J Pharmacokinet Pharmacodyn (2013) 40:S15–S149
DOI 10.1007/s10928-013-9308-2

ABSTRACTS

Abstracts Accepted for American Conference on Pharmacometrics 2013

Publication Draft for Journal of Pharmacokinetics and Pharmacodynamics

M-001 Modeling Sitagliptin Effect on Dipeptidyl Peptidase IV (DPP4/CD26) Activity in Adults with Hematological Malignancies After Umbilical Cord Blood (UCB) Hematopoietic Stem Cell Transplant (HSCT)

Nieves Vélez de Mendizábal[1,2,*], Robert M. Strother[3], Steven Messina-Graham[4], Sherif S. Farag[1], Hal Broxmeyer[4], Robert R. Bies[1,2]

[1]Indiana University School of Medicine, Indianapolis, IN, USA; [2]Indiana Clinical and Translational Sciences Institute (CTSI), Indianapolis, IN, USA; [3]Christchurch Hospital, Christchurch, NZ, USA; [4]Indiana University-Purdue University, Indianapolis, IN, USA

Objectives: UCB is a promising resource for HSCT, however, the delayed engraftment observed has resulted in increased morbidity and mortality resulting in less frequent use of UCB. Inhibition of DPP4, previously shown to enhance stem cell engraftment in mice, have been examined in human subjects in an effort to improve time to engraftment in UCB HSCT [1, 2]. Based on data from this clinical trial, a semi-mechanistic model was developed to simultaneously describe DPP-4 activity after multiple doses of sitagliptin in subjects with hematological malignancies after a single-unit UCB HSCT.
Methods: The clinical study included 24 patients (21–58 years) that received myeloablative conditioning followed by oral sitagliptin 600 mg on days −1 to +2, with single-unit UCB HSCT on day 0. Sitagliptin plasma concentrations were determined via HPLC–MS/MS and plasma DPP-4 activity was determined using the DPP4-Glo Protease Assay (Promega, Madison, WI, USA). These data were simultaneously analyzed using the population approach with NONMEM 7.2.
Results: Disposition of sitagliptin in plasma was best described by a 2-compartment model. Drug absorption was best described by a first order rate constant. Inter-subject variability (ISV) was found to be significant for the apparent total plasma clearance (CL/F), apparent volume of distribution in the central compartment (V_2/F), apparent volume of distribution in the peripheral compartment (V_3/F), and relative bioavailability (F). None of the PK parameters were time or dose dependent. ISV was significant on $DPP4_0$, k_{unb} and EC_{50}. The inclusion of covariance (positive correlation) between the random effects associated to EC_{50} and bioavailability (F) parameters significantly improved the model predictions. Different doses and administration schedules were evaluated with the selected model with the aim of maximizing the DPP-4 inhibition minimizing drug exposure and/or C_{max}.
Conclusions: A PKPD model was developed that accurately described the relationship between sitagliptin dosing schedules and DPP4 activity in vivo. This model is valuable for exploration of new dose regimes to maximize DPP-4 inhibition with the aim of improving time to engraftment in UCB HSCT.

References

[1] Broxmeyer HE, Hoggatt J, O'Leary HA, Mantel C, Chitteti BR, Cooper S, Messina-Graham S, Hangoc G, Farag S, Rohrabaugh SL, Ou X, Speth J, Pelus LM, Srour EF, Campbell TB (2006) Dipeptidylpeptidase 4 negatively regulates colony-stimulating factor activity and stress hematopoiesis. Nat Med 18(12): 1786–1796.

[2] Farag SS, Srivastava S, Messina-Graham S, Schwartz J, Nelson R, Robertson M, Abonour R, Cornetta K, Wood L, Secrest A, Strother RM, Jones D, Broxmeyer HE (2007) In-vivo DPP-4 inhibition to enhance engraftment of single-unit cord blood transplants in adults with hematological malignancies. Stem Cells Dev

M-002 Pharmacokinetic/Pharmacodynamic Analysis of an Antibacterial Agent Administered in a Phase II Study for the Treatment of Acute Bacterial Skin and Skin Structure Infection (ABSSSI)

David Tenero* and John Zhu

GlaxoSmithKline, Clinical Pharmacology Modeling & Simulation, King of Prussia, PA, USA

Objectives: Investigate the pharmacokinetic/pharmacodynamic (PK/PD) relationship for an orally administered antibacterial agent in patients with acute bacterial skin and skin structure infection and attempt to identify breakpoint(s) for clinical response.
Methods: In a multicenter, randomized, double-blind, Phase II trial, an antibacterial drug was administered as 1500 mg twice daily for up

to 10 days in patients with suspected Gram-positive ABSSSI who were not currently receiving antibacterial therapy. A population PK model was first developed using PK data from three Phase I studies in healthy volunteers. Population mean parameters were fixed to the final Phase I estimates to obtain Bayesian estimates of apparent clearance for each patient from the current Phase II study. Subsequently, individual Bayesian pharmacokinetic estimates were used to predict drug exposure, as measured by the steady-state AUC(0-24),ss for each patient. Logistic regression and classification and regression tree (CART) analyses were conducted to investigate the PK/PD relationship between microbiological/clinical cure and exposure [AUC(0-24),ss or free (f) AUC/MIC] as well as patient covariates (age, gender, and race). NONMEM (version 7.2) was used for population PK model building and R (version 2.12.0) was used for logistic regression, CART, and Fisher's exact test analyses and model evaluation.

Results: The healthy volunteer data were best described by a two-compartment model with first-order input and a lag time for absorption. Body weight was a statistically significant covariate on oral clearance (CL/F) and central volume of distribution (V/F). Population mean parameters were fixed to the final Phase I estimates to obtain Bayesian estimates of PK parameters for each patient from the Phase II study. The distribution of the Bayesian estimated CL/F and V/F from the Phase II study were comparable to the individual post hoc estimates from the Phase I studies used to developed the population PK model, indicating that the Bayesian estimation approach was appropriate to estimate CL/F (and AUC) for the Phase II patients.

The plan was to evaluate the PK/PD relationship in the intent-to-treat bacteriology (ITTB) and clinical (ITTC) populations and the per protocol bacteriology (PPB) and clinical (PPC) populations; however, the number of treatment failures in the per protocol populations was to low ($n = 3$) for this type of PK/PD analysis. Thus, PK/PD analyses were only conducted for the ITTB and ITTC populations with results shown for the ITTB population ($n = 37$; 22 cure/15 failure). Results for the ITTC population were similar.

Univariate logistic regression analyses showed that age, gender, race, fAUC/MIC, and AUC(0-24),ss were not statistically significant predictors of microbiological cure in the ITTB population. AUC(0-24),ss had the lowest P value ($P = 0.137$) and residual deviance and provided the most informative model for these data, and the Hosmer–Lemeshow test ($P = 0.86$) indicated there is not sufficient evidence to conclude that this model has lack of fit. However, the area under the receiver operating characteristic (ROC) curve was 0.63, indicating poor discrimination and predictability of the model. At the median AUC(0-24),ss value of 90.3 μg h/mL, the corresponding model-predicted probability of microbiological success is 58.9 %, concordant with the observed 59.5 % microbiological success rate.

CART analyses identified a breakpoint for AUC(0-24),ss (78.2 μg h/mL) as a predictor of microbiological cure. When AUC(0-24),ss was ≥ 78.2 μg h/mL, the microbiological success rate was 67.9 % (19 success, 9 failure), whereas when AUC(0-24),ss was <78.2 μg h/mL, the microbiological success rate was only 33.3 % (3 success, 6 failure) ($P = 0.118$). Logistic regression analysis was re-run with the independent variable AUC(0-24),ss included as a categorical variable, based on the CART-identified clinical breakpoint. AUC(0-24),ss as a categorical covariate showed a more significant influence ($P = 0.077$) on microbiological cure than AUC(0-24),ss as a continuous covariate. Additionally, the model had the lowest residual deviance and more precise parameter estimates.

Conclusions: Logistic regression and CART analyses were conducted to investigate the PK/PD relationship between microbiological/clinical cure and exposure [AUC(0-24),ss or fAUC/MIC] as well as patient covariates (age, gender, and race) in this Phase II study. AUC(0-24),ss and fAUC/MIC were not significant predictors for microbiological success or clinical success but, overall, AUC(0-24),ss provided the most informative model for these data. However, the analyses were conducted on a small patient population that included many non-drug related dropouts and these data need to be interpreted with caution.

M-003 Design of Informative Renal Impairment Studies: Evaluation of the Impact of Design Stratification on Bias, Precision and Dose Adjustment Error

J. G. Coen van Hasselt[1,2,*], Jan H. M. Schellens[1,3], Jos H. Beijnen[2,3], Alwin D. R. Huitema[2]

[1]Department of Clinical Pharmacology, The Netherlands Cancer Institute, Amsterdam, The Netherlands; [2]Department of Pharmacy & Pharmacology, Slotervaart Hospital/Netherlands Cancer Institute, Amsterdam, The Netherlands; [3]Division of Pharmacoepidemiology & Clinical Pharmacology, Department of Pharmaceutical Sciences, Faculty of Science, Utrecht University, Utrecht, The Netherlands

Objectives: Renal impairment (RI) studies are conducted to estimate the impact of RI on pharmacokinetics (PK). In some therapeutic areas (e.g. oncology), these studies can be difficult to conduct, for instance due to the limited number of eligible patients available. The objective of this analysis was to evaluate bias and precision of population PK parameters, and the dose adjustment error (DAE) for RI studies (i) with different levels of study design imbalance in the stratification of subjects across RI categories, and (ii) which include additional patients in the control arm of RI studies, that may be available from previously conducted PK studies.

Methods: Study designs were simulated and re-estimated using a hypothetical 2-compartmental PK model, varying the magnitude of the fraction of renal elimination (FR) and the magnitude of between-subject variability (BSV). The DAE was computed based on the difference between the theoretical dose adjustment versus the empirical estimated dose adjustment.

Results: Although some design imbalance may still lead to DAEs of acceptable magnitude (DAE ≤11.05–14.44 % inter-quartile range, IQR), at least some patients are necessary in the more severe RI groups in order to adequately estimate RI effects. Secondly, when 100 additional patients with normal renal function were included in a sub-informative design, the DAE changed from ≤17.63–16.64 % IQR, to ≤8.89–8.69 % IQR, indicating that inclusion of these patients may substantially improve a RI analysis.

Conclusions: We quantified the impact of study design imbalance on bias and precision of PK parameters and DAE, as may occur for RI studies in some indications. Adding additional data from earlier studies to the analysis dataset improves the bias and precision of PK parameters.

M-004 A Modified Approach to Assess the Relationship Between Plasma Eltrombopag Concentrations and QTc Intervals from Phase III Studies in Patients with Hepatitis C Virus Infection

Xiaohua Gong, Jianping Zhang*

GlaxoSmithKline, Research Triangle Park, NC, USA

Objectives: Eltrombopag is an orally bioavailable, small molecule thrombopoietin receptor (TPO-R) agonist developed for the treatment

of thrombocytopenia in patients with hepatitis C virus (HCV) infection. An earlier thorough QT (TQT) study in healthy subjects had shown no relationship between plasma eltrombopag concentration (Cp) and time-matched change from baseline in QTc between active and placebo (ddQTc) at therapeutic (50 mg QD) and supratherapeutic (150 mg QD) doses [1]. However, patients with HCV have demonstrated increased eltrombopag exposure due to impaired hepatic function [2], and they are more susceptible to QTc prolongation [3, 4]. Although assessment of the potential impact of eltrombopag on the QTc interval was incorporated in phase III studies, time-matched QTc data between placebo and active treatment were not available within subject to allow standard Cp-ddQTc evaluation. A modified calculation of ddQTc was developed, such that the mean time-matched QTc change from baseline in subjects from placebo group was subtracted from the individual time-matched QTc change from baseline in subjects treated with eltrombopag. This approach allowed method similar to TQT analysis to be used to determine the effect of plasma eltrombopag concentrations on QTc intervals in patients with HCV from Phase III studies. The objectives of this analysis were (1) To determine whether a relationship exists between plasma eltrombopag concentration and the QT/QTc interval in patients with HCV; (2) To identify influential covariates that might impact any relationship between plasma eltrombopag concentration and QT/QTc interval in patients with HCV.

Methods: Plasma eltrombopag concentration and ECG data were obtained from 98 subjects with HCV in two phase III studies. Mixed effects modeling was conducted for the Cp-QT and Cp-ddQTc analyses. A stepwise modeling process was applied in which inter-individual and inter-occasion variability and a circadian component (for Cp-QT modeling) were added to the model. Graphical exploration of random effects (η) against each covariate was inspected and covariate analysis was conducted where effects of covariates manifested. Data from Study 2 served as a validation dataset for the models developed based on data from Study 1 alone. In addition, visual predictive check and non-parametric bootstrap methods were implemented for final model evaluation. The final Cp-ddQTc model developed from the combined data was used to simulate the ddQTc at therapeutic (up to 100 mg QD) and supratherapeutic (200 mg QD) doses of eltrombopag in the analysis population (with time-matched QTc data) as well as the entire PK population from both studies.

Results: (1) The final Cp-QT model fitted to the combined data revealed an estimated correction coefficient (α) of 0.32. The estimated slope for the effect of the plasma eltrombopag concentration on QT interval was 0.243 (RSE = 9 %) m s/(μg/mL) with a 95 % confidence interval from bootstrap analysis slightly above zero (0.059, 0.447 msec/(μg/mL)), suggesting a linear relationship between plasma eltrombopag concentration and QT interval. However, a conservative calculation using the upper limit of 95 % CI of the slope estimate (0.447 msec/(μg/mL)) and assuming a fixed heart rate of 60 bpm (RR = 1000 msec) demonstrated that the predicted QTc change from baseline at 100 mg QD dose (median C_{max} = 22.55 μg/mL) would be approximately 10.1 msec, which suggests that impact of eltrombopag concentrations on QT interval is not clinically significant. (2) The final Cp-ddQTcF model fitted to the combined data also provided good estimates of model parameters. The estimated slope for the effect of the plasma eltrombopag concentration on ddQTcF was 0.136 (RSE = 10 %) msec/(μg/mL) with a 95 % confidence interval from bootstrap analysis (-0.049, 0.394 msec/(μg/mL)) containing zero, suggesting that the eltrombopag exposure does not have significant affect on ddQTcF. (3) Simulations based on the final Cp-ddQTcF model developed with either the analysis population or the entire PK population suggested no significant QT prolongation over the studied dosages of 25–100 mg once daily or with a supratherapeutic dose of 200 mg once daily.

Conclusions: (1) The slopes of the relationship between eltrombopag concentrations and QT/ddQTc were slight. (2) The risk of QT prolongation in response to daily dose of eltrombopag up to 100 mg is negligible in patients with HCV infection. (3) The risk of QT prolongation due to supratherapeutic doses of eltrombopag as high as 200 mg QD is predicted to be negligible in patients with HCV infection.

References

[1] Matthys G, Park JW, McGuire S, Wire MB, Zhang J, Bowen C, Williams D, Jenkins JM, Peng B (2010) Eltrombopag does not affect cardiac repolarization: results from a definitive QT study in healthy subjects. Br J Clin Pharmacol 70(1): 24–33

[2] Zhang J, Williams DD, Moore KP (2009) Use of eltrombopag exposure-platelet response relationship for dose optimization in patients with chronic HCV-infection with and without interferon. PAGE Abstr. 1494

[3] Bernardi M, Calandra S, Colantoni A, Trevisani F, Raimondo ML, Sica G, Schepis F, Mandini M, Simoni P, Contin M, Raimondo G (1998) Q-T interval prolongation in cirrhosis: prevalence, relationship with severity, and etiology of the disease and possible pathogenetic factors. Hepatology 27(1): 28–34

[4] Bal JS, Thuluvath PJ (2003) Prolongation of QTc interval: relationship with etiology and severity of liver disease, mortality and liver transplantation. Liver Int 23(4): 243–248

M-005 Pharmacokinetic-Pharmacodynamic Modeling of the Antitumor Effects of SGN-CD19A, a Novel Antibody–Drug Conjugate, in Mice

Baiteng Zhao[1,*], Faith Stevison[1], Che-Leung Law[2], Tae H Han[1]

[1]Clinical Pharmacology, Seattle Genetics, Inc., Bothell, WA 98021, USA. [2]Preclinical Research, Seattle Genetics, Inc., Bothell, WA 98021, USA

Objectives: SGN-CD19A is a novel antibody–drug conjugate under investigation for the treatment of acute lymphoblastic leukemia and B cell non-Hodgkin lymphoma. It comprises a humanized antibody, specific for human CD19, conjugated to the microtubule disrupting agent monomethyl auristatin F. Preclinical evaluations of SGN-CD19A demonstrated antitumor activities in the SCID mouse xenograft models [1]. The objectives of this study were to characterize the relationship of SGN-CD19A pharmacokinetics (PK) and antitumor effects in a mouse Ramos xenograft model.

Methods: SGN-CD19A PK was characterized following intraperitoneal (IP) administration of a single dose to nontumor-bearing mice and to Ramos tumor-bearing. The pharmacodynamic (PD) antitumor effect was characterized following IP administration of SGN-CD19A in the mouse Ramos xenograft model. A dose fractionation approach was used in the PD study, where a total dose of 8 mg/kg SGN-CD19A was administered as either a single dose of 8, 4 mg/kg q21dx2, 4 mg/kg q7dx2, 2 mg/kg q7dx4, or 0.8 mg/kg q2dx10 [2]. Tumor sizes were measured during the treatment. Sequential PK/PD models were developed to describe the plasma PK and antitumor activity of SGN-CD19A using NONMEM v7.1.2. Both the signal distribution model and cell distribution model were tested for antitumor effects. Nonlinear tumor cell kill function with loss of drug sensitivity was incorporated in the PD model.

Results: SGN-CD19A PK was dose proportional across the range of doses tested and was similar between those in nontumor-bearing and tumor-bearing mice. The plasma concentration–time profiles of SGN-CD19A in mice were described well by a two-compartment PK model with a depot compartment. The antitumor effects were dependent on dose and schedule although all animals received the same total dose

of SGN-CD19A. A single dose resulted in the greatest antitumor effect while the highest fractioned dose resulted in reduced antitumor activity. A cell distribution model with exponential growth and incorporation of resistance development to the drug described the PD data.

Conclusions: A semi-mechanistic PK/PD model characterized the PK and antitumor effect of SGN-CD19A in a mouse Ramos xenograft model. The antitumor effect of SGN-CD19A is dependent on the dose and schedule in mouse xenograft model.

References

[1] Law et al., AACP 2011

[2] Hartsfield et al., AAPS NBC 2012

M-006 Model Based Meta-analysis of Children's Depression Rating Scale: Revised (CDRS-R) in Children and Adolescents with Major Depressive Disorder

Diansong Zhou*, Nidal Al-Huniti

Clinical Pharmacology & Pharmacometrics, AstraZeneca, Wilmington, DE, USA

Objectives: Major depressive disorder (MDD) leads to significant morbidity and mortality in children and adolescents. Many antidepressants failed to demonstrate superiority in double blinded clinical trials due to the significant placebo response. The purpose of current study was to evaluate the time course of antidepressants in treatment of MDD through longitudinal modeling, to explore the placebo response effect and guide clinical trial design.

Methods: A PubMed search was conducted to obtain clinical trials for antidepressive agents with reporting Children's Depression Rating Scale-Revised (CDRS-R) in children and adolescent. Only randomized controlled trials in youths (6–18 years of age) with MDD that studied selective serotonin reuptake inhibitors as well as other novel antidepressants were included as the placebo response in major depression trials was higher than for other indications and could be influenced by patient and trial characteristics [1]. A total of 10 clinical trials for 7 drugs representing 2410 patients were included in the final analysis. The average CDRS-R score at study entry was in the range of 54.5–64.6 for these patients. An E_{max} like model was applied to describe depression effect as shown below:

$$\text{Response}_i = (E_0 + \eta_1) - \frac{(E_{\max} + \eta_2) * \text{Time}_i}{(ET_{50} + \eta_3) + \text{Time}_i} + \frac{\varepsilon}{\sqrt{n}}$$

Response_i is CDRS-R score for observation i.

$E_{max} = E_{max,placebo} + D * E_{max,drug}$, where D equals 1 for drug and 0 for placebo.

Model parameters were estimated by using nonlinear mixed effect modeling software (NONMEM 7.2). A 1000 trial simulation was then conducted with final parameter estimates and normally distributed eta and epsilon with mean and variance estimated by the model to evaluate the variability of placebo/drug and potential impact of sample size in clinical trial design.

Results: The baseline CDRS-R score was estimated to be 58.9 (1.5 % RSE) for MDD clinical trials in children and adolescent. The maximum effect with treatment of placebo was 24.5 (7.9 % RSE), while the maximum effect was increased in the range of 1.4–7.7 by treating with different antidepressive agents. The ET_{50}, the time induced a response equal to one-half of E_{max}, was estimated to be 1.9 weeks (9.1 % RSE). The 1000-trial simulation (Figure below) indicated

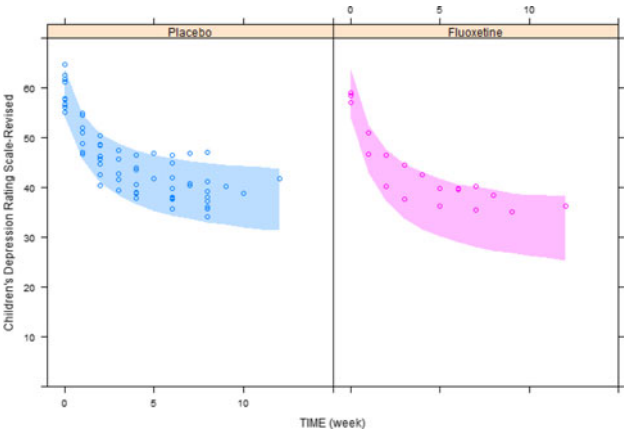

model performance was acceptable (fluxetine results). In addition, the model also demonstrated significant variability of placebo effect in MDD clinical trials.

Conclusions: The meta-analysis of a longitudinal model permitted a good fit to the antidepressive effect in children and adolescent. Model based meta-analysis incorporates potential effect of different study populations and designs from multiple clinical studies, and would guide drug development programs to design new clinical trials.

References

[1] Bridge JA, Birmaher B, Iyengar S, Barbe RP, Brent DA (2009) Placebo response in randomized controlled trials of antidepressants for pediatric major depressive disorder. Am J Psychiatry 166(1):42–49

[2] Ahn JE, French JL (2010) Longitudinal aggregate data model-based meta-analysis with NONMEM: approaches to handling within treatment arm correlation. J Pharmacokinet Pharmacodyn. 37(2):179–201

M-007 Diabetes Toolkit: A Multi-Function Clinical Trial Simulation Program

Dongwoo Kang*, Raymond Miller

Translational Medicine and Clinical Pharmacology, Daiichi Sankyo Pharma Development, Edison, NJ, USA

Objectives: To develop a general multi-function clinical trial simulation tool for diabetes compounds to compute the probability of trial success.

Methods: An R based trial simulation package consisting of 2 modules was developed using a diabetes drug PKPD (pharmacokinetic-pharmacodynamic) model established using rivoglitazone [1], a peroxisome proliferator-activated receptor gamma (PPARγ) agonist. A publicly available R package of MSToolkit together with the internally developed modules is used to simulate and analyze the data. There also is an option to call a NONMEM run to simulate the model. Module 1 simulates a conventional clinical trial to test if a new compound produces large enough effect to be approved for marketing. An example decision criterion is to observe a 10 mg/dL or larger drop in FPG (fasting plasma glucose) compared with baseline value and/or to observe a 3 % or larger decrease in HbA1c (glycosylated haemoglobin). Module 2 evaluates the viability of replacing a long term study with a relatively short term study with the objectives of reducing time and cost of development. To assess such a hypothesis, a

Table 1 Probability of success with respect to dose groups considered

Dose (mg)	PoS.FPG (%)	PoS.HBA (%)
0.5, 1, 2, 3, 5	5	0
1, 2, 3, 5	8	0
2, 3, 5	30	0
3, 5	56	6
5	82	20

Table 2 Probability of success with respect to different decision criteria

Criteria·ΔFPG ≥ (mg/dL)	PoS·FPG (%)	Criteria·ΔHBA ≥ (%)	PoS·HBA (%)
2.5	82	0.075	50
5	78	0.15	26
10	56	0.3	6
20	16	0.6	0

long term (e.g., 16 weeks) study data is generated. Then a short term (e.g., 2 or 4 weeks) study is mimicked by subsetting the long term study observations. Using the short term subset data, PD model parameters are reestimated to obtain a new model based on short term data only. Projected endpoint values at the end of the required long term period are obtained from the new short term data model, to be compared with the original long term study output. If both values are similar enough according to specific clinical criteria, the short term study can replace the long term study because the conclusions will be statistically similar. Diabetes Toolkit also produces extensive graphic summary of the simulation results.

Results: Diabetes Toolkit was tested under various trial scenarios. Example cases for Module 1 are shown in the tables below. Table 1 shows the probability of success (PoS) for FPG criteria of 10 mg/dL or greater decrease from baseline at the end of 16 weeks of treatment, and HbA1c criteria of 3 % or greater decrease, with respect to different sets of doses considered to determine trial success. Focusing on high dose groups increases the PoS. Table 2 shows the PoS of FPG or HbA1c with respect to various criteria values to identify the sensitive or dull regions with respect to changes in the decision criteria.

Conclusions: A multi-function R package Diabetes Toolkit was developed to perform diabetes clinical trial simulations. FPG and HbA1c are the output variables to determine the drug response. Diabetes Toolkit can be a useful tool during drug development to do trial simulations quickly and with minimum or no reliance on other software. Diabetes Toolkit can be easily modified for simulation of different class drugs with different mechanisms of action.

References

[1] Shashank Rohatagi, Timothy J. Carrothers, JinYan Jin, William J. Jusko, Tatiana Khariton, Joseph Walker, Kenneth Truitt, and Daniel E. Salazar (2008) Model-based development of a PPARγ agonist, rivoglitazone, to aid dose selection and optimize clinical trial designs. J Clin Phamacol 48:1420–1429

M-008 Population Pharmacokinetic Modeling for Edoxaban in Healthy Subjects and Patients with Non-valvular Atrial Fibrillation (NVAF)

Ophelia QP Yin, Raymond Miller

Daiichi Sankyo Pharma Development, Edison, NJ, USA

Objectives: Edoxaban is a novel, oral, once-daily, highly specific direct inhibitor of factor Xa that is currently being developed for the treatment and prevention of venous thromboembolism and prevention of stroke and systemic embolism in patients with non-valvular atrial fibrillation (NVAF). The objective of this analysis was to characterize edoxaban population pharmacokinetics (PK), including estimation of its absolute bioavailability, and quantification of the effects of renal impairment or co-administration of P-gp inhibitors on edoxaban PK.

Methods: Data from 7 phase I studies in healthy volunteers ($n = 225$) or renal impairment patients ($n = 24$), and one phase II study in patients with NVAF ($n = 732$) were included in this analysis. NVAF patients with mild or moderate renal impairment were enrolled in the phase II study. Edoxaban was given as a single dose of 15 or 60 mg orally, or a single dose of 30 mg intravenously in phase I studies. In the phase II study, edoxaban doses were 30 or 60 mg once-daily orally, or 30 or 60 mg twice-daily orally. Full PK samples were obtained from all phase I studies, while in the phase II study there were approximately 2 samples per patient. Population PK analysis was performed by using nonlinear mixed effects modeling (NONMEM). The final selected model was assessed by goodness-of-fit, visual predictive check and bootstrap analysis.

Results: Edoxaban PK was described by a two-compartment model, with first-order absorption and elimination. Absolute bioavailability (F) was estimated to be 58.1 %. Renal creatinine clearance was identified as a significant covariate on clearance (CL), with typical CL values being 28.7, 25.6, 22.7 and 20.4 L/h respectively, in subjects with normal renal function, or with mild, moderate or severe renal impairment. With intravenous dosing of edoxaban, concurrent administration of the P-gp inhibitor quinidine statistically significantly decreased edoxaban CL and volume of distribution of central compartment (Vc), resulting in an increase of 32 % in AUC and 66 % in C_{min}. With oral dosing of edoxaban, concurrent administration of P-gp inhibitors (including quinidine, ketoconazole, erythromycin, verapamil, and amiodarone) significantly increased edoxaban F and decreased Vc, resulting in moderate increases in AUC (range 33–77 %) and C_{max} (range 65–104 %), but a much smaller increase in C_{min} (range −24 to 38 %) due to shortened terminal elimination half-life. Visual predictive check suggested the final model described the data well, and all parameter estimates had reasonable precision as per bootstrap analysis.

Conclusions: Overall, population PK analysis was consistent with the known biopharmaceutical characteristics of edoxaban. The final model provided reasonable estimation with regard to the absolute bioavailability of edoxaban, impact of renal impairment on edoxaban clearance, and the magnitude of change in edoxaban exposure measures upon co-administration of P-gp inhibitors. The population PK model also aided the prediction of edoxaban PK in NVAF patients, which will be used in a subsequent exposure–response analysis.

M-009 Understanding Placebo Responses in Alzheimer's Disease (AD) Clinical Trials from the Literature Meta-data and CAMD Database

Kaori Ito[1,*], Brian Corrigan[1], Klaus Romero[2], Richard Anziano[1], Jon Neville[2], Diane Stephenson[2], Richard Lalonde[1]

[1]Pfizer Inc., Groton, CT, USA; [2]Critical Path Institute, Tucson, AZ, USA

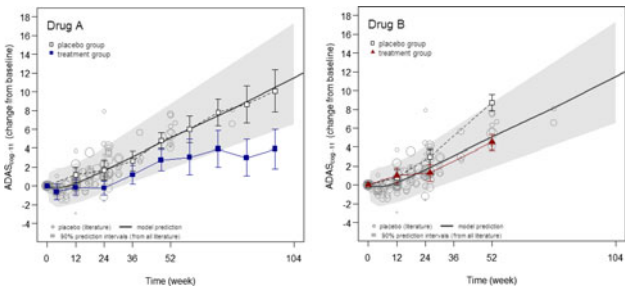

Fig. 1 Using drug models to facilitate interpretation of study results

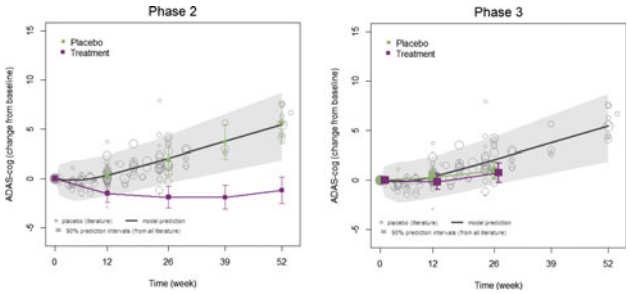

Fig. 2 Abnormal placebo response or lack of drug treatment effect?

Objectives: Understanding both the placebo response and the underlying disease progression is crucial to designing clinical trials and interpreting results in Alzheimer's disease (AD) research. It is sometimes difficult to differentiate the placebo effect and underlying disease progression in individual longitudinal studies, resulting in potential misinterpretation of the study results. In this analysis, the placebo response in the Alzheimer's disease assessment scale cognitive subscale (ADAS-cog) was evaluated across studies. The placebo response component from a previously published disease progression model for ADAS-cog model was used to estimate the placebo response with cognitive function over time in mild to moderate AD patients, and the disease progression in the placebo group in various case studies were compared to model predictions. In addition, placebo group data from the coalition against major diseases (CAMD) AD database in mild to moderate AD patients is described.

Methods: Historical placebo response data were obtained from a literature search from 1990 to 2010, as described in a previous publication [1]. The disease progression model was developed based on these trials [1], and the placebo response components were used in this analysis. Data used in each Case Study was double blind, placebo controlled studies taken from the public domain or Pfizer internal data bases (placebo arm only), and the CAMD database (http://www.c-path.org/CAMD.cfm). The CAMD AD database (cut-off date for this analysis: Dec 2011) had patient level information from more than 3,700 individual subjects obtained from 10 trials, spanning the continuum of mild cognitive impairment (MCI) to mild and moderate AD trials.

Results: Figure 1 (Case Study 1) shows side by side results from two Phase II clinical trials for two different compounds (Drugs A and B). In both cases, it appears as though a treatment effect was present as compared with the placebo group in each study. However, when historical control data is overlaid, along with model predictions conditioned for baseline severity, it appears that the placebo response in Drug B trial was much worse than what would be predicted. Conversely, the treatment arm in Trial B appears to be where the expected response for placebo usually falls. Given this result, and without clear rationale for why a difference in placebo response would be observed, the clinical team concluded that the placebo response or Drug B was not normal, and needed more data to confirm the efficacy before moving to Phase III.

In the next example, drug X demonstrated a significant treatment effect in a Phase II study, followed by a large Phase III study. The Phase III results appeared different from the Phase II study; there was no significant difference between treatment group versus placebo group. The clinical team questioned the placebo response in the Phase III study, which appeared almost flat. In this case, the placebo response in Phase III can be quantitatively assessed, and was deemed well within the normal range; it was still within the 90 % prediction intervals when compared with historical placebo response and model prediction (Fig. 2). It was revealed that the placebo responses in both Phase II and Phase III were reasonable, and that it was the treatment effects that appeared different, resulting in a failed Phase III trial (point size in Fig. 2 is proportional to the sample size of the study).

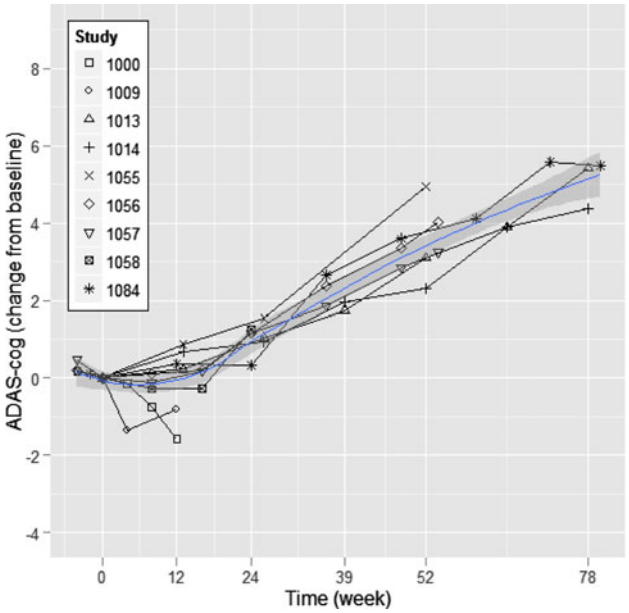

Fig. 3 Mean change from baseline ADAScog from CAMD database

Figure 3 illustrates the mean change from baseline ADAS-cog over time by study from the CAMD database. The blue line and gray-shaded area in the figure indicate a lowess fit line with 95 % confidential intervals. Across studies, the placebo effect is evident to at least week 12. Interestingly, the short Phase II studies (Studies 1000 and 1009, 12 weeks Phase II studies) had larger placebo effects, again perhaps due to expectations from both investigators and patients. Also, these studies had a relatively small sample size ($N = 102$ and 164 for placebo arm), which might have effects on patient selection or trial results.

Additional case studies will be presented at the conference.

Conclusions: Recent failures in Phase III AD clinical studies are not likely due to insufficient cognitive decline/disease progression in the placebo group to demonstrate separation of treatment effect. A meta-analytic approach using all available data provides a robust understanding of placebo effect, and the disease progression, and the placebo response predicted from the model allows us to quantitatively evaluate the clinical study results, and to compare placebo responses across trials. Baseline severity of cognitive deterioration is an important covariate of disease progression, and must be accounted for when comparing across trials.

Reference

[1] Ito K et al. (2010) A disease progression meta-analysis model in Alzheimer's disease. Alzheimer's & Dementia 6: 39–53

M-010 Pharmacokinetic-Pharmacodynamic Modeling of Adalimumab and its Efficiency in the Management of Rheumatoid Arthritis Patients

David Stepensky

Department of Clinical Biochemistry and Pharmacology, The Faculty of Health Sciences, Ben-Gurion University of the Negev, Beer-Sheva, Israel

Background: Anti-TNF-α antibodies that are used to manage rheumatoid arthritis (RA) can interact with TNF-α in the synovial fluid, in the systemic circulation, and in other locations in the body. Unfortunately, only partial data on the time course of synovial and systemic concentrations of TNF-α and adalimumab is available due to the difficulties with collection of synovial fluid from the RA patients. Thus, there is lack of clarity regarding the mechanisms anti-TNF-α effects of adalimumab in RA and its optimal use in this disease. Outcomes of the recent pharmacokinetic-pharmacodynamic modeling analysis of adalimumab effects in the RA indicated that subcutaneous, intravenous and intraarticular administration of the clinically-used doses of adalimumab (40 mg) exert similar anti-TNF-α effects [1]. At these doses, adalimumab appears to exhibit predominantly systemic anti-TNF-α effects (i.e., adverse effects) and the contribution of the local effects in the rheumatic joints is small (∼7 %). On the other hand, the balance of local versus systemic effects can be potentially improved using intraarticular sustained release (SR) formulations of adalimumab. It is not clear to which extent the efficiency of the local and systemic effects of adalimumab (administered by different routes, as a solution or as a SR formulation) is affected by the inter-patient variability of the RA disease state and of the adalimimab pharmacokinetics.

Objectives: To estimate the inter-patient variability in the rheumatoid arthritis (RA) disease state and in the pharmacokinetics and pharmacodynamics of adalimumab. To estimate the resulting variability in the time course of local (intraarticular) versus systemic concentrations of TNF-α and in the optimal local delivery rate of adalimumab.

Methods: The data on the variability in the RA disease state and the pharmacokinetics of adalimumab were collected from the scientific literature [2–8]. The data included the following parameters: the TNF-α baseline levels and its turnover in the plasma and the synovial fluid of the RA patients, adalimumab absorption, distribution and elimination, and the affinity between the adalimumab and TNF-α. The collected data have been analyzed using a target-mediated drug disposition (TMDD) model with three sites of antibody-TNF-α interaction[1]. Individual model parameters have been simulated for one hundred virtual patients using Monte-Carlo approach, and the time course of the local (intra-articular) and systemic TNF-α and adalimumab concentrations have been analyzed. Furthermore, the dose–response of intraarticular adalimumab in the individual patients and its dependence on the individual variability factors have been evaluated.

Results: The time course of the local (intra-articular) and systemic TNF-α and adalimumab concentrations exhibited significant inter-patient variability. The RA disease state (the baseline TNF-α secretion rates in the individual compartments) was identified as the highest source of variability in the baseline TNF-α levels and the anti-TNF-α effects of adalimumab. Based on the simulations, intraarticular adalimumab administration using sustained release formulations can improve the balance of local versus systemic anti-TNF-α effects. For the average patient, the optimal rate of intraarticular adalimumab delivery (the therapeutic window) was in the range of 4.4–14.1 pmol h L. However, for the individual simulated patients, the optimal local delivery rates of adalimumab ranged from 0.3–4.0 to 52–66 pmol h L (Figs. 1, 2).

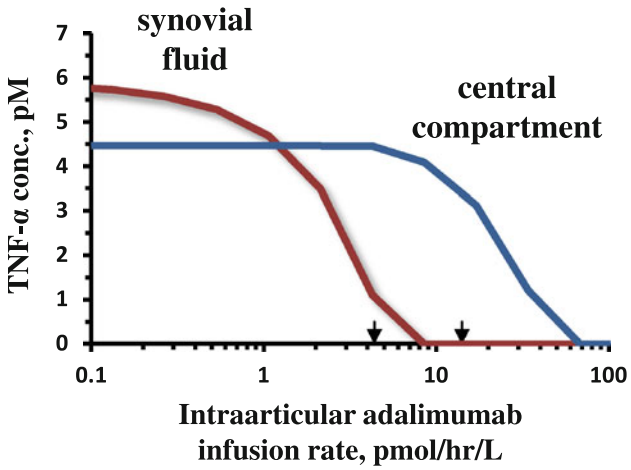

Fig. 1 The dose–response of intraarticular adalimumab infusions in the average patient. The average pharmacokinetic and pharmacodynamics parameters of TNF-α and adalimumab and the TMDD model with three sites of antibody-TNF-α interaction were used to simulate the effect of the intraarticular adalimimab infusion rate on the local (synovial fluid) and systemic (plasma) TNF-α levels in the rheumatoid arthritis patients. The arrows indicate the higher and the lower boundaries of the therapeutic window: at least 80 % of desired effect (reduction of the TNF-α levels in the synovial fluid) and up to 20 % of the adverse effect (reduction of the TNF-α levels in the plasma)

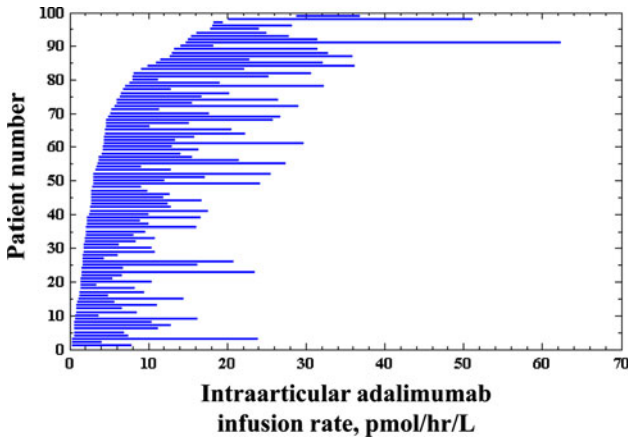

Fig. 2 The therapeutic window of intraarticular adalimumab in the individual patients. The dose–response of intraarticular adalimumab infusions has been simulated for one hundred patients using Monte-Carlo approach based on the inter-patient variability of the pharmacokinetic and pharmacodynamics parameters of TNF-α and adalimumab and the TMDD model with three sites of antibody-TNF-α interaction. The lines indicate the higher and the lower boundaries of the therapeutic window of for the intraarticular adalimumab infusions in the individual patients

Conclusions: Despite the extensive clinical use of TNF-α-neutralizing antibodies, parameters that govern their efficiency in individual RA patients have not been identified yet. Simulations using the TMDD model with three sites of antibody-TNF-α interaction and the estimated variability parameters indicate that the disease state is the highest source of variability of the baseline TNF-α levels and of the adalimumab pharmacological effects. Therefore, sustained release formulation that continuously releases anti-TNF-α antibody at a certain pre-set rate can lead to suboptimal responses in a high proportion of the individual patients. Efficient RA treatment using TNF-α-neutralizing antibodies should take into account the inter-patient variability of local vs. systemic factors derived from the disease state. Adjustment of drug dosage based on the individual variability factors is required to optimize the balance of local versus systemic anti-TNF-α effects. Correlation of local TNF-α levels in the affected joints with the clinical markers of RA warrants further investigation. Inter-patient variability should be taken into account for other drugs acting on soluble targets (growth factors, interferons, interleukins, immunoglobulins, etc.).

References

[1] Stepensky D (2012) Local vs. systemic anti-TNF-alpha effects of adalimumab in rheumatoid arthritis: pharmacokinetic modeling analysis of interaction between a soluble target and a drug. Clin Pharmacokinet 51(7):443–455

[2] Gamm H, Lindemann A, Mertelsmann R, et al (1991) Phase I trial of recombinant human tumour necrosis factor alpha in patients with advanced malignancy. Eur J Cancer 27(7): 856–863

[3] Mittelman A, Puccio C, Gafney E, et al (1992) A phase I pharmacokinetic study of recombinant human tumor necrosis factor administered by a 5-day continuous infusion. Invest New Drugs 10 (3): 183–190

[4] McNearney T, Baethge BA, Cao S, et al (2004) Excitatory amino acids, TNF-alpha, and chemokine levels in synovial fluids of patients with active arthropathies. Clin Exp Immunol 137(3): 621–627

[5] Pejovic M, Stankovic A, Mitrovic DR (1995) Determination of the apparent synovial permeability in the knee joint of patients suffering from osteoarthritis and rheumatoid arthritis. Br J Rheumatol 34(6): 520–524

[6] Kaymakcalan Z, Sakorafas P, Bose S, et al (2009) Comparisons of affinities, avidities, and complement activation of adalimumab, infliximab, and etanercept in binding to soluble and membrane tumor necrosis factor. Clin Immunol 131(2): 308–16

[7] den Broeder A, van de Putte L, Rau R, et al (2002) A single dose, placebo controlled study of the fully human anti-tumor necrosis factor-alpha antibody adalimumab (D2E7) in patients with rheumatoid arthritis. J Rheumatol 29(11): 2288–98

[8] Weisman MH, Moreland LW, Furst DE, et al (2003) Efficacy, pharmacokinetic, and safety assessment of adalimumab, a fully human anti-tumor necrosis factor-alpha monoclonal antibody, in adults with rheumatoid arthritis receiving concomitant methotrexate: a pilot study. Clin Ther 25(6): 1700–1721

M-011 Qualification of Ocular CFD Models to Aid Development of Intravitreal Anti-VEGF Therapies

Paul Missel*

Modeling & Simulation, Alcon Research Ltd., Fort Worth, TX, USA

Objectives: Develop qualified computational fluid dynamic models for rabbit, monkey and human eyes to simulate ocular PK after intravitreal (IVT) administration. This engineering approach explicitly represents ocular anatomic geometry and simulates the patterns of physiologic fluid flows and mass transport of drug by convective diffusion. The model enables estimation of target ocular tissue exposure across species and following various modes of administration (e.g. IVT, topical and subconjunctival). This abstract summarizes current model qualification using available literature data.

Methods: Drug advection after central bolus injection was simulated using methods published previously [1]. A regional drug sink, applied to the choroid, was adjusted to provide the best fit to the rabbit data. The same values of material properties, sink and boundary conditions were applied for all species.

Results: Simulations fit the time course of drug concentration in both vitreous and aqueous humor compartments for both Avastin and Lucentis in the rabbit (data from Bakri et al. [2, 3], Fig. 1a, b). The

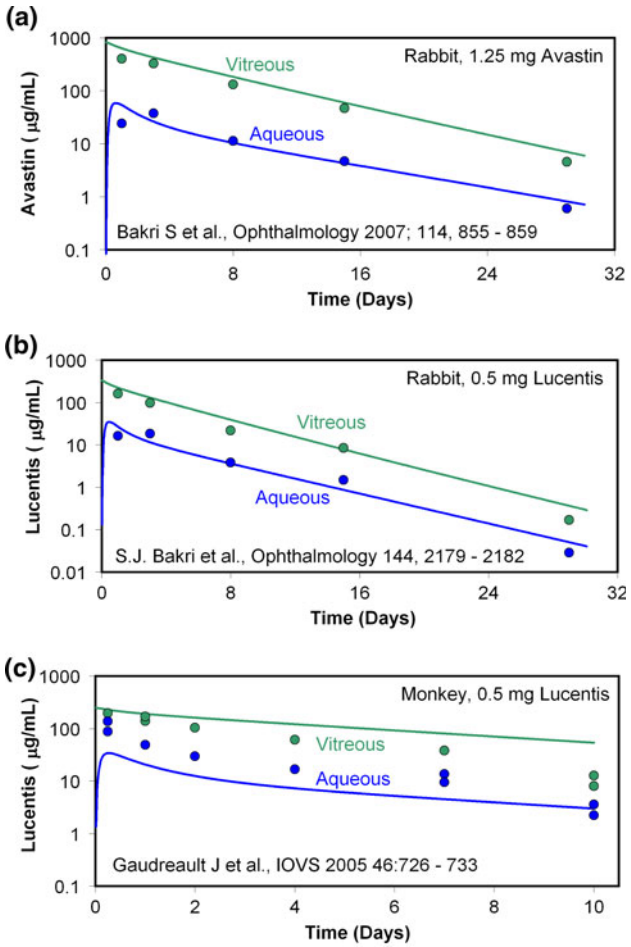

Fig. 1 Comparison between simulated and experimental pharmacokinetic measurements after IVT injection in animals. In each case, the initial condition at the beginning of the simulation was a spherical bolus in the mid vitreous with concentration set as required to administer the amount of drug specified. Solid curves represent the average concentrations in the entire vitreous and aqueous compartments as indicated. (a) 1.25 mg Avastin administered in 50 µL to Dutch-belted rabbits. (b) 0.5 mg Lucentis administered in 50 µL to Dutch-belted rabbits. (c) 0.5 mg Lucentis administered in 50 µL to Cynomolgus monkeys

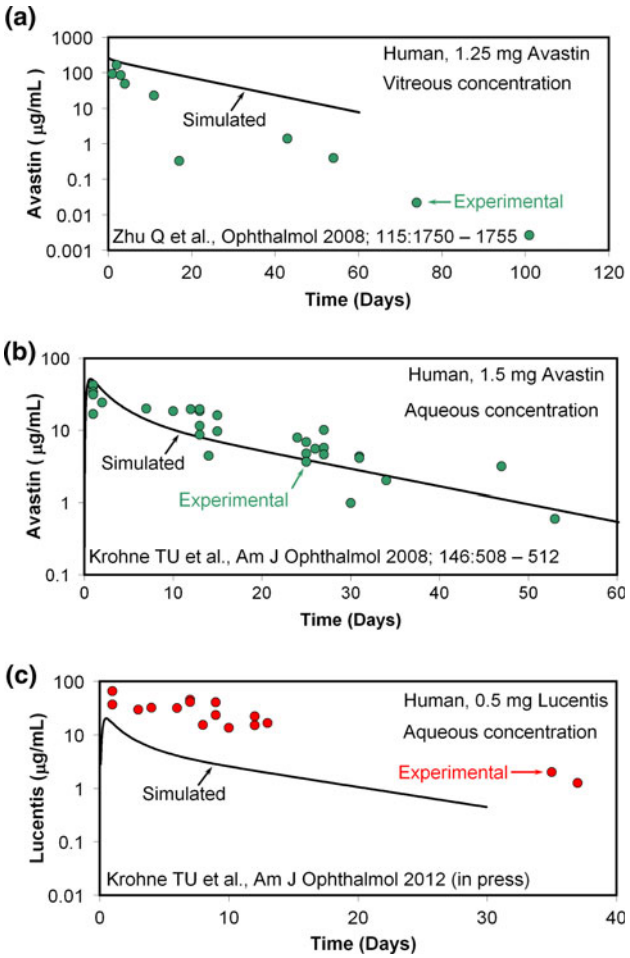

Fig. 2 Comparison between simulated and experimental pharmacokinetic measurements after IVT injection in humans. In each case, the initial condition at the beginning of the simulation was a spherical bolus in the mid vitreous with concentration set as required to administer the amount of drug specified. Solid curves represent the average concentrations in the entire vitreous or aqueous compartments as indicated. **a** 1.25 mg Avastin administered in 50 µL to patients with submacular hemorrhage and CNV due to age-related macular degeneration. **b** 1.25 mg Avastin administered in 100 µL to patients with macular edema secondary to neovascular age-related macular degeneration, diabetic retinopathy, or retinal vein occlusion. **c** 0.5 mg Lucentis administered in 100 µL to patients with macular edema secondary to neovascular age-related macular degeneration, diabetic retinopathy, or retinal vein occlusion

rate of clearance from man reproduced the aqueous humor measurements of Krohne et al. [4, 5], although the absolute magnitude was only reproduced for Avastin (Fig. 2b, c). Clearance of Avastin simulated for the vitreous compartment was slower than the clinical data of Zhu et al. [6] obtained from patients exhibiting choroidal neovascularization (Fig. 2a). Clearance simulated from the monkey was slower than the experimental data of Gaudreault et al. [7], and the aqueous humor concentrations were underpredicted (Fig. 1c).

Conclusions: The model seems best qualified for the rabbit eye, and reproduces the clearance rate in man. However, there may be physiologic differences between species that provide an additional means of drug clearance from the vitreous in the monkey, with the possibility of an additional mechanism of transfer from the vitreous to the aqueous compartment. Drug clears from the monkey eye about as quickly as from the rabbit eye despite the fact that the monkey eye is slightly larger. Model physiology will need to be altered to account for disease effects. The strong sink required in the choroid suggests that clearance may be coming close to being limited by diffusion.

References

[1] Missel PJ (2012) Simulating intravitreal injections in anatomically accurate models for rabbit, monkey and human eyes. Pharm Res 29:3251–3272. http://rd.springer.com/content/pdf/10.1007%2Fs11095-012-0721-9

[2] Bakri SJ, Snyder MR, Reid JM, Pulido JS, Singh RJ (2007) Pharmacokinetics of intravitreal Bevacizumab (Avastin). Ophthalmology 114: 855–859

[3] Bakri SJ, Snyder MR, Reid JM, Pulido JS, Ezzat MK, Singh RJ (2007) Pharmacokinetics of intravitreal Ranibizumab (Lucentis). Ophthalmology 114:2179–2182

[4] Krohne TU, Eter N, Holz FG, Meyer CH (2008) Intraocular pharmacokinetics of Bevacizumab after a single intravitreal injection in humans. Am J Ophthalmol 146:508–512

[5] Krohne TU, Liu Z, Holz FG, Meyer CH (2012) Intraocular pharmacokinetics of Ranibizumab folloing a single intravitreal injection in humans. Am J Ophthalmol 154:682–686

[6] Zhu Q, Ziemssen F, Henke-Fahle S, Tatar O, Szurman P, Aisenbrey S, Schneiderhan-Marra N, Xu X, Tubingen Bevacizumab Study Group, Grisanti S (2008) Vascular Endothelial growth factor-A in patients with choroidal neovascularization. Ophthalmology 115:1750–1755.

[7] Gaudreault J., Fei D, Rusit J, Suboc P, Shiu V (2005) Preclinical pharmacokinetics of Ranibizumab (rhuFabV2) after a single intravitreal administration. Invest Ophthalmol Visual Sci 46: 726–733.

M-012 Prediction of Shrinkage of Individual Parameters Using Bayesian Information Matrix in Nonlinear Mixed Effect Models with Evaluation in Pharmacokinetics

François Combes[1,2,3], Sylvie Retout[2], Nicolas Frey[2], France Mentré[1,*]

[1]INSERM, UMR 738, Univ Paris Diderot, Sorbonne Paris cité, Paris, France; [2]Pharma Research and Early Development, Clinical Pharmacology, F. Hoffmann-La Roche Ltd, Basel, Switzerland; [3]Institut Roche de Recherche et Médecine Translationnelle, Boulogne-Billancourt, France

Objectives: In population pharmacokinetics (PK), precision of population parameter estimates depends on design and are evaluated using Fisher information matrix. Individual parameters are usually estimated by the maximum a posteriori (MAP) and precision of individual estimates can be evaluated using the Bayesian fisher information matrix (M_{BF}) [1]. Shrinkage of individual parameters towards the mean occurs when information is sparse and can be quantified as a reduction of variance of the estimated random effects (RE) [2]. This study aims at (1) exploring the relationship between BM_F and shrinkage in order to propose a prediction of shrinkage and (2) evaluating by simulation the prediction of individual parameter precision and shrinkage.

Methods: We first derived the expression of M_{BF} for additive RE and constant residual error and then extended it for exponential RE and/or combined residual error, using first order approximation of the model.

Using the formula of shrinkage in linear mixed effects models, we derived a prediction of shrinkage from M_{BF}. Regarding the evaluation by simulation, we simulated data from sparse and rich design for two PK examples: a simple one (one compartment) with six different scenarios (additive or exponential RE, with low and high variabilities, additive or combined residual error); a more complex example derived from a real case study [3] (two compartment, dual linear and non-linear elimination). We used NONMEM 7.2 and MONOLIX 4.0 to perform individual estimation via MAP assuming known population parameters and fixed to their exact value. We also recorded individual standard errors (SE). We then compared predicted and estimated individual SE for each scenario and example as well as the predicted and estimated shrinkage, evaluated using the formula with ratio of variances.

Results: For the simple example, considering all scenarios and designs, predicted SE of the two parameters using M_{BF} were close to the estimated SE with both software and varied as expected with the richness of the design and the variabilities. There were also a very good agreement (almost identity line) between estimated shrinkage (which varies from 0 to 70 %) and predicted shrinkage. Similar results were observed for all the parameters of the real example.

Conclusion: The Bayesian Information Matrix allows to evaluate impact of design on precision of individual parameters and to predict shrinkage. It can be used for design optimization and will be implemented in PFIM.

References

[1] Merlé Y, Mentré F (1995) Bayesian design criteria: computation, comparison and application to a pharmacokinetic and a pharmacodynamic model. J Pharmacokinet Biopharm 23(1):101–25

[2] Savic R, Karlsson M (2009) Importance of shrinkage in empirical Bayes estimates for diagnostics: problems and solutions. The AAPS J 11(3):558–569

[3] Frey N, Grange S, Woodworth T (2010) Population pharmacokinetics analysis of tocilizumab in patients with rheumatoid arthritis. J Clin Pharmacol 50(7):754–66

Results in this abstract have been previously presented in part at PAGE 2012, Venice, Italy, June 2012 and published in the conference proceedings as abstract 2442.

M-013 Systems Modeling of Bortezomib and Dexamethasone Combinatorial Effects on Bone Homeostasis in Multiple Myeloma Patients

Li Zhang*, Donald E. Mager

Department of Pharmaceutical Sciences, University at Buffalo, State University of New York, Buffalo, NY, USA

Objectives: Osteolytic bone disease is one of the most debilitating manifestations of multiple myeloma (MM), and bisphosphonates are often administered to inhibit bone resorption by suppressing osteoclast activity. Bortezomib, a proteasome inhibitor that combines potent anti-myeloma properties with bone anabolic effects, is being evaluated for its positive effects on MM with skeletal complications. Dexamethasone is often given in conjunction with bortezomib for its potent antineoplastic effects; however, osteolysis is a major adverse event of long-term steroid-based therapies [2]. The purpose of this study is to develop a pharmacodynamic model that integrates the bone anabolic effects of bortezomib with the osteolytic activity of dexamethasone in MM associated bone disease.

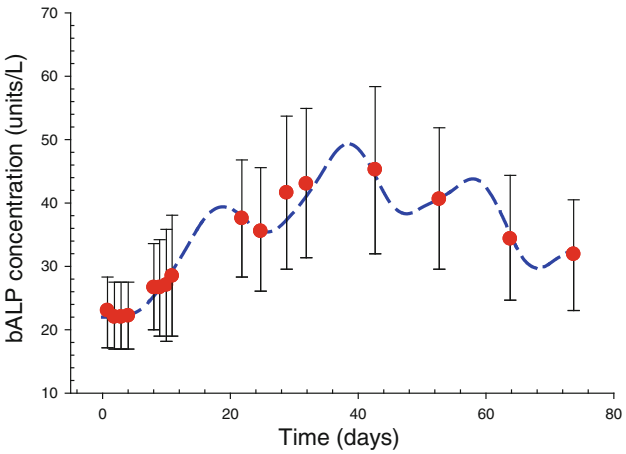

Fig. 1 Model predicted and observed serum bALP concentration–time profile after multiple dosing of 1.3 mg/m^2 bortezomib concomitant with 20 mg dexamethasone in MM patients. Original data were obtained from literature [1]. Symbols represent the observed data (mean ± S.E.), and dashed line represents the model fitted profile

Methods: Mean temporal profiles of bortezomib plasma concentration, 20S proteasome activity, serum Dickkopf-1 (DKK1) concentrations following bortezomib monotherapy, and concentrations of bone specific alkaline phosphatase (bALP), a bone formation biomarker, following bortezomib and dexamethasone exposure in MM patients were extracted from literature [1, 3].

A systems pharmacological model was developed to describe bortezomib bone anabolic effects by integrating the temporal cascades of bortezomib PK, inhibition of proteasome activity, suppression of myeloma cell-derived DKK1 secretion, DKK1 regulation of cellular bone homeostasis, and bALP dynamics following bortezomib multiple dosing in MM patients. Furthermore, an interaction model was developed to simultaneously characterize bortezomib induction and dexamethasone inhibition of bALP by coupling the effects of dexamethasone modulation of myeloma burden and osteoblast apoptosis into the bortezomib anabolic model. Model parameters were estimated in sequential stages by maximum likelihood with the ADAPT5 computer program. Simulations were performed to assess the bone anabolic effects under various bortezomib and dexamethasone combination regimens.

Results: A three-compartment PK model with time-dependent elimination well described bortezomib exposure, and a sigmoidal direct response model well characterized proteasome activity suppression after bortezomib administration. An indirect response model reasonably captured myeloma cell-mediated DKK1 turnover, and bALP dynamics was well captured by integrating DKK1 inhibition on responding osteoblast production following bortezomib monotherapy. The dynamics of bALP following bortezomib and dexamethasone combination therapy in MM patients (Fig. 1) was well described by the combination model that was developed by integrating the apoptotic effects of dexamethasone on myeloma and osteoblast cells into bortezomib bone model. The final model parameters were all estimated with good precision (low CV %). Furthermore, model simulations suggest that bortezomib monotherapy, or combined with low-dose dexamethasone (10 mg), might represent appealing therapeutic strategies for MM patients with skeletal complications.

Conclusion: A systems pharmacology model was developed and successfully characterized the time-course of clinical biomarkers following bortezomib and dexamethasone combination therapy in

MM patients. The interaction model is based on codifying multiple regulatory mechanisms of drug action and provides a platform for probing optimized bortezomib and dexamethasone combination dosing regimens to minimize skeletal side effects during myeloma therapy.

References

[1] Lund T, Soe K, Abildgaard N, Garnero P, Pedersen PT, Ormstrup T, Delaisse JM, Plesner T (2010) First-line treatment with bortezomib rapidly stimulates both osteoblast activity and bone matrix deposition in patients with multiple myeloma, and stimulates osteoblast proliferation and differentiation in vitro. Eur J Haematol 85:290–299

[2] Terpos E, Sezer O, Croucher P, Dimopoulos MA (2007) Myeloma bone disease and proteasome inhibition therapies. Blood 110:1098–104

[3] Reece DE, Sullivan D, Lonial S, Mohrbacher AF, Chatta G, Shustik C, Burris H, Venkatakrishnan K, Neuwirth R, Riordan WJ, Karol M, von Moltke LL, Acharya M, Zannikos P, Keith Stewart A (2011) Pharmacokinetic and pharmacodynamic study of two doses of bortezomib in patients with relapsed multiple myeloma. Cancer Chemother Pharmacol 67:57–67

M-014 Compliance Spectrum as a Drug Fingerprint of Drug Intake and Drug Disposition Based on Limited Sampling Information

Olivier Barrière, Jun Li, Fahima Nekka*

Université de Montréal, Montreal, QC, Canada

Objectives: Poor adherence to a drug prescription has significant impact on the efficacy and safety of a planned therapy. The relationship between drug intake and drug disposition can only be partially obtained through the positive influence investigation of the former on the latter. The so-called "inverse problem", which is concerned with the issue of retracing the patient compliance scenario using limited clinical knowledge, provides a platform to assess this complex issue.
Methods: Based on the reported Pop-PK model of a specific drug, imatinib in this work, where the PK parameters and the associated variability were well determined, we were able to simulate a whole range of drug concentration values at a given sampling point for once daily regimens. Then, all possible drug compliance profiles were mimicked for a population of patients. We designed a heatmap-style image, named compliance spectrum, which provides an intuitive and interactive way to evaluate the relationship between drug input and drug disposition along with their consequences on PK profile [1]. Construction of the compliance spectrum is based on the Bayesian decision method we previously developed for the inverse problem of patient compliance within the framework of Population-PK [2].
Results: The adopted approach allows, for the first time, to quantitatively acquire knowledge about the compliance patterns having a causal effect on a given PK. Moreover, using a simulation approach, we were able to evaluate the evolution of success rate of the retracing process in terms of the considered time period before sampling a well as the model-inherited variability. Moreover, our invented visual representation clearly presented the heterogeneity of different sampling concentrations for susceptible drug compliance profiles.
Conclusions: This work allows, from a probability viewpoint, to propose a solution for this inverse problem of compliance determination. And for the first time, we provide a direct visualization of complex relationship of drug input and disposition such that these two currently separated topics can be studied in the same framework.

References

[1] Barrière O, Li J, Nekka F (2012) Compliance spectrum as a drug fingerprint of drug intake and drug disposition. J Pharmacokinet Pharmacodyn (in press)

[2] Barrière O, Li J, Nekka F (2011) A Bayesian approach for the estimation of patient compliance based on the last sampling information. J Pharmacokinet Pharmacodyn. 38(3):333–351

M-015 Introduction of an Information-Loaded Metric to Improve the Comparison of Antibiotic Performance for Different Dosing Regimens

Jun Li*, Fahima Nekka

Université de Montréal, Montreal, QC, Canada

Objectives: The determination of an optimal dosing regimen is a critical step to enhance the drug efficacy and avoid toxicity. Rational dosing recommendations based on mathematical considerations are increasingly being adopted in the process of drug development and use.
Methods: We propose a quantitative approach to evaluate the efficacy of antibiotic agents by integrating both in vivo pharmacokinetic (PK) and in vitro pharmacodynamic (PD) information into a unified formalism. In this way, the dosing regimens, including doses and associated timings, can be mathematically defined as a causal variable that influences the drug therapeutic effect. The hypothetical but realistic drug models, representatives of concentration– and time–dependents antibiotic agents, will be used to investigate the proposed approach on several typical dosing regimens, including QD, BID, TID and QID.
Results: We succeeded to reveal unexpected, but relevant behaviours of drug performance when different drug regimens and drug classes are considered [1]. First, the new pharmacometric formalism allows covering a whole range of antibiotics, including the two well known concentration and time dependent classes, through the introduction of the Hill-dependency concept. Second, we found that the doses required to reach the same therapeutic effect, when scheduled differently, exhibit completely different tendencies for concentration– and time–dependent drugs. Moreover, we theoretically confirmed the previous experimental results of the superiority of the once daily regimen of aminoglycosides.
Conclusions: The proposed methodology is appealing for its computational features and can easily be applicable to design fair clinical protocols or rationalize prescription decisions.

References

[1] Li J, Nekka F (2012) A rational quantitative approach to determine the best dosing regimen for a target therapeutic effect:

a unified formalism for antibiotic evaluation. J Theor Biol. 319C:88–95. doi:10.1016/j.jtbi.2012.11.019.

[2] Bi GD, Li J, Nekka F (2009) Antimicrobial breakpoint estimation accounting for variability in pharmacokinetics. Theor Biol Med Model. 6:10. doi:10.1186/1742-4682-6-10.

M-016 Characterization of In Vitro Antimicrobial Activity of Vertilmicin Alone and in Combination with Ceftazidime by Using Semi-mechanistic Pharmacokinetic/Pharmacodynamic Model

Luning Zhuang[1,*], Sherwin K. B. Sy[1], Huiming Xia[2], Rajendra P. Singh[1], Changxiao Liu[3], Hartmut Derendorf[1]

[1]Department of Pharmaceutics, College of Pharmacy, University of Florida, Gainesville, FL 32610, USA; [2]Department of ophthalmology, University of Florida, Gainesville, FL 32610, USA; [3]Tianjin State Key Laboratory of Pharmacokinetics and Pharmacodynamics, Tianjin Institute of Pharmaceutical Research, Tianjin 300193, China

Objectives: Vertilmicin is a novel semisynthetic aminoglycoside derived from verdamicin. The goal of this study is to develop a semi-mechanistic pharmacokinetic/pharmacodynamic (PK/PD) model to describe the relationship between bacterial responses and drug concentrations and to predict the optimized dose required to achieve maximum efficacy of vertilmicin alone and in combination with ceftazidime in the future clinical trials.
Methods: Static and dynamic time-kill curves were adopted to study in vitro antibacterial activity of vertilmicin alone against methicillin-susceptible *Staphylococcus aureus* (MSSA), methicillin-resistant *Staphylococcus aureus* (MRSA) and *Pseudomonas aeruginosa*. In the static time-kill curve studies, the bacterial burden was determined under a wide range of drug exposures ranging from 0.25- to 16-fold of minimum inhibitory concentration (MIC) over a 24-h period. The dynamic time-kill experiments were performed at 20 μg/mL and carried out using a manual dilution system with half-life of 2 h. Constant time-kill study against *Pseudomonas aeruginosa* will be utilized to study the combined antimicrobial activity of vertilmicin and ceftazidime based on 0.25- to 4-fold MIC of vertilmicin in the presence of five different concentrations of ceftazidime. Subsequently, two-compartment PK/PD model was developed to fit the data of mono- and combination therapies simultaneously. The Loewe additivity was used as reference to evaluate the drug–drug interactive effect.
Results: The result of time-kill kinetics showed that vertilmicin was concentration-dependent antibacterial agent against the three bacterial strains. The elimination half-life of vertilmicin had a dramatic impact on its antimicrobial activities, which was further confirmed by the EC_{50} estimates from the semi-mechanistic PK/PD model. The combination of vertilmicin and ceftazidime against *Pseudomonas aeruginosa* showed significantly enhanced bactericidal capacity compared to either drug at the same level. The drug–drug interaction model that incorporates PK/PD model and Loewe additivity was able to elucidate the time course of bacterial growth and death in each combination treatment. The estimates from the drug–drug interaction model showed that the overall drug–drug interactive effect between vertilmicin and ceftazidime was additive, but highly varied with respect to the combinations. The optimal dose regimen of vertilmicin in combination with ceftazidime could be easily identified using there-dimensional surface response.
Conclusions: The result of PK/PD modeling demonstrated that vertilmicin has promising prospect for future clinical application. It also suggested that drug–drug interaction model modified from PK/PD modeling was capable of assisting dose selection for combination therapy of vertilmicin and ceftazidime to maximize the probabilities of positive clinical outcomes. Undoubtedly, PK/PD model is a powerful tool to evaluate the in vitro antibacterial activity of novel antibiotics, as well as to make key decisions in drug development.

References

[1] Schmidt S, Sabarinath SN, Barbour A, Abbanat D, Manitpisitkul P, Sha S, Derendorf H (2009) Pharmacokinetic-pharmacodynamic modeling of the in vitro activities of oxazolidinone antimicrobial agents against methicillin-resistant *Staphylococcus aureus*. Antimicrob Agents Chemother 53:5039–5045

[2] Tam VH, Schilling AN, Nikolaou M (2005) Modelling time-kill studies to discern the pharmacodynamics of meropenem. J Antimicrob Chemother 55:699–706

M-017 Relationship of Model Selection Criteria to Prediction Accuracy

Mark Sale[1,2,*], Rob Bies[2]

[1]Next Level Solutions, Raleigh, NC, USA; [2]Indiana University School of Medicine, Indianapolis, IN, USA

Objectives: to examine the relationship between commonly used model selection criteria and predictive performance of the resulting models. Six model selection criteria were used:

1. −2ll + 2 points per parameter (AIC [1])
2. AIC + Requirement for successful covariance step
3. −2ll + 3.84 points per parameter (Chi square test with $p < 0.05$, 1 df)
4. −2ll + 6.64 points per parameter (Chi square test with $p < 0.01$, 1 df)
5. −2ll from cross validation [2,3] with 0 points per parameter
6. Normalized prediction distribution errors (NPDE) global p value [4]

Methods: A data set was provided by an independent party and was selected based on having a large number of potential candidate covariates (13) on several parameters (4). This data set was divided into a 2/3 fraction used as the training data set and the remaining 1/3 used as the validation data set. The model search was limited to covariates. NONMEM analyses on the training data set were performed using a global search method; single objective hybrid genetic algorithm (GA, [5]). GA is an automated, reproducible, robust and objective model selection algorithm. It is objective in the sense that all models were constructed and evaluated by strictly objective measures. No learning effect between analyses will occur with the GA, as might occur with an individual doing six sequential analyses of the same data. No subjective decisions about what covariates to include, or the sequence in which to include them were made. In this algorithm the model population size was set to 300 models, with 4 niches. For each analysis the model was considered to be final after no improvement is seen for 8 generations. Each modeling exercise constructed, ran and evaluated approximately 12,000 models.
The covariates include both discrete ($N = 3$) and continuous ($n = 10$) covariates. One of the discrete covariates had 5 levels, the others had only 2. An exponential model (e.g., TV = TV*EXP(COV*THETA()) was used for discrete covariates candidate relationships, where TV is the typical value, COV has values of 0 or 1 and THETA() is an estimate parameter. For the discrete covariate with 5 possible values,

Table 1 Results of modeling exercises

Model selection criteria	# Covariates	−2ll for validation set	NPDE global *p* value
AIC	26	648.16	1.58e-06
AIC + $COV success	24	651.80	6.33e-08
LRT ($p < 0.05$)	13	648.47	2.27e-06
LRT ($p < 0.01$)	6	652.84	6.44e-07
Cross validation	32	623.74	7.12e-07
Npde	21	785.80	3.47e-04

The first column lists the model selection criteria used, the 2nd column the number of covariates in the final model. The 3rd column lists the −2ll from the fixed model, using the validation data set, and the last column the global *p* value from NPDE

the initial covariate was reparameterized into 3 separate covariates, representing different combinations of the most common values.

For the continuous covariates, two derived covariates were created: one centered (e.g., CSCOV = (COV-Mean)/SD, where CSCOV is the centered value, COV is the covariate, Mean is the covariate mean and SD is the standard deviation) and scaled (e.g., SCOV = COV/Mean. In the model search, the centered, scaled covariate was used for candidate exponential relationships (TV = TV*EXP (COV*THETA()) and the scaled covariate was used for candidate power relationships (TV = TV*COV**THETA()), as the covariates must be non-negative to avoid numerical errors.

The model search included all covariates on all parameters (ADVAN3, TRANS4). The parameters were:

- Clearance
- Central volume of distribution
- Intercompartmenal clearance
- Peripheral volume of distribution

For the cross validation, four data splits into four data sets was used. Commonly for cross validation, 10 data splits and 10 data sets are recommended. However, this resulted in unacceptable run times (i.e., 100 NONMEM runs for each of ~12,000 models).

The full model selection exercise was repeated six times with the same training data set; once with each different model selection criteria. The final model from each model selection exercise was then used (with fixed model structure and parameters) to calculate the −2ll and NPDE of the validation data set.

The endpoints for the analysis were:

- # of covariates in the final model.
- −2ll for the validation data set, with a model (structure and parameters) fixed to the final training data set model.
- NPDE global p value for the validation data set, with a model fixed to the final training data set model.

Results:
The analysis was run on a local network of between 1 and 6 Windows computers. Run times for the each modeling exercise was between 38 h (LRT with $p < 0.01$) on 1 computer and 132 h (cross validation) on 6 computers.

Results are given in Table 1

Conclusions: In general, performance of the final model reflects the model selection criteria used. If NPDE is used as the model selection criteria, the results will best predict a large (better) global *p* value in a validation data set. However, the −2ll is significantly larger (worse). The larger the parsimony penalty used in the model selection process, the more parsimonious the resulting model will be. The price paid for a more parsimonious model is a larger −2LL on both the training data set (not shown) and the validation data set. A requirement for a successful covariance step yields a slight smaller and slightly less predictive model than a similar modeling exercise that does not require a successful covariance step.
Cross validation (with no parsimony penalty) resulting in the largest and most predictive model. A modeling exercise with a parsimony penalty of 3.84 ($p < 0.05$) using the traditional −2ll on the training data set resulted in a model that was somewhat less predictive than using cross validation (with no parsimony penalty), but significantly smaller.

In general cross validation resulted in the most predictive model. A requirement for a successful covariance step resulted in a less predictive model than a similar analysis not requiring a successful covariance step.

References

[1] Akaike H (1974) A new look at the statistical model identification. IEEE Transactions on Automatic Control 19(6):716–723

[2] Kohavi R (1995) A study of cross-validation and bootstrap for accuracy estimation and model selection. Proceedings of the fourteenth international joint conference on artificial intelligence, Morgan Kaufmann, San Mateo, 2(12): 1137–1143

[3] Katsube T, Khandelwal A, Harling K, Hooker AC, Karlsson MO (2011) Evaluation of stepwise covariate model building combined with cross-validation. Department of Pharmaceutical Biosciences, Uppsala University, Uppsala, Sweden; Clinical Research Department, Shionogi & Co., Ltd., Japan. PAGE meeting, Athens Greece

[4] Brendel K, Comets E, Laffont C, Mentré F (2010) Evaluation of different tests based on observations for external model evaluation of population analyses. J Pharmacokinet Pharmacodyn 37(1): 49–65

[5] Sherer EA, Sale ME, Pollock BG, Belani CP, Egorin MJ, Ivy PS, Lieberman JA, Manuck SB, Marder SR, Muldoon MF, Scher HI, Solit DB, Bies RR (2012) Application of a single-objective, hybrid genetic algorithm approach to pharmacokinetic model building. J Pharmacokinet Pharmacodyn 39(4):393–414

M-018 Population Pharmacokinetic/Pharmacodynamic Modeling the Concentration: QTc Prolongation Relationship of LDZ856 Using Jacketed Telemetry in Beagle Dogs

Lance Wollenberg[1,2,*], Haiying Sun[1], Samira Garonzik[2], Haisong Ju[3], Peter Hoffmann[3], Venkateswar Jarugula[1]

[1]Novartis Institutes for Biomedical Research, Drug Metabolism and Pharmacokinetics (DMPK), East Hanover, NJ, USA; [2]The State University of New York, University at Buffalo, Buffalo, NY 14216, USA; [3]Novartis Pharmaceuticals, Modeling and Simulation (M&S), East Hanover, NJ, USA; [4]Novartis Institutes for Biomedical Research, Pre-Clinical Safety Pharmacology (PCS), East Hanover, NJ, USA

Objective: Dose–response based electrocardiogram (ECG) studies are used to evaluate the potential of compounds to promote cardiac arrythmia. Cardiac arrythmia is often characterized by prolongation of QT interval which may lead to an increased risk of fatal arrhythmias

including torsades de pointes. Our objective in this work is to develop a population-based pharmacokinetic/pharmacodynamic (PK/PD) model to describe the exposure–response relationship of LDZ856 on the prolongation of the QT interval in preclinical animal models. This approach would allow for a quantitatively robust method to identify QT positive compounds earlier in the development process, and would be helpful in developing safety margins for QT prolongation between clinical and preclinical studies.

Methods: LDZ856 was administered at three dose levels (30, 150, 300 mg/kg) as an oral gavage to three beagle dogs. Plasma concentration was measured at 0.5, 1, 3, 7 and 24 h post dose and samples were analyzed by a validated LC–MS/MS method. Measurement of the QT interval was obtained hourly by jacketed telemetry during the single ascending dose PK studies. Telemetry jackets were equipped with a digital ECG transmitter box. ECG signals were recorded continuously by emka system for approximately 26 h (2 h prior to dosing followed by 24 h post-dose). Heart rate and ECG intervals were digitally analyzed by emka ECG-Auto software. QT intervals were corrected for heart rate using Van de Water's QT correction formula (QTcVW) [1]. Population PK/PD modeling was performed using First Order Conditional Estimation with Interaction (FOCE-INT) in NONMEM 6. Final model selection was based on various goodness-of-fit indicators, including comparisons based on the minimum objective function value, visual inspection of diagnostic scatterplots, parameter plausibility and precision of parameter estimates.

Results: Time-matched, PK/QTcVW observation analysis indicated a positive linear slope [0.00074 ms/(ng/mL) (16.9 %), parameter mean (%RSE)]. This limited data set did not include the complete time course of QTcVW measurements, and was unable to adequately describe a physiologically relevant exposure–response relationship. To better describe the exposure–response relationship, the PK data was best fit with a one compartment model with a proportional error model [30.6 (11.8 %)] to predict the full concentration–time course. The bioavailability of the low dose (30 mg/kg) was fixed to a value of (1), and the relative bioavailability of the increasing dose levels were fit as model parameters [0.55 (10.3 %)] and [0.53 (10.7 %)] for the higher dose levels (150 and 300 mg/kg), respectively, to account for dose non-linearity due to limited absorption at higher doses. The clearance [1.28 L/h (14.3 %)] and volume of distribution of [29.9 L (9.86 %)] were precisely estimated by the PK model. Upon selection of a final PK model, a sequential approach was taken to fit the PD data, where parameter values from the PK fitting exercise were fixed to subject specific values to drive the PD effect. The model predicted PK concentrations were utilized to characterize the full time course QTcVW effect, allowing for the use of a more complex PD model. The PD data was best fit with a non-linear, sigmoid E_{max} model, using an additive error model [10.5 ms (4.69 %)]. This model describes a physiologically relevant exposure–response relationship of LDZ856 concentration to QTcVW prolongation. The concentration of LDZ856 associated with a 50 % increase (EC_{50}) [9.12 μg/mL (26.8 %)] in the maximum effect on QTcVW prolongation (E_{max}) [33.6 ms (19.3 %)] and Hill parameter [1.54 (22.0 %)], were precisely estimated by the final PD model (Fig. 1).

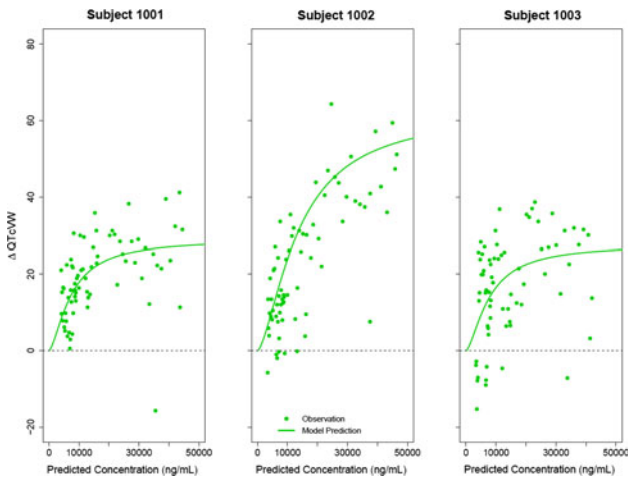

Fig. 1 The final exposure–response relationship from the population PK/PD analysis is indicated for each individual subject (1001,1002, 1003). Observed data is indicated by the green dots, and the individual model predicted response is indicated by the solid green line. The dashed line (ΔQTcVW = 0) is used as a reference and indicates no change in ΔQTcVW value

Conclusion: The exposure–response relationship was successfully developed to describe the prolongation of the QT interval as a function of LDZ856 concentration. In future studies we would like to apply this approach to preclinical studies of Novartis compounds to evaluate its capacity to predict QTc prolongation in clinical studies and generate safety margins between preclinical and clinical studies. In turn, this method will be employed to better evaluate go/no go decisions for preclinical data when transitioning into clinical trials.

Reference

[1] Van de Water A, Verheyen J, Xhonneux R, Reneman RS (1989) An improved method to correct the QT interval of the electrocardiogram for changes in heart rate J Pharmacol Method 22:207–217

M-019 PKPD Modeling of Retrospective Data to Guide Study Design for Phase II Trial

Hongmei Xu[1,*], Jianguo Li[1], Paul Dickinson[2], Stuart McIntosh[2], Nidal Al-Huniti[1]

[1]Clinical Pharmacology and Pharmacometrics, AstraZeneca Pharmaceuticals, Wilmington, DE, USA; [2]Global Medicines Development, AstraZeneca Pharmaceuticals, Alderley Park, UK

Objectives: Significant and reversible reductions in testosterone levels were observed with Compound A (Cmpd A), in both preclinical and clinical testing. Modeling and simulation were used to quantify Cmpd A pharmacological effects and to support optimal dosing in further clinical development. The objectives of this analysis were: (1) to develop a population pharmacokinetic pharmacodynamic (PKPD) model to characterize the relationship between Cmpd A and testosterone concentration; (2) to characterize the food effect on Cmpd A PK and simulate food effect on PD response; (3) to perform simulation and predict the differences of testosterone suppression effect between BID and QD dosing strategy.

Methods: Population PKPD modeling of Cmpd A and testosterone concentrations from four phase I studies and one phase II study was performed to quantify the exposure–response relationships between plasma concentrations of Cmpd A and testosterone. PKPD analyses were conducted using sequential approach via nonlinear mixed-effects modeling with NONMEM® VII. The PK model was developed first and the predicted concentrations from the empirical Bayes estimates of the PK parameters were used in the PD response model building. Different absorption rate constant (Ka) was introduced to characterize the PK in fed state compared to fasted state. The developed PKPD model was used to explore different dosing regimens (40 mg BID vs. 80 mg QD) targeting reduction of plasma

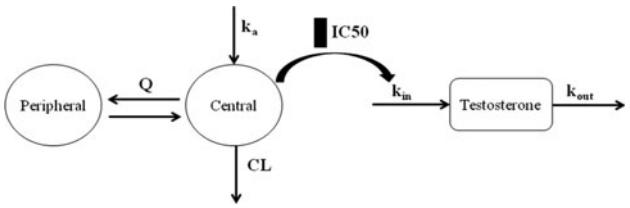

Fig. 1 PKPD model scheme of Cmpd A

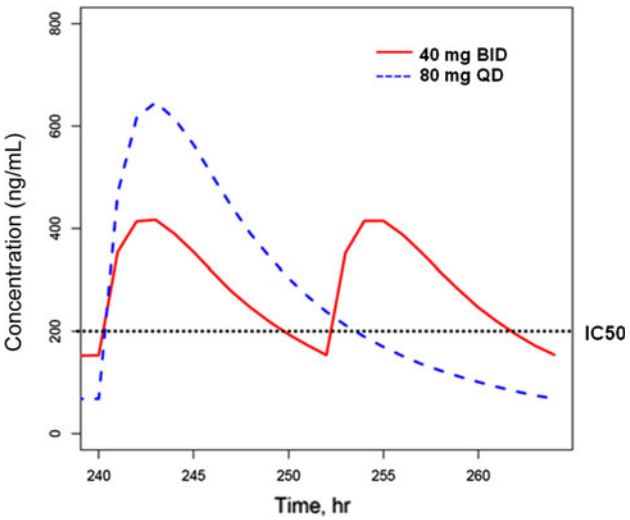

Fig. 2 Predicted steady state Cmpd A concentration after administering 40 mg BID or 80 mg QD of Cmpd A

testosterone levels and predict PD response at fasted and fed state at different dosing regimen.

Results: Data including 3597 Cmpd A PK observations and 786 testosterone concentrations from 139 healthy volunteers were investigated. A two-compartment model with first-order elimination best described Cmpd A PK. Covariates of interest included weight, age, sex and race. Weight was found to be the significant covariate on central volume of distribution (Vc), peripheral volume of distribution (Vp) and the inter-compartmental clearance (Q). Significant higher Ka (0.739 h^{-1}) was found in volunteers at fed state compared to 0.337 h^{-1} at fasted state. Circadian rhythm of baseline testosterone concentrations was well described by a cosine function. Indirect response model (inhibition on testosterone production) was used to link the drug effect to PD response. The scheme of PKPD model is illustrated in Fig. 1. Age was found to influence the baseline testosterone significantly. This result was supported by the findings of significant higher testosterone concentrations in healthy young male than healthy elder male from Diver et al. [1]. Based on simulations, the observed PK difference (significant higher C_{max}, similar AUC) in fed volunteers compared to fasted volunteers, did not lead to significant difference in testosterone change. It was also concluded that following 40 mg BID treatment, trough Cmpd A concentration will be much higher compared to 80 mg BID. The time above IC50 for testosterone concentration after 40 mg BID of Cmpd A is 80.9 % time of the dosing interval compared to only 55.7 % after 80 mg QD (Fig. 2). The mean predicted peak testosterone concentration at steady state are lower and overall less variable during 24 h for 40 mg BID dose compared to 80 mg QD dose (Fig. 3). These findings suggest 40 mg BID dosing provide sustained testosterone suppression effect during dose interval and is preferred in future clinical trial.

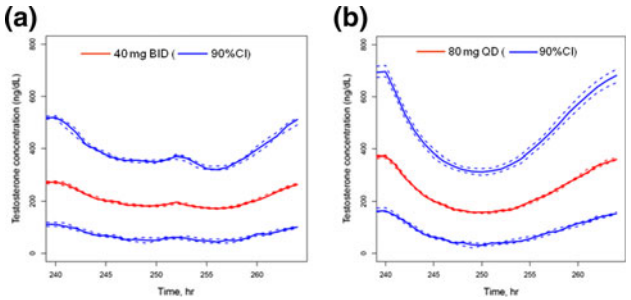

Fig. 3 Predicted steady state testosterone concentration after administering 40 mg BID or 80 mg QD of Cmpd A

Conclusions: Population pharmacokinetic and pharmacodynamic analysis demonstrates that 40 mg administered twice a day is better than 80 mg once a day to maximally and more consistently suppress testosterone during the entire dosing interval. Dose modification is not needed for volunteers at fed state to achieve comparable testosterone suppression effect at fasted state.

Reference

[1] Diver MJ, Imtiaz KE, Ahmad AM et al (2003) Diurnal rhythms of serum total, free and bioavailable testosterone and of SHBG in middle-aged men compared with those in young men. Clin Endocrinol 58:710–717

M-020 Simplification of Complex Physiologically-based Pharmacokinetic Models of Monoclonal Antibodies

Mohamed Elmeliegy*, Wojciech Krzyzanski

Department of Pharmaceutical Sciences, University at Buffalo, the State University of New York, Buffalo, NY, USA

Objectives: Monoclonal antibodies (mAbs) are a promising and exponentially growing category of targeted agents. In contrast to small molecules, elimination of mAbs occurs predominantly via endosomal catabolism to amino acids and peptides. Their long half-life is attributed to binding to endosomal neonatal Fc (FcRn) receptor which protects them from catabolic degradation. Binding of mAb to FcRn is pH-dependent such that higher binding affinity occurs in acidic environment. Previously published PBPK models explaining the gradual change in endosomal pH are useful in describing the effects of pH-dependent FcRn-mAb binding on mAb half-life. However, several processes in these models occur in distant compartments with minimal impact on plasma or tissue concentrations. Such models exhibit exceeding complexity and high number of compartments. The goal of the current work is to reduce the complexity of these models by making physiologically sound assumptions regarding the rate of binding and transfer processes.

Methods: We applied a previously published catenary PBPK model [1] that describes the endosomal transit of mAb and pH dependency in mAb–FcRn association and dissociation. The model represents the endosomal space as five subcompartments with different pH levels and binding affinities to mAb. The five endosomal subcompartments can be classified into one initial (highest pH), three intermediate, and one terminal subcompartment (lowest pH). Following mAb transfer from the vascular space of each tissue to the initial endosomal subcompartment, the drug is transferred through intermediate subcompartments with an inter-compartmental transit time, tau. Recycling of FcRn-bound mAb to vascular and interstitial compartment occurs from the terminal

endosomal subcompartment. Two basic assumptions were made. First, binding and dissociation of the mAb to FcRn was assumed to occur instantaneously (i.e. binding and dissociation constants, k_{on} and $k_{off} \rightarrow \infty$) relative to other processes (e.g. mAb internalization and terminal elimination rates) [2]. Thus, we assumed that free mAb, free FcRn receptor, and mAb-FcRn receptor complex are at rapid equilibrium conditions. The mAb binding affinity to FcRn was described as the dissociation equilibrium constant (KD), which was defined as k_{off}/k_{on}. Similar KD value was used for mAb and endogenous IgG. Second, given the short total endosomal transit time ($\sim$10.8 min), we assumed instantaneous transfer time between endosomal sub-compartments (i.e. tau $\rightarrow$ 0) [3]. All model coding and simulations were conducted using ADAPT 5. Simulations of plasma and tissue profiles from full and simplified models were analyzed via non-compartmental approaches using Phoenix WinNonlin.

Results: Following mAb uptake from the vascular space, initial endosomal subcompartment was rapidly equilibrated with intermediate subcompartments. Given the competitive binding of two moieties (endogenous IgG and exogenous mAb) to the same receptor, a new term that represents the total of free endogenous IgG and free exogenous mAb ($free_{endo+mAb}$), was introduced and solved as a quadratic equation. This term was then used to calculate free mAb. Equations relating total (i.e. free and FcRn-bound) mAb concentration in initial and terminal subcompartments to concentrations in vascular and interstitial compartments, uptake rate, and tau were derived. The FcRn-bound mAb was calculated by subtracting the amount of free mAb from the total amount. The simplified model (36 differential equations) recapitulated the typical biexponential plasma profile from the original model (236 differential equations). Plasma AUCs from full and simplified model were in good agreement (97.7 %). Concentrations profiles from the simplified model in different tissues were similar to the original model (AUCs were in close agreement 98.2 $\pm$ 0.5 %, mean $\pm$ SD).

Conclusions: A significant reduction in number of compartments associated with catenary PBPK models was achieved while accurately describing plasma and tissue concentrations. The proposed method eliminates processes with minimal impact on plasma and tissue concentration profiles. Attempts to further reduce PBPK model complexity are ongoing.

References

[1] Chen Y, Balthasar JP (2012) Evaluation of a catenary PBPK model for predicting the in vivo disposition of mAbs engineered for high-affinity binding to FcRn. AAPS J, 14(4):850–859

[2] Mager DE, Krzyzanski W (2005) Quasi-equilibrium pharmacokinetic model for drugs exhibiting target-mediated drug disposition. Pharm Res 22(10):1589–1596

[3] Ober RJ, et al (2004) Visualizing the site and dynamics of IgG salvage by the MHC class I-related receptor, FcRn. J Immunol 172(4): 2021–2029

M-021 Population Pharmacokinetics of BMN 673, a Novel PARP Inhibitor, in Beagle Dogs

Yulan Qi*, Don Musson, Laurie Tsuruda, Huiyu Zhou, Alphonsus Cheng, Charles O'Neill

BioMarin Pharmaceutical Inc., 105 Digital Dr., Novato, CA 94949, USA

Objectives: BMN 673 is a highly potent, specific Poly ADP-ribose polymerase (PARP) inhibitor in tumors bearing DNA repair deficiencies [1]. PARP plays important roles in the repair of single-stranded breaks in DNA through the base excision repair path way [2]. As a result of PARP inhibition, accumulation of single-stranded breaks leads to the replication fork collapse and conversion of single-stranded breaks to double-stranded breaks. The inability of tumor cells with deficiency in homologous recombination DNA repair to repair the double-stranded breaks then induces cell death [3]. The goal of this study was to develop a population Pharmacokinetic model of BMN 673 in beagle dogs.

Methods: BMN 673 was administered orally to beagle dogs once daily at 0.003, 0.01, 0.03 and 0.1 mg/kg for 5 days followed by28-day recovery. Intensive PK samples were collected on Days 1 and 5, and sparse PK samples were collected from Days 6 to 26. The PK properties of BMN 673 were investigated using nonlinear mixed-effects models via NONMEM VII.

Results: The PK of BMN 673 was adequately characterized by a two-compartment model with first order absorption and elimination. The final PK model fitted the data well as demonstrated by goodness of fit plots and visual predictive check. The population mean (relative standard error) values for PK parameters such as clearance, absorption rate constant, central volume of distribution and peripheral volume of distribution are 0.2 L/h (7.6 %), 0.97 h^{-1} (14.0 %), 6.54 L (11.4 %), and 4.53 L (21.9 %), respectively. The relative standard errors are between 8 and 22 % indicating that the precision of PK parameter estimation was generally good.

Conclusions: The population PK model developed was appropriate to describe the time course of BMN 673 plasma concentration in beagle dogs after 5-day repeated dosing. This model can be used for simulations to plan future studies.

References

[1] Shen Y, Feng Y, Wang B, Chu D, Myers P, Post L (2010) LT-00673, a highly potent PARPIs, shows antitumor activity against tumor cells with DNA repair deficiencies. AACR 101st Annual Meeting, Washington DC Poster # 3514

[2] Ame J, Rolli V, Schreiber V, Niedergang C et al (1999) PARP-2, A novel mammalian DNA damage-dependent poly(ADP-ribose) polymerase. J Biol Chem 274(25):17860–17868

[3] Huang S, Das B, Renaud A, Zhang Y, Doroshow J, Ji J, Takeda S, Pommier Y (2012) Trapping of PARP1 and PARP2 by Clinical PARP Inhibitors. Cancer Res 72(21):5588–5599

M-022 Mechanistic Modeling of Ligand Displacement by MEDI-575, a Human Monoclonal Antibody Against Platelet-derived Growth Factor Receptor Alpha (PDGFRα)

Bing Wang[1,*], Meina Liang[1], Amy Schneider[1], Brandon Lam[1], Inna Vainshtein[1], Carlos Chavez[1], Kathleen McKeever[2], Lorin Roskos[3]

[1]Clinical Pharmacology & DMPK, MedImmune LLC, Hayward, CA, USA; [2]Biological Safety Assessment, MedImmune LLC, Gaithersburg, MD, USA; [3]Clinical Pharmacology & DMPK, MedImmune LLC, Gaithersburg, MD, USA

Objectives: To develop a mechanistic model incorporating the interactions of MEDI-575, PDGFRα and the endogenous ligand PDGF-AA, to describe the nonlinear pharmacokinetics (PK) of MEDI-575 and observed PDGF-AA profiles in cynomolgus monkeys.

Methods: The PK and pharmacodynamic (PD, PDGF-AA) data from a single-dose and a multiple-dose studies were merged and simultaneously modeled using NONMEM (Version 7.2). The PK-PD model structure is shown below:

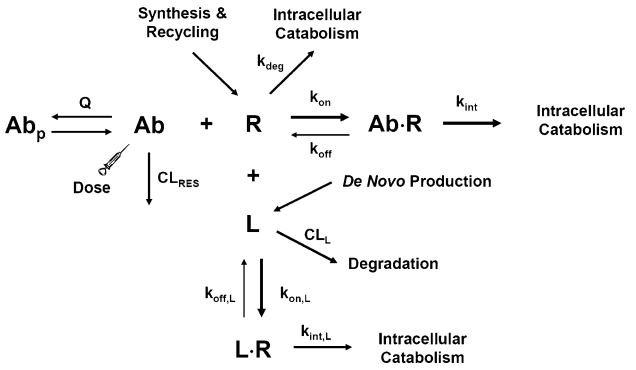

Ab, R and L represent MEDI-575, PDGFRα and PDGF-AA ligand, respectively. Both PDGF-AA and MEDI-575 bind to PDGFRα with high affinities in vitro. After the initial transition period after MEDI-575 dosing, the complexes Ab·R and L·R were assumed to quickly reach a dynamic pseudo-equilibrium (steady-state). A cubic equation depicting the tri-molecular interaction system was solved using a novel differential-equation approach [1].

Results: Six differential equations delineating the overall interactions and kinetics of MEDI-575, PDGFRα and PDGF-AA ligand were reduced to four by pseudo-equilibrium assumptions. The free (unbound) concentrations of MEDI-575 and PDGF-AA were deduced by solving a cubic equation system in NONMEM. The model also incorporated PDGFRα internalization kinetics as determined from in vitro confocal imaging studies. The mechanistic model adequately described the observed nonlinear PK of MEDI-575 and elevating PDGF-AA profiles. By fitting to the PK and PD data, the model not only predicted the target receptor occupancy by a mAb, but also the biologically active agonistic ligand-receptor complex.

Conclusions: This work represents the first successful application of a mechanistic model to delineate the in vivo tri-molecular interactions of a drug, its target receptor, and a competing endogenous ligand. The model also supported clinical utilization of a displaced ligand upon mAb dosing as a relevant PD biomarker to assist the optimal dose recommendation for early clinical studies.

Reference

[1] Krzyzanski W, Yan X, Chen Y (2012) Methods of solving rapid binding target-mediated drug disposition model for two drugs competing for the same receptor. PAGE Conference, Venice

M-023 Lopinavir Population Pharmacokinetics in HIV-infected Patients from Resource-limited Settings Receiving Second-line Treatment with Lopinavir/Ritonavir Monotherapy in AIDS Clinical Trials Group (ACTG) Study 5230

Heather E. Vezina[1,*], Jeong-Gun Park[2], Carole L. Wallis[3], John A. Bartlett[4,5], Nagalingeswaran Kumarasamy[6], Wendy S. Stevens[7], Karin L. Klingman[8], Heather J. Ribaudo[2], David A. Katzenstein[9] on behalf of the A5230 team

[1]The Children's Hospital of Philadelphia, Philadelphia, PA, USA; [2]Statistical Data Analysis Center, Harvard University, Boston, MA, USA; [3]Lancet Laboratories, Johannesburg, South Africa; [4]Duke University Medical Center, Durham, NC, USA; [5]Kilimanjaro Christian Medical Centre, Moshi, Tanzania; [6]YRG CARE Medical Centre, Chennai, India; [7]University of Witswatersrand, Johannesburg, South Africa; [8]Division of AIDS, National Institute for Allergy and Infectious Diseases, National Institutes of Health, Bethesda, MD, USA; [9]Stanford University Medical Center, Stanford, CA, USA

Objectives: Lopinavir/ritonavir (LPV/r) is a co-formulated protease inhibitor (PI) used to treat HIV-1 infection. Lopinavir (LPV) inhibits HIV-1 protease and ritonavir (RTV) inhibits CYP3A-mediated LPV metabolism thereby increasing LPV plasma concentrations [1]. ACTG 5230 was a multicenter, open-label, single arm pilot trial that evaluated LPV/r monotherapy (400/100 mg twice daily) as second-line antiretroviral therapy (ART) in PI-naïve HIV-infected patients from resource-limited settings (RLS) experiencing virologic failure on a first-line nonnucleoside reverse transcriptase inhibitor-based regimen [2]. Given this novel treatment strategy and unique patient population, the objectives of the present work were to characterize LPV plasma pharmacokinetics (PK) and identify patient-specific characteristics associated with PK variability.

Methods: A single, random, steady-state plasma sample was drawn from each subject during study visits at weeks 8, 12, 16, and 24 and analyzed for LPV concentrations by HPLC–UV. RTV concentrations were not measured. LPV concentrations below the assay's limit of quantification (BLQ) were excluded from the analysis. Several structural models were evaluated including one- and two-compartment models with and without absorption lag time. Model parameter estimates were obtained using the first order conditional estimation with interaction (FOCE-I) method in NONMEM version 7.2. Covariate data consisted of the continuous variables (mean ± SD) weight (63 ± 12.3 kg) and age (39.3 ± 8.4 years), and the categorical variables sex and race (Thai or Black African). Concomitant medications were not tested because drugs known or suspected of interacting with LPV/r were prohibited in the study. Covariate models were developed based on clinical relevance of the covariates and likelihood ratio testing during stepwise forward inclusion and backward elimination. In the stepwise procedure, a change in the objective function value of 7.88 units was defined as significant ($p < 0.005$, $df = 1$). A bootstrap re-sampling technique with 1000 runs was used to evaluate stability of the final model and precision of the parameter estimates.

Results: 427 LPV concentrations from 111 subjects were used in the population PK analysis. 7 concentrations (6 BLQ; 1 near BLQ) were excluded. A one-compartment model with first-order absorption and elimination best described the data. Sex and race modeled by a power function were significant covariates on apparent oral clearance (CL/F) and were included in the final model. Males had 32 % faster CL/F than females. Thai subjects had 24 % faster CL/F than Black African subjects from Malawi, Tanzania, and South Africa. Eta-shrinkage for CL/F was 12.2 %. All parameter estimates, relative standard errors (RSE) and 95 % confidence intervals (CIs), as well as bootstrap estimates and 95 % CIs are below. Successful estimation and covariance steps were achieved in 99.8 % of the bootstrap runs suggesting a robust model.

Parameter	Final estimate	RSE (%)	95 % CI	Bootstrap estimate	Bootstrap 95 % CI
CL/F (L/h)	2.83	4.28	2.59–3.07	2.82	2.57–3.06
SEX (M/F) effect	1.32	5.77	1.17–1.47	1.33	1.18–1.50
RACE (Thai/African) effect	1.24	7.15	1.07–1.41	1.25	1.06–1.43
V/F(L)	45.4	26.2	22.1–68.7	44.6	20.4–74.5
Ka	0.364	34.6	0.117–0.611	0.375	0.127–0.699

Table contiuned

Parameter	Final estimate	RSE (%)	95 % CI	Bootstrap estimate	Bootstrap 95 % CI
Intersubject variability in CL/F (CV %)	0.071 (26.7 %)	18.7	0.045–0.097	0.069	0.044–0.097
Residual variability by proportional error model (CV %)	0.089 (29.8 %)	10.9	0.070–0.108	0.089	0.071–0.108

RSE (%) = 100 % × SE/estimate; *V/F* apparent volume of distribution; *Ka* absorption rate constant

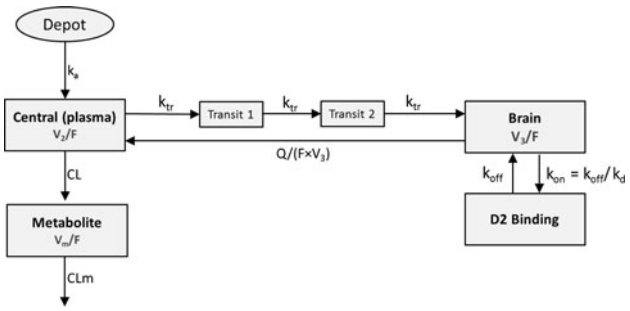

Fig. 1 PKPD model schema

Conclusions: The PK of LPV in PI-naïve HIV-infected subjects from RLS receiving LPV/r monotherapy as second-line ART were adequately described by a one-compartment model. LPV CL/F was influenced by sex and race with males and Thai subjects exhibiting faster clearances. After accounting for sex and race, the remaining interindividual variability in CL/F is small and contributions from other sources such as host genetics are as yet unknown.

References

[1] Kaletra® [package insert]. North Chicago, IL: Abbott Pharmaceuticals PR Ltd.; 2012. www.rxabbvie.com/pdf/kaletratabpi.pdf. Accessed January 18, 2012.

[2] Bartlett JA, Ribaudo HJ, Wallis CL, Aga E, Katzenstein DA, Stevens WS, Norton MR, Klingman KL, Hosseinipour MC, Crump JA, Supparatpinyo K, Badal-Faesen S, Kallungal BA, Kumarasamy N (2012) Lopinavir/ritonavir monotherapy after virologic failure of first-line antiretroviral therapy in resource-limited settings. AIDS 26:1345–1353.

M-024 Predicting Human Brain Concentrations and Receptor Occupancy of Clozapine Using Pharmacokinetic-pharmacodynamic Modeling of Clozapine in Rats

Claire H. Li[1,2,*], Robert E. Stratford Jr[3], Nieves Velez de Mendizabal[1,2], Robert R. Bies[1,2]

[1]Indiana University School of Medicine, Indianapolis, IN, USA; [2]Indiana Clinical and Translational Sciences Institute (CTSI), Indianapolis, IN, USA; [3]Xavier University of Louisiana, New Orleans, LA, USA

Objectives: Clozapine is highly effective in treating schizophrenia, in particular with hard-to-treat patients that present with predominantly negative symptoms. Despite this, there remains significant variability in the response to this drug. To better understand the variability, the objective of this study was to predict human ECF concentrations of clozapine by translating rat brain concentrations and receptor occupancy for this drug, coupling this with known human disposition of clozapine in the plasma and predicting human brain concentrations and occupancy from human plasma concentration measurements.
Methods: Unbound concentrations of clozapine and Nor-clozapine in four rats were previously measured in brain using quantitative microdialysis for up to 480 min after administration of a 10 mg/kg dose given subcutaneously [1]. Rich data were available from rats in both plasma and extracellular fluid (ECF) of brain for the modeling analysis. A compartmental modeling approach was first constructed to assess plasma and brain concentration data and subsequently explore transfer to the brain compartments. A transit model [2] was used to describe the delay observed in the appearance of clozapine in brain. The receptor occupancy model published by Johnson et al. [3] was adapted to describe the connection between brain ECF concentrations and receptor occupancy in the final model as shown in Fig. 1. The final rat PK-PD model was carried forward to simulate human ECF concentrations by scaling rat ECF concentration data using allometric principles with exponent to 0.75 for clearance, 1 for volume of distribution and 0.25 for transit rate constants. Human plasma PK parameters from a published PK model for clozapine in humans (Ismail [4]) were coupled with the scaled transfer rates and clearances determined from the rat data [4].
Results: A one compartment model with first order absorption and elimination best described plasma concentrations in rats. Clearance and volume of distribution of clozapine in plasma were 0.582 L/min and 25.8 L, respectively. A delay of concentration enriching in the brain ECF compartment was captured by a transit model that consisted of two transit compartments. Drug was assumed to pass through these two transit compartments using the same k_{tr} constant rate to the brain. The estimated k_{tr} was 0.0129 L/min. The PD parameter of k_{off} was estimated using dissociation constant (k_d) of 72 nM; k_{on} was calculated from k_d and k_{off}. The model was evaluated using goodness-of fit-plots and visual predictive checks. Between subject variability was significant for volume of distribution in plasma (V2), bioavailability (F1) and the transit rate constant (k_{tr}). Human clozapine concentrations in ECF were simulated based on published human plasma PK parameters and allometric scaling of the rat ECF PK parameters.
Conclusions: This PKPD model of clozapine, developed using rich plasma and brain concentrations in rats, adequately described drug transport across the brain barrier in rats and accounted for target receptor occupancy. This model was also useful to predict clozapine concentration in human ECF. Linking these occupancies to responses using this model may be improved if 5HT2 receptor occupancy is also implemented to reflect additional mechanisms of action for clozapine.

References

[1] Cremers TI, Flik G, Hofland C, Stratford RE (2012) Microdialysis evaluation of clozapin and *N*-desmethylclozapine pharmcokinetics in rat brain. Drug Metab Disposition 40(10): 1909–1016

[2] Savic RM, Jonker DM, Kerbusch T, Karlsson MO (2007) Implementation of a transit compartment model for describing drug absorption in pharmacokinetic studies. J Pharmacokinet Pharmacodyn 34(5):711–726

[3] Johnson M, Kozieiska M, Reddy VP, Vermeulen A, Li C, Grimwood S, Greef RD, Groothuis GMM, Danhof M, Proost JH

[4] Ismail Z, Uchida H, Mamo DC, Pollock BG, Bies RR (2012) Age and sex impact clozapine plasma concentrations in inpatients and outpatients with schizophrenia. Am J Geriatr Psychiatry 20(1):53–60

M-025 Amenorrhea and Breast Pain Profiles of the Combinations of Bazedoxifene and Conjugated Estrogens (BZA/CE) and Other Hormone Replacement Therapies in Postmenopausal Women, Modeling Assessment and Simulation of Comparative Study Designs

Juif (Frank) Jen*, Sima Ahadieh, Kuan Gandelman, John R Thompson, Sebastian Mirkin, Bill McKeand and Kevin Sweeney

Pfizer Inc., New York, NY, USA

Objectives: (1) To explore the amenorrhea (AM) and breast pain (BP) profiles of BZA/CE, Prempro (Conjugated Estrogens/Medroxyprogesterone Acetate or CE/MPA) and Premarin (CE). (2) To support BZA/CE post-marketing studies and development.
Methods: A comprehensive literature search through September 15, 2011 was performed for clinical trials that reported CE, MPA, BZA or other hormone replacement therapies (HRTs) as treatments, the AM and/or BP event rates as endpoints, and postmenopausal women as the patient population. The trial results from ten selected publications were extracted and combined with the summary information from four internal studies to create the analysis databases. As the response variables, the logit transformed AM and BP rates were modeled separately. The dose amounts of the components in the combination HRTs were the independent variables. Mixed-effects modeling was used to analyze the data with trial/study as a random effect. Trial simulations based on the developed models were used to estimate the probability of success (PoS) of trial scenarios. The software R was used for data preparation and analysis.
Results: AM rates were higher for BZA/CE than Prempro across all dose combinations. The AM rates of BZA/CE were flat at all CE/BZA dose combinations while those of Prempro decreased as the CE dose increased. BZA/CE at CE 0.45 mg and BZA 10–40 mg had a mean AM rate of 84 % with a 90 % CI: (82–85 %), compared to 59 % (52–65 %) for Prempro at CE 0.45 mg and MPA 1.5 mg. A higher MPA dose in Prempro tended to slightly decrease the AM rates further. BP rates were lower for BZA/CE across all CE/BZA dose combinations, compared to those of Prempro. BZA doses in the range of 10–40 mg had little effect on BP rates. Mean BP rates were estimated at 7 % (6–8 %) for BZA/CE with CE 0.45 mg/BZA 20 mg and 21 % (17–25 %) for Prempro with CE 0.45 mg/MPA 1.5 mg. The MPA effect on BP rates was not assessed due to limited Prempro treatment arms. To compare the AM rates of BZA/CE and Prempro at the aforementioned dose combinations, 50 patients per treatment arm were required to achieve an 80 % PoS. Twice the number of patients might be needed to achieve a >80 % PoS if BP rate was the primary endpoint. Dropout was not considered in the PoS estimation.
Conclusions: BZA/CE had better AM and BP profiles among postmenopausal women who received HRTs. Additional post-marketing studies may be conducted to confirm our findings from these analyses.

M-026 Using Bayesian-PBPK Modeling for Assessment of Inter-Individual Variability and Subgroup Stratification

Markus Krauss[1,2,*], Rolf Burghaus[3], Jörg Lippert[3], Mikko Niemi[4,5], Andreas Schuppert[1,2], Stefan Willmann[1], Lars Kuepfer[1], Linus Görlitz[1]

[1]Bayer Technology Services GmbH, Computational Systems Biology, 51368 Leverkusen, Germany; [2]Aachen Institute for Advanced Study in Computational Engineering Sciences, RWTH Aachen, Schinkelstr. 2, 52062 Aachen, Germany; [3]Bayer Pharma AG, Clinical Pharmacometrics, 42117 Wuppertal, Germany; [4]Department of Clinical Pharmacology, University of Helsinki, Helsinki, Finland; [5]HUSLAB, Helsinki University Central Hospital, Helsinki, Finland

Objectives: Tailor-made therapeutic designs require a functional understanding of the processes governing the distribution of substances within an organism. Anthropometric parameters like age or weight have great influence on the level of drug exposure in the human body [1]. Furthermore, the genetic predisposition of a patient is very important, since different genotypes can have significant effects on drug metabolization processes [2, 3]. In the worst case, side effects due to increased (off-)target tissue drug concentrations become critical for patient safety [3]. The early identification of subgroups showing significantly increased adverse event rates is a difficult task since only limited information about a new drug is available but is of utmost importance to prevent costly drug withdrawals in later phases of the drug development process [4]. Therefore, a mechanistic understanding of pharmacokinetics (PK) is essential in drug development to optimize the benefit-risk profile of a drug. This involves in particular the identification of high-risk subgroups in which an unfortunate combination of predisposition and non-optimal dosing schemes lead to potentially life-threatening side effects. In clinical practice, such subgroups have to be treated with individualized dosing schemes, which need to be designed and surveyed with adequate diagnostics. Here we combine Bayesian statistics with detailed mechanistic physiologically-based pharmacokinetic (PBPK) models. On a pravastatin example, we demonstrate that this combination provides a powerful tool to investigate inter-individual variability in groups of patients and to identify clinically relevant homogenous subgroups in an unsupervised approach. Since PBPK models allow the identification of physiological, drug-specific and genotype-specific knowledge separately, our approach supports knowledge-based extrapolation to other drugs or populations.
Methods: PBPK models are based on a large amount of prior physiological and anthropometric information which is integrated in the model structure [5, 6], Since PBPK models explicitly distinguish between properties of the compound and properties of the patients, respectively, they allow separation of physiological and drug-induced effects. PBPK models have previously been used for mechanistic analyses of drug PK [7], pharmacogenomics [2], multiscale modeling [8] or analysis of rare adverse events [3]. However, current use of such models often provides only a single value time-concentration curve, describing the behavior of a mean patient, neglecting potentially relevant individual properties. Therefore, PBPK models frequently lack the rigorous quantification of inter-individual variability in parameters which cannot be derived from the patients' anthropometry. To systematically account for parameter variability within patient populations, a Bayesian-PBPK approach is developed rigorously quantifying the probability of a parameter given the amount of information contained in the measured data. Since these parameter distributions are high-dimensional, a Markov Chain Monte

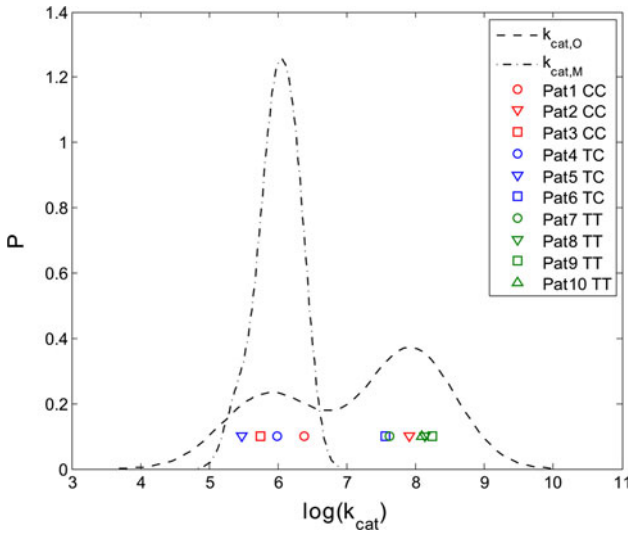

Fig. 1 Identification of clinically relevant subgroups related to the hepatic uptake transporter OATP1B1 ($p < 0.1$) using a Shapiro–Wilk test. Estimated kernel densities of logarithmic mean values of the posterior transporter activities (k_{cat}) for MRP2 and OATP1B1 are shown together with the single patient logarithmic mean values for OATP1B1

Carlo (MCMC) algorithm is used, where the physiological and drug-specific parameters are considered in separate blocks. MCMC covers a large group of algorithms containing usual [9], adaptive [10] and hierarchical [11] approaches to take samples from the posterior distribution of a parameter vector. The core idea of MCMC is to sample the unknown variables along a Markov chain, which has the posterior distribution as its stationary distribution. If several parameters are considered, such probability distributions are high dimensional. Thorough analysis of this posterior distribution quantifies inter-individual variability of a group of patients as well as the co-variability of the parameters, allowing the identification of homogenous subgroups. Bayesian approaches have already been used in conjunction with PBPK modeling, especially in toxicological questions [11], but also for population PK [12]. However, often the PBPK models used have been comparatively small and have contained lumped parameters carrying mixed information of different physiological or drug specific parameters. By using a large-scale PBPK model, which separates drug specific from population specific information, in combination with Bayesian approaches iterative characterization of special populations by optimally leveraging information from different drugs can be achieved.

Results: Considering pravastatin pharmacokinetics as an application example, Bayesian-PBPK is used to investigate inter-individual variability in a cohort of 10 patients. Correlation analyses infer structural information about the PBPK model. Moreover, homogeneous subpopulations are identified a posteriori by examining the parameter distributions and this subgroup stratification can even be assigned to a polymorphism in the hepatic organ anion transporter OATP1B1 (Fig. 1).

Conclusions: The presented Bayesian-PBPK approach systematically characterizes inter-individual variability within a population by updating prior knowledge about physiological parameters with new experimental data. Moreover, clinically relevant homogeneous subpopulations can be mechanistically identified. The large scale PBPK model separates physiological and drug-specific knowledge which allows, in combination with Bayesian approaches, the iterative assessment of specific populations by integrating information from several drugs.

References

[1] Willmann S, et al (2007) Development of a physiology-based whole-body population model for assessing the influence of individual variability on the pharmacokinetics of drugs. J Pharmacokinet Pharmacodyn 34(3):401–431

[2] Eissing T, Lippert J, Willmann S (2012) Pharmacogenomics of codeine, morphine, and morphine-6-glucuronide: model-based analysis of the influence of CYP2D6 activity, UGT2B7 activity, renal impairment, and CYP3A4 inhibition. Mol Diagn Ther, 16(1):43–53

[3] Lippert J, et al (2012) A mechanistic, model-based approach to safety assessment in clinical development. CPT: Pharmacomet Syst Pharmacol 1:e13

[4] Kuepfer L, Lippert J, Eissing T (2012) Multiscale mechanistic modeling in pharmaceutical research and development. Adv Exp Med Biol 736: 543–561.

[5] Rowland M, Peck C, Tucker G (2011) Physiologically-based pharmacokinetics in drug development and regulatory science. Annu Rev Pharmacol Toxicol 51(1):45–73

[6] Nestorov I (2007) Whole-body physiologically based pharmacokinetic models. Expert Opin Drug Metab Toxicol 3(2): 235–249

[7] Meyer M, et al (2012) Using expression data for quantification of active processes in physiologically-based pharmacokinetic modeling. Drug Metab Dispos 40(5):892–901

[8] Krauss M, et al (2012) Integrating cellular metabolism into a multiscale whole-body model. PLoS Comput Biol 8(10):e1002750

[9] Hastings WK (1970) Monte Carlo sampling methods using Markov chains and their applications. Biometrika 57(1):97–109

[10] Roberts GO, Rosenthal JS (2009) Examples of adaptive MCMC. J Comput Graph Stat 18(2): 349–367

[11] Bois FY, Jamei M, Clewell HJ (2010) PBPK modelling of inter-individual variability in the pharmacokinetics of environmental chemicals. Toxicology 278(3):256–267

[12] Yang Y, Xu X, Georgopoulos PG (2009) A Bayesian population PBPK model for multiroute chloroform exposure. J Exposure Sci Environ Epidemiol 20(4):326–341

M-027 Population Pharmacokinetic and Exposure–Response Analyses of Apremilast in Subjects with Active Psoriatic Arthritis

Yong Liu[1], Nastya Kassir[2], Samer Mouksassi[2], Simon Zhou[1], Jean-Francois Marier[2], Maria Palmisano[2]

[1]Celgene Corporation, Summit, NJ, USA; [2]Pharsight, A Certara Company, Montreal, QC, Canada

Objectives: Apremilast is a phosphodiesterase type 4 inhibitor evaluated for the treatment of psoriatic arthritis (PsA), psoriasis, ankylosing Spondylitis, and Behçet's disease. The aim of this study is to assess the population pharmacokinetics (PK) of apremilast (CC-10004) and the relationship between apremilast exposure and clinical endpoints ACR20, ACR50 and HAQ-DI (American College of Rheumatology 20 or 50 Response, and Health Assessment Questionnaire, Disability Index) in PsA patients.

Methods: The dataset pooled from a phase 2 study and a phase 3 study ($N = 160$), and several phase 1 studies ($N = 98$) was used to construct the population PK model. Upon identification of the structural population PK model, key covariates were evaluated to identify statistically and clinically relevant covariates explaining the sources of variability in apremilast PK. The final population PK model was used to predict apremilast exposure measures and perform PK/PD modeling of clinical endpoints. Individual clinical endpoints (ACR20 and ACR50) were characterized as a binary response (0 or 1) over time. The relationship between exposure to apremilast and response was modeled using logistic regression.
The logit of this model had the following form:

$$F = \gamma + \text{Placebo} + \text{DrugEffect} + \text{eta}$$

where γ intercept for clinical response; Placebo = Placebo model which is a function of time; DrugEffect = Drug action (i.e., PD model described using either a direct, indirect, or effect site maximum pharmacological effect (E_{max}) models, driven by exposure or concentration values of apremilast); eta = Individual random effect. Population PK and PK/PD modeling was performed using NONMEM version 7.2.
Results: A one-compartment model with first-order absorption resulted in the best quality of fit of apremilast plasma concentrations. Typical apparent clearance (CL/F) and volume of distribution (Vc/F) of apremilast were 11.5 L/h and 129 L, respectively. Significant effects of body weight, sex and disease status were observed on CL/F or Vc/F. PK/PD modeling of ACR20, ACR50 and HAQ-DI were described using time-dependent placebo models and E_{max} models for drug effects. Average steady-state minimum concentration values of apremilast following administration of placebo, 20 mg BID, 30 mg BID and 40 mg QD at Week 16 were 0, 133.6, 202.7 and 76.3 ng/mL, respectively. The above apremilast exposures allowed predictions of ACR20 proportions (7.6, 25.1, 28.3 and 20.5 %, respectively), ACR50 proportions (1.3, 11.2, 18.4 and 5.8 %, respectively) and change from baseline of HAQ-DI (−0.10, −0.20, −0.22 and −0.18, respectively) at Week 16.
Conclusions: PK/PD model reasonably described the change from placebo for apremilast ACR20/ACR50 results, but underestimated the ACR20 probability of placebo at week 16. The exposure-efficacy analyses suggest that 30 mg BID and 20 mg BID treatments may provide a greater probability of ACR20 and ACR50 responses; and better HAQ-DI response compared to the 40 mg QD treatments in PsA subjects and suggest that BID dosing regimen may be more appropriate than QD dosing regimen.

Reference

[1] Hutmacher MM, Krishnaswami S, Kowalski KG. Exposure–response modeling using latent variables for the efficacy of a JAK3 inhibitor administered to rheumatoid arthritis patients. J Pharmacokinet Pharmacodyn. 2008 Apr; 35(2):139-57.

M-028 Modeling the Intrinsic Factor Xa From Edoxaban Treatment

SaeHeum Song*, Dongwoo Kang, Jeanne Mendell, Abdel-Baset Halim, and Raymond Miller

Translational Medicine and Clinical Pharmacology, Daiichi Sankyo Pharma Development, Edison, NJ, USA

Objectives: To quantitatively describe the relationship between intrinsic Factor Xa (Intr FXa) and the exposure of Edoxaban, an oral, once-daily, direct Factor Xa inhibitor under development for the prevention of stroke and systemic embolism in patients with non-valvular-atrial fibrillation (NVAF) and treatment and prevention of recurrence of venous thromboembolism.
Methods: Edoxaban is an oral, direct, selective Factor Xa inhibitor. Reduced Factor Xa activity results in hypocoagulation. A population PK (pharmacokinetic) model of edoxaban was built using 18 phase 1 and 2 studies including 11,444 PK samples from 1,624 patients. Individual predicted concentration values were used to model the Intr FXa data from a phase 2 study [1] evaluating the safety of the four fixed doses of edoxaban (30 mg QD, 60 mg QD, 30 mg BID, and 60 mg BID) in patients with NVAF compared to an active control arm of warfarin. Subjects were randomized to 1 of the 5 treatment arms administered for 3 months. The Intr FXa data from 585 patients who received edoxaban was modeled using a dynamic binding model to describe the relationship between Factor Xa inhibition and edoxaban concentration. Intr FXa was determined in citrated plasma samples by activating endogenous Factor X to Factor Xa and then measuring the activity of Factor Xa with a two-stage chromogenic method. In the first stage, plasma Factor X is activated by Russel's Viper Venom (Pentapharm, Basel, Switzerland), in the presence of calcium ions, and in the second stage, Factor Xa hydrolyses a chromogenic substrate (Biogenic, Tokyo, Japan). The intensity of the color is directly proportional to FXa and, hence, intrinsic FX activity. Linearity of the assay was demonstrated between 9 and 100 % of normal human plasma, and the assay was reliable as shown by inter-run CV % of ≤14 %. Markov chain Monte Carlo stochastic approximation expectation maximization estimation implemented in NONMEM V.7.2 was used to estimate the model parameter values for association (K_{on}) and dissociation (K_{off}) of edoxaban with Intr FXa and the associated variability. Scatter plots of predicted vs. observed Intr FXa, pre-dose and post-dose boxplots of predicted vs. observed Intr FXa were used along with numerical evaluations to assess the goodness of model fit.
Results: The estimated binding affinity of Intr FXa was 9.04 ± 0.411 ng/mL (mean ± standard error) and the dissociation constant was 0.220 ± 0.0188 h. Simulated daily mean and peak values of Intr FXa activity for all the subjects are shown in Table 1 with respect to dosing regimens along with the observed incidence of all bleeding events from the phase 2 study. The order of daily mean Intr FXa values, from the smallest to the largest, concurs with the order of observed bleeding events from the phase 2 study. The proportion of subjects with Intr FXa exceeding a certain cutoff value along with the dosing schedule showed correlation with bleeding risk. For example, 30 mg BID dosing exhibited an average of 80 % or greater inhibition of Factor Xa activity throughout the day, whereas 60 mg QD dosing exhibited an average of 80 % or greater inhibition for 75 % of the time (i.e., for about 18 h per day).
Conclusions: The established pharmacokinetic-pharmacodynamic model of edoxaban has good predictability with respect to the

Table 1 Daily mean and peak values of Intr Factor Xa (mean ± standard deviation) with respect to edoxaban dosing regimens versus the observed bleeding risk

	30 mg QD	60 mg QD	30 mg BID	60 mg BID
Mean Intr FXa (%)	24.39 ± 11.16	15.65 ± 8.71	12.37 ± 8.40	7.13 ± 5.84
Peak Intr FXa (%)	48.53 ± 19.28	35.35 ± 17.96	22.53 ± 14.14	14.20 ± 11.43
Observed incidence of all bleeding events (%[N])	5.5 [13]	7.3 [17]	12.7 [31]	18.3 [33]

observed data. The simulated daily Intr FXa agrees with the observed bleeding risk across dosing regimens. The prolonged period of Intr FXa suppression, despite the same total daily dose, may provide a biological explanation to the greater bleeding risk observed from 30 mg BID compared to 60 mg QD. The 60 mg QD and 30 mg QD regimens showed similar and less bleeding risk to the warfarin control treatment (8.0 %), respectively, and were chosen for on-going phase 3 trials.

Reference

[1] Weitz JI, Connolly SJ, Patel I, Salazar D, Rohatagi S, Mendell J, Kastrissios H, Jin J, Kunitada S (2010) Randomised, parallel-group, multicentre, multinational phase 2 study comparing edoxaban, an oral factor Xa inhibitor, with warfarin for stroke prevention in patients with atrial fibrillation. Thrombosis and Haemostasis 104(3):633–641

M-029 Translation of Linezolid PK/PD Relationship from In Vitro Killing Kinetics Against *Staphylococcus aureus* Isolates to Mouse and Human Efficacy

Beesan Tan, Michele Johnstone, Virna Schuck

Infection Innovative Medicines, AstraZeneca R&D Boston, Waltham, MA, USA

Objectives: In antibacterial drug discovery and development, three PK/PD indices are commonly used: duration a drug remains above the minimum inhibitory concentration (MIC) ($T > MIC$), the ratio of the maximal drug concentration to the MIC (C_{max}/MIC) and the ratio of the area under the concentration time-curve to the MIC (AUC/MIC). This approach presents limitations relative to understanding the system or disease progression, mainly because only the summary PK parameters are being linked to a point estimate of efficacy. On the other hand, understanding the relationship between the full concentration–time profile and bacterial killing kinetics provides better insight into optimizing dosing strategy of the drugs. The aims of this study were (1) to simultaneously describe the in vitro killing kinetics of linezolid against four different *S. aureus* isolates using a semi-mechanistic PK/PD model; and (2) to demonstrate translation of linezolid PK/PD relationship from in vitro data to preclinical and clinical data using the model.

Methods: In vitro time-kill profiles of four different *S. aureus* isolates exposed to various static linezolid concentrations were modelled simultaneously using a mechanism-based population PK/PD model implemented in NONMEM 7.1. Linezolid PK was described by a one-compartment model. The bacterial dynamics in the system was characterized by a two sub-population model: one replicating and linezolid-susceptible population, and the other resting and linezolid-non-susceptible population [1, 2]. In the model, linezolid was assumed to enhance the killing rate of the bacteria in growing stage. The translatability of the model to in vivo and clinical data was evaluated in two parts: (a) the ability of the model to predict the magnitude of mouse- and clinically-derived linezolid PK/PD index (AUC/MIC); and (b) the ability of the model to predict the recommended linezolid clinical dosing regimen. In part (a), a dose fractionation study was simulated for each isolate in mouse and human. In each dose fractionation study, a total of 75 dosing regimens were simulated from the combinations of 15 different total daily doses fractionated into 5 different dosing intervals. The doses were chosen such that the full exposure–response relationship was explored. The relationship between bacterial load at 24 h and AUC/MIC were fitted with a sigmoidal E_{max} model (2), and the magnitude required to achieve stasis and 1-log drop in bacterial load at 24 h were calculated. In part (b), linezolid concentration–time profiles and corresponding *S. aureus* load in human were simulated using the PK/PD model built and previously published human PK parameters (3). Simulations were conducted for doses of 600, 800, 1000, 1200, 1400 mg/day divided into either once, twice or three times daily, administered as IV infusion over 30 min.

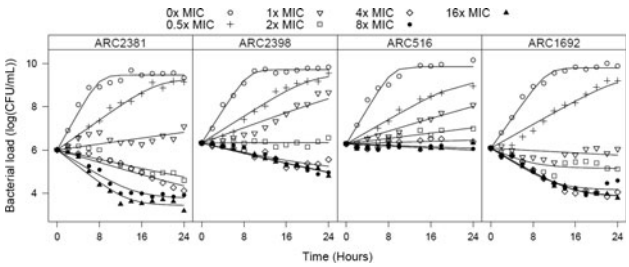

Fig. 1 Observed (symbols) and predicted (lines) time-kill profiles for four different *S. aureus* isolates exposed to linezolid at static concentrations ranging from 0 to 16 times the MIC

Results: The PK/PD model adequately described the killing kinetics of linezolid against all four isolates of *S. aureus* (Fig. 1). The growth rate was found to be the only statistically significant parameter accounting for the difference in killing kinetics seen between isolates. The model predicted the average (±SD) AUC/MIC required to achieve stasis and 1-log drop in bacterial load at 24 h in mouse infection model were 75 ± 40 and 144 ± 97, respectively, in accordance with previously published experimental values for stasis (83 ± 57) in a neutro-penic mouse thigh model [4]. The results here demonstrate the predictability of the model from in vitro to preclinical response, and provide a tool for selecting doses for testing in vivo, therefore optimizing the study design and potentially decreasing animal use in research. In human, the reported linezolid AUC/MIC breakpoints for different infection sites in severely ill patient population ranged from 51 to 164 [5]. This value is in good agreement with our model-predicted AUC/MIC ratio required for one log reduction in human infection (96 ± 59). Free linezolid concentration–time profiles and the corresponding bacterial count from the simulations of human dosing regimen are presented in Fig. 2. Greater maximum bacterial killing was associated with once daily dosing compared to twice or three times daily dosing. However, more rapid regrowth was also seen after once daily dosing. Overall, the predicted minimal dosing regimen (least amount of drug given least frequently) required to achieve stasis and 1-log reduction at 24 h were 400 mg q12 h and 600 mg q12 h, respectively. This is in good agreement with the recommended linezolid dosing guidelines: 400 mg q12 h for adults with uncomplicated skin and skin structure infection or 600 mg q12 h for other approved infection.

Conclusions: The simultaneous modeling of the in vitro killing kinetics of linezolid against four different *S. aureus* isolates using a semi-mechanistic PK/PD model with subsequent simulations of response in vivo allowed us to translate a PK/PD relationship from in vitro to in vivo preclinical studies and into to the clinical setting. In addition, we demonstrated that our semi-mechanistic PK/PD model offers advantages toward rational selection of optimal dosing regimen.

References

[1] Schmidt S, Sabarinath SN, Barbour A et al (2009) Pharmacokinetic-pharmacodynamic modeling of the in vitro activities of oxazolidinone antimicrobial agents against methicillin-resistant

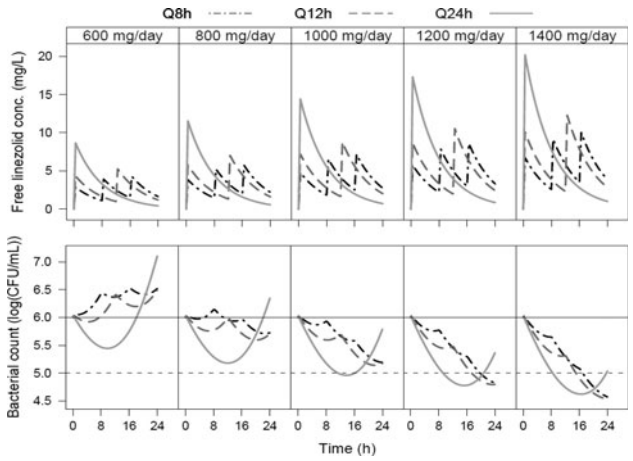

Fig. 2 Simulated free linezolid concentration–time profile (top panel) and corresponding *S. aureus* count (bottom panel) for different dosing regimens of linezolid. The solid and dashed horizontal lines in the bottom panel represent stasis and one log reduction in bacterial count, respectively

Staphylococcus aureus. Antimicrob Agents Chemother 53: 5039–5045

[2] Nielsen EI, Cars O, Friberg LE (2011) Pharmacokinetic/pharmacodynamic (PK/PD) indices of antibiotics predicted by a semimechanistic pkpd model: a step toward model-based dose optimization. Antimicrob Agents Chemother 55:4619–4630

[3] Abe S, Chiba K, Cirincione B et al (2009) Population pharmacokinetic analysis of linezolid in patients with infectious disease: application to lower body weight and elderly patients. J Clin Pharmacol 49:1071–1078

[4] Andes D, van Ogtrop ML, Peng J, Craig WA (2002) In vivo pharmacodynamics of a new oxazolidinone (linezolid). Antimicrob Agents Chemother 46:3484–3489

[5] Rayner CR, Forrest A, Meagher AK et al (2003) Clinical pharmacodynamics of linezolid in seriously ill patients treated in a compassionate use programme. Clin Pharmacokinet 42: 1411–1423

M-030 Longitudinal Analysis of Vabicaserin and Olanzapine Treatment Effects on PANSS Total Scores Using an Informed Dropout Model

Adam Ogden[1,*], Jing Liu[1], Thomas A. Comery[1], and Diane Mould[2]

[1]Worldwide Research and Development, Pfizer Inc., Groton, CT, USA; [2]Projections Research, Inc., Phoenixville, PA, USA

Objectives: Vabicaserin (VABI), a potent and selective 5-HT2C full agonist, has potential utility for the treatment of schizophrenia. Results of a Phase 2a trial of VABI, which included olanzapine (OLZ) as a positive control, in subjects with acute exacerbation of schizophrenia were recently reported [1]. VABI treatment improved positive and negative syndrome scale (PANSS Total) scores, relative to placebo, as determined using ANCOVAs with last observation carried forward (LOCF). Due to the large percentage of dropouts (> 50 % distributed across all treatment groups) observed in this study, a disease progression model accounting for dropouts was developed to better characterize the effect of VABI treatment.

Methods: Time-dependent functions were evaluated as the base PANSS Total models for VABI, OLZ, and placebo. Treatment effect was estimated in all models. The models also included a LOGIT function to constrain the predictions to be within the range of possible PANSS Total scores. Time-to-event dropout models were then added to the base PANSS Total models, and both models were fit simultaneously. Using the combined models, model-predicted mean changes from baseline were estimated for VABI, OLZ, and placebo.

Results: A proportional quadratic function was determined to produce the best model fit of the VABI data, whereas a linear function best fit the OLZ data. A Weibull hazard model resulted in the best fit of the dropout data. Inclusion of a dropout model resulted in a less steep slope of drug effect relative to the previous LOCF analysis. Due to the significant overlap of observed VABI trough plasma concentrations at the doses tested, subject-level VABI concentrations could not be incorporated into the treatment effect model but were a significant covariate in the dropout model. A statistically-significant treatment effect was observed for both VABI and OLZ relative to placebo. The model-predicted mean change from baseline of PANSS Total scores was −25.4, −17.0, and −6.8 for OLZ, VABI, and placebo, respectively.

Conclusions: Inclusion of a dropout model significantly improved the model fits relative to the previous LOCF analysis. This analysis suggests that VABI treatment demonstrated greater improvement on PANSS Total scores compared to placebo. However, the magnitude of response was less than that observed following OLZ treatment in this clinical study.

Reference

[1] Shen et al (2011) A 6-week randomized, double-blind, placebo-controlled, comparator-referenced, multicenter trial of vabicaserin in subjects with acute exacerbation of schizophrenia. Neuropsychopharmacology 36:S106

M-031 Population Pharmacokinetic Model-based In Vitro-In Vivo Correlation Approach to Predict Plasma Concentration Profiles of a Prodrug Orally Administered as Controlled Release Formulations and its Active Metabolite in Healthy Volunteers

Yan Ji[*], Michael Heathman, David Sperry, Matthew Deverall, Ahmad Almaya, Evelyn Lobo

Eli Lilly and Company, Indianapolis, IN, USA

Objectives: To develop an in vitro-in vivo correlation (IVIVC) model connecting the time-profiles of in vitro dissolution of controlled release (CR) formulations with in vivo plasma concentrations by utilizing a population pharmacokinetic (PK) approach to predict plasma concentration profiles of both a prodrug and its active metabolite.

Methods: Three CR formulations, A, B and C corresponding to slow, intermediate and fast release rates, were developed for a prodrug. In vitro dissolution profiles of the CR formulations were determined and plasma concentrations of both the prodrug and the active metabolite were obtained from two clinical studies in fasted healthy volunteers following oral administration of the prodrug as solution or as one of the three CR formulations. The CR formulation dissolution profiles were incorporated into a population PK model, which was used to fit the plasma concentrations of both the prodrug and active metabolite, using NONMEM VI. The model was then used to predict plasma concentration profiles of the prodrug and the active metabolite in fasted healthy volunteers following oral administration of three

new CR formulations of the prodrug based on their in vitro dissolution profiles.
Results: The final population PK model included five compartments: CR formulation, depot compartment representing absorption of prodrug, central compartment of prodrug, peripheral compartment of prodrug, and active metabolite compartment. A fourth-order polynomial function was used to describe in vitro dissolution kinetics of the CR formulation, which was linked to the depot compartment of the prodrug. A model event time (MTIME) was used to estimate the absorption time window to characterize the extent of absorption of the prodrug. PK of the prodrug was described by a two-compartment model, which included first-order absorption from the depot, distribution to the peripheral compartment and clearance to the active metabolite. The active metabolite was then eliminated from the body. The model adequately characterized the PK of both the prodrug and the active metabolite for CR formulation A, B and C based on the goodness-of-fit criteria, visual predictive checks, and parameter precision (percentage standard errors of estimation were below 30 %). Using the in vitro dissolution profiles of three new CR formulations, the model reasonably captured the observed concentration profiles of both the prodrug and the active metabolite. The prediction errors for area under the concentration–time curve (AUC) and maximal plasma concentration (C_{max}) of both the prodrug and the active metabolite were generally below 100 %.
Conclusions: Avoiding data transformation and utilizing a population PK model, this approach provides more information of in vivo drug performance for not only the prodrug but also the active metabolite which is of primary clinical interest, and allows greater flexibility in assessing PK variability and potential covariate effects, compared to conventional IVIVC approaches. The method was applied to select the optimal CR formulation and guide dose selection of new untested formulations in clinical studies.

M-032 Longitudinal Model Based Meta Analysis of Positive and Negative Syndrome Scale (Panss) in Patients with Schizophrenia

Sima Ahadieh*, Thomas Tensfeldt, Vikas Kumar

Pfizer Inc., Groton, CT, USA

Objectives: To support go/no go drug development decisions, a longitudinal model based meta-analysis (L-MBMA) for PANSS Total was updated with recently published studies and recently approved antipsychotics.
Methods: A database of 43 published clinical studies (28 in acute and 15 in chronic schizophrenic (SCZ) patients) from MEDLINE, and FDA summary basis of approval (SBA) was created. Treatments included in the dataset were either placebo, atypical antipsychotics or more recently approved antipsychotic drug such as asenapine, lurasidone, iloperidone, and paliperidone ER. A large drop-out frequency in this patient population required the use of the reported last observation carried forward (LOCF) data. The model consisted of additive baseline, placebo, and drug effects. The between study variability was accounted by a random effect on the slope and asymptote of the placebo model. Between arm variability was included through an additive residual variance term. Chronic or acute disease status was used as a covariate in the model. Both placebo and active treatments were characterized by an exponential model vs. time. Model parameters were estimated using NONMEM 7.1.2. Stochastic simulations were performed to assess the predictive power of the model. The mathematical models were defined as:

$$\text{Effect}_{\text{placebo}} = (B + \eta 2) \times \left(1 - e^{-(K \times e^{\eta 1}) \times \text{time}}\right) \times (1 + \text{condition})$$

$$\text{Effect}_{\text{drug}} = \text{Eff} \times \left(1 - e^{-S \times \text{time}}\right) \times (1 + \text{condition})$$

$$\text{Effect}_{\text{treatment}} = \text{Baseline} - \text{Effect}_{\text{placebo}} - \text{Effect}_{\text{drug}} + W \times \varepsilon$$

B and K are the asymptote and onset of placebo effect, while Eff and S were asymptote and onset of the drug effect. Condition was the patient status covariate (chronic or acute).
Results: The placebo effect was estimated as −5.8 [−17.6, 4.2] points reduction in PANSS Total after 6 weeks. There seemed to be a rising in placebo response by the trial date. The estimated mean placebo adjusted drug effect in acute patients at 6 weeks for various antipsychotics (in decreasing order) was: olanzapine ~ risperidone (−8.8) > haloperidol (−8.46) > aripiprazole (−8.3) > paliperidone ER (−7.56) > ziprasidone ~ lurasidone ~ asenapine (−5.48) > iloperidone (−3.8). Newly approved antipsychotic drugs do not seem to demonstrate superior efficacy compared to the standard of care (risperidone/olanzapine).
The estimated mean placebo adjusted drug effect in patients with chronic SCZ at 6 weeks, in decreasing order, were olanzapine ~ risperidone (−8.2) > paliperidone ER (−6.3) > ziprasidone (−5.4) > aripiprazole (−4.9) > haloperidol (−4.5). The drop in PANSS total was estimated to be larger in the acute patient population compared to chronic patients.
Conclusions: Quantitative modeling of PANSS Total provided an integrated approach for comparing treatment effects across marketed antipsychotics. The updated model estimates were used to support decision making by comparing the efficacy of internal compounds in development with marketed antipsychotics in both chronic and acute SCZ patients. In addition, the placebo response increase by time of trial needs further investigation and could be used as a covariate on the placebo effect in the future models.

References

[1] http://www.nature.com/clpt/journal/v85/n1s/pdf/clpt2008290a.pdf?free=1
[2] Beal et al. (1998) NONMEM users guides: parts I–VIII. NONMEM project group. University of California, San Francisco

M-033 Development of a Population PK Model to Describe Dovitinib Pharmacokinetics

Samira Garonzik*, Jerry Nedelman, Jeff Scott, Ovidiu Chiparus, Jane Xia and Eugene Tan

Novartis Pharmaceuticals, East Hanover, NJ, USA

Objectives: Dovitinib is a potent oral inhibitor of Receptor Tyrosine Kinases (FGFR, VEGFR, PDGFR). Dovitinib is anticipated to be efficacious in patients with tumors dependent on FGF-activated pathways (mutation, amplification or overexpression). Moreover, dovitinib may augment management of tumors with FGF activation secondary to VEGF resistance.The objective of this analysis was to improve upon a previously developed PK model [1] to better describe the time dependencies and dose dependent nonlinearities of dovitinib PK.
Methods: PK data from 127 patients receiving dovitinib, 50–600 mg daily or intermittently over 15–859 days were available. Plasma concentration–time data were available after the first dose and at steady state. NONMEM versions 6 and 7 were used for nonlinear mixed effects modeling of the data; R version 2.1.3 was used for data display and summarization.

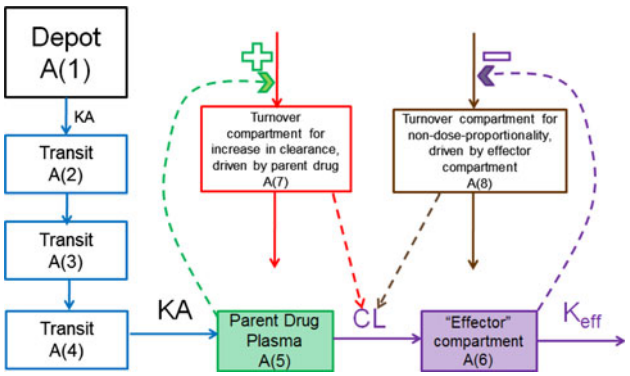

Fig. 1 Schematic for improved model

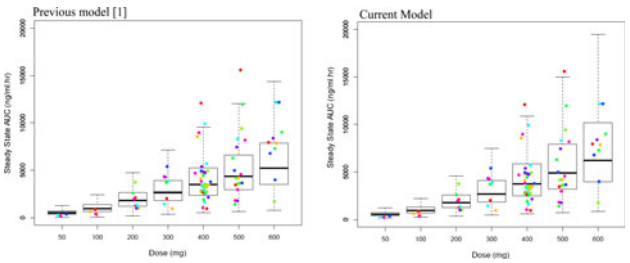

Fig. 2 Comparison of predicted steady state AUC by dose with data overlaid for previous model [1] and current model

Results: Dovitinib exposures on Day 1 were characterized by dose proportionality following single doses ranging from 50 to 600 mg. At steady state, there was a slight non-proportional increase in exposure with dose, but with lower accumulation than expected under time-independent PK. Absorption was prolonged, with t_{max} 6–8 h post dose.

A previously reported PK model used two parallel clearance terms allowing for either lower than expected steady-state exposure or non-dose-proportionality to manifest, with both phenomena depending on a single time dependent process [1]. This model predicted non-dose-proportionality only for patients with the highest exposures [1].

The multi-compartment model developed here (Fig. 1) exhibited increased flexibility and was able to better capture the complex features of dovitinib PK. Oral doses of dovitinib enter into a depot compartment. Transit compartments accommodate the absorption lag. The two turnover compartments (driven by either the parent drug concentration or by a downstream effector) modulate the clearance of dovitinib in opposing ways. The first turnover compartment has a very small EC50 making it act like a switch that causes an amplification in dovitinib clearance which is essentially the same for all doses. The resulting increase in clearance causes the concentrations at steady state to be lower than projections based on day 1. The second turnover compartment induces reductions in clearance relative to baseline. It has a more moderate EC50, which leads to an observable dose dependence in exposure at steady state.

A predictive check was performed in order to compare the previous model [1] with the current model by simulating 5000 subjects at each dose from each model with the same seed. Boxplots were used to display the range of steady state AUC's predicted by each model for each dose level. Observed data was then overlaid (Fig. 2). The new model demonstrates an improved predictive capacity at the higher doses, implying that the non-dose-proportionality is better described by this model.

Conclusions: The PK model developed in this work described the data well and captured both time dependent processes including decrease in exposure as well as the more subtle dose non-proportionality over time. This model will be used to characterize data from additional studies and perform a full covariate analysis.

Reference

[1] Garonzik S, Nedelman J, Tan E, Chiparus O, Dugan M (2012) Development of PK/PD models to describe pharmacokinetics and biomarker responses for dovitinib (TKI258)

M-034 Comparative Dose Response Modeling of Efficacy, Adverse Events and Discontinuation Rates in Neuropathic Pain

Evelyn D. Lobo[1], Michael A. Heathman[1,*], William F. Ebling[2]

[1]Eli Lilly and Company, Indianapolis, IN, USA; [2]Emergent Insights, Newark, DE, USA

Objectives: To compare the dose response relationships for efficacy (pain score), adverse events (frequency of somnolence and dizziness) and total discontinuation rates (due to lack of efficacy, adverse events) of gabapentin, pregabalin and duloxetine in specific types of neuropathic pain.

Methods: A database consisting of 14 placebo controlled dose ranging clinical trials of gabapentin, pregabalin and duloxetine was developed from publicly available sources: journal articles, regulatory documents, package inserts, and web documents. The clinical trials investigated various neuropathic pain such as diabetic neuropathic pain, post-herpetic neuropathic pain and general neuropathic pain. A dose response with time course model with inter-study and inter-arm variability for pain score (using 11-point Likert scale) was developed to characterize improvements in mean pain score for each treatment arm (placebo or drug) as shown below:

$$\text{PainScore} = \text{Baseline} - \text{Placebo} \cdot \left(1 - e^{-Kpb \cdot Time}\right) - E_{\max} \cdot \frac{\text{Dose}^{\gamma}}{\text{Dose}^{\gamma} + ED_{50}^{\gamma}} \left(1 - e^{-K\text{drug} \cdot \text{Time}}\right)$$

where Kpb is the rate of decline in pain score in placebo; E_{max} is the maximal effect of the drug; γ is Hill coefficient; ED_{50} is the dose associated with 50 % maximal effect; Kdrug is the rate of decline in pain score in drug treated arm.

A logistic regression model was developed to characterize the total discontinuation rates due to lack of efficacy, adverse events, or other reasons, as well as the frequency of somnolence and dizziness. Covariates such as pain subtype, drug, age, titration, and duration of treatment were investigated. All analyses were conducted using NONMEM VI and SPLUS 6.2.

Results: The treatment period for gabapentin was 8 weeks (daily dose: 900–3600 mg), for pregabalin was 5–13 weeks (50–600 mg) and for duloxetine was 12 weeks (20–120 mg). The baseline pain score was lower for duloxetine (5.86) trials compared to pregabalin or gabapentin (6.56). The model characterized the time course of change in pain score from baseline well. The ED_{50} for pregabalin and duloxetine were 105 and 19.5 mg, respectively, while there appeared to be no dose dependency for gabapentin.

Similar to the pain score model, discontinuation due to lack of efficacy declined with dose for both pregabalin and duloxetine, while there was no dose response relationship for gabapentin.

Discontinuation due to adverse events showed a clear dose response relationship for all three drugs, although discontinuation rates were lower for diabetic neuropathic pain than for the other indications. While there was no dose response for discontinuation due to other reasons, age
did have an effect, with older patients being less likely to drop out of the study. Frequency of somnolence and dizziness were lower in trials that used dose titration as compared to trials that did not use titration.

Conclusions: The dose–response relationships for the efficacy, adverse events and discontinuation rates were quantified for 3 currently approved drugs for neuropathic pain. The results of the meta-analyses provided insights into the relative efficacy, tolerability and dropout rates at the approved doses that guided decisions regarding the selection of dose and active comparator for use in Phase 2 studies and optimization of study design of novel compounds under investigation for neuropathic pain.

M-035 Population PK-PD Modeling of Everolimus in the Treatment of Patients with Tuberous Sclerosis Complex (TSC) Who Have Subependymal Giant Cell Astrocytomas (SEGA)

William Sallas[1,*], Ovidiu Chiparus[1], Wing Cheung[1], Shweta Urva[1], Jixian Wang[2], Helene Cauwel[2], Du Lam[1], Gaurav Shah[1], Celine Sarr[1]

[1]Novartis, East Hanover, NJ, USA; [2]Novartis, Basel, Switzerland

Background: TSC is an autosomal dominant genetic disorder characterized by the growth of non-malignant tumors in multiple organ systems [1–2]. Brain lesions (SEGAs) are the primary cause of morbidity and mortality in children with TSC. In the EXIST-1 trial the primary endpoint was overall SEGA response rate—the percentage of patients with at least 50 % shrinkage in sum of target SEGA volumes (SV) with no new or worsening non-target SEGA lesions or hydrocephalus. Everolimus led to a statistically significant difference ($p < 0.0001$) in the overall SEGA response rate in favor of everolimus versus placebo (34.6 vs. 0 %). The study is ongoing. Current results are for double-blind treatment period, but not after the predefined cutoff date. Dose was titrated from 4.5 mg/m^2 to reach a trough (C_{min}) of 5–15 ng/mL, subject to tolerability. Limited pharmacokinetics (PK) was assessed 2 weeks after first dose, at each visit, and 1–2 weeks following dose adjustments. SEGAs assessed by brain MRI at baseline, week 12, week 24, and week 48 were measured centrally [3].

Exploratory objective: Assess target C_{min} range for therapeutic drug monitoring through modeling of the relationship between everolimus exposure and sum of target SEGA volume (SV) while accounting for interpatient differences

Methods: The sum of target SEGA volumes (SV, cm^3) was modeled as a function of everolimus exposure (C_{min}, ng/mL) over time based on actual daily dosing history, including dose changes and interruptions. Baseline SV, age, body size, sex, and concomitant medications were examined to help explain patient differences in both their PK (not shown) and their impact on sensitivity to everolimus for SV shrinkage. An indirect response model was developed that modeled the rate of change in SV for $C_{min} = 0$ (placebo) by a nonnegative input rate "Kin" (cm^3/h) and nonnegative output rate "Kout × SV" (1/h × cm^3). The difference in input and output rates tell you the rate of change in SV. The drug effect is the inhibition "I" (fraction 0–1) of the input rate Kin through everolimus C_{min} by an I_{max} model:

$$I = Imax \times Cmin/(IC50 + Cmin),$$

where Imax is between 0 and 1, and IC50 is nonnegative. Initially $C_{min} = 0$ (and $I = 0$) until after everolimus treatment starts; then I is estimated daily. If $C_{min} = IC50$, then $I = I_{max}/2$. For placebo and everolimus, the differential equation for the rate of change of SV was represented in terms of SV, C_{min}, and the individual pharmacodynamic parameters (Kin, Kout, IC50, and I_{max}) as:

$$dSV/dt\ [cm^3/h] = Kin \times (1 - I) - Kout \times SV.$$

A separate population PK analysis provided the individual PK parameters from all patients in the everolimus arm to estimate daily C_{min} used in the population PK-PD model. NONMEM with METHOD = 1 INTERACTION was used for both the population PK (not shown) and the population PK-PD models.

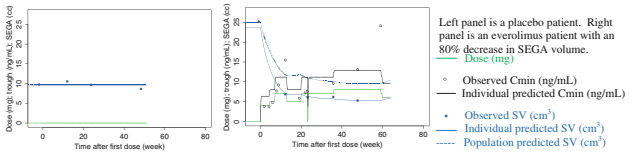

Fig. 1 Dose (mg), observed and predicted C_{min} (ng/mL) and SEGA volume (cm^3) versus time (week) Left panel is a placebo patient. Right panel is an everolimus patient with an 80 % decrease in SEGA volume

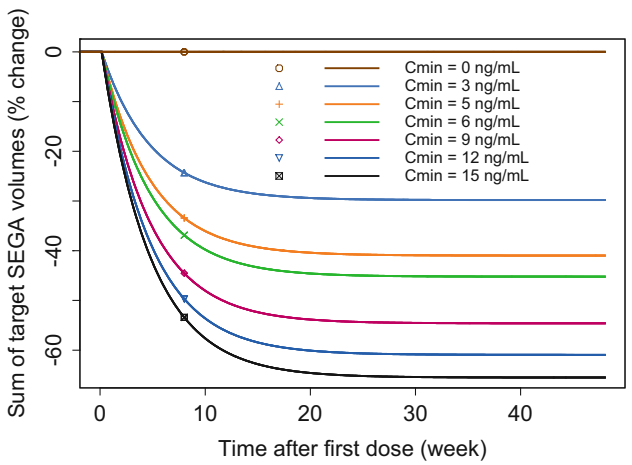

Fig. 2 Typical change in SV by C_{min} vs. time

Table 1 Typical decrease in SV and model-based percentage of patients with at least a 50 % decrease by C_{min}

C_{min} (ng/mL)	Typical SV decrease after baseline (95 % CI)	Model-based % patients with ≥50 % decrease
0	0 (−4 to 9)	2
3	30 (22 to 36)	12
5	41 (30 to 46)	31
6	45 (32 to 50)	38
9	55 (37 to 59)	58
12	61 (40 to 65)	70
15	66 (42 to 70)	78

Table 2 Individual target C_{min} for patients with poor early SV shrinkage

	Past individual SV shrinkage			Future individual goal for SV shrinkage		
	10%	20%		30%	50%	75%
Individual observed Cmin (ng/mL)		1	Individual target Cmin (ng/mL)	1.7	4.2	14.9
	1			3.9	9.6	NA
		2		3.5	8.4	NA
		3		5.2	12.7	NA
	2			7.9	NA	NA
	3			11.8	NA	NA
		4		6.9	NA	NA
		6		10.4	NA	NA
		8		13.9	NA	NA
	≥4			NA	NA	NA
		≥9		NA	NA	NA

This table is based on limited data, and is not appropriate to use at this time.

NA means goal is not likely to be achievable, i.e., individual target Cmin exceeds 15 ng/mL – the upper limit of the target Cmin range (based on limited safety experience in patients with higher Cmin).

Good chance to reach 50-75% shrinkage
Good chance to reach 50% shrinkage
Good chance to reach 30% shrinkage
Poor chance to reach 30% shrinkage

Results: There were 78 patients randomized to everolimus with median age 9.5 years (range 1.0–23.9), and there were 39 patients randomized to placebo with median age 7.1 years (range 0.8–26.6). Two patients randomized to everolimus had no target SEGA lesion observed at baseline by central assessment and were excluded from the population PK-PD analysis. The remaining 115 patients in the population PK-PD analysis population contributed a total of 510 sums of target SEGA volumes. The observed and predicted C_{min} and SEGA volume for two patients are below (Fig. 1).

Typical sum of target SEGA volumes (SV) after baseline as a function of C_{min} was estimated (Fig. 2; Table 1).

Models with C_{min} replaced by AUC calculated using the population PK model provided similar results. C_{min} was chosen because it was used in therapeutic drug monitoring. The median observed C_{min} was 3.7 ng/mL at week 2, and the median increased to 7.1 ng/mL at week 48 due to corresponding increases in dose. IC50 was variable, ranging from 1 to 25 ng/mL with typical IC50 = 6.4 ng/mL. Some subpopulations were too small to distinguish their IC50. Thus, there was no evidence to individualize starting dose beyond that found from population PK (not shown).

At 24 weeks, 21.6 % of everolimus patients had less than 30 % SV shrinkage. Some of these patients may benefit from individualized dosing. A patient SV reaches steady state typically after 12–24 weeks of everolimus. Then, the model can theoretically provide some guidance toward an individual target C_{min} to meet a patient goal for SV shrinkage (Table 2).

Conclusions: The PK-PD model generally supports the 5–15 ng/mL target C_{min} range, but also recognizes patients with tolerability issues requiring a dose reduction and a C_{min} below 5 ng/mL could still have benefit from tumor shrinkage in this long-term, life-threatening disease.

References

[1] Franz DN, Bissler JJ, McCormack FX (2010) Tuberous sclerosis complex: neurological, renal, and pulmonary manifestations. Neuropediatrics 41:199–208

[2] Dixon BP, Hulbert JC, Bissler JJ (2011) Tuberous sclerosis complex renal disease. Nephron Exp Nephrol 118:e15–e20

[3] Franz DN, et al (2013) Efficacy and safety of everolimus for subependymal giant cell astrocytomas associated with tuberous sclerosis complex (EXIST-1): a multicentre, randomised, placebo-controlled phase 3 trial. Lancet 381:125–132

The results in this abstract have been previously presented in part at International TSC Congress, September 6–9, 2012, Naples, Italy.

M-036 Exposure–Response Modeling in Support of Phase 3 Dose Selection of MK-3222 for Treatment of Psoriasis

Anthe Zandvliet[1,*], Hanbin Li[2], Russ Wada[2], Kristine Nograles[3], Rich Shames[4], Devan Mehrotra[6], Sandy Allerheiligen[6], Thomas Kerbusch[1], Robin Mogg[6], Bill Hanley[5]

[1]Merck Research Laboratories, Oss, The Netherlands; [2]Quantitative Solutions, Menlo Park, CA, USA; [3]Merck Research Laboratories, Kenilworth, NJ, USA; [4]Merck Research Laboratories, Palo Alto, CA, USA; [5]Merck Research Laboratories, Westpoint, PA, USA; [6]Merck Research Laboratories, Upper Gwynedd, PA, USA

Objectives: MK-3222 is a high affinity humanized anti-IL 23 p19 specific MAb being developed for treatment of psoriasis. The Phase 2b dose ranging study of MK-3222 was carefully designed to establish the dose–response relationship [1]. The results from this Phase 2b study were used to develop an exposure–response model to analyze PASI75 and PASI90 response rates. Model-based simulations were used to support dose selection for Phase 3 development.

Methods: PASI75 and PASI90 responder status (yes/no) at week 16 were modeled as a saturable function of exposure using logistic regression. PASI75 and PASI90 were analyzed separately and were also co-modeled as correlated endpoints. Subject exposures were calculated from a population PK model. The effect of body weight, prior biologic experience (yes/no), psoriasis vs. psoriatic arthritis status, and baseline PASI on model parameters were evaluated. Model robustness was evaluated by fitting data subsets (i.e. only PASI75 data, or only PASI90 data), dose–response data, and combined PASI75 and PASI90 data.

Key Assumptions

- Phase 2b study P05495 subjects are representative for the Phase 3 population.
- The average serum concentration (Cavg) up to week 16 is a reasonable measure of exposure that is predictive of week 16 PASI75 and PASI90
- A logistic regression model with a steep increase of response at lower exposure levels, leading to a plateau at higher exposure levels, is appropriate to describe MK-3222 PASI75 and PASI90 response.

Results:

Exposure–response model

The model fit is shown in Fig. 1 for PASI75 (left panel) and PASI90 (right panel). EC50 for PASI75 was estimated to be 0.2 μg/mL (i.e. the concentration resulting in half-maximal efficacy). Since the median exposure for the 100 mg dose group was 4.67 μg/mL, both

Table 1 PASI75 response rate at week 16

Dose group	5 mg	25 mg	100 mg	200 mg	Placebo
N	42	90	89	86	45
n PASI75 responders (week 16)	14	58	59	64	2
% PASI75 responders (week 16)	33.3 %	64.4 %	66.3 %	74.4 %	4.4 %

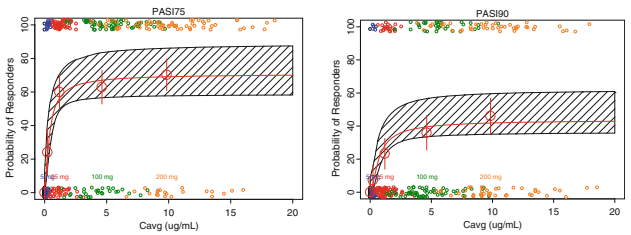

Fig. 1 Model fit for week 16 PASI75 and PASI90 response (difference from placebo) versus exposure. Scenario: joint model of combined PASI75 and PASI90 data. Dashed area is 95 % CI from simulations based on the variance–covariance matrix

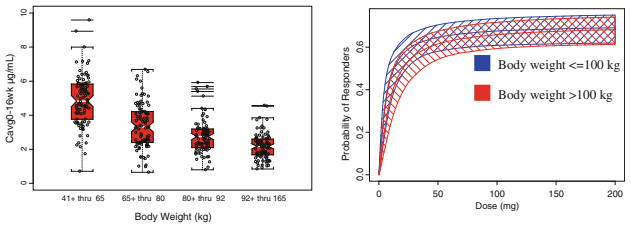

Fig. 2 Impact of body weight on drug exposure (left panel) and on the dose–response relationship for PASI75 at W16 (right panel). Exposure was estimated per subject using a population

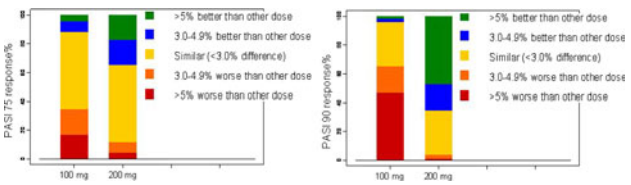

Fig. 3 Results from clinical trial simulations for PASI75 (left) and PASI90 (right) in cohorts of n = 300 based on exposure–response models. Scenarios: model of PASI75 data (left) and PASI90 data (right)

100 and 200 mg are towards the top of the exposure–response curve (Table 1).

Impact of body weight

The population PK analysis demonstrated that drug clearance increased with body weight. Figure 2 shows the impact of body weight on drug exposure (left panel) and on the dose–response relationship (right panel). Drug exposure decreases with increasing body weight. Body weight was a relevant determinant of the PASI75 response rate in the lower dose range. However, impact was minimal at the plateau of the dose–response relationship. These results justify the conclusion that there is no need for a body weight based dosing strategy.

Model-based dose selection

The model-based analysis of the clinical data from the Phase 2b study suggested that the 100 mg dose was near the plateau of the exposure–response relationship for PASI75. The incremental benefit for 200 versus 100 mg was estimated to be ~2 % for PASI75 and 2–6 % for PASI90. Clinical trial simulations were conducted to investigate the impact of these differences on the potential outcome of Phase 3 clinical trials. In total, 10,000 trials were simulated with cohorts of 300 subjects. Results are shown in Fig. 3 which demonstrates that the observed response rates for 200 versus 100 mg are likely similar for PASI75 and may be higher for PASI90. All model scenarios (only PASI75 data, only PASI90 data, dose–response data, and combined PASI75 and PASI90 data) suggested fairly similar mean differences between 100 and 200 mg dose groups, although models that fit PASI90 only showed larger, possibly clinically meaningful benefits of 200 over 100 mg as compared to models that fit combined PASI75 and PASI90 data.

Conclusions: There is no need from a clinical pharmacology perspective to tailor the dose based on body weight. The 100 and 200 mg doses are likely near or at the plateau of the exposure–response relationship and were both selected for Phase 3 development. The 200 mg dose may have a clinically meaningful higher PASI90 response rate.

Reference

[1] Thomas Kerbusch et al (2011) Phase 2b dose selection for the treatment of autoimmune disorders leveraging comparator data, ACoP 2011

M-037 Population Pharmacokinetic and Pharmacokinetic/Pharmacodynamic Analyses of Dutasteride in Male Subjects with Androgenetic Alopecia

Géraldine Ferron-Brady[1,*], Walter Gubelin Harcha[2], Julia Maria Barboza Martinez[3], Tsen-Fang Tsai[4], Allison Barnes[1], Dushen Chetty[1], Makoto Kawashima[5], Kensei Katsuoka[6], Ryoji Tsuboi[7], Michael Fossler[1]

[1]GlaxoSmithKline, King of Prussia, PA, USA; [2]Centro Medico Skinmed, Santiago, Chile; [3]Clinica International, Lima, Peru; [4]National Taiwan University Hospital, Taipei, Taiwan; [5]Tokyo Women's Medical University, Tokyo, Japan; [6]Kitasato University, Kitasato, Japan; [7]Tokyo Medical University, Tokyo, Japan

Objectives: The objectives of these analyses were (1) To develop a population pharmacokinetic (PPK) model characterizing for the first time the pharmacokinetics of dutasteride in male subjects with androgenic alopecia (2) To develop a population pharmacokinetic/pharmacokinetic (PPKPD) model that characterizes the effects of dutasteride on dihydrotestosterone and hair count following once daily oral administration to male subjects with androgenetic alopecia.

Methods: Dutasteride and dihydrotestosterone concentrations and target area hair count within a 2.54-cm diameter circle [1] were

available from a phase II-III multicenter randomized placebo-controlled study. Male subjects with androgenetic alopecia aged 20–50 years received placebo or dutasteride (0.02, 0.1 or 0.5 mg) daily for up to 24 weeks. Data were analyzed by non-linear mixed effect modeling using NONMEM 7.0 using first order or first order conditional estimation allowing for interaction (FOCE-I). As the 0.02 mg dose group could not be included in the PPK model (see Results), observed dutasteride concentrations were used for the PPKPD analysis. Dihydrotestosterone concentrations below the limit of quantitation (LLQ) were replaced by half the LLQ and dutasteride concentrations below the LLQ were replaced by half the LLQ for the active treatment groups and by zero for the placebo group for the PPKPD analyses. Model evaluation comprised non-parametric bootstrap and visual predictive checks.

Results: More than 50 % of dutasteride concentrations were below the LLQ for the dose of 0.02 mg and attempts to include these data using the M3 method were unsuccessful. Initial runs were done with models with linear and non-linear elimination with FOCE-I. These runs showed consistent under estimation of concentrations for the dose of 0.5 mg. This issue was solved by switching to the FO estimation method as previously done [2]. The pharmacokinetics of dutasteride for the dose of 0.1 and 0.5 mg were best described by a one-compartment model with linear and non-linear elimination (Table 1). Body weight and age were covariates on the linear clearance and body weight was a covariate on the volume of distribution. Race and ethnic Heritage did not have any additional effect on the linear clearance and volume of distribution. The bootstrap analysis as well as the visual predictive check showed that the model was reasonably robust.

Dihydrotestosterone concentrations measured at the end of treatment were better predicted with dutasteride concentration than dutasteride dose. The PK/PD relationship ($N = 694$ subjects) followed a simple E_{max} model where E_{max} is the maximum drug induced effect and was 91.0 % (95 % CI: 88.5–93.5 %). The concentration providing 50 % of E_{max} (EC_{50}) was estimated to be 0.191 ng/mL (95 % CI: 0.104–0.278 ng/mL). No covariates were identified for E_{max}.

The effect of dutasteride on change from baseline in 2.54-cm target area hair count ($n = 610$ subjects) was best described by a simple E_{max} relationship with dutasteride concentration (Table 2). The placebo effect showed greater hair loss in subjects with higher baseline hair count with an average loss of 8 hairs for a median baseline hair count of 760 and a hair loss of 33 for the 95th percentile baseline hair count of 1110. Cluster (Hispanic versus non-Hispanic countries) and baseline Norwood-Hamilton (BNHS) alopecia score significantly impacted E_{max}. Subjects from non-Hispanic countries had 53 % lower hair gain and subjects with a baseline Norwood-Hamilton score of V had 43 % higher hair gain than subjects with a score of III or IV.

Conclusions: A one-compartment population pharmacokinetic model for dutasteride with linear and non-linear elimination was successfully developed and validated. Dutasteride linear clearance and volume of distribution were related to body weight with standard

Table 1 Population PK model for dutasteride in male subjects with androgenetic alopecia ($n = 309$ subjects)

Parameter	NONMEM estimate	Bootstrap estimate	NONMEM RSE	Bootstrap RSE	Bootstrap 2.5th percentile	Bootstrap 97.5th percentile
Θ_1 (L/h) in TVCL = $\theta_1 \cdot (1 + (AGE-40) \cdot \theta_5) \cdot (BW/70)^{\wedge 3/4}$	0.467	0.462	4.32	4.85	0.420	0.508
Θ_2 (K_m, ng/mL)	1.63	1.52	22.9	33.6	0.567	2.54
Θ_3 (V_{max}, μg/h)	3.66	3.60	9.26	11.8	2.82	4.41
Θ_4 (L) in TVVC = $\theta_4 \cdot (BW/70)^{\wedge 1}$	461	455	5.86	7.44	400	530
Θ_5 (%) in TVCL = $\theta_1 \cdot (1 + (AGE-40) \cdot \theta_5) \cdot (BW/70)^{\wedge 3/4}$	−2.16	−2.19	19.6	20.3	−3.11	−1.28
Variability (CV %)						
Interindividual variability on CL	69.4	67.8	15.8	19.2	53.9	80.7
Interindividual variability on VC	63.2	60.8	19.0	23.1	46.4	73.9
Interoccasion variability on F	16.4	15.7	31.2	35.4	8.12	20.4
Residual variability (proportional)	12.3	12.5	26.3	26.9	7.23	20.2

RSE percentage of relative standard error (100 % * SE/Estimate)

Table 2 Population PK/PD model for change from baseline in 2.54-cm target area hair count ($n = 610$ subjects)

Parameter	Estimate	RSE (%)	95 % CI lower	95 % CI upper
E_{max} for BNHS III or VI and Hispanic countries, hair	134	10.6	106	162
E_{max} for BNHS V and Hispanic countries, hair	192	14.5	138	246
EC50, ng/mL	0.245	53.1	−0.0098	0.500
Θ_1 (hair) in E0 = θ_1 + (BTAHC-760) · θ_2	−7.96	93.6	−22.6	6.64
Θ_2 in E0 = θ_1 + (BTAHC-760) · θ_2	−0.0705	27.0	−0.108	−0.0333
Θ_3 in E_{max}_Non Hispanic Countries = E_{max}_Hispanic countries · θ_3	0.472	14.4	0.339	0.605
Residual variability: σ (additive)	93.2	9.45	85.3	101

RSE percentage of relative standard error (100 % * SE/Estimate); *BTAHC* baseline target area hair count, *BNHS* baseline Norwood–Hamilton score, *E0* placebo effect; *Cluster 1* Argentina, Chile, Mexico and Peru. *Cluster 2* Japan, Philippines, Thailand, Taiwan and Russia

allometric relationships and the linear clearance decreased by 2.16 % for each year increase in age. These effects were not clinically significant and no dose adjustment is recommended.

The effect of dutasteride on DHT was best described by a simple E_{max} model with no covariate with a maximum 91 % decrease from baseline. The effect of dutasteride on hair count was also best described by a simple E_{max} relationship with dutasteride concentration. Hispanic countries and a baseline Norwood–Hamilton score of V were shown to provide higher E_{max}. Both models provided similar concentrations leading to 50 % of maximum effect around 0.2 ng/mL or slightly greater than the concentrations obtained with the 0.02 mg dose of dutasteride. The mean concentrations observed with the 0.1 and 0.5 mg dose would lead to 90 and 99 % of E_{max}, respectively.

References

[1] Olsen EA, Hordinsky M, Whiting D, et al (2006) The importance of dual 5α-reductase inhibition in the treatment of male pattern hair loss: Results of a randomized placebo controlled study of dutasteride versus finasteride. J Am Acad Dermatol 55:1014–1023

[2] Gisleskog PO, Hermann D, Hammarlund-Udenaes M, Karlsson M (1999) Validation of a population pharmacokinetic/pharmacodynamic model for 5 alpha-reductase inhibitors. Eur J Pharm Sci 8:291–299

M-038 Assessment of Adalimumab Dose Selection for Adult Ulcerative Colitis Using Exposure–Response Analyses

Michael Bewernitz[1], Christine Garnett[2,4], Klaus Gottlieb[3], Kevin Krudys[4], Andrew E. Mulberg[3], Aisha P. Johnson[3], Anil Rajpal[3], Yow-Ming Wang[5], Lin Zhou[5], Kevin Bugin[3], Nitin Mehrotra[4,*]

[1]Division of Clinical Pharmacology 1, Office of Clinical Pharmacology (OCP), U.S. Food and Drug Administration (FDA), Silver Spring, MD, USA; [2]Current address: Certara L.P., Saint Louis, MO, USA; [3]Division of Gastroenterology and Inborn Errors Products, Office of New Drugs, FDA, Silver Spring, MD, USA; [4]Division of Pharmacometrics, OCP, FDA, Silver Spring, MD, UDA; [5]Division of Clinical Pharmacology 3, OCP, FDA, Silver Spring, MD, USA

Objectives: On September 28 2012, FDA approved adalimumab (Humira™) for inducing and sustaining clinical remission in adult patients with moderately to severely active ulcerative colitis (UC). Phase 2 dose ranging trials were not conducted to establish the dose of adalimumab for the treatment of patients with UC. However, in one of the two registration trials in UC patients, the sponsor studied two induction doses 80/40 (80 mg, followed 2 weeks later by a dose of 40 mg) and 160/80 (160 mg, followed 2 weeks later by a dose of 80 mg). There was no difference in remission rate observed between adalimumab 80/40 and placebo. In the other registration trial, only the 160/80 mg induction dose was studied. Induction doses higher than 160/80 were not studied. The trial utilized co-primary efficacy endpoints of clinical remission (defined as proportion of patients with a total Mayo score ≤2 with no individual subscore >1) at week 8 (induction of clinical remission) and clinical remission at week 52. The trial demonstrated a statistically-significantly greater proportion of patients presenting induction of clinical remission in the adalimumab arm (41 of 248, or 16.5 %) compared to the placebo arm (23 of 246, or 9.3 %), $p < 0.05$. In view of the relatively modest effect size seen in the trial we hypothesized that a higher dose could have been more effective. Exposure–response analyses were performed by the FDA to assess the appropriateness of the adalimumab dose for the treatment of moderately to severely active UC.

Methods: The data originated from a multicenter, randomized, double-blind, placebo-controlled phase 3 clinical trial to evaluate the efficacy and safety of the human anti-Tumor Necrosis Factor (TNF) monoclonal antibody, adalimumab in patients with UC. There were 258 patients randomized to the adalimumab arm (receiving a 160/80 mg induction dose followed by 40 mg every other week) and 260 patients randomized to the placebo arm. Logistic regression analysis was conducted to assess the relationship between the week 8 trough adalimumab concentration and the probability of achieving clinical remission at week 8. Beginning at week 12, patients who demonstrated an inadequate response switched to open-label 40 mg adalimumab every other week. Kaplan–Meier plots were generated to visualize the relationship between week 8 trough adalimumab concentration and the time until inadequate response. Finally, the relationship between week 8 trough adalimumab concentration and time until inadequate response was assessed with a Cox proportional hazards model. Numerous baseline risk factors (such as age, baseline Mayo score, prior exposure to anti-TNF therapy, weight, etc.) were evaluated in the logistic regression and Cox proportional hazards analyses.

Results: The results of the logistic regression and Kaplan–Meier analyses are presented in Fig. 1.

A statistically-significant ($p = 0.0002$) relationship was established between week 8 trough adalimumab concentration and clinical remission at week 8 (induction phase) using logistic regression (Fig. 1a). Notably, the trend of increasing remission rate with increasing adalimumab concentration does not appear to plateau over the range of observed trough adalimumab concentrations, suggesting that a higher dose may increase the probability of clinical remission at week 8. The relationship between probability of achieving clinical remission per Mayo score at week 8 and week 8 trough adalimumab concentration was also modeled using multivariate logistic regression. The results showed that week 8 trough adalimumab concentration ($p = 0.0003$), baseline Mayo score ($p < 0.0001$), and prior-anti-TNF therapy experience at baseline ($p = 0.025$) were all significantly related to week 8 remission. Patients with higher concentrations have higher probability of induction of clinical remission. Patients with prior anti-TNF therapy experience have a lower probability of induction of clinical remission which is consistent with the observed

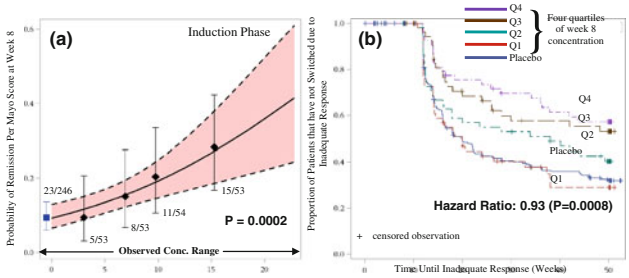

Fig. 1 Panel A: Probability of Remission at Week 8 Increases with Increasing Week 8 Adalimumab Trough Concentration. The predicted mean and 95 % CI interval are represented by the solid and dashed curves as well as the shaded area. The observed remission versus the mean and 95 % CI within observed concentration quartiles are represented by the black diamonds and bars, and the placebo group is represented by the blue square and bars. Panel B: Inadequate Response Occurred Earlier in Patients with Lower Week 8 Concentrations

clinical data. In addition, patients with higher baseline Mayo scores have a lower probability of induction of clinical remission at week 8.

The Kaplan–Meier analysis results (Fig. 1b) indicate that patients with higher week 8 trough adalimumab concentrations sustained their response (i.e. did not exhibit inadequate response) over a longer period of time compared to patients with lower week 8 trough adalimumab concentrations who demonstrate inadequate response earlier. In addition, the proportion of patients who did not demonstrate an inadequate response increased with increasing concentration (32 % for placebo, 29 % for Q1, 40 % for Q2, 53 % for Q3, and 57 % for Q4).

Univariate Cox-proportional hazards analyses were performed to assess the relationship between time to inadequate response and week 8 trough adalimumab concentration as well as various baseline risk factors (such as age, baseline Mayo score, prior exposure to anti-TNF therapy, weight, etc.). The week 8 trough adalimumab concentration ($p = 0.0006$) and prior exposure to anti-TNF therapy ($p = 0.0031$) were statistically significant covariates indicating that patients with lower concentrations or prior exposure to anti-TNF have higher probability of an inadequate response. A multivariate proportional hazards model showed that the week 8 trough adalimumab concentration was a significant covariate ($p = 0.0008$) after accounting for prior exposure to anti-TNF therapy. The hazard ratio for week 8 trough adalimumab concentration (HR = 0.93) indicates that increasing the concentration by 1 μg/mL decreases hazard for inadequate response by 7 %. These results demonstrate that the time to inadequate response (requiring an open-label switch) increases with increasing adalimumab concentration after correcting for potentially confounding risk factors.

A robust exposure–response relationship for clinical remission at week 52 could not be established due to the large number of patient drop outs during the course of the trial and resulting missing PK data.

Conclusions: The pharmacometric analyses presented herein demonstrate that higher week 8 trough adalimumab concentrations are associated with: (1) greater proportion of patients achieving clinical remission at week 8, and (2) increased duration of clinical remission. Given the modest effect size (16.5 % remission induction rate for adalimumab 160/80/40 versus 9.3 % for placebo) and the observation that remission rate does not plateau over the observed concentration range, we conclude that a higher dose for the induction of remission may provide greater benefit to UC patients. These analyses were presented by the FDA review team at the gastrointestinal drugs advisory committee (GIDAC) Meeting on August 28th 2012. A majority (14 of 17) of the GIDAC members voted that the optimal adalimumab dose for UC has not been established, although the dosage studied demonstrated clinical efficacy.

Exposure–response analyses were pivotal in enhancing our understanding the adequacy of the proposed adalimumab induction dosing regimen. Based on the results of these analyses along with the observed clinical data, FDA required the Sponsor to conduct a post marketing clinical trial to evaluate the efficacy and safety of adalimumab induction regimens utilizing doses higher than those previously studied.

References

[1] FDA Slides for Gastrointestinal Disease Advisory Committee Meeting on August 28th, 2012 (http://www.fda.gov/downloads/AdvisoryCommittees/CommitteesMeetingMaterials/Drugs/GastrointestinalDrugsAdvisoryCommittee/UCM318077.pdf)

[2] Meeting minutes for Gastrointestinal Disease Advisory Committee Meeting on August 28th, 2012 (http://www.fda.gov/downloads/AdvisoryCommittees/CommitteesMeetingMaterials/Drugs/GastrointestinalDrugsAdvisoryCommittee/UCM319690.pdf)

[3] FDA briefing document for Gastrointestinal Disease Advisory Committee Meeting on August 28th, 2012 (http://www.fda.gov/downloads/AdvisoryCommittees/CommitteesMeetingMaterials/Drugs/GastrointestinalDrugsAdvisoryCommittee/UCM316786.pdf)

[4] Humira approval letter for UC (http://www.accessdata.fda.gov/drugsatfda_docs/appletter/2012/125057Orig1s232ltr.pdf)

[5] FDA approved package insert for Humira (http://www.accessdata.fda.gov/drugsatfda_docs/label/2012/125057s232lbl.pdf)

M-039 Model-Based Meta-Analysis Informs Phase 3 Head-to-Head Trial Simulations of Brodalumab and Competitors in Psoriasis

David H Salinger[1,*], Jaap W Mandema[2], Richard D Newmark[3] and Megan A Gibbs[1]

[1]Amgen Inc., Seattle, WA, USA; [2]Quantitative Solutions, Menlo Park, CA, USA; [3]Amgen Inc., Thousand Oaks, CA, USA

Objectives: Model-based meta-analysis leverages all publically available competitor trial data to provide a framework for quantitative comparison between compounds for which no head-to-head trials have been performed [1]. Inclusion in the meta-analysis of internal (unpublished) data for a compound under development expands the framework to allow quantitative comparison with marketed competitors and other compounds under development. This modeling can then be applied as the basis for simulation of head-to-head trials with the purpose of exploring suitable sample sizes and probability of superiority (and non-inferiority) success.

Head-to-head trial powering has typically been done assuming a certain difference in treatment effect and variance. Sample size determination based on model-based meta-analysis can provide the following advantages:

- All available data is used (rather than a single chosen "representative" trial result)
- Co-modeling provides a global estimate of placebo rate and normalizes all efficacy results relative to that placebo rate (rather than point estimates)
- Model-based analysis of trials provides a distribution of relative treatment effect (rather than a point estimate) from which to base trial simulations.

Here, we present a case study exploring sample sizes (based on the psoriasis area and severity index; PASI) for prospective head-to-head trials between brodalumab (AMG 827) and ustekinumab (Stelara®) and adalimumab (Humira®) for subjects with psoriasis.

The objectives of this work were to use model-based meta-analysis to determine the time course of the dose–response relationship for PASI50, 75, 90 and 100 % response rates of brodalumab in relation to other compounds (with published clinical trial data) for psoriasis; and to present a case study illustrating how model-based meta-analysis can be used to inform head-to-head trial simulation and optimize phase III trial strategy

Methods: The analysis proceeded in two stages. In the first stage, a model-based meta-analysis (MBMA) of all publically available data from placebo controlled double blind trials of approved (or nearing approval) drugs for psoriasis. Data to inform the meta-analysis was found via literature search (PubMed, etc.) and review of reference

lists from previous meta-analyses, clinicalstudyresults.org, conference abstracts and corporate websites. Internal data from a phase II trial of brodalumab was also included. The included data represented over 14000 subjects in 34 trials of 10 drugs.
The MBMA was accomplished as joint modeling of the probability of achieving PASI 50, 75, 90, 100—by treatment arm of each trial. Placebo and treatment effect were modeled for each drug. The base model assumed a different E_{max} for each endpoint but similar for all drugs. The assumption was tested by allowing different E_{max} by drug class. We evaluated impact of endpoint, drug, drug class, regimen, indication, failure of prior treatment, baseline PASI score, disease duration, age, weight and gender on model parameters. From this MBMA, we derive a distribution of effect difference between treatments of interest.

In the second stage of this analysis, head-to-head trials for brodalumab vs. adalimumab and ustekinumab were simulated based on the distribution of the effect difference between treatments. Trial level assumptions included, most importantly, sample size, but also PASI endpoint, weight distribution, and MBMA modeling assumptions. For each set of trial level assumptions of interest, 10,000 trials were simulated. The probabilities of achieving statistically significant treatment effect outcomes (superiority, non-inferiority, inferiority and inconclusive outcome) were calculated from the 10,000 trials. All tests were done at a one-sided alpha of 0.025 and a non-inferiority margin of 5 %.
Results: For chosen sets of trial level assumptions, plots comparing treatment effect outcome probability vs. sample size were made to illustrate the results. Results of primary interest were also tabled.
Conclusions: We successfully used model-based meta-analysis to characterize the time-course of the dose–response relationship for PASI50, 75, 90 and 100 of brodalumab in relation to competitor drugs.
This case study illustrates how model-based meta-analysis can be used to inform head-to-head trial simulation and optimize phase III trial strategy under various trial level assumptions.

Head-to-head trial simulations allowed for assessment of the probability of success for clinical studies of brodalumab vs. ustekinumab and adalimumab

Reference

[1] Mandema JW, Salinger DH, Baumgartner SW, Gibbs MA (2011) A dose–response meta-analysis for quantifying relative efficacy of biologics in rheumatoid arthritis. Clin Pharm Therapeutics 90(6):766–769

M-040 Population Pharmacokinetics of Pyrazinamide in Patients with Tuberculosis

Abdullah Alsultan[1,*], Kelly E. Dooley[2], Marc Weiner[3], William Whitworth[4], William R. Mac Kenzie[4], Charles A. Peloquin[1] and the Tuberculosis Trials Consortium

[1]University of Florida, Gainesville, FL, USA; [2]Johns Hopkins University School of Medicine, Baltimore, MD, USA; [3]San Antonio VA Medical Center, San Antonio, TX, USA, [4]Centers for Disease Control and Prevention, Atlanta, GA, USA

Objectives: The treatment of active tuberculosis (TB) requires multiple drugs and a treatment duration of at least 6 months. The standard regimen for drug-susceptible TB consists of rifampin, isoniazid, pyrazinamide (PZA), and ethambutol. Of these four TB drugs, PZA is the only one known to be bactericidal against TB organisms in acidic environments [1]. The use of PZA during the first 2 months of TB treatment allows for the shortening of treatment from nine to 6 months. Recent evidence suggests that PZA activity is dose dependent and that maximum concentration (C_{max}) values >35 μg/ml are associated with better efficacy [2]. Higher doses than those currently recommended in the USA (25 mg/kg) might be needed to achieve this C_{max} target. The goal of this study was to determine the proportion of patients with a $C_{max} > 35$μg/ml and to estimate the pharmacokinetics (PK) of PZA among patients enrolled in Tuberculosis Trial Consortium (TBTC) trials 27 and 28.
Methods: The data are from PK sub-studies of TBTC Studies 27 and 28. In both studies, PZA was dosed at approximately 25 mg/kg daily, rounded to the nearest 500 mg. Seventy-two patients participated in the sub-studies. Blood was collected pre-dose then 1, 2, 6, 8, 12 and 24 h post dose. Blood PK sampling was performed after the fourth or fifth dose of PZA, administered under directly observed therapy. Noncompartmental analysis (NCA) was performed with WinNonlin Professional Version 4.0. Population PK analysis was analyzed using nonlinear mixed effect modeling software, Monolix version 3.2.
Results: The median dose patients received in the two studies was 1500 mg. The median (interquartile range) for C_{max} and time to maximum concentration (Tmax) were 29.77 (25.89-34.99) μg/ml and 1 (1-2) h respectively (NCA). Only 18 patients (25 %) had $C_{max} > 35$ μg/ml. A one-compartment model best described PZA PK. Because PZA was rapidly absorbed, and there were limited data prior to two hours post dose, the final population estimate for ka was high. Therefore, ka was fixed at 3, as used in previous studies. Residual variability was described using a combined error model. The median population estimates for total body clearance (Cl/F) and volume of distribution (V/F) were 44.1 L/h and 4.35 L respectively. Significant covariates for PZA's V/F were sex and weight. Only body weight was a significant covariate for PZA clearance. Women had a lower V/F compared to men, and both Cl/F and V/F increased with body weight. Table 1
Goodness of fit plots are shown in Figs. 1 and 2.

Table 1 Final model parameter estimates

Parameter	Median (%RSE)	IIV%
C_{max}	29.77 μg/ml	
T_{max}	1 h	
V/F(L)	44.1 L (5)	10.4
Cl/F (L/h)	4.35 L/h (4)	23
Slope effect of weight on CL/F[a]	0.586 (26)	
Slope effect of weight on V/F[a]	0.792 (13)	
Effect of sex on V/F[a]	0.178 (27)	

IIV inter-individual variability

[a] Reported as mean, RSE: relative standard error

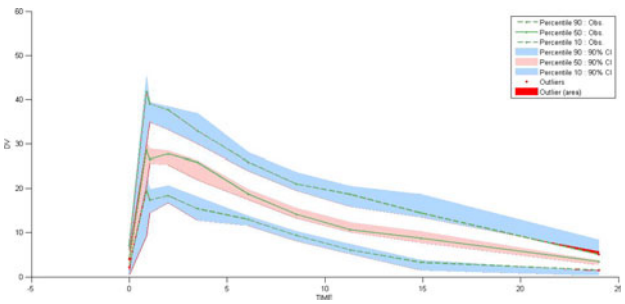

Fig. 1 Visual Predictive Checks

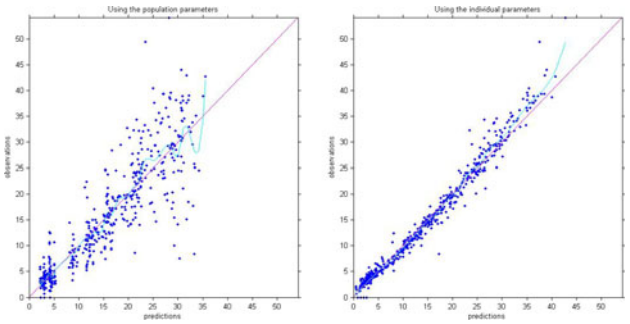

Fig. 2 Observed vs predicted concentrations

Conclusions: Higher doses of PZA than those currently used in the U.S. and globally for TB will be required to achieve the proposed C_{max} target of 35 μg/ml. Sex and weight both significantly affected PZA pharmacokinetics, and patients with higher mg/kg doses were more likely to achieve target concentrations, suggesting that weight-based dosing for this drug is appropriate.

References

[1] Zhang Y and Mitchison D (2003) The curious characteristics of pyrazinamide: a review. Int J Tuberc Lung Dis 7:6–21

[2] Donald PR, Maritz JS and Diacon AH (2012) Pyrazinamide pharmacokinetics and efficacy in adults and children. Tuberculosis 92:1–8

M-041 Population Pharmacokinetics of Levofloxacin in Children Treated for, or Exposed to, Multidrug Resistant Tuberculosis in the Federated States of Micronesia and Republic of Marshall Islands

Daniel Gonzalez[1,2,3,*], Sundari Mase[4], John Jereb[4], Fatma Martin[5], Charles Daley[6], Dorina Fred[7], Kennar Briand[8], Ann Loeffler[9], Terence Chorba[4], Charles Peloquin[1]

[1]University of Florida, Gainesville, FL, USA; [2]University of North Carolina, Chapel Hill, NC, USA; [3]Duke Clinical Research Institute, Durham, NC, USA; [4]Centers for Disease Control and Prevention, Atlanta, GA, USA; [5]North Bay Pediatrics, Vallejo, CA, USA; [6]National Jewish Health, Denver, CO, USA; [7]TB/Leprosy Program, Chuuk, Federated States of Micronesia; [8]TB/Leprosy Program, Ebeye, Republic of Marshal Islands; [9]Francis J. Curry National TB Center, San Francisco, CA, USA

Objectives: Levofloxacin, a fluoroquinolone with gram-positive and -negative coverage, has bactericidal activity against *Mycobacterium tuberculosis* [1–3]. As a result, current treatment guidelines for tuberculosis (TB) advocate a role for fluoroquinolone use in cases of multi-drug resistant TB (MDR TB) as the use of traditional regimens is not feasible [4]. Although the population pharmacokinetics (PK) of levofloxacin has been studied previously in children, no studies have been performed in pediatric patients treated for, or exposed to, TB [5,6]. During two simultaneous outbreaks of TB in the Federated States of Micronesia (FSM) and Republic of Marshall Islands (RMI), PK studies were performed by the Centers for Disease Control and Prevention to characterize the drug disposition in this patient population [7]. The goal of the analyses described herein is to characterize the population PK in 50 children studied during these MDRTB outbreaks.

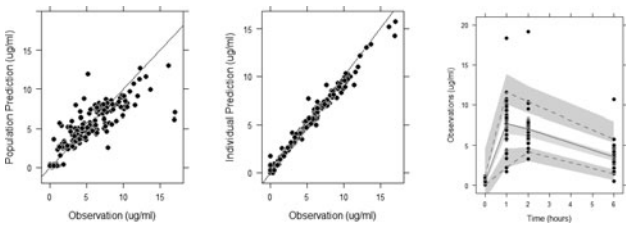

Figs. 1-3 Goodness of fit plots and a visual predictive check for the final population PK model

Methods: In Chuuk, a state in the FSM, 33 children (age 1–14 years) were administered levofloxacin (5–20 mg/kg/day) as an oral gel for the treatment of MDR-TB or presumed MDR latent TB infection (LTBI). In Majuro, the capital of the RMI, during another outbreak, 17 children (1–15 years) were treated with levofloxacin (11–16 mg/kg/day) as an oral gel for LTBI. Following 6 weeks of treatment or longer, plasma samples were taken in all 50 children after 1, 2, and 6 h. In Majuro, a 0-h time point was also taken in all children. Following collection, samples were stored at −70 °C before being shipped on dry ice to University of Florida for analysis using a validated HPLC method with fluorescence detection.

A population PK analysis was performed in the software nonlinear mixed effects modeling (NONMEM, version 7.2). The first-order conditional estimation method with interaction algorithm was used for all models. All collected data was included in the analyses. NONMEM execution and run management was performed using Pirana, while prediction-corrected visual predictive checks (pcVPC) and a bootstrap analysis ($n = 1{,}000$ simulations) was performed using Perl-speaks-NONMEM (PsN). For the bootstrap analysis, the 2.5th and 97.5th percentile were calculated based on the samples generated. Goodness of fit and pcVPCs were generated using the R (version 2.15.2) packages lattice and Xpose. Addition of covariates (age, gender, weight, heigh, and breakfast status) was tested using generalized additive modeling implemented in the Xpose package. One- and two-compartment PK models were tested. A fixed exponent allometric model was applied to both CL/F and V/F using a 70 kg standardized weight. Additive and combined additive with proportional error models were tested. Using the final population PK model, simulations were performed in NONMEM to evaluate target attainment; whereby an area under the free drug concentration versus time curve over the minimum inhibitory concentration (*f*AUC/MIC) ≥100 was evaluated as a target. A total of 1,000 simulations were performed for varying dosing regiments (5, 10, 15, and 20 mg/kg) and target attainment was calculated for various potential MIC values.

Results: A one-compartment body model provided an adequate data fit (Fig. 1). The population parameter estimates for the absorption rate constant (K_A), and the standardized clearance (CL/F) and volume of distribution (V/F) were 2.69 h^{-1}, 11.61 L/h, and 88.39 L, respectively (Table 1). Inter-individual variability estimates in K_A, CL/F, and V/F were 82.5, 33.2, and 24.5 %, respectively. Aside from weight, no other covariates resulted in statistically significant improvements in the data fit. Assuming a conservative drug exposure target, *f*AUC/MIC ≥100, for the lowest assumed MIC (0.25 μg/mL), a dose of 10 mg/kg resulted in a highly likelihood of target attainment; while for an MIC of 0.5 μg/mL, a dose of 20 mg/kg was needed (Table 2). Poor target attainment rates were obtained with higher MIC values.

Conclusions: Levofloxacin may be an effective treatment option for children with MDR-TB or presumed MDR LTBI. Further clinical research is needed to evaluate appropriate targets for PK/PD indices that can be used to optimize drug dosing.

Table 1 Parameter and bootstrap estimates for the final population PK model

	Parameter estimate	RSE (%)	Bootstrap estimate (95 % CI)
Structural			
K_A ($HOUR^{-1}$)	2.69	22	2.77 (1.89–5.31)
CL/F (L/H)	11.61	5	11.61 (10.34–12.82)
V/F(L)	88.39	4	87.86 (80.8–95.26)
Variance			
ω^2 (K_A)	0.68	42	0.69 (0.22–1.43)
ω^2 (CL/F)	0.11	28	0.11 (0.05–0.17)
ω^2 (V/F)	0.06	50	0.06 (0.01–0.11)
Residual			
Proportional	0.02	38	0.01 (0–0.03)
Addittive (μg/ml)	0.08	56	0.1 (0–0.28)

Table 2 Percentage target attainment (%, *f*AUC/MIC $\geq$ 100) for varying levofloxacin dosing regimens (mg/kg) and representative MIC (μg/mL) values for *M. tuberculosis*

DOSAGE/MIC	0.25	0.5	1	2
5	16.3	0.1	0	0
10	100	16.6	0.1	0
15	97.5	57	3.5	0
20	99.7	83.6	16.6	0.1

References

[1] Johnson JL, Hadad DJ, Boom WH, et al (2006) Early and extended early bactericidal activity of levofloxacin, gatifloxacin and moxifloxacin in pulmonary tuberculosis. Int J Tuberc Lung Dis. 10:605–612

[2] Yew WW, Chan CK, Leung CC, et al (2003) Comparative roles of levofloxacin and ofloxacin in the treatment of multi-drug resistant tuberculosis: preliminary results of a retrospective study from Hong Kong. Chest 124:1476–1481

[3] Peloquin CA, Hadad DJ, Molino LP, et al (2008) Population pharmacokinetics of levofloxacin, gatifloxacin, and moxifloxacin in adults with pulmonary tuberculosis. Antimicrob Agents Chemother 52:852–857

[4] American Thoracic Society/Centers for Disease Control and Prevention/Infectious Diseases Society of America (2003) Treatment of Tuberculosis. Am J Respir Crit Care Med 167(4): 603–662

[5] Chien S, Wells TG, Blumer JL, et al (2005) Levofloxacin pharmacokinetics in children. J Clin Pharmacol. 45:153–160

[6] Li F, Nandy P, Chien S, et al (2010) Pharmacometrics-based dose selection of levofloxacin as a treatment of post-exposure inhalational anthrax in children. Antimicrob Agents Chemother 54:375–379

[7] Centers for Disease Control and Prevention (2009) Two simultaneous outbreaks of multidrug-resistant tuberculosis–Federated States of Micronesia, 2007–2009. MMWR Morb Mortal Wkly Rep 58:253–256

M-042 Abatacept Exposure–Response Analysis and its Impact on Dose Selection in Lupus Nephritis

Satyendra Suryawanshi, Michael Tagen, Bindu Murthy, Jan Hillson, Amit Roy

Bristol-Myers Squibb, Princeton, NJ

Background: Recent post hoc analyses of patients participating in a trial of abatacept (ABA) vs. placebo, in combination with mycophenolate mofetil and corticosteroids for treatment of active lupus nephritis (IM101075) have provided an evidence-based rationale for choosing among alternative definitions of complete renal response (CRR) used in recent Phase 2/3 clinical trial in lupus nephritis [1].
Objective: The objective of this analysis was to characterize the relationship between ABA exposure and CRR using these alternative definitions to guide the dose selection for a follow-on Phase 3 study.
Methods: In IM101075, patients with biopsy-proven active, proliferative lupus nephritis were randomized to receive placebo ($n = 100$) or one of two intravenous ABA regimens: 30 mg/kg on Days 1, 15, 29 and 57 followed by $\sim$10 mg/kg every 4 weeks (30/10; $n = 99$), or $\sim$10 mg/kg for the entire 12 months (10/10; $n = 99$). Pharmacokinetic (PK) data collected in the study were analyzed by population PK analysis, and were used to determine various summary measures of exposure (Cavg and C_{min} over Month 1and 3, C_{min} at Month 12 based on clearance observed at Month 1) in each subject. We assessed rates of CRR at 12 months according to 3 sets of criteria, from (1) an ongoing National Institutes of Health trial of ABA (Abatacept and Cyclophosphamide Combination: Efficacy and Safety Study [NCT00774852]), (2) the Aspreva Lupus Management Study trial of mycophenolate mofetil (NCT00377637), and (3) the Lupus Nephritis Assessment with Rituximab (LUNAR) trial of rituximab [2]. The probability of achieving a CRR at 12 months was described by a logistic regression exposure–response (E–R) model. Age, weight, sex and baseline urine protein creatinine ratio (UPCR) were assessed as covariates in the model. LUNAR criteria were selected for further model evaluation based on largest observed difference (CRR of $\sim$6 % in placebo group, compared to $\sim$20–24 % in ABA group). The final model using CRR (assessed by the LUNAR criteria) was applied to predict efficacy in a proposed Phase III trial.
Results: The average model-predicted minimum concentration of ABA over the first month ($C_{min\ (1\ month)}$) was a significant predictor of CRR at Month 12. Higher baseline UPCR was also identified as a positive predictor of CRR at Month 12. There was a strong relationship between $C_{min\ (0–1\ month)}$ and the probability of achieving CRR in nephrotic (UPCR >339 mg/mmol) and non-nephrotic (UPCR $\leq$339 mg/mmol) pts. An association was identified between proteinuria and exposure suggesting that ABA is cleared more rapidly in nephrotic subjects and that ABA exposure increased over time in some nephrotic subjects suggesting that reduction in proteinuria may reduce clearance over time. Model evaluation shows reasonable agreement between model-predicted and observed response rates predicting that there may be incremental benefit from induction with 30 mg/kg of ABA for 57 days. This regimen provides the most benefit compared to placebo over time.
Conclusions: CRR based on LUNAR criteria shows a positive E–R relationship for ABA in the treatment of lupus nephritis and identifies proteinuria as a confounder in dose selection and a target of treatment effect. This supports further evaluation of ABA and dose selection for the treatment of lupus nephritis in an ongoing Phase III study.

References

[1] Wofsy D, et al (2012) Arthritis Rheum 64:3660–3665

[2] Rovin B, et al (2012) Arthritis Rheum 64:1215–1226

M-043 Benefits of an Item Response Theory Based Analysis of ADAS-cog Assessments

Sebastian Ueckert[1,*], Elodie L. Plan[1,2], Kaori Ito[3], Mats O. Karlsson[1], Brian Corrigan[3] and Andrew C. Hooker[1]

[1]Pharmacometrics Research Group, Uppsala University, Uppsala, Sweden; [2]Metrum Research Group, Tariffville, CT, USA; [3]Primary Care Business Unit, Pfizer Inc., Groton, CT, USA

Objectives: Despite an increasing interest in biomarkers, cognition remains the primary regulatory accepted clinical endpoint in Alzheimer's Disease (AD). The most frequently used test, ADAS-cog, consists of a broad spectrum of tasks evaluating cognition [1]. The total ADAS-cog score is obtained by summing up the subscores resulting from rating a subject's performance in each of the subtests. Despite its frequent application, the total ADAS-cog score has a number of practically relevant weaknesses. A major problem is the low sensitivity of the assessment in mild cognitive impairment (MCI) patients and severe AD patients and the consequential necessity to adapt the assessment. This adaptation is often not only heuristic in nature but also reduces the ability to compare results across trials. Additionally, a potential bias arises if a subject refuses to perform one or more tests and a subscore has to be imputed.
The objective of this work was to develop an alternative method to analyze ADAS-cog assessments data with the ability to combine data from different assessment variants and without the need to impute subscores. Furthermore, the possibility to determine the most informative ADAS-cog variant for a specific population was to be investigated.
Methods: Data: Baseline ADAS-cog assessments with item level data from the Alzheimer's Disease Neuroimaging Initiative (ADNI) [2] and the Coalition Against Major Diseases (CAMD) [3] databases were used to estimate model parameters in the developed IRT model. In total the data consisted of 2651 subjects from 7 studies with a total of 152313 baseline observations.
Data Analysis: Based on the statistical framework of item response theory (IRT), each test was interpreted as a surrogate measure for the hypothetical unobserved variable "cognitive disability". For each subtest of the cognitive assessment, depending on the nature of the arising data, a binary, count or ordered categorical model was developed, describing the probability of a failed test outcome as a function of the latent cognitive disability. All parameters characterizing the individual subtest were expressed as fixed effects, whereas the cognitive disability was modeled as a subject specific random effect. The model performance was evaluated through comparison of observed and simulated data for each subtest.
Optimal Test Design: From the developed IRT model, the Fisher information for estimating a patient's cognitive disability was calculated for each item in the ADAS-cog test. The test items were ranked by information content within a mild cognitively impaired (MCI) and a mild AD (mAD) patient population. Furthermore, the additional amount of information added to an ADAS-cog assessment through incorporation of additional components ("delayed word recall" and "number cancellation") were evaluated in both populations.
Results:ADAS-cog IRT Model: The final ADAS-cog IRT model consisted of 39 binary, 5 binomial, 1 generalized Poisson and 5 ordered categorical submodels with a total of 166 parameters. Simulations from each of the models were in excellent agreement with the observed data. All but one estimated characteristic curves for the test items were well defined with a low failure probability for healthy subjects and high failure probability for severely impaired patients. Only the characteristic curve for the task "state your name" was essentially flat.
Optimal Test Design: The information content ranking of the subcomponents in a classical ADAS-cog assessment differed between the two patient populations. For the MCI population the word recall component was most informative, while for the mAD population the orientation component carried most information. Similarly, there was an apparent difference in the relative amount of information added by including the "delayed word recall" and "number cancellation" components. With the additional components, the information content of the complete ADAS-cog assessment increased by 78 % in the MCI population compared to only 35 % for the mAD population.
Conclusions: By treating each item of the ADAS-cog assessment as a measurement for "cognitive disability", the approach presented in this work takes into account each single item response instead of only one summary score. As a consequence, the assessment data from different ADAS-cog variants can easily be combined in a common analysis and results from one variant can be translated to another. Missing subscore data due to refusal of a subject or omission by a physician does not bias the outcome but are reflected in an increased uncertainty of the analysis. Furthermore, the availability of individual response functions for each test item allows for explicit quantification of the information content of the individual components as well as the ability to adapt a cognitive assessment test to a specific patient population's degree of disability. A population specific test would not only be more sensitive to changes due to disease progression or drug effect, but also reduce the assessment time and thus burden for the patient.

References

[1] Rosen WG, Mohs RC, Davis KL (1984) A new rating scale for Alzheimer's disease Am J Psychiatry 141(11):1356–1364
[2] ADNI (Alzheimer's Disease Neuroimaging Initiative). http://www.adni-info.org/
[3] CAMD (Coalition Against Major Disease). http://www.c-path.org

M-044 The use of Bayesian MCMC Methods on Development of Tools to Predict the Impact of Immunogenicity on Pharmacokinetics

Steven Kathman[1,*], Peiming Ma[2], Lei Zhou[1], Theingi Thway[1], Naren Chirmule[1], Vibha Jawa[1]

[1]Amgen, Thousand Oaks, CA, USA; [2]GlaxoSmithKline, Shanghai, China

Objectives: Development of therapeutic proteins (TP) involves the understanding of dose-exposure-efficacy, and safety/toxicity relationships. These analyses are complex due to the multi-factorial effects of, for example, nonlinear pharmacokinetics (PK) that can be caused by saturable target-mediated drug disposition. The induction of immune responses introduces additional complexities to achieving this understanding. Given the substantial increase in the number of biological products, including biosimilars, there is a need to quantify and predict the effects of immunogenicity and any resulting changes in TP pharmacokinetics. The primary objective of this work is to examine the utility of population-based modeling and simulation approaches for investigating the development of immunogenicity and assessing its impact on TP pharmacokinetics. Potential uses of the

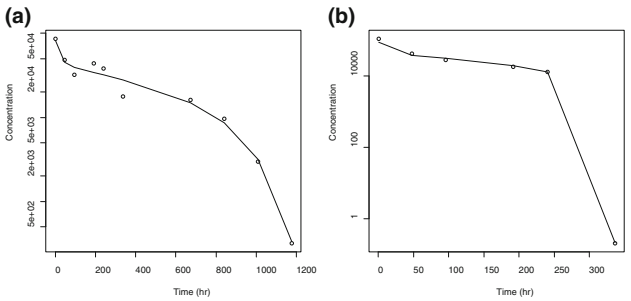

Fig. 1 Example model fit plots for two individual animals. (a) an animal that did not develop antibodies. (b) an animal that developed antibodies

resulting models include: assessing the impact of anti-drug antibodies (ADA) on PK as a means of determining exclusion criteria when calculating exposure metrics, determining whether concentration values from animals with low magnitude of ADA should be excluded from exposure calculations, and addressing the technical limitation of drug interference on preclinical assays at early time points by providing the impact of ADA even with a lack of actual analytical ADA data.

Methods: Using data from two separate studies of single intravenous infusion into cynomolgus monkeys, models were developed to assess the development of immunogenicity and its impact on pharmacokinetics.

The first study was a single dose infusion of antibody clones from a fully human monoclonal antibody. The same dose level was given to all animals. There were five separate clones included in this study; each clone had a different complementary determining region sequence and binding affinity to the target, but identical framework sequences. Up to eleven PK samples were taken from 0.5 to 1176 h post dose from each subject. Four ADA serum samples were collected at 168, 336, 504, and 672 h post dose.

The second study involved a single dose regimen with a range of doses of a single antibody clone given to different animals. This clone had not been evaluated in the first study, but did have the similar target as above tested clones. Up to ten PK samples were taken from 0.5 to 1176 h post dose from each subject. Sparse sampling, at two or three time points post dose, was utilized for the assessment of ADA.

The model developed for these studies was a two-compartment simplified target-mediated disposition model [1]. The expression for the clearance included a linear and nonlinear (Michaelis–Menten) term. The linear term of the model was allowed to change at a particular point in time, presumably due to the presence of antibody formation. The probability that the clearance changes and the time at which the clearance changes were estimated in the model. These estimates were then compared to the actual time at which antibodies were detected, to explore whether or not the changes in clearance could be due to antibody formation. The differential equation for the central compartment of this model is as follows:

$$dC/dt = \text{Input} - (CL * I(t < \alpha) + \eta * I(t > \alpha)) * C/V - (V_{max}/(KM + C)) * C/V + Q/V * (C_2 - C)$$

where C is concentration in the central compartment, C_2 is the concentration in the peripheral compartment, CL is the linear clearance term prior to time = α, η is the linear clearance term after time = α, α is the estimated point at which the clearance term changes, Vmax is the maximum nonlinear elimination rate, KM is the Michaelis–Menten constant, V is the volume of distribution for the central compartment, and Q is the inter-compartmental clearance.

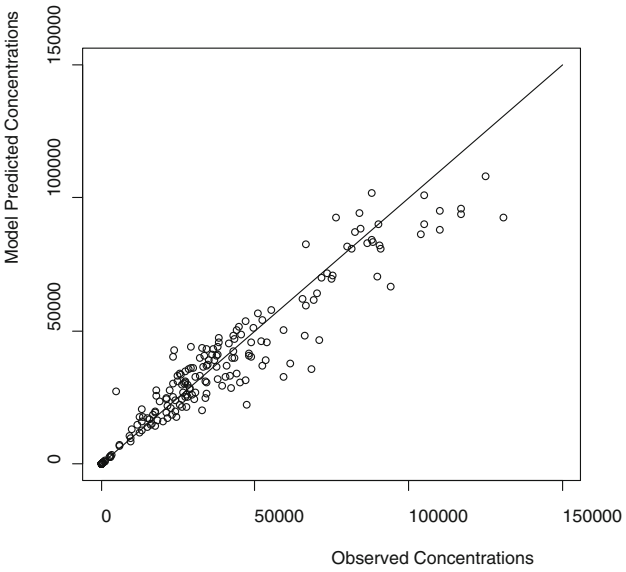

Fig. 2 Observed concentration versus model predicted concentrations (based on medians from Bayesian posterior simulations)

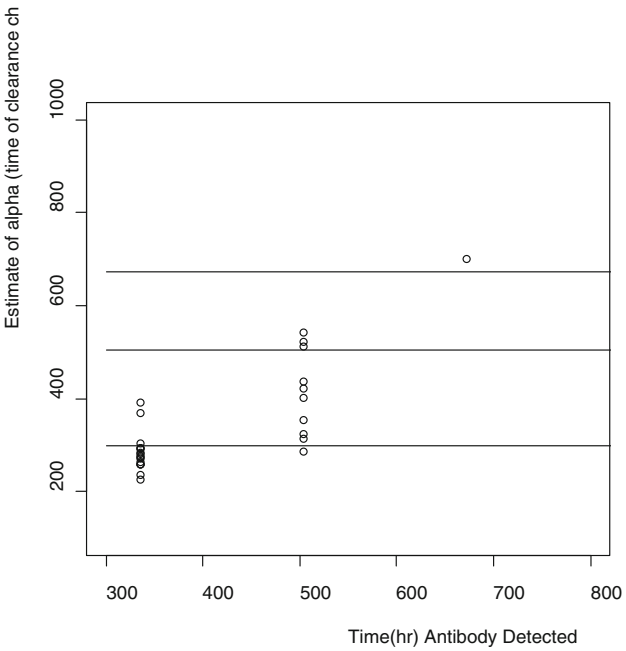

Fig. 3 Time the antibodies were detected versus the estimated time of linear clearance change (median of the posterior distribution)

The model was fit using Bayesian Markov-Chain Monte Carlo (MCMC) methods within the WinBugs software (http://www.mrc-bsu.cam.ac.uk/bugs/welcome.shtml). The WBDiff add-on was used to solve the differential equations. Non-informative prior distributions were used for each of the unknown terms in the model.

The five clones (from the first study described above) were analyzed together in a single hierarchical model, with the clones representing an additional level in the hierarchy. This approach is the same as that typically used in model based meta-analyses.

Results: For both studies, individual plots reveal that the model fit the data well. Figure 1 shows examples of concentration–time profiles

and model fits from the first study. Figure 1a illustrates the model fit for an animal that did not develop antibodies while Fig. 1b illustrates the model fit for an animal that did develop antibodies. Figure 2 shows the actual concentrations versus the model predicted concentrations from the first study to further illustrate the model fit. Similar results are seen with the second study.

Figure 3 shows the actual time of antibody detection versus estimated time of clearance change for the animals that had antibodies detected in the first study. In most instances, the estimated time at which the clearance changed was close to or before the actual time at which the antibodies were detected. There were two animals that did not have antibodies detected in this study. One had an estimated time for clearance change of 767 h (the last sample for ADA detection was 672 h). The other animal had a probability of 0.95 that their clearance did not change. Similar results were seen for the second study.

Conclusions: The Bayesian MCMC method offers a novel and rigorous approach to investigate the impact of immunogenicity on biologic PK by evaluating the onset time and magnitude of the ADA signal.

Reference

[1] Ma, P (2012) Theoretical considerations of target-mediated drug disposition models: simplifications and approximations. J Pharm Res 29:866–882

M-045 A Model for Maturation of Renal Function in Pediatric Population Developed from the Clearance of Vancomycin and Gentamicin

Hong Lu*, Sara Rosenbaum

Department of Biopharmaceutical Science, University of Rhode Island, Kingston, RI, USA

Objectives: Population modeling in pediatric pharmacokinetic (PK) studies often uses size and age as covariates. Covariate-parameter correlations are described in simple exponential relationships used by allometric scaling. However, extrapolations based on such parameter estimates have limited value due to the differences in the impact of developmental growth across populations [1]. The quantitative models used to describe the clearance maturation processes across the age range may be required to improve extrapolation and predictive performance. The aim of this study is to use previously published pharmacokinetic parameters from two renal excreted drugs (due to glomerular filtration), gentamicin and vancomycin, to develop a model for the maturation of renal clearance. The post conception age (PCA) is used as the variable in the modeling practice.

Methods: A literature search (MEDLINE, 1976-present) were conducted to find references or publications describing pharmacokinetics of vancomycin and gentamicin in children, using words such as, neonate, infant, children and crossing these with terms such as drug names, pharmacokinetics. Additionally, a variety of pediatric pharmacology reviews were examined. Through these sources, a database of age-dependent observed clearances for 2 therapeutic probes was created. A developmental renal excretion model was developed for both gentamicin and vancomycin clearance using the following equation [2, 3]:

$$CL_i = CL_{std} \times \left(\frac{w_i}{70}\right)^{0.75} \times \frac{PCA^{\theta}}{Tcl^{\theta} + PCA^{\theta}}$$

CL_{std} is a population clearance estimate standardized to a 70 kg person; Tcl is a parameter describing the age (PCA) to reach 50 % of standardized adult CL value; and θ is the Hill coefficient. The allometric weight scaling describes the size effect and the Hill function in this equation is used as an empirical capacity limited model for the maturation of renal function. The predictive performance of the model was assessed by visual inspection of fits and precision of estimates.

Results: The age-dependent clearance datasets included PK studies on neonates, young infants, children, adolescents and adults. The population clearance (CL) estimates for gentamicin and vancomycin were 111 and 93.5 mL/min/70 kg, separately. The time to reach 50 % of adult clearance was 11 months (PCA) for gentamicin and 9.5 month (PCA) for vancomycin. By 1 year of age, both vancomycin and gentamicin clearance had attained more than 90 % of the adult level. The two renally excreted compounds presented similar developmental profiles when the percentage fractions of adult clearance were plotted versus PCA.

Conclusions: Use of the developmental renal excretion model to quantify renal GFR—mediated gentamicin and vancomycin clearance resulted in similar parameter estimates and maturation profiles, suggesting that this model may be applicable to other drugs via renal glomerular filtration across the age range from newborn to young adults.

References

[1] Cella M, et al (2011) Paediatric drug development: are population models predictive of pharmacokinetics across paediatric populations? Br J Clin Pharmacol 72(3):454–464

[2] Anderson BJ, Holford NH (2008) Mechanism-based concepts of size and maturity in pharmacokinetics. Annu Rev Pharmacol Toxicol 48:303–332

[3] Tod M, et al (2001) Pharmacokinetics of oral acyclovir in neonates and in infants: a population analysis. Antimicrob Agents Chemother 45(1): 150–157

M-046 Physiological Model Qualification Best Practices

Karim Azer[1,*], Stefan Willmann[2], Antonio Cabal[3], Thomas Kerbusch[4]

[4]Merck, Rahway, NJ, USA; [2]BTS, Leverkusen, Germany, [3]Merck, Upper Gwyned, PA, USA; [4]Merck, Oss, The Netherlands

Objectives: Our goal is to establish a framework that would allow for the qualification of physiological models and their effective communication internally to senior management and development teams at Merck and externally to regulatory authorities for decision-making.

Methods: As in many other industries, the use of models is very common in the pharmaceutical research and development process. Throughout various stages of this process, valuable information is obtained using in vitro (e. g. based on tissue samples, cells, or cell components) or in vivo models (e. g. laboratory animal models and humans). In the past 20 years, computational models (sometimes referred to as in silico models) have entered the drug development process and become an increasingly accepted pillar in drug research and development. Among the computational models, physiological models form an important subset. This class of models is characterized by the incorporation of a substantial amount of relevant prior physiological knowledge and data (see definition below). Such physiological models are currently used in drug discovery and development programs to enable decisions. The ability to qualify models and model results is essential for the use of physiological models in enabling internal decisions and incorporation of physiological

model sections into regulatory interactions and submissions. However, there is limited guided or deliberate effort for qualifying developed models.

Model qualification involves both technical and scientific qualification. Once a model is in place, *technical qualification* seeks to ensure that model formulation is accurately translated into a computer code, and that the numerical solution of the model is accurate. *Scientific qualification* is the process of identifying and describing the question that a model is to be used for, as well as appropriately formulating a model with acceptable assumptions and limitations. In some computational fields, this distinction is referred to as model validation (scientific aspects) vs. model verification (technical aspects). In this presentation, we will be concerned with the scientific qualification of models. We opt to use the terminology "qualification" instead of "validation" because it emphasizes that models are built to be fit for purpose, and that models may be regularly updated or improved with the advent of emerging data or advancements in scientific knowledge and thinking. Hence, despite assumptions made, limitations in the model, or incomplete representation of the complete physiology or biology, a model can still provide added value within a well-defined scope.

Results: It is important that the scope of the modeling activity, which is typically a scientific question that is to be addressed, is well defined at the beginning of the model development phase. Since a model is designed to be fit for a purpose, this purpose needs to be clearly described and a set of questions that need to be addressed clearly defined. Once the background and associated questions are identified, a discussion of whether a model can be used to address the questions at hand needs to take place. We will be focused on the case where a physiological model is identified, as part of this discussion, to help address the questions being raised by the development or discovery team. Subsequently, one needs to understand how the model will contribute to addressing questions being raised. Upon establishing this link between the modeling effort and the questions being raised, we will review topics that we propose to be addressed and documented, as part of the qualification process.

The guidance for model developers will be exemplified using two published physiological models. One of these models is the glucose-insulin model (GIM) of Dalla-Cobelli and co-workers. The model of Dalla-Cobelli and co-workers has been used as a decision support system for insulin dosing in type 1 diabetic patients. It is further applied in the context of glucose sensor evaluation and for the preclinical testing of control strategies in artificial pancreas studies. Several implementations of this model are available from commercial vendors. The second model we will review is a finite element model of bone strength by Cabal et al. [1] The model uses micro-architecture images of the wrist bone and uses finite element methods to estimate the strength of the bone in silico.

Conclusions: Physiological models are currently used in drug discovery and development programs to enable decisions. We have developed a framework for the qualification of physiological models in the context of drug discovery and development. The adoption and application of this framework will support the goals of effective physiological model development, communication and increased acceptance of physiological models to enable critical decisions in the discovery and development environments.

References

[1] Cabal A, et al (2012) High-resolution peripheral quantitative computed tomography and finite element analysis of bone strength at the distal radius in ovariectomized adult rhesus monkey demonstrates efficacy of odanacatib and differentiation from alendronate. JBMR (submitted)

[2] Dalla Man C, Raimondo DM, Rizza RA, Cobelli C (2007) Meal simulation model of the glucose-insulin system. IEEE Trans Biomed Eng 54(10):1740–1749

M-047 Population Pharmacokinetic Analysis of Plasma, Cerebrospinal Fluid, and Brain ELND005 in Patients with Mild to Moderate Alzheimer's Disease

Earvin Liang[1], Michelle Green[3,*], Li Yan[3], Jonathan Wagg[3], Jesse Cedarbaum[2], Susan Abushakra[1]

[1]Elan Pharmaceuticals, South San Francisco, CA, USA; [2]Bristol-Myers Squibb, Wallingford, CT, USA; [3]Pharsight, a Certara Company, Sunnyvale, CA, USA

Objectives: ELND005 (scyllo-inositol) is being investigated as an orally administered agent to treat Alzheimer's Disease (AD). The objective of this analysis was to develop a population pharmacokinetic (PK) model to describe plasma, cerebrospinal fluid (CSF), and brain ELND005 concentration profiles following multiple oral doses.

Methods: ELND005 or placebo was administered twice daily for 78 weeks to 351 mild to moderate AD patients randomized to placebo ($n = 83$), 250 mg ($n = 88$), 1000 mg ($n = 89$) or 2000 mg ($n = 91$). Sparse plasma samples were collected from all patients ($n = 351$) and cerebrospinal fluid (CSF) samples were collected via lumbar puncture from a subset of subjects ($N = 20$–26/dose), both of which were analyzed for ELND005 via validated liquid chromatography–tandem mass spectrometry. Brain ELND005 levels from a subset of subjects ($N = 25$–26/dose), estimated by Magnetic Resonance Spectroscopy, were considered for brain PK modeling. Population PK and statistical methods were conducted following the FDA Guidance for Industry Population Pharmacokinetics and the EMA Guideline on Reporting the Results of Population Pharmacokinetic Analyses. To help inform the PK model structure, plasma and CSF ELND005 PK data from two Phase 1 studies in healthy subjects were pooled with the Phase 2 AD patient data. The structure of the model for the human brain PK compartment was also informed by prior analyses of preclinical brain ELND005 PK data obtained from mice and rat studies.

Results: Plasma concentrations of ELND005 were adequately characterized by a 2-compartment population PK model with zero-order input and first order elimination from the central (plasma) compartment. Apparent ELND005 plasma clearance was inversely related to estimated creatinine clearance. CSF ELND005 levels were well described as a function of the concentration of ELND005 in a third compartment (CSF), in series with the plasma compartment. Brain ELND005 levels were well described by a fourth compartment (brain), in series with the plasma compartment and in which transfer from plasma to the brain compartment occurred via a saturable transport process.

Conclusions: The final population PK model can be properly constructed and characterized as moderate absorption, rapid distribution into peripheral compartments, slow redistribution into central compartment, slow apparent clearance, and long apparent terminal half-life. CSF and brain levels of ELND005 were dependent on plasma ELND005 concentration with relatively slow clearance from the brain compartment.

The resultsin this abstract (with slight revision) have been previously presented in part at International Conference on Alzheimer's Disease (ICAD), July 2011, Paris, France and published in the conference proceedings as abstract P2-509.

M-048 A Dose Adaptation Approach of Methylphenidate for Children with Attention Deficit Hyperactivity Disorder (ADHD)

Guillaume Bonnefois[1,*], Olivier Barrière[1], Jun Li[1,2], Fahima Nekka[1,2,3]

[1]Faculté de pharmacie, Université de Montréal, Montréal, QC, Canada; [2]Centre de Recherches Mathématiques, Université de Montréal (CRM), Montréal, QC, Canada; [3]Centre for Applied Mathematics in Bioscience and Medicine, McGill University, Montréal, QC, Canada

Objectives: Attention deficit hyperactivity disorder (ADHD) is a serious neuro-behavorial disorder that affects up to 12 % of children worldwide. Stimulant medications have been used for about 50 years, with methylphenidate (MPH) as the main agent. A variety of oral formulations are made available under immediate, to circumvent known limitations of immediate release, while keeping its advantages [1].
Indeed, immediate release formulations have shown problems in terms of effectiveness duration, patient compliance and issues of privacy and inconvenience caused by frequent administration outside home. In the current practice, three levels of doses, from high to medium to low, are prescribed, in alignment with the observed therapeutic effect.

In this study, we propose a computational strategy of dose adaptation using a Population pharmacokinetic (Pop-PK) approach to identify the most efficient PK profile of immediate release MPH.
Methods: Inspired by these practical problems, we will apply our recently developed methodology to investigate the best dosing regimen of MPH using a grid search for best dose and time schedules. With the aim to reduce the considerable constraints related to the MPH use, we will base our work on a reported Pop-PK model [2] to investigate the use of PK as informative surrogate to enhance the predictability of therapeutic effect, using clinical data for doses and reported effect scales.
Results: The developed computational algorithm was applied to delineate drug regimens in terms of their efficacy without recourse to direct blood sampling.
Conclusions: The generated methodology and knowledge can be translated to help designing new drug formulation and used to develop educational tools.

References

[1] Swanson et al (1999) Acute tolerance to methylphenidate in the treatment of attention deficit hyperactivity disorder in children. Clin Pharmacol Ther 66(3):295–305

[2] Shader et al (1999) Population pharmacokinetics of methylphenidate in children with attention-deficit hyperactivity disorder. J Clin Pharmacol 39(8):775–785

M-049 Population Pharmacokinetic Model for Azithromycin (AZI) in Blood, Peripheral Blood Mononuclear Cells (PBMCs), and Polymorphonuclear Cells (PMNs) of Healthy Adults

Mario Sampson[1,*], Teodora Pene Dumitrescu[2], Kim L.R. Brouwer[1], Virginia Schmith[2]

[1]University of North Carolina Eshelman School of Pharmacy, Chapel Hill, NC, USA; [2]GlaxoSmithKline, Research Triangle Park, NC, USA

Objectives: AZI, a macrolide, is under investigation as an anti-inflammatory agent. AZI accumulates in white blood cells, distributes extensively into tissues, and is eliminated primarily by biliary excretion. Intracellular accumulation is thought to be due to lysosomal trapping. Data suggest that AZI accumulates more in inflamed than non-inflamed tissues. Previous studies have not simultaneously modeled concentrations in blood, PBMCs, and PMNs over time. The purpose of this study was to develop a model to describe the distribution of AZI between whole blood and pro-inflammatory cell compartments, and to characterize the inter-individual variability in parameter estimates.
Methods: AZI was administered to 20 healthy adults as a single, 250 mg or 1000 mg oral dose. Blood samples were collected pre-dose, and at specified times for three weeks post dose. PBMCs and PMNs were isolated from blood using density gradient centrifugation. Drug concentrations were measured in blood, PBMCs, and PMNs by tandem mass spectrometry. Data were analyzed by nonlinear mixed effects modeling using Phoenix NLME 2.1. Model evaluation consisted of bootstrapping ($n = 1000$) and visual predictive check ($n = 1000$).
Results: The dataset was well described by a four-compartment mamillary model with first-order absorption, first-order elimination from the central (Comp1) and small peripheral ("cellular", Comp2 and Comp3) compartments, and bidirectional distribution between the central compartment and large peripheral ("tissue/rest of body", Comp4) compartment (Fig. 1). Blood concentrations were modeled as the sum of concentrations in each compartment multiplied by a coefficient (Eq. 1). Population central clearance (CL1) and volume of distribution (V1) were 67.3 L/h and 336 L, respectively. Peripheral compartment volumes of distribution (V2, V3, and V4) were 0.62,

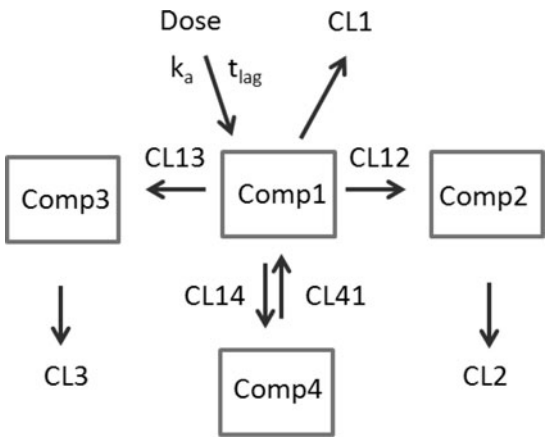

Fig. 1 Structural Model

2.96, and 4597 L, respectively. Inter-subject variability in Ka, CL1, distributional CL (CL12/CL13), V1, V2, and V3 were 41, 114, 75, 122, 51 and 53 %, respectively. Twenty of 23 model parameters exhibited <10 % difference (no parameters >20 % difference) between model estimate and bootstrap median estimate. In the visual predictive check for blood, PBMC, and PMN, 12.3, 9.7, and 6.7 % of observed concentrations were outside the 90 % prediction interval, respectively.

Conclusions: AZI distribution between blood, PBMCs, and PMNs was well-described by a four-compartment model. Parameters were estimated precisely and there was good overlap between observed and simulated datasets. Future directions include using this model to simulate AZI blood, PBMC, and PMN concentrations under various dosing regimens used in inflammatory conditions.

Funding: This work was supported by T32GM086330 from the National Institute of General Medical Sciences.

$$\text{Cblood} = \text{A} * [\text{Comp1}] + \text{B} * [\text{Comp2}] + \text{C} * [\text{Comp3}], \quad (1)$$

where Cblood is the blood concentration, and A, B, and C are estimated (A, B) or fixed (C) coefficients multiplied by the concentration in the respective compartment.

M-050 Population Pharmacokinetic Analysis of a Novel Pan-HER Inhibitor, HM781-36B, in Patients with Advanced Malignant Solid Tumors

Yook-Hwan Noh*, Hyeong-Seok Lim, Kyun-Seop Bae

Ulsan University College of Medicine, Asan Medical Center, Seoul, South Korea

Objectives: HM781-36B is an orally active inhibitor of human epidermal growth factor receptors HER1, HER2, and HER4 tyrosine kinase. The objectives of this work were to quantitatively describe the pharmacokinetic (PK) characteristics of HM781-36 in Phase I oncology patients and to evaluate the potential sources of its PK variability.

Methods: The HM781-36 population PK analysis were performed using the data from three phase I clinical studies, which included 1933 HM781-36 plasma concentrations from 58 patients with advanced solid cancers (101 PK study: 39 patients, 102 PK study: 11 patients, 102 food effect PK study: 8). In 101 PK study, HM781-36B was administered once-daily oral doses ranged from 0.5 to 32 mg (0.5, 1, 2, 4, 8, 12, 16, 20, 24 and 32 mg/day) and were given for 14 days. Blood samples for PK were collected up to 24 h on the first dosing day and up to 48 h after the last dosing. In 102 PK and 102 food-effect studies, HM781-36B was administered with once-daily oral doses ranged from 12 to 24 mg (food effect study—16 mg only) and was given for 28 days. Blood samples for PK were collected up to 24 h on the first and last dosing day. Plasma HM781-36 concentrations were analyzed using liquid chromatography-mass spectrometry. PK analyses were performed by non-compartment method, as well as compartmental method. Nonlinear mixed effects modeling for the population pharmacokinetic analysis of HM781-36 was performed using NONMEM version 7.2 with ADVAN2 subroutine and a combined exponential and additive error model to estimate the residual unexplained error. The model selection was based on the generated objective function value (OFV) and diagnostic plots. The robustness of the final model was evaluated using a bootstrap procedure and model stability and appropriateness using numerical and visual predictive checks.

Results: A one-compartment model with first order absorption and mixed residual error model best described the pharmacokinetic data. The final base model predicted a population apparent clearance (CL/F) of HM781-36 of 16.74 L/h. The absorption rate constant, central volume of distribution, and apparent clearance were 1.69 h^{-1} (between-subject variability, BSV: 10.7 %), 120 L (BSV: 4.8 %), and 16.7 L/h (BSV: 4.3 %), respectively. The model fitted well with the observed data, and the bootstrap and predictive checks guaranteed robustness and appropriateness of the population pharmacokinetic model. No significant relationship was observed between PK parameters and patient demographics.

Conclusions: A population pharmacokinetic model for HM781-36 in patients with advanced malignant solid tumors has been developed. This model will be used as HM781-36 basic drug model for dose individualization and adjustment and for designing later Phase II and III clinical trials. This study provided a rationale for further clinical evaluation of HM781-36B.

Reference

[1] JaeWoo Kim, Kyun-Seop Bae (2011) Pharmacokinetics of the pan-HER inhibitor, HM781-36B, in patients with advanced malignant solid tumors (Abstract), JSCPT-KSCPT-ASCPT Joint conference 2011 and the 32nd JSCPT Annual Scientific meeting

M-051 Estimability of Transit Compartments Model Parameters From Steady State Pharmacokinetic Data

Ying Zhang*, Wojciech Krzyzanski

Department of Pharmaceutical Sciences, State University of New York at Buffalo, Buffalo, NY, USA

Objectives: The transit compartments model is commonly used to describe a delay in signal processing. The number of transit compartments can be determined by trial and error or by estimation when applying the gamma function [1]. The objectives of this study were to assess the performance of the gamma function for estimation of the number of transit compartments, assess the bias and precision of the parameter estimates, and verify utility of the steady-state concentration data for parameter estimation.

Methods: The transit compartments model was used to describe a delay between the site of drug administration and the central compartment with a first-order elimination. 100 replications of drug concentration at the central compartment were generated at nine time points with single dose administration, and fourteen time points with multiple dose administration for steady state and washout using the transit compartments model with varying compartment number N and three levels of residual error CV % = 5, 10 and 20 %. Additional PK parameters included mean transit time (τ), volume of distribution (V), and clearance (CL). The model parameters were estimated for each scenario using the Phoenix WinNonlin. The bias and precision of parameter estimates were examined. The bias was calculated as (Q2-True)/True × 100 %, and the precision was (Q3–Q1)/True × 100 %, where Q1, Q2, Q3 denote the quartiles of the parameter estimates distribution.

Results: The precision of parameter estimates improved with decreasing residual error. The bias decreased with decreasing residual error. For the multiple dose administration in the model with 4 transit compartments and the 10 % residual error, the percent bias of PK parameters ranged: −0.13–25.21 and −0.45–0.27, for steady state only data set and steady state with washout data set, respectively. The percent precision ranged: 4.86–135.79 and 5.38–26.4 for steady state only data set and steady state with washout data set, respectively.

The steady state data did not allow accurate resolution of *N*. This flaw can be resolved by addition of washout data. The correlation coefficients between *N* and τ were about 0.95 across all scenarios.
Conclusions: The estimates of the number of compartments in the transit compartments model can be obtained from steady-state PK data with washout, but not steady state data alone. We provide explicit solutions for transit compartments with bolus input allowing implementation of gamma function method for single dose administration and steady state plasma concentration data.

Reference

[1] Savic RM, Jonker DM, Kerbusch T and Karlsson MO (2007) Implementation of a transit compartment model for describing drug absorption in pharmacokinetic studies. J Pharmacokinet Pharmacodyn 34:711–726

T-001 Bridging Sunitinib Exposure and Time-to-tumor Progression in Hepatocellular Carcinoma Patients by Mathematical Modeling of an Angiogenic Biomarker

Sihem Ait-Oudhia[1,*], Donald E. Mager[1], Robert M. Straubinger[1], Garin Tomaszewski[2], Adrienne Groman[2], Patricia Zagst[2], Gerald Fetterly[2] and Renuka Iyer[2]

[1]State University of New York at Buffalo, Buffalo, NY 14260, USA; [2]Roswell Park Cancer Institute, Buffalo, NY 14263, USA

Objectives: Hepatocellular carcinoma (HCC) is the third leading cause of death worldwide and therapy is a significant unmet medical need [1]. Sunitinib (SU) is a selective tyrosine kinase inhibitor of the angiogenic biomarker soluble vascular endothelial growth factor receptor-2 ($sVEGFR_2$) [2]. SU failed its primary overall survival endpoint in patients with advanced HCC in a phase III trial compared to Sorafenib [3]. The current work applies PK/PD modeling to analyze and link drug exposure and $sVEGFR_2$ dynamics to tumor growth inhibition (TGI) and time-to-tumor progression (TTP). Our analysis suggests that (i) the concentration of active drug (i.e., sunitinib and metabolite) inhibits the release of $sVEGFR_2$ from endothelial cells, thus leading to TGI, and (ii) daily $sVEGFR_2$ exposure is likely a reliable predictor for the TTP endpoint in HCC patients. Moreover, this work provides one of the first quantitative links between the dynamics of a surrogate biomarker of angiogenesis and TTP, and predicts with fidelity the clinical results observed in the placebo arm.
Methods: Data were obtained from 16 patients with unresectable HCC enrolled in a phase II study. SU was orally administered daily at 37.5 mg on days 1–7 prior to chemoembolization with Doxil, and again on days 15–35 after the start of the study. Subsequent treatment cycles were 4 weeks on daily SU followed by 2 weeks off. Plasma concentrations of SU and its active metabolite (SU12662) were measured using a liquid chromatographic tandem mass spectrometric method. The lower limits of quantifications (LOQ) were 0.099 and 0.088 ng/mL for SU and SU12662. Plasma levels for $sVEGFR_2$ were determined using an enzyme-linked immunosorbent assay, for which the lower LOQ was 7 pg/mL. DCE-MRI was performed in all available patients ($n = 8$) to determine baseline tumor volumes and then on days 8, 10, 28, and 35. All 16 patients were monitored for TTP and overall survival (OS). The RECIST criterion for the TTP event was defined as an increase in tumor diameter of $\geq$20 % over baseline. TTP and OS were reported as probabilities using Kaplan–Meier plots generated in Prism (GraphPad Software). A MAP-Bayesian approach was utilized to model drug and metabolite PK, which both were captured with a two-compartment model including linear clearances. Inhibition of $sVEGFR_2$ production was mediated by the model-predicted active unbound concentration (AC_{ub}) of SU and SU12662. $sVEGFR_2$ concentrations served as the driver for tumor growth. The probability of TTP was modeled using an exponential hazard function that is dependent on a time varying covariate—the difference in $sVEGFR_2$ concentration from its baseline ($\Delta sVEGFR_2$). The final model is shown in Fig. 1. The nonlinear mixed-effects modeling and simulations were performed using MONOLIX 4.1 and Berkeley Madonna. Internal model evaluation was performed using a visual predictive check, and the precision of the parameter estimates was assessed by the percent of relative standard errors (%RSE).

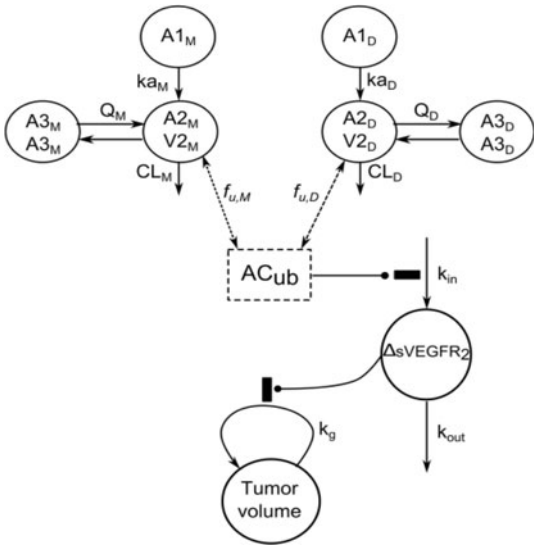

Fig. 1 Pharmacokinetic/pharmacodynamic model for sunitinib and SU12662. Drug (D) and metabolite (M) were captured with two-compartment models including linear elimination (CL_D, CL_M) and first-order absorption from gastrointestinal tract (ka_D, ka_M). The fraction of drug metabolized into SU12662 was $f_M = 21$ %. The active unbound concentration $AC_{ub} = f_{ub,D}.C_D + f_{ub,M}.C_M$, where $f_{ub,D}$ and $f_{ub,M}$ are the fractions of unbound drug and metabolite driving the inhibition of $sVEGFR_2$ production, which was captured with an indirect response model with a zero-order production rate (k_{in}) and a first-order removal rate constant (k_{out}). The difference in $sVEGFR_2$ concentrations from its baseline level ($\Delta sVEGFR_2$) drive the inhibition of net HCC growth (k_g)

Results: The apparent clearance of the drug and its metabolite (CL_D, CL_M) were estimated at 30.3 and 19.7 L/h with a %RSE of 19 and 14, respectively. Their corresponding apparent volumes of distribution (V_D, V_M) were 1,780 and 1,840 L (39 and 25 %RSE). Sunitinib exposure achieved was within the target range for $sVEGFR_2$ inhibition. The half-life of $sVEGFR_2$ in plasma calculated at 4 h was consistent with the known half-life for this angiogenic factor [4]. The slope (α) for AC_{ub} effect on $sVEGFR_2$ production was 0.77 $(\mu g/L)^{-1}$ with 14 %RSE. The $sVEGFR_2$ effect on the inhibition of tumor growth was assumed maximal ($I_{max} = 1$), whereas its potency (ΔIC_{50}) was estimated at 1.83 μg/L with 41 %RSE. The between-subjects variabilities for CL_D, CL_M, V_D, V_M, α, and ΔIC_{50} were 37.4, 51, 44.7, 64.8, 21, and 36 %. The median observed tumor volume baseline was 91 mm^3. Visual predictive checks for model outputs are shown in Fig. 2. The simulated mean TTP was 7.4 months and was in good agreement with average observed data (7.8 months) (Fig. 3).
Conclusions: The final PK/PD models effectively captured the plasma concentration–time course profiles of SU, SU12662, and $sVEGFR_2$ for all patients involved in the study. The profiles of

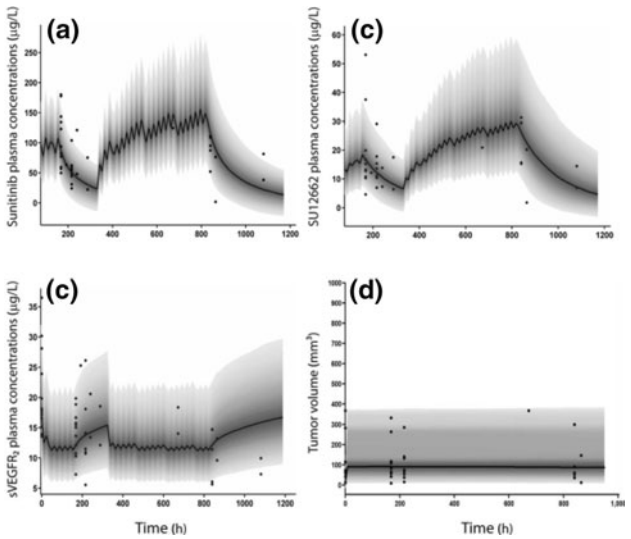

Fig. 2 Temporal visual predictive check (VPC) plots for (A) sunitinib plasma concentrations, (B) SU12662 plasma concentrations, (C) sVEGFR2 plasma concentrations, and (D) tumor volumes. Solid circles represent observed data. The gray area identifies the 5th and 95th percentiles of the predicted data, and solid lines represent the 50th percentile (median) of the predicted data. The confidence interval includes the majority of the data and the median is centrally located. These VPCs show no specific deviation of predicted versus observed data, which qualifies the model as being structurally sound and supports the veracity of the predicted parameter values and concentrations

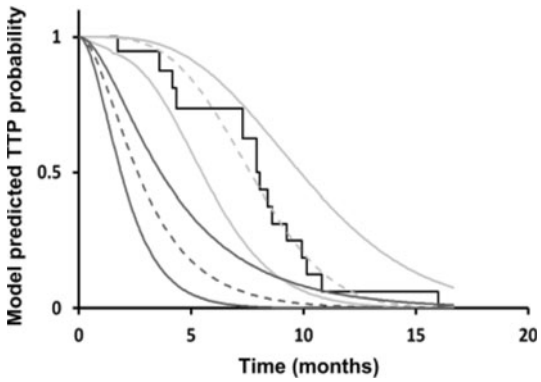

Fig. 3 Model predicted TTP probabilities. The solid black line represents the observed TTP probability. The solid light gray lines are the 5th and 95th percentiles of the predicted data, and the light gray dashed line is the 50th percentile (median) of the predictions in patients treated with SU. Model simulated TTP probability in placebo patients is shown with the dark gray color, where solid lines represent the 5th and 95th percentiles and the dashed line is the 50th percentile (median)

$sVEGFR_2$ plasma concentrations over time successfully linked drug exposure to tumor volume shrinkage and the time-to-progression. Moreover, $sVEGFR_2$ was a reliable predictor for the time-to-progression event. This model may serve as a general platform for the dynamics of anti-angiogenic drugs.

References

[1] El-Serag HB (2011) Hepatocellular carcinoma. N Engl J Med 365(12):1118–1127

[2] Rini BI (2007) Sunitinib. Expert Opin Pharmacother 8(14): 2359–2369

[3] Cheng A, et al (2011) Phase III trial of sunitinib (Su) versus sorafenib (So) in advanced hepatocellular carcinoma (HCC). J Clin Oncol, 29. Suppl; Abstract no. 4000

[4] Lindauer A, et al (2010) Pharmacokinetic/pharmacodynamic modeling of biomarker response to sunitinib in healthy volunteers. Clin Pharmacol Ther 87(5):601–608

T-002 Lifespan Based Pharmacokinetic-Pharmacodynamic Model of Tumor Growth Inhibition by Anticancer Therapeutics

Gary Mo[1,*], Frank Gibbons[2], Patricia Schroeder[2], Wojciech Krzyzanski[1]

[1]University at Buffalo, Buffalo, NY, USA; [2]AstraZeneca R&D Boston, Waltham, MA, USA

Objectives: Accurate prediction of tumor growth is critical in modeling the effects of anti-tumor agents. In recent years, both empirical and semi-mechanistic models have been developed to capture the relationship between pharmacokinetics and tumor growth inhibition. More recent tumor growth mechanistic models have been proposed that account for the first-order tumor growth that is determined by the tumor size and maturation of the tumor cells exposed to chemotherapy, which leads to their death [1–3]. We propose a tumor growth model based on the lifespan of tumor cells and changes to the lifespan as a result of anti-cancer drug treatment.

Methods: We are presenting a lifespan model to predict the growth of tumors based on the doubling time of tumor cells. The fundamental concept of our model is that tumor growth is accounted for by the cell division that occurs after the time T_D when the mitotic tumor cells reach the end of their lifespan, and that tumor loss is due to loss of the parent cell after division. Previous reports have demonstrated that preclinical xenograph tumors grow exponentially during early phases and linearly afterwards. To account for this, our model uses a previously published bifurcation system [1] that can automatically switch the tumor growth to a linear rate once a threshold tumor weight is reached. Our model describes the effects of chemotherapeutic agents as a dose-dependent shift of a fraction of the mitotic tumor cells into a population of non-proliferating cells with a lifespan T_N. The non-proliferating cells die due to apoptosis when their age reaches T_N, and this contributes to the overall tumor cell loss. The chemotherapeutic drug effect is described by the E_{max} model where EC_{50} serves as a potency parameter.

Results: We compared our lifespan model to existing models through simulations and refitting the literature data. Simulations showed that the lifespan model accurately describes the same stages of tumor growth as reported in the Simeoni model [3]. Lifespan parameters T_D and T_N, as well as pharmacological parameters E_{max} and EC_{50} were all identifiable. The estimates of lifespans T_D and T_N in our model correspond to the exponential tumor growth rate and apoptotic maturation parameters, respectively, reported in [3]. Simulations of the lifespan model with parameter values derived from an exponential growth rate of 0.146/day, linear growth rate of 0.334 g/day, and initial tumor weight of 0.085 g [3] showed that decreasing the value of T_D causes the lifespan model to eventually collapse to the Simeoni model with the same parameter estimates (exponential growth = 0.147/day,

linear growth rate = 0.334 g/day and initial tumor weight = 0.085 g). Simulations with increasing values of T_D indicated that a nonlinear relationship exist between cell doubling time and exponential growth rate. The exponential growth rate and the threshold tumor weight can both be accurately calculated from T_D. Furthermore, the EC_{50} parameter of our model corresponds to the second-order rate constant used to describe drug potency [3].

Conclusions: We have developed a mechanistic model that is based on the lifespan of tumor cells to predict tumor growth and inhibition of growth by anti-tumor agents. The model was compared to the existing models of tumor growth. It performed equally well and in addition the doubling time of mitotic tumor cells and lifespan of apoptotic tumor cells affected by the drug were estimated. This lifespan model is able to capture the relationship between the pharmacokinetics of therapeutic agents with tumor growth inhibition using physiologically relevant model parameters.

References

[1] Harrold JM, Straubinger RM, Mager DE (2012) Combinatorial chemotherapeutic efficacy in non-Hodgkin lymphoma can be predicted by a signaling model of CD20 pharmacodynamics. Cancer Res 72(7):1632–1641

[2] Jumbe NL, et al (2010) Modeling the efficacy of trastuzumab-DM1, an antibody drug conjugate, in mice. J Pharmacokinet Pharmacodyn 37(3):221–242

[3] Simeoni M, et al (2004) Predictive pharmacokinetic-pharmacodynamic modeling of tumor growth kinetics in xenograft models after administration of anticancer agents. Cancer Res 64(3):1094–1101

T-003 ADOPT (A Dynamic HbA_{1c} EndpOint Prediction Tool): A framework for Predicting Primary Endpoint in Phase 3 Diabetes Trials

Jonas B Møller[1,*], Rune V Overgaard[1], Maria C Kjellson[2], Niels R Kristensen[1], Søren Klim[1], Steen H Ingwersen[1], Mats O Karlsson[2]

[1]Quantitative Clinical Pharmacology, Novo Nordisk A/S, Søborg, Denmark; [2]The Pharmacometrics Group, Uppsala University, Uppsala, Sweden

Objectives: Phase 2 trials within diabetes generally have a long duration of 12–24 weeks, where 12 weeks may be too short to reach steady state HbA_{1c} and 24 weeks significantly increase time and cost of development. The main determinant for HbA_{1c} is blood glucose, which reaches steady state much sooner. We propose a framework for predicting phase 3 end-of-trial HbA_{1c} based on phase 2 data that potentially avoids this issue by quantifying the longitudinal relation between glucose and HbA_{1c}.

Methods: Individual data from 4 clinical trials covering 12 treatment arms with different anti-diabetic treatments (OADs, GLP-1 analogues, and insulins) were included in this analysis (Table 1, Refs. [1–4]). HbA_{1c} was sampled at screening and 3-5 times during the treatment period. In addition, 3 times during the treatment period, each subject was sampled regularly to obtain 24-hour plasma glucose

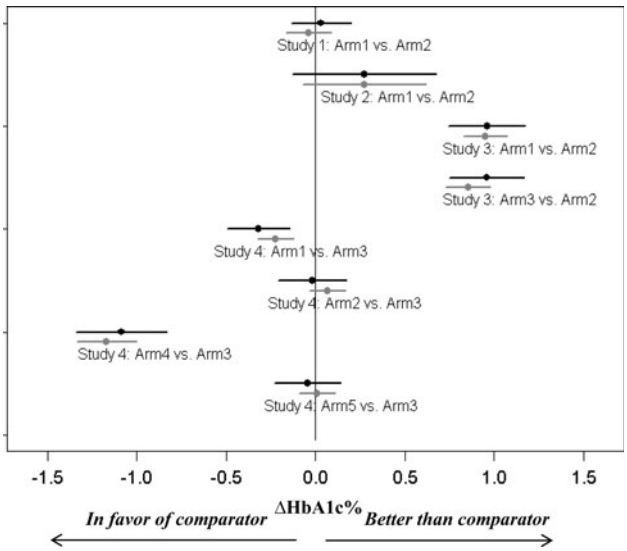

Fig. 1 Overview of prediction performance in each arm. The abscissa shows the change in HbA_{1c} % (ΔHbA_{1c} %) following 24-28 weeks of treatment vs. comparator. Each line presents 95 % confidence interval for the treatment effect vs. comparator calculated based on observations (black) and predictions from 12 week data (gray). Dots present mean difference in ΔHbA_{1c} % between comparator and the specific arm

Table 1 Summary of trials included

Treatment type	Arm	Trial and arm—short name	N	HbA_{1c} baseline	Ref.
Basal Insulin	Insulin glargine (comparator)	Trial1-arm1	259	8.6	[1]
Basal Insulin	Insulin detemir	Trial1-arm2	248	8.6	
Pre-mixed insulin	Novo mix	Trial2-arm1	99	9.7	[2]
Basal insulin	Insulin glargine (comparator)	Trial2-arm2	110	9.8	
GLP-1 analog + Biguanide + TZD	Liraglutide	Trial3-arm1	176	8.6	[3]
Biguanide + TZD	1.8 mg + Metformin + Rosiglitazone	Trial3-arm2		8.4	
GLP-1 analog + Biguanide + TZD	Metformin + Rosiglitazone (comparator)	Trial3-arm3	159	8.5	
	Liraglutide 1.2 mg + Metformin + Rosiglitazone		170		
GLP-1 analog + Biguanide	Liraglutide 0.6 mg + Metformin	Trial4-arm1	238	8.4	[4]
GLP-1 analog + Biguanide	Liraglutide 1.8 mg + Metformin	Trial4-arm2	234	8.3	
SU + Biguanide	Glimeperide + Metformin (comparator)	Trial4-arm3	232	8.3	
Biguanide	Metformin	Trial4-arm4	116	8.4	
GLP-1 analog + Biguanide	Liraglutide 1.2 mg + Metformin	Trial4-arm5	224	8.4	

profiles. The link between glucose and HbA_{1c} was implemented as an indirect response model with mean plasma glucose (MPG) and HbA_{1c} as dependent variables estimated using a non-linear mixed-effects model. The predictive performance of the model was evaluated using 12-week data to predict HbA_{1c} at end-of-trial. Thus, HbA_{1c} was predicted for each individual subject from screening up to 24–28 weeks using MPG and HbA_{1c} samples up to 12 weeks. Besides directly comparing predicted HbA_{1c} values (mean and variance) to observations, we sought to evaluate whether the model could predict the primary endpoint (ΔHbA_{1c} vs. comparator) in each trial (Fig. 1).
Results: A total of five model parameters were estimated while two model parameters reflecting glycosylation of hemoglobin were fixed to predetermined values. HbA_{1c} % at end-of-trial was predicted with a mean numerical error in each treatment arm ranging from 0.0 to 0.24 % with an average of 0.14 % error across treatment arms. The ratio of the variance of predictions versus observations ranged from 0.75 to 0.86 indicating a slight under-prediction of variance. Calculations of the mean ΔHbA_{1c} versus comparator and the corresponding confidence intervals were shown to provide identical conclusions based on predictions from 12-week data and observations at end-of-trial (Fig. 1).
Conclusions: The proposed link between glucose and HbA_{1c} provides a framework for accurate and precise prediction of end-of-trial (24–28 weeks) HbA_{1c} based on 12-week MPG and HbA_{1c} measurements. Application of this framework thus provides a basis for improved phase 3 dose selection using phase 2 data within diabetes drug development.

References

[1] Rosenstock J, Davies M, Home PD, Larsen J, Koenen C, Schernthaner G (2008) A randomised, 52-week, treat-to-target trial comparing insulin detemir with insulin glargine when administered as add-on to glucose-lowering drugs in insulin-naive people with type 2 diabetes. Diabetologia 51:408–416

[2] Raskin P, Allen E, Hollander P, Lewin A, Gabbay RA, Hu P, Bode B, Garber A (2005) Initiating insulin therapy in type 2 diabetes: a comparison of biphasic and basal insulin analogs. Diabetes Care 28:260–265

[3] Zinman B, Gerich J, Buse JB., Lewin Andrew, Schwarz S, Raskin P, Hale PM, Zdravkovic M, Blonde L, LEAD-4 Study Group (2009) Efficacy and safety of the human glucagon-like peptide-1 analog liraglutide in combination with metformin and thiazolidinedione in patients with type 2 diabetes (LEAD-4 Met + TZD). Diabetes Care 32:1224–1230

[4] Nauck M, Frid A, Hermansen K, Shah NS, Tankova T, Mitha IH, Zdravkovic M, Düring M, Matthews DR; LEAD-2 Study Group (2008) Efficacy and safety comparison of liraglutide, glimepiride, and placebo, all in combination with metformin, in type 2 diabetes: the LEAD (liraglutide effect and action in diabetes)-2 study. Diabetes Care 32(1):84–90

T-004 Single-cell Pharmacokinetics of an Auristatin-Based Antibody–Drug Conjugate

Tae H Han, David Julian, Baiteng Zhao*

Clinical Pharmacology, Seattle Genetics, Inc., Bothell, WA, 98021 USA

Objectives: Antibody–drug conjugates (ADC) represent a new modality in the treatment of cancer that enables target specific delivery of potent cytotoxic agents. The pharmacokinetics of ADCs are complex and requires consideration of multiple pathways. The objectives of the study were to develop a mechanistic single-cell PK model to account for these multiple pathways
Methods: A network model of ADC pharmacokinetics in a single cell was developed in silico. Both specific and non-specific pathways for ADC internalization were incorporated in this single-cell model. Nodes that represent analytes in different locations in tissue were connected by first-order or second-order reactions. Parameter values were fixed based on literature, internal data, model fits, or scientific judgment. MATLAB (R2012a) and SimBiology (v. 4.1) were used to develop the model and for simulations.
Results: The model performed well in fitting auristatin data from in vitro experiments. Across cell lines, efflux of the auristatin was found to vary while the uptake of auristatin was similar. In addition, specific delivery of ADC to the target cell accounted for the majority of the in vitro cytotoxicity. Based on a sensitivity analysis, the key reaction pathways were those directly involved in auristatin release from the ADC.
Conclusions: The single-cell pharmacokinetic model describes in vitro results well. Further work to extrapolate the ability of this model to fit data from in vivo experiments is planned.

T-005 A Population Pharmacokinetic Model of Caffeine and Paraxanthine to Investigate Methylxanthine Abstinence and CYP1A2 Activity

Vidya Perera[1,2,3,*], Annette S Gross[1,4], Alan Forrest[3], Gauri Rao[3], Andrew J McLachlan[1,2]

[1]Faculty of Pharmacy, The University of Sydney, NSW, Australia; [2]Centre for Research and Education on Ageing, Concord Hospital, Sydney, NSW, Australia; [3]School of Pharmacy and Pharmaceutical Sciences, SUNY at Buffalo, Buffalo, NY, USA; [4]Clinical Pharmacology Modeling and Simulation, GlaxoSmithKline R&D, Sydney, NSW, Australia

Objectives: The drug metabolizing enzyme cytochrome P4501A2 (CYP1A2) demonstrates a large degree of inter-individual and population variability [1]. Currently, caffeine is the probe drug utilized to investigate CYP1A2 activity in vivo in humans [2]. The apparent clearance of caffeine is considered to be the gold standard measurement of CYP1A2 activity. However, phenotyping methodologies differ, in particular the time period of methylxanthine abstinence (MA) prior to administration of the study dose of caffeine [3]. Understanding the impact of a methylxanthine abstinence period on caffeine and paraxanthine pharmacokinetics is critical to ensure an accurate estimate of CYP1A2 activity. The aim of this study was to evaluate caffeine and paraxanthine pharmacokinetics with and without a methylxanthine abstinence (MA) period in subjects with a range of caffeine consumption and to analyze the impact of MA on metrics of CYP1A2 activity.
Methods: This study developed and evaluated a mixed effects pharmacokinetic model for caffeine and paraxanthine pharmacokinetics derived from a sequential single dose cross-over study in health non-smoking male volunteers ($n = 30$) who received an oral 100 mg caffeine dose. Participants received caffeine on 2 occasions: during their usual diet of methylxanthines and after a 24 h period of methylxanthine abstinence. Blood samples were obtained at 0, 0.5, 1, 1.5, 2, 4, 6, 8, 10 and 24 h in both periods. Participants were classed as heavy caffeine consumers if they had a usual caffeine intake of >200 mg per day [1]. Plasma concentrations of caffeine and paraxanthine were measured by high performance liquid chromatography [4]. Data was modeled using the maximum likelihood estimation method in ADAPT V [5].

Table 1 Model parameters in the 24 h methylxanthine abstinence period and no methylxanthine abstinence period

Parameter	24 h Methylxanthine abstinence period			No methylxanthine abstinence period		
	Mean	RSE %	CV %	Mean	RSE %	CV %
ka	3.65	41.6	103	3.55	54.9	56.0
k_{12}	1.71	19.4	32.5	1.54	71.5	62.6
k_{21}	2.02	14.4	23.1	2.40	64.9	29.7
V_1	31.2	38.8	17.7	27.7	56.8	20.2
V_3	24.4	47.2	24.6	18.4	52.8	37.2
Tlag	0.15	54.5	107	0.14	76.2	81.2
CL_{CAPX}	2.73	15.0	22.7	2.63	17.3	19.6
CL_{PX}	3.81	11.2	13.4	3.70	14.2	10.9
CL_{CAO}	4.86	40.1	57.1	3.74	49.0	68.1
IC(1)	1.72	82.3	229	3.40	144	187
IC(2)	1.20	Fixed	–	1.21	Fixed	–
IC(3)	4.06	22.8	48.2	6.93	77.2	103
IC(4)	1.37	Fixed	–	1.18	Fixed	–
SD1int	0.05	Fixed	–	0.05	Fixed	–
SD1Slope	0.02	38.8	–	0.07	13.7	–
SD2int	0.05	Fixed	–	0.05	Fixed	–
SD2slope	0.04	32.2	–	0.04	29.9	–

RSE % relative standard error of parameter as a percentage; *CV %* coefficient of variation percent; k_a rate constant from absorptive compartment; k_{12} rate constant from compartment 1 of caffeine to peripheral compartment; k_{21} rate constant from peripheral compartment to caffeine central compartment; V1 volume of distribution of caffeine in compartment 1; V3 volume of distribution of paraxanthine in compartment 3; *Tlag* lag time for caffeine from absorptive compartment; CL_{CAPX} Clearance of caffeine to paraxanthine; CL_{PX} Clearance of paraxanthine; CL_{CAO} Clearance of caffeine renally plus clearance of caffeine to theophylline and theobromine; *IC(i)* Initial condition in ith compartment; *SD1int* variance model parameter describing intercept of caffeine; *SD1slope* variance model parameter describing slope of caffeine; *SD2int* variance model parameter describing intercept of paraxanthine; *SD2slope* variance model parameter describing slope of paraxanthine

Results: Caffeine and paraxanthine concentration–time data were modeled simultaneously with first order absorption (and lag), elimination rate constants and error variance models for both caffeine and paraxanthine. Caffeine was described by a two compartment pharmacokinetic model with two linear clearance parameters (CL_{CAPX}, which describes the clearance of caffeine to paraxanthine, and CL_{CAO} which describes clearance by all other elimination pathways of caffeine), while paraxanthine was described by a one compartment pharmacokinetic model with one linear clearance (CL_{PX}). The model fit the data very well in the MA (overall r^2 = 0.99 for caffeine and r^2 = 0.91 for paraxanthine) and no MA (r^2 = 0.98 for caffeine, and r^2 = 0.91 for paraxanthine) periods. Table 1 displays the parameters obtained from data in the 24 h MA and no MA periods. The apparent clearance of caffeine (CL_{TOT}) was calculated as the sum of CL_{CAPX} and CL_{CAO}. A difference was observed between the apparent caffeine clearance (CL_{TOT},) in the MA period (n, mean, 95 % CI) (30, 8.44, 7.21–9.68 L/h) and no MA period (30, 7.27, 6.14–8.40 L/h) ($p < 0.05$). When stratified by caffeine consumption the difference in the CL_{TOT} in heavy caffeine consumers between the no MA and MA was only significant for heavy caffeine consumers ($n = 5$, 6.30, 3.39–9.19 L/h) and (10.48, 5.62–15.32 L/h), respectively ($p < 0.05$) (Fig. 1). The apparent paraxanthine clearance was not significantly altered in heavy or light caffeine consumers between the two study periods. The model indicated that the difference in the CL_{TOT} in heavy caffeine consumers between the two periods was related to the CL_{CAO} pathway rather than the pathway describing CYP1A2 mediated metabolism (CL_{CAPX}).

Conclusions: A methylxanthine abstinence period has a significant impact on the pharmacokinetics of caffeine in heavy caffeine consumers. The decrease in the total apparent caffeine clearance, in the

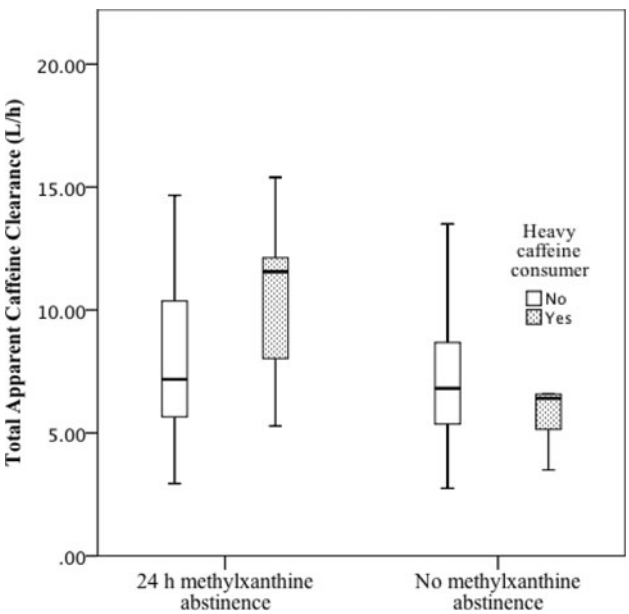

Fig. 1 Total apparent caffeine clearance in the 24 h MA and no MA periods stratified by caffeine consumption. The upper and lower bounds of the boxplot represent the 75th and 25th percentiles; the median is also indicated by the line within each box

no MA period does not appear related to saturation of the CYP1A2 enzyme pathway, indicated by the lack of change in the clearance of caffeine to paraxanthine and the clearance of paraxanthine. The results may reflect a change in the sensitivity to the diuretic effect of caffeine among heavy caffeine consumers following methylxanthine abstinence. These results have implications for measurement of CYP1A2 activity, dose optimization of CYP1A2 metabolized drugs and studies linking CYP1A2 activity to intrinsic or extrinsic factors. The results highlight the importance of population pharmacokinetic analysis compared to traditional pharmacokinetics approaches when interpreting drug metabolism.

References

[1] Perera V, Gross AS, McLachlan AJ (2012) Influence of environmental and genetic factors on CYP1A2 activity in individuals of South Asian and European ancestry. Clin Pharmacol Ther 92(4): 511–519

[2] Perera V, Gross AS, McLachlan AJ (2012) Measurement of CYP1A2 activity: a focus on caffeine as a probe. Curr Drug Metab 13(5): 667–678

[3] Perera, V, et al (2011) Pharmacokinetics of caffeine in plasma and saliva, and the influence of caffeine abstinence on CYP1A2 metrics. J Pharm Pharmacol 63(9): 1161–1168

[4] Perera V, Gross AS, McLachlan AJ (2010) Caffeine and paraxanthine HPLC assay for CYP1A2 phenotype assessment using saliva and plasma. Biomed Chromatogr 24(10):p. 1136–1144

[5] D'Argenio DZ, Schumitzky A, Wang X (2009) ADAPT 5 User's Guide: Pharmacokinetic/Pharmacodynamic Systems Analysis Software, B.S. Resource, Editor 2009: University of Southern California, Los Angeles

T-006 Comparison of Different Efficacy Endpoints in Neuropathic Pain Trials: An Application of Meta-analysis

Chih-Wei Lin*, Wei Liu, Walid Awni, Sandeep Dutta

Clinical Pharmacology and Pharmacometrics, AbbVie, North Chicago, IL, 60064, USA

Objectives: Pain intensity (PI) scale with the "0–10 numerical rating" is widely used as efficacy endpoint in pain trials. Although many other endpoints are also used in pain evaluation and seem to show similar trends for multiple efficacy endpoints typically evaluated in pain trials, there have been no systemic comparison between these efficacy endpoints for pain reduction. The objective of this work was to compare PI with a variety of pain endpoints, including patient global impression of change (PGIC), short from McGill (SFMAC), short form 36 (SF36), brief pain inventory (BPI), clinical global impression of change (CGIC) used in neuropathic pain trails.

Methods: The initial database of 82 trials was created by a systemic search for published controlled clinical trials for neuropathic pain including diabetic peripheral neuropathy, postherpetic neuralgia and fibromyalgia. 9 endpoints were identified in the database: PI in 74 trials, PGIC in 49 trials, SFMAC in 37 trials, SF36 in 30 trials, BPI in 25 trials, CGIC in 23 trials, fibromyalgia impact questionnaire (FIQ) in 16 trials, clinical global impression-Severity (CGI-S) in 11 trials, and pain relief (PR) in 7 trials (Table 1). Majority of the trials had 3–4 different efficacy endpoints. To investigate the relationships between efficacy endpoints, the data were regrouped for paired endpoints into small subgroups by trial, arm, time and imputation. The observed endpoint relationships were linear and evaluated by mixed effects models. Between trial variability was described by random effects, and residual error was weighted according to the size of the subgroups. The correlation between observations within an arm was evaluated by a compound symmetry correlation structure. Akaike information criterion was used in model selection. Analyses were performed in R.

Results: The relationships between PI (0–10 scale) and other endpoints were evaluated, except FIQ, CGI-S and PR because of the small sample size of the regrouped data. All the endpoint relationships were well described by linear mixed effects models.

The mean score reduction in PI at endpoint was 1.4 for placebo groups and 2.3 for active groups. By using PI as a bridge, it is possible to compare different scales for pain assessments in neuropathic pain trials for placebo and active groups (Fig. 1). When a change in PI was compared to different efficacy endpoints, a 1.4 point mean score PI reduction for placebo response was associated with the following changes in different efficacy endpoints:

(i) 34.1 or 20.7 % of the trial subjects had achieved 30 or 50 % pain reduction in PI, respectively;

(ii) 0.78 point drop from baseline in PGIC (1–7 scale, baseline = 4) or 29.9 % rate to achieve much improved/very much improved in PGIC;

(iii) 0.56 point reduction in SFMAC-present pain intensity (PPI) (0–5 scale) and 17.1 point reduction in SFMAC-visual analog scale (VAS) (0–100 scale);

(iv) 8.7 point reduction in SF36-body pain (0–100 scale);

(v) 1.43 point reduction in BPI (0–10 scale); (f) 0.81 point drop from baseline in CGIC (1–7 scale, baseline = 4) or 29.2 % rate to achieve much improved/very much improved in CGIC.

Conclusions: These analyses provide direct comparisons between PI and other efficacy endpoints, and allow indirect comparisons among other efficacy endpoints for placebo and drugs included in this analysis. This work enables rough conversions between main score reductions and responder rates for different endpoints, and provide

Table 1 Summary of Evaluated Efficacy Endpoints in Neuropathic Pain Database

Endpoint category	*N* of trials	Evaluated endpoint (*N* of trials)
Pain Intensity	74	average pain (73), 50 % reduction (43), 30 % reduction (34),
Patient Global Impression of Change (PGIC)	49	Mean score (20), %much improved/very much improved (16)
Short From McGill (SFMAC)	37	VAS Pain (26), present pain intensity (23)
SF36	30	Bodily pain (25)
Brief Pain Inventory (BPI)	25	Average pain (22)
Clinical Global Impression of Change (CGIC)	23	%much improved/very much improved (10), mean score (7)
Total	82	

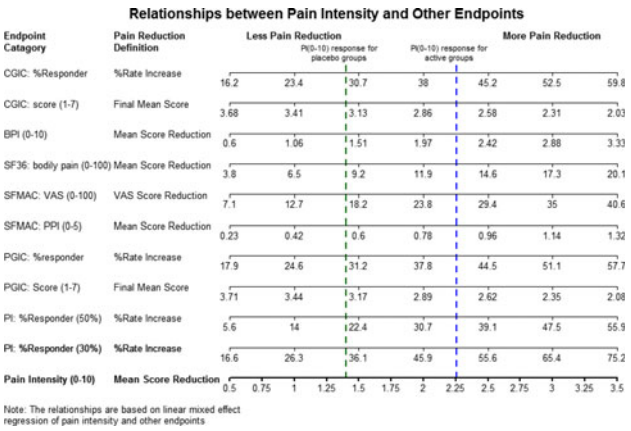

Fig. 1 Relationship between Pain Intensity and Other Endpoints for Pain Assessments

approximate placebo and active responses for different endpoints for neuropathic pain.

T-007 Application of a Literature-Based Model of Weight Loss in Diabetes and Obesity Drug Development

Karen Schneck[1,*], Jeanne Geiser[1], Haoda Fu[2], David Manner[2], Beth Sheets[4], Jenny Chien[1]

[1]Global Pharmacokinetics/Pharmacodynamics and Pharmacometrics; [2]Global Statistics; [3]Data Sciences and Solution, Eli Lilly and Company, Indianapolis, IN, USA

Objectives: Published literature can be used to develop drug-disease models to inform decisions about study design or drug development strategy. Two models describing weight loss in obese patients with or without Type 2 diabetes mellitus (T2DM) were developed to predict the contribution of placebo, drugs, exercise, diet, and disease state on the magnitude and time course of weight reduction.
Methods: A database of study-level aggregate data from multiple trials published in literature (1 week to 1 year duration) was curated. Study arms were categorized by disease status—obesity with or without T2DM. Models included placebo and drug treatment (e.g., sibutramine, rimonabant, dexfenfluramine, exenatide, pramlintide, liraglutide, taspoglutide, and albiglutide). Non-pharmacological intervention (diet, exercise) or concomitant metformin use was treated as a categorical covariate. The effect of baseline weight on change from baseline was explored. An indirect dose–response model was implemented in a nonlinear mixed effects modeling software (NONMEM) using the first order conditional estimation (FOCE) method [1]. The $PRIOR option and proprietary densely sampled data was utilized to stabilize estimation of the rate constant describing the weight loss time course [1]. The indirect dose–response model was translated into SPLUS to simulate varying treatment conditions. The Integrated Two-Component Prediction (ITP) longitudinal model [2] was executed using BUGS software [3]. Predictions from the models described potential scenarios for the probability of technical success as represented by the percentage of the simulated population achieving the desired target weight loss.
Results: The models revealed the differing time course and extent of weight loss in the obese patient populations with and without T2DM for the various interventions and conditions. A model and data from a Phase 1 proof-of-concept study were used together to simulate alternative study design scenarios to streamline a development program and to predict plausible outcomes of a Phase 2 trial, including the relative performance of a compound in development against marketed comparators. The ITP weight loss model maximized the use of dropout data to support dose allocation in an adaptive design trial.
Conclusions: Models for weight loss developed from literature data are advantageous tools to support key drug development decisions. In this case example, the models guided decisions dependent upon the time course of weight reduction, the effectiveness of marketed comparators, and the influence of study population on weight loss.

References

[1] Bauer R (2011) NONMEM User's Guide, Introduction to NONMEM 7.2.0. ICON Development Solutions, Ellicott City, MD

[2] Haoda F, Manner D (2010) Bayesian adaptive dose-finding studies with delayed responses. J Biopharm Stat 20(5):1055–1070

[3] http://www.mrc-bsu.cam.ac.uk/bugs

T-008 Population Pharmacokinetic Model for Levomilnacipran in Healthy Subjects and Patients with Major Depressive Disorder

Timothy J Carrothers[1,*], Tatiana Khariton[1], ChunLin Chen[1], Antonia Periclou[1], Laishun Chen[1], Michelle Green[2], Leon Bax[2], Helen Kastrissios[2], and Parviz Ghahramani[1]

[1]Forest Research Institute, Jersey City, NJ, USA; [2]Pharsight, Sunnyvale, CA, USA

Objectives: To characterize the population pharmacokinetic (PPK) profile of levomilnacipran in patients with major depressive disorder (MDD) and to quantify the potential effects of demographic characteristics, renal and liver function, and relevant classes of concomitant medications on steady-state exposures.
Methods: The PPK analysis data set included 11,863 non-zero observations from 1,256 subjects (567 males, 689 females), including 8,928 observations from 458 healthy subjects in 13 Phase I studies and 2,935 observations from 798 patients with MDD in three Phase III studies. Doses of levomilnacipran sustained release (SR) formulation ranged from 20 to 300 mg once daily in the combined dataset. A structural PPK model was developed based on exploratory evaluations of the phase I data and evaluation of goodness of fit plots. Possible parameter-covariate relationships were initially identified using exploratory graphical and regression analyses, then subsequently evaluated using nonlinear mixed effect modeling. Covariates were screened one at a time and selected using a stepwise forward-selection ($p < 0.01$), backward-elimination ($p < 0.001$) method based on the likelihood ratio test. Model evaluation was based on statistical criteria, numerical stability of the minimization, and graphical presentations of goodness-of-fit. Goodness-of-fit graphs included population and individual predicted concentrations versus observed concentrations, conditional weighted residuals versus time after first dose, and conditional weighted residuals versus predicted plasma concentrations. During model refinement, statistically significant covariates that were not clinically relevant were removed from the model and parameter estimates were examined to ensure that they were well estimated and plausible. The resultant model was considered the final practical PPK model. This final model was further evaluated using visual predictive check and bootstrap analysis. Modeling was performed in NONMEM, Version VII.1.0 (FOCE-I),

Table 1 Parameter estimates of the final practical PPK model

Parameter	Estimate	RSE	IIV(ETA)	IIV(as %CV)
CL/F (L/h)	24.0	0.93	0.0674	26.0[a]
Vc/F (L)	495	1.24	0.0657	25.6[a]
Ka (1/h)	0.519	2.64	0.307	55.4
Tlag (h)	1.73	0.58	–	–
CLCR ≥50 mL/min on CL/F	0.475	8.46	–	–
CLCR<50 mL/min on CL/F	0.525	7.43	–	–
WTKG on Vc/F	0.605	11.2	–	–
Residual error, Ph 1, proportional	0.150	3.95	–	–
Residual error, Ph 1, additive	2.71	7.93	–	–
Residual error, Ph 3, proportional	0.352	4.52	–	–
Esidual error, Ph 3, additive	21.4	12.1	–	–

RSE relative standard error, *IIV* interindividual variability, *CV* coefficient of variation

[a] Correlation of CL/F IIV and Vc/F IIV was 0.391

Covariate effects listed above modeled as PKPAR = TypicalPKParValue * (Cov/TypCov)^(theta)

IIV modeled as PKPAR*exp(ETA)

Cij = C + SQRT(additive + proportional*C), for ith subject and jth plasma concentration measurement

with Perl-speaks-NONMEM Version 3.2.12 used to conduct the bootstrap analysis.

Simulations of the final PPK model were performed to identify dose adjustment strategies for subjects with varying degrees of renal impairment, including mild (CLCR 60–89 mL/min), moderate (CLCR 30–59 mL/min) and severe (CLCR 15–29 mL/min). Various dose reduction strategies, covering both the titration period and the maintenance period, were evaluated through comparison to subjects with normal renal function.

An exploratory evaluation of the impact of medications co-administered with levomilnacipran on model-predicted steady-state exposures to levomilnacipran was conducted for subjects in the three Phase III studies. Groupings of drugs that influence the human cytochrome P450 (CYP) system were created according to a reputable, publicly-accessible source table [1]. Groupings of interest included CYP 3A4/5/7 inducers, CYP 3A4/5/7 inhibitors, CYP 2D6 inhibitors, CYP inducers as a combined group, and cyclosporine. In addition, strong P-glycoprotein (P-gp) inhibitors and groupings of drugs influencing renal transporters OCT2, OAT1, and OAT3 were assessed, based on a list provided by US-FDA [2].

Results: A one compartment pharmacokinetic model with delayed first order absorption and first order elimination best described the pharmacokinetics of levomilnacipran. Pharmacokinetics were linear over the therapeutic range. The model for levomilnacipran was parameterized in terms of apparent systemic clearance (CL/F) and apparent central compartment volume (Vc/F), an absorption rate constant (Ka) and absorption lag time (Tlag). Interindividual variability was modeled in an exponential format and estimated to be 26 % for CL/F and Vc/F and 55 % for Ka. Covariance between CL/F and Vc/F was modeled. Additive and proportional residual error terms were estimated separately for sparse data and phase I data. The additive and proportional error terms for Phase I data were 13 and 43 %, respectively, of the residual error variances for sparse data. The structural model provided an adequate fit to the data as demonstrated by diagnostic plots and symmetrical parameter distributions. All parameters (Table 1) were well estimated as shown by precise parameter estimates, reasonable ETA shrinkage (10–40 %) and low epsilon shrinkage (8 %).

The primary clinical covariate influencing exposure to levomilnacipran was renal function. For a subject with normal renal function (CLCR of 120 mL/min and body weight of 79 kg), typical CL/F was 24.0 L/h and typical Vc/F was 495 L. The median absorption lag time was estimated to be 1.73 h and the median absorption half-life was 1.3 h. Variations in renal function explained 35 % of between-subject variability in CL/F. For subjects with mild, moderate and severe renal impairment, the final model shows reductions in median CL/F of 20, 40 and 58 %, respectively, compared with a typical subject with normal renal function. A piece-wise model with separate parameters for the impact of CLCR on CL/F was utilized to significantly improve the goodness-of-fit at values of CLCR under 50 mL/min. The only clinically relevant covariate for Vc/F was body weight. For a 100 kg subject, Vc/F would be expected to increase by 15 % (571 L) compared to a subject with the typical weight of 79 kg, while in a subject weighing 60 kg, Vc/F would be expected to be reduced by 15 % (419 L) compared to a subject with the typical weight of 79 kg. However, over the full range in body weight of 45–143 kg observed in the dataset, the influence of body weight on C_{max},ss resulted in less than 20 % variation. Fewer than 3 % of subjects were taking clinically relevant concomitant medications. In the exploratory evaluation of the concomitant medication groups, none of the groupings listed above showed an impact on model-predicted levomilnacipran AUC,ss, C_{max},ss, or C_{min},ss.

Table 2 Population PK-based recommendations for titration schedule by renal function category

Dose (mg, QD)	Day 1	Day 2	Days 3 and 4	Days 5–7	Days 8+
Renal function					
Normal or mild	20	20	40	80	120
Moderate	20	20	20	60	80
Severe	20	20	20	40	60

Due to the influence of renal impairment on levomilnacipran exposures, dosing adjustments are needed in subjects with moderate or severe renal impairment to achieve steady-state exposures similar to that in subjects with normal renal function (Table 2). At pharmacokinetic steady-state, the maximum doses for subjects with moderate and severe renal impairment are 80 once daily and 60 mg once daily,

respectively, compared to a dose of 120 mg once daily in subjects with normal renal function or mild renal impairment. Simulations also indicated that dose reductions during the up-titration phase in patients with moderate or severe renal impairment allow reduction of levomilnacipran plasma exposures to levels similar to those in normal and mildly impaired patients. This would ensure peak plasma concentrations and AUCs in subjects with moderate to severe renal impairment during the first 4 days of dosing are comparable to those of subjects with normal renal function.

Conclusions: A one compartment pharmacokinetic model with delayed first order absorption and first order elimination described the pharmacokinetics of levomilnacipran. Creatinine clearance and body weight were clinically relevant covariates influencing the pharmacokinetics of levomilnacipran. Concomitant medications, including those that influence renal transporters, P-gp and CYP, did not show an impact on levomilnacipran exposures including AUC,ss, C_{max},ss, and C_{min},ss. No dose adjustment is needed for subjects with mild renal impairment, but the maintenance dose for subjects with moderate and severe renal impairment should not exceed 80 mg once daily and 60 mg once daily, respectively. In addition, adjusted dose titration schedules are recommended for subjects with moderate and severe renal impairment to achieve levomilnacipran exposures similar to those in subjects with normal renal function.

References

[1] Flockhart DA. Drug Interactions: Cytochrome P450 Drug Interaction Table. Indiana University School of Medicine (2007). http://medicine.iupui.edu/clinpharm/ddis/table.aspx, accessed 13 March 2012.

[2] Table 12. Examples of In Vivo Inhibitors and Inducers of Selected Transporters, in http://www.fda.gov/Drugs/DevelopmentApprovalProcess/DevelopmentResources/DrugInteractionsLabeling/ucm080499.htm, accessed 13 March 2012.

T-009 Effect of Celecoxib on Aspirin-Mediated Inhibition of Cox-1 Enzyme: Pharmacokinetic-Pharmacodynamic Modeling Analysis

David Stepensky and Gilad Rimon

Department of Clinical Biochemistry and Pharmacology, The Faculty of Health Sciences, Ben-Gurion University of the Negev, Beer-Sheva, Israel

Background: COX-1 is a homodimer enzyme that is involved in prostaglandin biosynthesis from the arachidonic acid (AA) and can be inhibited by non-steroidal anti-inflammatory drugs (NSAIDs). This inhibition leads to reduced thromboxane B_2 (TxB_2) synthesis in the circulating platelets and reduced platelet aggregation, leading to cardioprotective activity. Aspirin can irreversibly inactivate the COX-1 enzyme via its acetylation at Ser530 residue. It has been found recently that COX-2 inhibitors from the coxib family, such as celecoxib and rofecoxib, are also able to bind to one subunit of COX-1 enzyme [1]. This binding to one monomer of COX-1 does not affect the normal catalytic processing of the AA by the second subunit, but does interfere with the inhibition of COX-1 by aspirin. Outcomes of the in vitro and animal studies (in dogs) indicate that coxibs, that are often prescribed in combination with low-dose aspirin, can interfere with the COX-1 inhibition and reduce the cardioprotective effects of aspirin [2]. The clinical studies that investigated the interaction between the coxibs and aspirin did not provide conclusive findings on its clinical importance, apparently due to the dose- and administration schedule-dependent extent of this interaction [3–4].

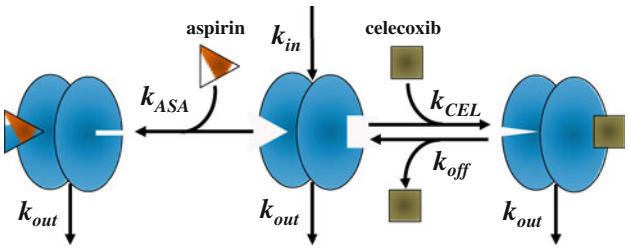

Fig. 1 The model of celecoxib and aspirin interaction with the COX-1 enzyme. The COX-1 in the platelets is produced at a constant rate k_{in} and is degraded according to the elimination rate constant k_{out}. Aspirin can irreversibly bind to the free COX-1 enzyme according to the 2-nd order k_{ASA} rate constant. Celecoxib can reversibly bind to the free COX-1 enzyme according to the 2-nd order k_{CEL} rate constant leading to the lower pool of COX-1 enzyme molecules that can be inhibited by aspirin. In presence of celecoxib, higher levels of aspirin-unbound COX-1 enzyme subsequently lead to increased thromboxane B_2 (TxB_2) synthesis in the circulating platelets and increased platelet aggregation

Objectives: To develop a quantitative model of celecoxib and aspirin binding to the COX-1 enzyme that takes into account the different mode of binding of these drugs to the individual subunits of the enzyme. To apply this model for analysis of the interaction between the celecoxib and aspirin on the inhibition of the COX-1 enzyme, TxB_2 synthesis and platelet aggregation for the clinically-relevant administration schedules of these drugs.

Methods: The data on the pharmacokinetics and pharmacodynamics of aspirin and celecoxib were collected from the scientific literature [5–7]. The data included the following parameters: the aspirin and celecoxib pharmacokinetics, turnover of platelet COX-1 enzyme, TxB_2 synthesis and platelet aggregation, and affinities of the aspirin and celecoxib to the COX-1. The collected data have been analyzed using a model of celecoxib and aspirin interaction with the COX-1 enzyme (Fig. 1) to determine the time course of the plasma drug concentrations, levels of the free and drug-bound COX-1, TxB_2 synthesis and platelet aggregation. The model validation was performed using the data from the clinical studies that investigated the interaction between the celecoxib and aspirin. Subsequent analysis included simulation of clinically-used doses and administration schedules of the investigated drugs; simultaneously at different time intervals.

Results: The applied model reflected the major pharmacokinetic and pharmacodynamics properties of the celecoxib and aspirin, and described appropriately the major findings of the clinical trials that analyzed the interaction between these drugs. The modeling outcomes indicated that celecoxib can interact with a substantial fraction of the COX-1 enzyme in the platelets and attenuate the COX-1-acetylation effect of aspirin. As a result, celecoxib can reduce the cardioprotective effects of aspirin. This interaction is most prominent at the high doses of celecoxib, low doses of aspirin, and in case that both drugs are administered simultaneously.

Conclusions: Celecoxib can interfere with the action of aspirin on COX-1 at the clinically-relevant doses of these drugs and can impede the action of low-dose aspirin on platelet aggregation in human subjects. The dosage regimens of both drugs should be modified to provide clinically effective COX-2 inhibition while minimizing interference with aspirin inhibition of platelet COX-1. Further studies should take into account the pharmacokinetic and

pharmacodynamic variability for both drugs to select their appropriate dosage regimens.

References

[1] Rosenstock M, et al (2001) Prostaglandin H synthase-2 inhibitors interfere with prostaglandin H synthase-1 inhibition by nonsteroidal anti-inflammatory drugs. Eur J Pharmacol 412(1):101–108

[2] Rimon G, et al (2010) Coxibs interfere with the action of aspirin by binding tightly to one monomer of cyclooxygenase-1. PNAS 107(1):28–33

[3] Renda G, et al (2006) Celecoxib, ibuprofen, and the antiplatelet effect of aspirin in patients with osteoarthritis and ischemic heart disease. Clin Pharmacol Ther 80:264–74

[4] Gladding P, et al (2008) The antiplatelet effect of six nonsteroidal anti-inflammatory drugs and their pharmacodynamic interaction with aspirin in healthy volunteers. Am J Cardiol 101(7):1060–1063

[5] Hong Y, et al (2008) Population pharmacodynamics modelling of aspirin- and ibuprofen-induced inhibition of platelet aggregation in healthy subjects. Clin Pharmacokinet 47:129–137

[6] Riendeau D, et al (2001) Etoricoxib (MK-0663): Preclinical profile and comparison with other agents that selectively inhibit cyclooxygenase-2. JPET 296:558–566

[7] Patrono C, et al (2008) Antiplatelet drugs. American college of chest physicians evidence-based clinical practice guidelines, 8th edn. Chest 2008, 133:199S–233S

T-010 Population Exposure–Response Analysis for an Escitalopram Thorough QT Study

Tatiana Khariton[1,*], Timothy J Carrothers[2], Antonia Periclou[1], Lars Lindbom[2], Parviz Ghahramani[1]

[1]Forest Research Institute, Jersey City, NJ, USA; [2]Pharsight, Sunnyvale, CA, USA

Objectives: To develop a population PK-QT model for evaluating the relationship between drug concentrations and the time-matched drug-placebo differences in heart rate corrected QT change for escitalopram doses 10–30 mg/day.

Methods: Data from 27 healthy volunteers in a Phase I study and 107 healthy volunteers in a dedicated Phase IV thorough QT (TQT) study were used to develop a population pharmacokinetic model for escitalopram (ESC) and S-demethyl-citalopram (SDC). The primary goal of the population PK modeling was to predict individual plasma concentrations of ESC and SDC corresponding to the times when the ECG measurements were taken using Holter monitoring following 10 and 30 mg/day doses. The secondary goal of the analyses was to provide estimates of plasma concentrations and C_{max} levels of ESC and SDC following a dose of 20 mg/day, a dosage that was not tested in the TQT study but may be used in clinical practice. The predicted C_{max} levels for 10, 20 and 30 mg/day doses were subsequently used to predict maximum expected QTc change. The population PK analyses for ESC and SDC were developed using the first order conditional estimation (FOCE) method with interaction in NONMEM^{TM} (version VI). For SDC, a direct approach was applied whereby the metabolite concentrations were modeled using a standard disposition model with first order absorption. Under this approach, ESC dose was assumed to drive the SDC model. The dose of SDC was set to 0.3 times the dose of ESC (based on the observed ratio between the mean steady state concentrations for SDC and ESC). The analysis examined the relationship between individual heart rate corrected QT interval (QTcNi) and the individual predicted plasma concentrations of ESC and SDC at 10 and 30 mg/day doses. A nonlinear mixed effects model for QTcNi over time was developed in S-PLUS® v.6.2 for Windows and consisted of additive effects of baseline, placebo, drug effect, and a normally distributed residual error: QTcNi = Baseline + Placebo + Drug Effect + Error. The influence of exposures on QTcNi drug effect was modeled using either ESC individual predicted plasma concentrations, or SDC individual predicted plasma concentrations. Drug effect was modeled either as a linear or an E_{max} relationship. Between-subject variability terms were added on each model parameter but were removed if either numerical convergence was not achieved by the estimation algorithm, or no significant improvement in the fit ($p > 0.001$) was achieved. To assess expected QTc change at 10 and 30 mg/day doses, QTcNi drug effect was simulated for typical steady state C_{max} values predicted the 10 and 30 mg/day doses assuming PK-QT model uncertainty. The expected QTc change at 20 mg/day dose was then interpolated using typical steady state C_{max} values at the same dose.

Results: The population PK models for ESC and SDC were based on 2,454 and 2,472 observations, respectively, collected from 134 subjects across both studies. A 2-compartment model with linear elimination and dose dependent bioavailability parameterized using clearance and volume of distribution best characterized the plasma concentration–time data of ESC. A 1-compartment model with linear elimination parameterized using clearance and volume of distribution best characterized the plasma concentration–time data of SDC. The QTcNi exposure response model was based on 27,164 observations collected from 117 subjects during baseline and active treatment visits. Baseline, placebo, and drug effects for ESC were well estimated (Table 1). For a male subject, typical baseline QTcNi was estimated at 398 ms, with between-subject variability of 16 ms. Mean baseline QTcNi for a female was 10 ms higher. As expected, baseline measurements also followed a strong diurnal pattern; a typical study subject experienced up to a 10 ms range of fluctuation in QTcNi over the course of the full 24-h cycle. After accounting for baseline and diurnal pattern, placebo effect was found to reduce the QTcNi prolongation by 3 ms. A modest diurnal pattern was present in placebo effect as well. Relationship between QTcNi and ESC concentrations was best described by an E_{max} model. The maximal QTcNi change (E_{max}) attributed to ESC was estimated to be 17 ms; the concentration causing half of this increase was estimated to be 47 ng/mL (EC_{50}), which incidentally is a typical C_{max} estimated for a 20 mg dose. Additional between-subject variability in E_{max} was estimated at 66 %. No evidence of hysteresis in the escitalopram exposure-QTc effect relationship was found. After accounting for baseline, placebo, escitalopram, and moxifloxacin effects, an 8 ms residual variability in QTcNi measurements remained. Residuals from the final escitalopram QTcNi model were explored for their association with individually predicted SDC concentrations; no evidence of any association was detected. Hence, most of the QTcNi prolongation observed after repeated administration of escitalopram can be described by the parent compound alone. An independent analysis was also performed assuming a linear relationship between the natural algorithm of the observed PK concentrations and time-matched, placebo-corrected changes in QTcF following 10 and 30 mg/day doses and interpolated for the 20 mg/day dose [1] (Fig. 1).

Conclusions: From the final PK-QT model of escitalopram, simulations estimated a non-clinically relevant placebo-corrected QTcNi prolongation at the recommended therapeutic dosage of 10 mg/day (mean 5.2 ms increase at a typical C_{max} after a steady state 10 mg/day dose with the upper bound of 1-sided 95 % confidence intervals (UCI) at 5.9 ms), a mean increase of 8.3 ms with 95 % UCI of 9.2 ms for the 20 mg/day dose, and a mean increase of 10.2 ms (with 95 % UCI of 11.4 ms) for the supratherapeutic dose of 30 mg/day dose. The independent analysis using linear model and observed concentrations

Table 1 Final Parameter Estimates for QTcNi Plasma Exposure Model with Bootstrap Standard Errors

Main model parameters	Population mean		Additive between-subject variability	
	Estimate	SE, %CV	Estimate	SE
Baseline for males (msec)	397.7	0.5	16.0	1.0
Increase in baseline for females (msec)	9.5	31	–	–
Placebo (msec)	−3.0	4.7	–	–
Log (E_{max}, msec) for escitalopram effect	2.81	3.2	0.66	0.07
Log (EC_{50}, ng/mL) for escitalopram effect	3.84	2.9	–	–
Residual variability (as st. dev.), msec	8.5	0.4	–	–

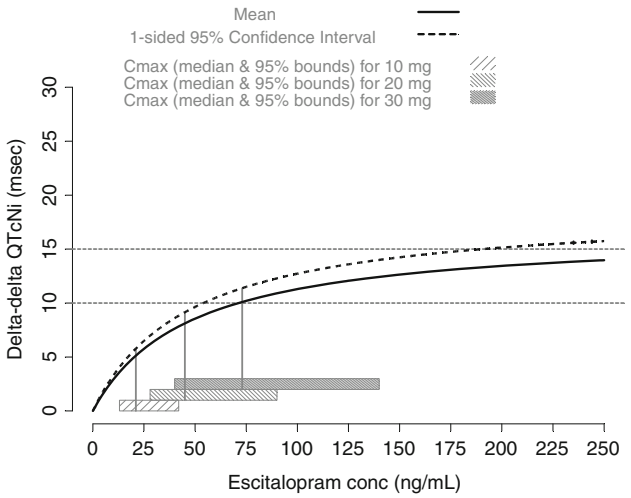

Fig. 1 Time-matched and placebo-corrected QTcNi associated with drug effect at a range of escitalopram concentrations

provided comparable estimates with a mean increase in QTcF of 6.6 ms (with 95 % UCI of 7.9 ms) for 20 mg/day dose [1].

Reference

[1] Prescribing Information for Lexapro® (escitalopram oxalate) Tablets and Lexapro® (escitalopram oxalate) Oral Solution, last modified on 12/2012. http://www.frx.com/pi/lexapro_pi.pdf. Accessed on January 24, 2013.

T-011 Role of Concentration–Response Modeling with Phase I Data in Evaluating QT Interval Prolongation: Results with Ten Compounds

Yeamin Huh[1], Wonkyung Byon[2], Steve Riley[2,*]

[1]University of Michigan, Ann Arbor, MI, USA; [2]Pfizer Inc., Groton, CT, USA

Objectives: The concentration-QT (CQT) relationship is routinely assessed in addition to the intersection–union test (IUT) in thorough QT (TQT) studies to quantify the effect of drugs on the QT interval. Single (SAD) and multiple (MAD) ascending dose studies conducted early in Phase 1 provide a data-rich basis to establish the CQT relationship since it contains wide range of drug concentration and time-matched ECG measurements. This study assessed the predictability of TQT study outcome using CQT analysis of pooled SAD/MAD data from ten compounds at Pfizer.

Methods: Based on availability of both TQT and SAD/MAD studies including ECG data, ten programs were identified. Linear mixed-effect (LME) models were applied using baseline-adjusted QTcF (Fridericia-corrected QT interval) as the dependent variable. Maximum baseline and placebo-adjusted QTcF (ΔΔQTcF) was estimated with the LME model from SAD/MAD data evaluated at the mean maximum concentration from the TQT study, and compared with the ΔΔQTcF estimated by IUT analysis from the TQT study. The same LME models were applied to the TQT data, and ΔΔQTcF and slope estimates from both TQT and SAD/MAD studies were compared.

Results: Positive/negative results of TQT IUT analysis were predicted by CQT analysis of SAD/MAD data for all ten compounds in terms of the mean predicted ΔΔQTcF being greater or less than 5 ms. When the LME model was applied to TQT data, slope estimates and 90 % confidence interval of ΔΔQTcF were generally in good agreement with those from the SAD/MAD data. Bootstrap datasets were additionally generated to account for variability in drug concentrations. When the LME model was applied to bootstrap datasets, maximum ΔΔQTcF estimates were very similar to those from the original data.

Conclusions: Equivalent information about QT prolongation of a drug was obtained from both IUT analysis of TQT data and CQT analysis of SAD/MAD data. Mean ΔΔQTcF <5 ms is a potential criterion for identifying negative compounds with CQT analysis of Phase 1 data to obviate a need for TQT study.

T-012 Modeling Discrete Bounded Outcome Scores Using Random Effects Coarsened Model: A Comparison of Performance of SAS and NONMEM® VII

Xu Steven Xu*, Mahesh Samtani, Partha Nandy

Model-Based Drug Development, Janssen Research & Development, 920 Route 202, Raritan, NJ, USA

Objectives: Random-effects coarsened (CO) models have been proposed for discrete bounded outcome scores (BOS) [1]. The CO model was originally implemented in SAS. Although the CO model has been used in pharmacokinetic/pharmacodynamics modeling with NONMEM [2], its performance with Laplacian approximation in NONMEM has not been formally evaluated. This study is to use Monte Carlo simulations to evaluate the performance of NONMEM VII for mixed effects CO models in comparison with the proc nlmixed in SAS, where numeric integration (Gaussian Quadrature) is often used.

Methods: Monte Carlo simulations were conducted are based on a CO model for Disability Assessment for Dementia Scores (DAD), a functional assessment of Alzheimer's disease. We assume that the normalized discrete response (BOS = R(t)/100) takes the form of k/m, where k = 0, 1, …, m = 100. A latent variable U on (0, 1) is assumed to cause the BOS outcome by:

$$\text{BOS} = \text{k/m if and only if } a_k \le U < a_{k+1}$$

where $a_k = (k - 0.5)/m$, $a_{k+1} = (k + 0.5)/m$, and $a_0 = 0$, $a_{m+1} = 1$. We assume that:

$$log\left(\frac{U_i}{1-U_i}\right) = \beta_{0i} + \beta_{1i} \cdot t + \varepsilon$$

where β_{0i} is the intercept that characterizes baseline disease state, β_{1i} characterizes the rate of disease progression and $\varepsilon \sim N(0, \sigma^2)$. The individual intercept and slope is assumed to follow a multivariate normal distribution. Seven samples per subjects during a 78-week period were simulated at baseline, 13, 26, 39, 52, 65, and 78 week. Two hundred trials were simulated, and each trial contained 2000 subjects.

Results: Both SAS and NONMEM could provide very accurate estimate for all the parameters (both fixed- and random-effects) of the CO model. The estimation bias for all the parameters was virtually identical for SAS and NONMEM, and the largest bias was no more than 2 %. The relative root mean square error (RRMSE) was also similar between SAS and NONMEM, and generally lower than 15 %.

Conclusions: The Laplacian approximation implemented in NONMEM VII provided almost identical performance for estimating both fixed- and random-effect parameters of the mixed effects CO model, compared to the numeric integration (Gaussian Quadrature) implemented in proc nlmixed in SAS. In addition, the run time of NONMEM VII for the mixed CO model was shorter than that of SAS.

References

[1] Molas, M, Lesaffre E (2008) A comparison of three random effects approaches to analyze repeated bounded outcome scores with an application in a stroke revalidation study. Stat Med 27(30):6612–6633

[2] Hu C, et al (2011) Bounded outcome score modeling: application to treating psoriasis with ustekinumab. J Pharmacokinet Pharmacodyn 38(4): 497–517

T-013 Modeling Continuous Bounded Outcome Scores Using Beta Regression with NONMEM® VII

Mahesh N. Samtani[1], Xu Steven Xu[1], Adrian Dunne[2], Partha Nandy[1], An Vermeulen[2], Filip De Ridder[2], the Alzheimer's Disease Neuroimaging Initiative

[1]Model-Based Drug Development, Janssen Research & Development, 920 Route 202, Raritan, NJ, USA; [2]Model-Based Drug Development, Janssen Research & Development, Beerse, Belgium

Objectives: Continuous bounded outcome scores (e.g., ADAS-cog and DAD measured in Alzheimer's disease) are often collected in clinical studies. Since these types of data are often bounded within a certain range, the expectation must be nonlinear due to the ceiling/floor effects, and the error distribution must be heteroskedastic since the variance must approach zero as their mean approaches either boundary score [1]. Therefore, regular regression models, such as normal linear or nonlinear models, are not applicable in such situations [1, 2]. Beta regression models have been recommended to describe these types of data. Implementing beta regression in NONMEM presents difficulties since NONMEM doesn't provide Gamma functions required by the beta distribution density function. The purpose of the study was to use Nemes' approximation to the Gamma function to facilitate the implementation of beta regression in NONMEM.

Methods: Monte Carlo simulations were conducted to simulate continuous outcomes within an interval of (0, 100) based on a beta regression model in the context of Alzheimer's disease. The responses ($R(t)$) re assumed to follow a beta distribution as follows:

$$\frac{R(t)}{100} \sim \text{beta}(\mu\tau, (1-\mu)\tau)$$

where τ is the precision parameter for the beta distribution, and the expected response (μ) for the ith subject on the logit scale is a linear function of time:

$$log\left(\frac{\mu_i(t)}{1-\mu_i(t)}\right) = \beta_{0i} + \beta_{1i} \cdot t$$

where β_{0i} is the intercept that characterizes baseline disease state, and β_{1i} characterizes the rate of disease progression. The individual intercept and slope are assumed to follow a multivariate normal distribution. Seven samples per subject over a 78-week period were simulated at 0, 13, 26, 39, 52, 65, and 78 weeks. Two hundred trials were simulated and each trial had 1000 subjects. The beta regression was applied to the Alzheimer's disease assessment scale (ADAS-cog) from the Alzheimer's Disease Neuroimaging Initiative (ADNI) study, a dataset that is publicly available.

Results: The simulation-reestimation exercise indicated that NONMEM could provide accurate estimates for the fixed-effect parameters with minimum bias (<2 %). There appeared to be some difficulties in estimating the interindividual variability (IIV), i.e. this approach underestimated the IIV of the rate of disease progression by approximately 20 %. In its current implementation, the mixed-effect beta regression model well described the disease progression for the cognitive component of the ADAS-cog from the ADNI study.

Conclusions: Using Nemes' approximation of the Gamma function, NONMEM provided reasonable estimates for both fixed and random-effect parameters of the mixed effects beta regression model. In addition, the NONMEM run time for the mixed beta regression models appeared to be fairly reasonable, i.e., the minimization step without the covariance step took ~2–3 s for the model and data used in the analysis.

Acknowledgements: Data used in preparation of this article were obtained from the Alzheimer's Disease Neuroimaging Initiative (ADNI) database (www.loni.ucla.edu/ADNI). As such, the investigators within the ADNI contributed to the design and implementation of ADNI and/or provided data but did not participate in analysis or writing of this report. A complete listing of ADNI investigators can be found at:www.loni.ucla.edu\ADNI\Collaboration\ADNI_Authorship_list.pdf

References

[1] Kieschnick R, McCullough BD (2003) Regression analysis of variates observed on (0, 1): percentages, proportions and fractions. St atistical Modelling 3:193–213

[2] Ospina R, Ferrari SP (2012) A general class of zero-or-one inflated beta regression models. Comput Stat Data Anal 56(6):1609–1623

T-014 The Population Pharmacokinetics of Subcutaneous Pasireotide in Healthy Volunteers and Cushing's Disease Patients

Jerry R. Nedelman[1,*], Roland Fisch[2], Ke Hu[3], Yanfeng Wang[3]

[1]Novartis, East Hanover, NJ, USA; [2]Novartis, Basel, Switzerland; [1]Novartis, Florham Park, NJ, USA

Objectives: Pasireotide is a novel cyclohexapeptide, injectable somatostatin analogue with high affinity to four of the five known human somatostatin receptors. Cushing's disease (CD) is a devastating disease caused by an adrenocorticotropic hormone (ACTH) secreting pituitary adenoma. The elevated ACTH secretion stimulates the adrenal glands to produce excess cortisol, leading to the subsequent development of the clinical signs and symptoms of hypercortisolism. By targeting somatostatin receptors in the pituitary adenoma, pasireotide can reduce cortisol levels. Its subcutaneous (s.c.) formulation has recently been approved for the treatment of CD in Europe and the US.

During the clinical development of pasireotide s.c., its population pharmacokinetics (PopPK) was assessed separately in healthy volunteers (HV) and CD patients. The results of the separate HV and CD PopPK analyses were qualitatively similar. A three-compartment, linear structural model was found to be adequate for both populations. Age and weight were identified as covariates for both populations, with similar trends where they appeared in common roles.

However, the separate analyses also differed in notable ways. Covariate dependencies were modeled in differently. Apparent clearance for CD was estimated to be about 63 % that of HV at the typical age and weight of HV; because of different dependencies on age and weight, the ratio varied across values of those covariates. Apparent clearance for CD was found to differ between the first and later days of treatment, which was not found for HV. Age and weight were significant covariates for both apparent clearance and apparent central volume for CD, but weight was not identified as significant for apparent clearance for HV. Lean body weight was found to be better than weight as a measure of body size for CD; it had not been considered for HV.

Understanding similarities and differences in the PK of HV and patients is important for information from clinical pharmacology studies conducted in HV to be bridged to clinical studies in patient populations. It is perhaps for this reason that as part of its review of the NDA, the FDA requested a pooled analysis of HV and CD with evaluation of the effect of disease status in addition to covariates as were studied separately. This report describes the combined analysis of HV and CD data, with comparison to the separate assessments.

Methods: The analysis in HV was based on data pooled from five phase I studies. The analysis data set had 4,244 observations from 216 male subjects. The studies included single and multiple s.c.-injection doses ranging from 2.5 to 1500 μg and 7 days' continuous s.c.-infusion doses of 450 to 2,250 μg per day.

The analysis in CD was based on data pooled from two studies. One was the 15-day Phase II study with one dose regimen, 600 μg b.i.d. The other was the 12-month Phase III study with two randomized dose regimens of 600 and 900 μg b.i.d., where dose increases were allowed to 1200 μg b.i.d. for efficacy and decreases were allowed to 300 μg b.i.d. for safety. Combined, the two studies in CD had 2368 observations from 197 CD patients.

Analysis data sets from the separate analyses were combined for the joint analysis of HV and CD. The same three-compartment structural model that was used for both HV and CD separately was used for HV and CD combined. Four covariates were considered in the combined PopPK modeling process: disease status (HV vs. CD), age, total body weight (WT), and lean body weight (LBW). The latter three comprised the union of covariates retained in the final models of the initial separate analyses in HV and CD. Model selection was done with LBW as the measure of body size. When the best model was identified with LBW, that model was refitted using WT in place of LBW, and the better of the two models was retained as the final model.

For model selection, a set of models was considered where the members of the set varied in the relationship between HV and CD. The set was constructed by considering two possibilities for that relationship—HV and CD are similar or HV and CD are different—for each of four components of the overall model: (1) CL/F and V/F; (2) k_a; (3) k_{23} and k_{32}; (4) k_{24} and k_{42}.

Thus, a priori $2^4 = 16$ possible models were considered. Each was fitted and the one with the lowest value of BIC was retained to the next step of replacing LBW by WT.

Results: The final model from the combined analysis had the following features:

- CL/F and V2/F: HV and CD have the same age effects on CL/F and V2/F, have the same LBW effect on CL/F and V2/F, and have the same covariance structure on Day 1. However, typical values of CL/F and V2/F differ between HV and CD.
- k_a: HV and CD are similar.
- k_{23} and k_{32}: HV and CD are similar.
- k_{24} and k_{42}: HV and CD are different.

Combined PopPK results show that pasireotide apparent clearance in CD is typically 59 % that of HV, similar to the value of 63 % derived from the separate analyses. Clearance increases with body size and decreases with age in a similar way for CD and HV, so the ratio of clearance between CD and HV remains constant across ages and weights. Apparent central volume of distribution in CD is typically 43 % that of HV. Volume increases with body size and age in a similar way for CD and HV. For CD, variation across ages and body sizes in summary measures of exposure is similar with the current model as with the model previously fitted to CD alone.

Let V_4/F denote the apparent volume of the deep peripheral compartment and Q_4/F the inter-compartmental clearance between the central compartment and the deep peripheral compartment. Then using

$$k_{24} = Q_4/V_2 \quad \text{and} \quad k_{42} = Q_4/V_4$$

one can compute Q_4/F and V_4/F from the known values of V_2/F, k_{24}, and k_{42}. The following table summarizes the results of such calculations using the final model's parameter estimates. Transfer of pasireotide between the central compartment and the deep peripheral compartment differed between CD and HV, associated with a larger apparent volume of distribution of the deep peripheral compartment among CD patients, being consistent with the fact of higher body fat in CD.

Parameter	Healthy volunteers	Cushing's disease
V_2/F (L)	38.0	16.2
k_{24} (1/h)	0.0398	0.0704
k_{42} (1/h)	0.00865	0.00290
Q_4/F (L/h)	1.51	1.14

Table continued

Parameter	Healthy volunteers	Cushing's disease
V_4/F (L)	175	392

Conclusions: Combined modeling of data from HV and CD confirmed similarities and harmonized dissimilarities between separate analyses, thereby providing further clarity in interpreting results of the clinical pharmacology studies in HV for clinical practice. Clearance for CD is 59 % that of HV at a given age and LBW, yielding correspondingly higher exposures for CD. No physiological explanation for this difference is known. CD patients, who are mostly women, tend to be older and to have lower LBW than the young males comprising the HV population. These differences in demographics tend to yield still lower clearances for CD, about which the model provides a quantification of the dependencies. Although lower in LBW, CD patients tend to be similar in total weight or even heavier than HV, in part due to the accumulation of body fat associated with CD. This might explain the larger deep peripheral volume inferred for CD.

T-015 Implementation of a Global NONMEM Modeling Environment

Lisa M. O'Brien[1,*], Ron J. Keizer[2], Jonathan Klinginsmith[1], Charles Ratekin[1], Michael A. Heathman[1]

[1]Eli Lilly and Company, Indianapolis, IN, USA; [2]Pirana Software & Consulting BV, The Netherlands

Objectives: Lilly is a global corporation with research facilities in many different parts of the world. Within Lilly, there is a large NONMEM [1] user community spread across several of these facilities, in North America, Europe, and Asia. A distributed NONMEM computing environment had previously been developed within Lilly to support these users, and had been in use for approximately 20 years. While this UNIX-based, command line system had many benefits for experienced users, a more user-friendly solution was desired.

Methods: System development was undertaken with the following goals:

- enable team members with varying technical backgrounds to perform modeling and simulation tasks within a unified framework
- take full advantage of existing infrastructure, including the distributed Linux computing environment and fully-automated parallel NONMEM execution
- leverage available open-source tools for automation of common analysis tasks
- reduce the amount of required training for new users, by providing a logical, user-friendly graphical interface
- provide command line access for experienced users who are proficient in using such environment
- automate the generation of report-ready figures and tables
- improve system performance for users outside of the United States (OUS).

Results: A group of PK/PD scientists was convened to evaluate available software, including both open-source and commercial solutions. Based on group consensus, PsN [2,3] and Pirana [4] were selected as the foundation of the new Lilly NONMEM system. PsN would provide an industry-standard automation tool for NONMEM analysis, while Pirana would provide a user-friendly interface with further automation capabilities.

Several solutions for hardware infrastructure were evaluated, including: Windows desktop deployment, Windows-based virtual desktop infrastructure, and a Linux server using NoMachine's NX Enterprise Server and Client software for remote desktop access. The Linux server implementation was chosen due to ease of support, superior performance, and the availability of UNIX command line access for experienced users.

Linux servers were installed in Lilly's Indianapolis, Basingstoke and Singapore research facilities to provide better network performance for OUS users. The servers were integrated with the existing computational infrastructure, using Sun Grid Engine (SGE) [5] for batch execution of NONMEM and PsN. A common file system for these servers was placed in the Indianapolis facility, with local scratch for the Erlwood and Singapore servers to facilitate local access.

Conclusions: Implementation of a user-friendly interface to the existing NONMEM system will significantly increase overall throughput and efficiency in performing PK/PD modeling tasks. The interface will make population analysis more readily available to scientists cross-functionally, thereby allowing PK/PD modeling and trial simulation to be applied to a broader range of drug development programs.

References

[1] Beal S, Sheiner LB, Boeckmann A, Bauer RJ (2009) NONMEM User's Guides. (1989–2009), Icon Development Solutions, Ellicott City, MD

[2] Lindbom L, Pihlgren P, Jonsson EN (2005) PsN-Toolkit–a collection of computer intensive statistical methods for non-linear mixed effect modeling using NONMEM. Comput Methods Programs Biomed 79(3):241–257

[3] Lindbom L, Ribbing J, Jonsson EN (2004) Perl-speaks-NONMEM (PsN): a Perl module for NONMEM related programming. Comput Methods Programs Biomed. 75(2):85–94

[4] Keizer RJ, et al (2011) Piraña and PCluster: a modeling environment and cluster infrastructure for NONMEM. Comput Methods Programs Biomed 101(1):72–79

[5] Gentzsch W (2001) Sun grid engine: towards creating a compute power grid. 1st International Symposium on Cluster Computing and the Grid

T-016 A Model Predicting Penetration of Rifampicin from Plasma to Epithelial Lining Fluid and Alveolar Cells

Oskar Clewe[1,*], Mats O Karlsson[1], Sylvain Goutelle[2,3], John E. Conte, Jr.[4,5], Ulrika SH Simonsson[1]

[1]Uppsala Pharmacometric Research Group, Department of Pharmaceutical Biosciences, Uppsala University, Uppsala, Sweden; [2]Hospices Civils de Lyon, Hôpital A. Charial, Service Pharmaceutique, ADCAPT, Francheville, France; [3]Université Lyon 1, UMR CNRS 5558, Biométrie et Biologie Evolutive, Villeurbanne, France; [4]Department of Epidemiology and Biostatistics, Infectious Disease Research Group, University of California, San Francisco, CA, USA; [5]American Health Sciences, San Francisco, CA, USA

Objectives: In a non-tuberculosis infected population describe rifampicin′s autoinduced plasma concentrations and predict the concentration ratios between epithelial lining fluid, alveolar cells and plasma.

Methods: Rifampicin plasma, epithelial lining fluid and alveolar cells in 40 adult subjects without tuberculosis [1] were included in this analysis. The subjects received rifampicin at 600 mg orally once a day for 5 days. Rifampicin plasma concentrations were measured on day 5 at approximately 2 and 4 h post dose. Concentrations in epithelial lining fluid and alveolar cells recovered by bronchoalveolar lavage were measured at approximately 4 h after the administration of the last dose.

Data analysis was performed with a nonlinear mixed-effects approach as implemented in the software NONMEM, version 7.2 (ICON Development Solutions), using the first order conditional estimation method with interaction (FOCE INTER). R (version 2.15.1) [2] was used for managing, exploring and visualizing data. The model building process was performed in a stepwise fashion, starting from a previously published rifampicin pharmacokinetic enzyme turn-over model [3]. Rifampicin's autoinduction was described with an enzyme turn-over-model, where rifampicin's plasma concentration increase the enzyme production rate which in turn increases the enzyme pool in a non-linear fashion by means of an E_{max}-model. The epithelial lining fluid and alveolar cell drug penetration were described using effect compartments [4], where the penetration coefficients between plasma and epithelial lining fluid (P_{elf}) and plasma and alveolar cells (P_{ac}) were estimated. The time rate constants k_{elf} and k_{ac} were fixed to a value mimicking an almost instantaneous transfer of drug from plasma to epithelial lining fluid or alveolar cells due to the sparse sampling design.

Model selection was based on the objective function value, parameter precision, goodness-of-fit plots (Xpose, version 4.3.5) [5], prediction corrected visual predictive checks (PsN, 3.5.5) [6–8] and scientific plausibility.

Results: The final rifampicin plasma model was a one compartment model with transit absorption compartments and an enzyme turn-over model describing rifampicin's autoinduction.

Parameters related to the absorption and enzyme turnover was fixed to previously published values [3]. Oral clearance and volume of distribution were estimated to 4.8 L/h and 50 L respectively. The data supported inclusion of inter individual variability on oral clearance (69 %).

At four hours post dose the rifampicin's penetration coefficients for epithelial lining fluid and alveolar cells were estimated to 0.27 and 1.17 respectively. This resulted in a mean epithelial lining fluid to plasma ratio of 1.36 and a mean alveolar cell to plasma ratio of 5.81 when compensating for the free fraction (0.2) of rifampicin concentration in plasma [9].

Conclusions: The final model propose a way to describe the often sparse data originating from the use of bronchoalveolar lavage, where only one or a few samples are possible to withdraw from each subject. The model characterizes rifampicin's plasma pharmacokinetic properties including auto-induction as well as the penetration of drug from plasma to epithelial lining fluid and alveolar cells.

References

[1] Conte JE, Golden JA, Kipps JE, Lin ET, Zurlinden E (2004) Effect of sex and AIDS status on the plasma and intrapulmonary pharmacokinetics of rifampicin. Clin Pharmacokine 43(6):395–404

[2] Team RC (2012) R: a language and environment for statistical computing. R Foundation for Statistical Computing

[3] Smythe W, Khandelwal A, Merle C, Rustomjee R, Gninafon M, Bocar Lo M, et al (2012) A semimechanistic pharmacokinetic-enzyme turnover model for rifampin autoinduction in adult tuberculosis patients. Antimicrob Agents Chemother. 56(4):2091–2098

[4] Kjellsson MC, Via LE, Goh A, Weiner D, Low KM, Kern S, et al (2012) Pharmacokinetic evaluation of the penetration of antituberculosis agents in rabbit pulmonary lesions. Antimicrob Agents Chemother 56(1):446–457

[5] Jonsson EN, Karlsson MO (1999) Xpose–an S-PLUS based population pharmacokinetic/pharmacodynamic model building aid for NONMEM. Comput Methods Prog Biomed 58(1):51–64

[6] Lindbom L, Ribbing J, Jonsson EN (2004) Perl-speaks-NONMEM (PsN): a Perl module for NONMEM related programming. Comput Methods Prog Biomed. 75(2):85–94

[7] Lindbom L, Pihlgren P, Jonsson EN (2005) PsN-Toolkit–a collection of computer intensive statistical methods for non-linear mixed effect modeling using NONMEM. Comput Methods Prog Biomed 79(3):241–257

[8] Bergstrand M, Hooker AC, Wallin JE, Karlsson MO (2011) Prediction-corrected visual predictive checks for diagnosing nonlinear mixed-effects models. The AAPS J 13(2):143–151

[9] Moffat AC, Osselton MD, Widdap (ed.) (2004) Clarke's analysis of drugs and poisons, 3rd ed. Pharmaceutical Press, London

Acknowledgments: The research leading to these results has received funding from the Innovative Medicines Initiative Joint Undertaking (www.imi.europe.eu) under Grant agreement no. 115337, resources of which are composed of financial contribution from the European Union's Seventh Framework Programme (FP7/2007-2013) and EFPIA companies' in kind contribution.

T-017 A Model-based Approach to Support Once-a-day Formulation Development for Topically Administered Brinzolamide in Glaucoma Patients

Matthew Fidler*, Allan Weber, Ramesh Sarangapani

Alcon Research, Fort Worth, TX, USA

Objectives: Carbonic Anhydryase II (CAII) changes cell fluid flow. Inhibiting CAII enzymes in the Iris Ciliary Body (ICB) slows aqueous humor production which lowers Intraocular pressure (IOP). Brinzolamide is a CAII inhibitor that is used to treat elevated IOP in ocular hypertensive and glaucoma patients (OAG/OHT).

We present a brinzolamide pharmacokinetics (PK)-pharmacodynamics (PD) model to describe the aqueous humor PK and IOP lowering following topical administration in rabbit, monkey and human. This model was applied to evaluate the operating parameters needed for a once-a-day brinzolamide formulation to give similar efficacy to BID Brinzolamide in OAG/OHT patients.

Methods: Brinzolamide aqueous humor PK data was available from three studies in Dutch Belt rabbits. The pooled rabbit PK data included a single topical dose PK study at 300 μg, a 300 μg BID 14-day topical dose PK study, and a single 1000 μg subconjunctival dose PK study. In addition, aqueous humor PK data was available from a PK study where cynomolgus monkeys were administered two 300 μg drops separated by 5 min. For each of these studies one aqueous humor sample was collected from each eye in a single animal.

Brinzolamide PD data was available in monkeys and humans. The preclinical data was pooled from 9 studies in cynomolgus monkeys. These studies measured IOP in the monkey over 24 h period following QD dosing or BID dosing of brinzolamide. As in the PK studies, the monkey studies administered a single 300 μg drop followed 5 min later by a second 300 μg drop. The human PD data was pooled from 8 clinical studies spanning a wide topical dose range of 90 μg (0.3 %) to 900 μg (3 %), either given as BID or TID dosing regimens.

All data was pooled to create a combined PK model and a linked PD model. A naïve pooled two compartment PK model was used to describe the aqueous humor concentration following topical dose. PK parameters were estimated simultaneously in all species by fitting the model to all available pooled data. Scaling factors were derived using a physiologically-based approach and applied to adjust for differences in a few key model parameters across species. Human or rabbit parameters were adjusted relative to parameters in monkey model. For instance, the absorption coefficient for the topical dose was estimated in monkey and adjusted for differences in rabbit and human corneal thickness. Similarly, inter-species differences in the volume of distribution and clearance from aqueous humor were accounted for using physiological differences in anterior chamber volume. The peripheral volume and inter-compartmental clearances were scaled by the lens weight (monkey-to-rabbit) or by volume (monkey-to-human). The PK model was linked to a direct-effect Hill (PD) model to describe the IOP reduction in humans and monkeys. This mixed-effect model characterized between subject changes in both the amount of IOP lowering (I_{max}), and the concentration required for IOP lowering (IC_{50}). Covariate analysis identified species as significant covariate (i.e. monkey vs human) for IOP lowering and this was incorporated in the model. Additional human covariates such as age, gender, race and iris color were graphically explored but were found not to be significant.

Results: The PK model was able to predict the PK profile of both rabbit and monkey for a wide range of topical dose and dosing regimens (Fig. 1). Similarly the direct effect model was able to capture the IOP response in monkeys and humans for a wide range of topical dose with BID or TID dosing regimens, as shown by a visual predictive plot (Fig. 1). The human IOP-lowering was 8.5 % higher than the Monkey IOP-lowering.

Conclusions: Based on human effect, this model-based simulation inferred that at least a four-fold increase in bioavailability or a two fold increase in bioavailability coupled with a 19 h increase in the retention time was needed for a Brinzolamide QD formulation to achieve and maintain the same efficacy as Brinzolamide BID 300 μg dose.

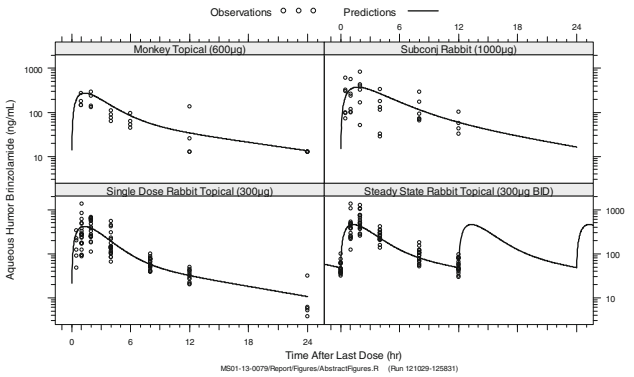

Fig. 1 PK fits for the Monkey & Rabbit

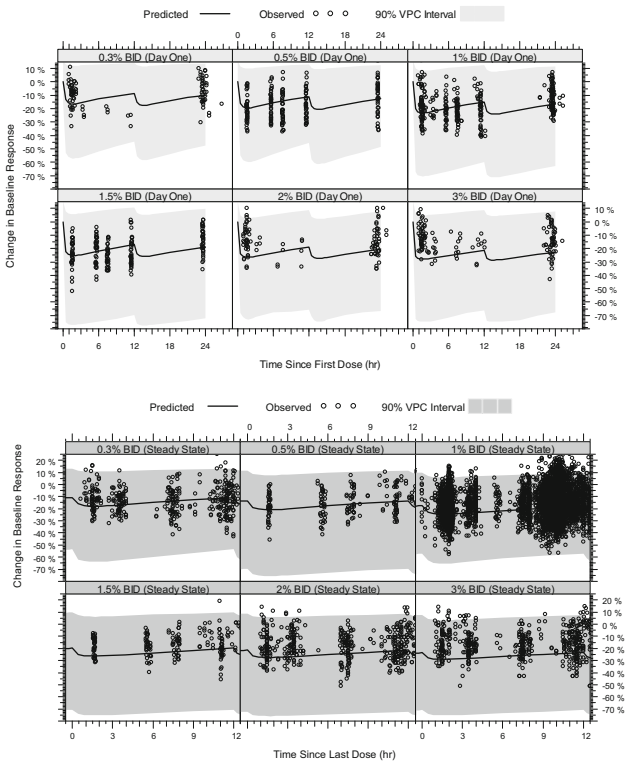

Fig. 2 Visual Predictive Check Plots for Day One and Steady State Change in IOP Response

T-018 Use of a Mechanistic Model of Drug-Induced Liver Injury (DILIsym™) to Support Interpretation of Elevated Liver Transaminase Levels in a Healthy Volunteer Pooled Safety Population for an Orphan Drug Designed for a Life-Threatening Situation

Brett A. Howell*, Lisl K.M. Shoda, Jeffrey L. Woodhead, Yuching Yang, Scott Q. Siler, Paul B. Watkins

The Hamner-UNC Institute for Drug Safety Sciences, Research Triangle Park, NC, USA

Objectives: Compound A is in development for a specific life-threatening situation. The severe nature of the circumstances under which Compound A would be administered is such that the FDA will assess efficacy based on animal studies alone. However, this "Animal Rule" does not apply to safety assessment, which must be determined in humans. In a pooled safety population involving 150 healthy adult volunteers (NHV), marked elevations of serum aminotransferases were observed in some subjects, suggesting possible liver injury. The DILIsym™ model was employed to help interpret the severity of the injury observed in the healthy volunteer population through a retrospective analysis.

Methods: DILIsym™ is a mechanistic, multi-scale, mathematical model being developed to assist in the safety characterization of compounds in clinical development [1–3]. The initial focus is on in vitro to in vivo preclinical and in vivo preclinical to first in human clinical. Simulated humans, dogs, rats, and mice are included, with differences in biochemical variability amongst populations captured in simulated sample populations generated via MATLAB's optimization toolbox. The primary goals for the model include understanding how in vitro toxicity assay results translate to pre-clinical animal models, the relevance of pre-clinical results for humans, and how biomarker results translate to patient safety. In this case study, we focused on the ALT sub-model within the larger DILIsym™ model. The ALT submodel has been constructed based on APAP overdose data, and provides reasonable agreement with data obtained in mice, rats, and man. We adjusted parameters of necrosis rate and transfer rate to generate simulation results consistent with the data obtained in the human volunteers treated

with Compound A. The half lives of the transaminases [4] and the mass per hepatocyte [5] were based on literature values. The predicted percent of hepatocytes lost were then analyzed to assess the relevance of the transaminase increases.

Results: The simulated alanine transaminase (ALT) levels agreed with the NHV data by design. Aspartate transaminase (AST) levels were then used as conformation that the baseline simulated human was reasonable. The AST simulation results were in line with the NHV outcomes observed. The predicted percentage of functional hepatocytes lost for the maximum observed ALT, 95th percentile observed ALT, and median observed ALT levels were around 3.5, 1, and 0.3 % of viable hepatocytes. When variability was introduced to the key parameter values, the percentage of hepatocytes lost was predicted to range from 2.5 to 4.5 % for the maximum ALT observed. The relevance of the magnitudes of the predicted hepatocyte loss values were put into context based on literature reports of liver excision [6], through simulation results compared to biomarker outcomes from NHV studies using heparins [7], and using historical liver biopsy data [8].

Conclusions: The simulations and associated analyses suggest that no subject in the clinical trial likely experienced more than a modest loss of hepatocytes, and that the levels lost were much lower than levels reportedly leading to serious health risks in other scenarios. This case study demonstrates the use of mechanistic models to interpret adverse event signals and how this information can help in communications with regulatory agencies.

References

[1] B.A. Howell, Y. Yang, R. Kumar, J.L. Woodhead, A.H. Harrill, H.J. Clewell III, M.E. Andersen, S.Q. Siler and P.B. Watkins, "In vitro to in vivo extrapolation and species response comparisons for drug-induced liver injury (DILI) using DILIsym^{TM}, a mechanistic, mathematical model of DILI," *Journal of Pharmacokinetics and Pharmacodynamics*, 39 (2012) 527-541.

[2] J.L. Woodhead, B.A. Howell, Y. Yang, A.H. Harrill, H.J. Clewell III, M.E. Andersen, S.Q. Siler and P.B. Watkins, "An Analysis of *N*-Acetylcysteine Treatment for Acetaminophen Overdose Using a Systems Model of Drug-Induced Liver Injury," *Journal of Pharmacology and Experimental Therapeutics*, 342 (2012) 529-540.

[3] S. Bhattacharya, L.K.M. Shoda, Q. Zhang, C.G. Woods, B.A. Howell, S.Q. Siler, J.L. Woodhead, Y. Yang, P. McMullen, P.B. Watkins and Melvin Andersen, "Modeling drug- and chemical-induced hepatotoxicity with systems biology approaches," *Frontiers in Physiology*, 3 (2012) 462: 1-18.

[4] D. Nicoll, C.M. Lu, M. Pignone, and S.J. McPhee, "Pocket Guide to Diagnostic Tests," Stamford, CT : Appleton and Lange, (1997).

[5] C.H. Remien, F.R. Adler, L. Waddoups, T.D. Box, and N.L. Sussman, "Mathematical modeling of liver injury and dysfunction after acetaminophen overdose: early discrimination between survival and death," *Hepatology*, 56 (2012) 727-734.

[6] S. Florman and C.M. Miller, "Live donor liver transplantation," *Liver Transpl.*, 12 (2006) 499-510.

[7] A.H. Harrill, J. Roach, I. Fier, J.S. Eaddy, C.L. Kurtz, D.J. Antoine, D.M. Spencer, T.K. Kishimoto, D.S. Pisetsky, B.K. Park and P.B. Watkins, "The effects of heparins on the liver: application of mechanistic serum biomarkers in a randomized study in healthy volunteers," *Clin Pharmacol Ther.*, 92 (2012) 214-220.

[8] B. Portmann, I.C. Talbot, D.W. Day, A.R. Davidson, I.M. Murray-Lyon and R. Williams, "Histopathological changes in the liver following a paracetamol overdose: correlation with clinical and biochemical parameters," *J Pathol.*, 117 (1975) 169-181.

T-019 Predicting Baseline ADAS-cog Scores from Screening Information using Item Response Theory and Full Random Effect Covariate Modeling

Sebastian Ueckert[1*], Elodie L. Plan[1], Kaori Ito[2], Mats O. Karlsson[1], Brian Corrigan[2] and Andrew C. Hooker[1]

[1]Pharmacometrics Research Group, Uppsala University, Uppsala, Sweden; [2]Primary Care Business Unit, Pfizer Inc., Groton, CT, USA

Objectives: The Mini-Mental-State Examination (MMSE) and the Alzheimer's Disease Assessment Scale - Cognitive Subscale (ADAS-cog) test are two of the most important cognitive assessments in Alzheimer's disease (AD). Both cognitive tests have specific advantages and are generally used for different purposes. While the MMSE is a brief 30-point questionnaire test which is often used for AD diagnosis by a primary care physician, ADAS-cog requires a training for individuals (rators) who administer the test and it takes more than 30 min to complete all the tasks, however, it is considered more sensitive and is one of the primary endpoints accepted by regulatory authorites for clinical studies in mild and moderate AD. Clinical studies generally use the MMSE to evaluate the cognitive capabilities of a potential participant at screening, for a variety of reasons. Consequentially, inclusion and exclusion criteria for the study are mostly written in terms of MMSE score thresholds.

The objectives of this work were to develop a pharmacometric model capable of predicting ADAS-cog assessment scores at baseline based on the results of an MMSE assessment and covariates available at screening.

Methods: Data: The data used for this work was from the Alzheimer's disease Neuroimaging Initiative (ADNI) [1] which was split into estimation and validation datasets. The validation dataset contained 30 randomly selected subjects from each arm of the study (healthy, mild cognitively impaired and mild AD subjects, i.e., 90 subjects in total), the estimation dataset consisted of the remaining 732 subjects from all 3 arms. MMSE (total score) is a sum of scores for each questionnaire in different sub-category tasks (e.g., orientation, command, etc.), and these individual scores were obtained from the ADNI database. For both datasets the MMSE assessment data from the screening visit, the ADAS-cog assessment data from the baseline visit as well as gender, age, and APOE4 genotype were used in this analysis.

Model: This work is based on the previously presented Item Response Theory (IRT) ADAS-cog model [2], which links the response of each test in the ADAS-cog assessment to the hidden variable "cognitive disability" using either a binary, binomial or ordered categorical probability model. The model was extended to MMSE data by adding additional binary models describing the MMSE response as function of the same hidden variable. Additionally, covariate information (gender, age and APOE4 genotype) was introduced into the model using a full random effect model (FREM) approach [3]. Fig. 1

ADAS-cog prediction: Only the information available at screening (MMSE and covariate data) from the validation dataset was used to determine the post hoc distribution (mode and standard error) of cognitive disability for all 90 individuals. The screening visit based cognitive disability distribution was compared to the estimate of cognitive disability after the baseline visit. Furthermore, expected

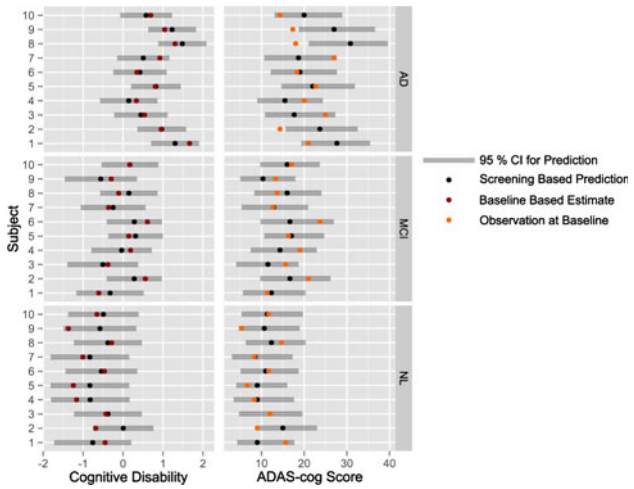

Fig. 1 Comparison of screening and baseline visit based estimates for cognitive disability as well as resulting prediction for ADAS-cog scores for 10 randomly chosen individuals from the validation dataset

ADAS-cog scores for the baseline visit were simulated based on the screening information and compared to the observed values. Information about the study arm, i.e., whether a subject was classified as healthy, mild cognitively impaired or mild AD, was not used for estimation and prediction, but only to evaluate the performance of the model in the different populations.

Results: All Individual MMSE test items were described through a 2 parameter binary model, yielding a total of 50 parameters. Item parameter estimates indicated a relatively low difficulty for most test items, only delayed recall and construction task had higher difficulty. The FREM model did not indicate any significant relationship between cognitive disability and gender or age. However, APOE4 genotype and cognitive disability were correlated with a correlation coefficient of 0.34. The whole FREM model was kept for the ADAS-cog prediction.

For all individuals in the validation dataset, estimates for cognitive disability based on the baseline visit were within the 95 % confidence intervals obtained from the screening information. Bias and imprecision were lowest in the AD and highest in the healthy subjects group, but generally not substantial.

Comparison of the predicted 95 % ADAS-cog score confidence intervals with the observed ADAS-cog scores at the baseline visit showed that the observed score was contained in the confidence interval in 93.2 % of the individuals. The average interval width was 15.3 points, with the largest intervals in the mild AD group and the smallest in the healthy subjects group.

Conclusions: The FREM covariate modeling approach, where covariate associations are estimated as correlations, is ideally suited for an IRT analysis which describes the unobservable disease status as a random effect. The failure to identify age as a relevant covariate might be a result of the age-matching in the healthy control group of the ADNI study.

This work illustrates how IRT can map the two most relevant cognitive tests, ADAS-cog and MMSE, to the same cognitive disability scale and utilizes the resulting model to predict baseline scores from screening information. Low bias and imprecision, especially in the most relevant populations (mild cognitively impaired and mild AD), illustrate the close correspondence between both assessments. These results also suggest the possibility to use the MMSE in longitudinal clinical studies, either in lieu of or interchanging with the ADAS-cog, leading to a significant reduction in assessment effort for both the physician and the patient, and a potential for additional longitudinal data.

References

[1] ADNI (Alzheimer's Disease Neuroimaging Initiative). http://www.adni-info.org/.

[2] Ueckert, S, Plan EL, Ito K, Karlsson MO, Corrigan B, Hooker AC (2012) Application of item response theory to ADAS-cog scores modelling in Alzheimer's disease. *PAGE 21* Abstr 2318. www.page-meeting.org/?abstract=2318

[3] Karlsson (2012) A full model approach based on the covariance matrix of parameters and covariates. *PAGE 21* Abstr 2455. www.page-meeting.org/?abstract=2455

T-020 Strategic Use of a Biomarker and Comparator Modeling to Optimize Dose Selection for Dose-range Finding and to Predict Efficacy and Aid Dose Selection for Ph II

Tomoko Freshwater[1*], Gene Marcantonio[1], Lee Hodge[2], Lars Lindbom[2], Jing Li[1], William Hanley[1], Holly Weng[1], Judith A Boice[1], Hani Houshyar[1], Marcella K. Ruddy[1]

[1]Merck & Co., Inc., Whitehouse Station, NJ, USA; [2]qPharmetra LLC, Andover, MA, USA

Objectives: MRL-1 is under development using a Phase IIa/IIb adaptive design development paradigm. To support the Phase IIa/IIb trial, a modeling and simulation (M&S) approach was extensively used to facilitate optimal dose/regimen selection of MRL-1 based on available Phase I PK and PD (as a biomarker) data as well as comparator Drug-X efficacy data.

Methods: PK and PD data from single and multiple rising dose studies were utilized to develop population PK and PK-PD models. Additional meta-analysis ($\sim$60 references) was conducted to characterize the extent, variability, and patient population impact on placebo effect and the active comparators in the therapeutic field. Furthermore, the expected level of MRL-1 efficacy was predicted by leveraging the published (Drug-X) data in integrated modeling using the relationship between PK-Biomarker-clinical efficacy of Drug-X and PK-Biomarker of MRL-1 to predict MRL-1 clinical efficacy.

Results: A two compartment PK model with a transit compartment to characterize drug absorption was found to best describe the PK data. The relationship between PK and biomarker was characterized using a direct link population PK/PD model. The doses selected and expected to fully characterize exposure–response were MRL-1 A-mg BID (98.8 % inhibition), B-mg QD (95.5 % inhibition), C-mg QD (78.6 % inhibition), D-mg BID (68.0 % inhibition), and E-mg QD (22.0 % inhibition). The MRL-1 A-mg BID and B-mg QD doses are expected to result in near maximal biomarker inhibition (99 %). The E-mg QD dose would be likely associated with sub-optimal efficacy as it has a $C_{average}$ biomarker inhibition of $\sim$22 %.

Conclusions: The modeling efforts were pivotal in helping to select doses expected to fully characterize the exposure–response for biomarker inhibition and efficacy parameter. The Phase II study doses selected were based on predictions of the range of biomarker inhibition (from $\sim$20 to 90 %). Further, a comparator model helped to link biomarker inhibition with the efficacy parameter. Overall, the

modeling approach was extensively and successfully utilized to enhance confidence in program decision making for MRL-1.

T-021 Exposure–Response Modeling and Simulation of the Efficacy Endpoints in Rheumatoid Arthritis

Lian Ma[1*], Ping Ji[1], Yaning Wang[2], Liang Zhao[1], Yun Xu[1], Suresh Doddapaneni[1], Chandrahas G Sahajwalla[1]

[1]Division of Clinical Pharmacology II, Center for Drug Evaluation and Research, Food and Drug Administration, Silver Spring, MD, USA; [2]Division of Pharmacometrics, Office of Clinical Pharmacology, Center for Drug Evaluation and Research, Food and Drug Administration, Silver Spring, MD, USA

Objectives: The common efficacy endpoints used in Rheumatoid Arthritis (RA) clinical trials are the response rate of American College of Rheumatology (ACR) score (ACR20, ACR50, and ACR70 represent at least 20, 50 and 70 % improvement, respectively) and the change from baseline in Disease Activity Score using 28 joints (DAS28). The aim of this current work was two fold: first, to develop pharmacokinetic/pharmacodynamic (PK/PD) models that describe the exposure–response relationships for these efficacy endpoints; and second, to apply this knowledge to aid in sensitive endpoint selection in RA.

Methods: The analysis used clinical data sets extracted from 11 phase II–III clinical trials describing 4,600 patients for 5 approved RA drugs. All these trials were randomized, double-blind, placebo-controlled, parallel group studies in RA patients treated with methotrexate (MTX) as background therapy. For each drug, the modeling was conduced with the pooled dataset combining different studies using sequential PK/PD approach in NONMEM VII. The contribution of drug effect was modeled with a mechanism-based indirect-response model with an E_{max} (maximal drug effect) inhibitory function on the formation rate (k_{in}). For ACR response, the longitudinal placebo/MTX response was modeled empirically with an exponential decay process. The probabilities of ACR response were then modeled with logistic regression combining the indirect-response model with placebo/MTX effect. For DAS28 score, the underlining placebo/MTX effect was incorporated into the E_{max} function in an indirect-response model. The final models were used to predict the clinical outcome at various time points following different treatment regimens. Relative sensitivity of these endpoints was assessed using power analysis based on results of trial simulation.

Results: The developed longitudinal exposure–response models adequately describe the relationship between drug concentrations and the observed ACR20, 50, 70 response rates and DAS28 scores based on various diagnostic plots. None of the covariate factors evaluated (e.g., demographics, baseline disease characteristics) significantly contributed to the between-subject variability in the pharmacodynamic parameters. The trial simulation and subsquential power analysis showed that the ACR20 response generally demonstrated the highest power in detecting significant effect of active treatment versus placebo at evaluated dosing regimens.

Conclusions: The developed exposure–response models can serve as a basis to support future clinical trials design in rheumatoid arthritis disease area.

References

[1] Hutmacher MM, Krishnaswami S, Kowalski KG (2008) J Pharmacokinet Pharmacodyn. 35(2):139–157

[2] Levi M, Grange S, Frey N (2012) J Clin Pharmacol (in press)

T-022 Development of a Complex Combined Parent-Metabolite Population Pharmacokinetic Model for Atorvastatin Acid and its Lactone Metabolite: Implication of Renal Transplantation

Joyce S. Macwan[1*], Wai-Johnn Sam[1], Reginald Y. Gohh[2], Fatemeh Akhlaghi[1]

[1]Clinical Pharmacokinetics Research Laboratory, Department of Biomedical and Pharmaceutical Sciences, University of Rhode Island, Kingston, RI, USA; [2]Division of Organ Transplantation, Rhode Island Hospital, Warren Alpert Medical School of Brown University, Providence, RI, USA

Objectives: The objective of the study was to develop a combined parent-metabolite population pharmacokinetic model of atorvastatin acid to identify and interpret demographic characteristics, genetic polymorphism as well as physiological and pathological factors that significantly alter pharmacokinetic properties of parent drug and its major metabolite.

Methods: The parent drug and metabolite plasma concentrations (1–11 per patient) of 132, male or female non-transplant (diabetic, $n = 46$; non-diabetic, $n = 53$) or stable kidney transplant recipients (diabetic, $n = 22$; non-diabetic, $n = 11$) who administered single or multiple oral doses of atorvastatin calcium (Lipitor®, Pfizer Pharmaceuticals, NY) were included in the study. Plasma concentrations of atorvastatin acid and atorvastatin lactone were quantified using previously validated liquid chromatography-tandem mass spectrometry assay [1]. A total of 639 concentrations including both acid ($n = 322$) and lactone ($n = 317$) form of atorvastatin were analyzed by nonlinear mixed-effects modeling approach (NONMEM®, version 7.2.0, ICON Development Solutions), to identify the influence of patients' specific characteristics on pharmacokinetic properties of both the parent drug and its lactone metabolite. The first-order conditional estimation with interaction method was used to fit the data. The inter-subject variability was assessed using additive, exponential and proportional models. Likewise, the residual variability was evaluated using additive, exponential, proportional and combined additive-proportional error models. The influential covariates affecting pharmacokinetic parameters of both the parent and metabolite were examined thorough PLT Tools (PLTsoft, San Francisco, CA). A stepwise covariate model building approach, forward addition (>3.84, $p < 0.05$, $df = 1$) followed by backward elimination (≥7.9, $p < 0.005$) was used. The final model was validated using visual predictive check and nonparametric bootstrap analysis ($n = 1000$).

Results: Pharmacokinetic characteristics of atorvastatin acid and atorvastatin lactone were well described using two-compartment model with first-order oral absorption and one-compartment with linear elimination, respectively with some degree of inter conversion between the two forms (Fig. 1). The inter-individual and the residual variability of pharmacokinetic parameters for both the parent drug and metabolite were modeled using an exponential and proportional error model, respectively. The population mean estimates of the final model parameters including absorption rate constant (K_a), apparent volume of distribution of atorvastatin acid in the central compartment (V_2/F), apparent oral clearance of atorvastatin acid to atorvastatin lactone (CL/F), apparent volume of distribution of atorvastatin acid in the peripheral compartment (V_3/F), apparent inter-compartmental clearance of atorvastatin acid (Q/F), apparent oral clearance of atorvastatin lactone to atorvastatin acid (CL_M/F), apparent volume of distribution of atorvastatin lactone in the central compartment (V_M/F), apparent inter-compartmental clearance of atorvastatin lactone (Q_M/F) were 0.771 h^{-1}, 481 L, 1126 L/h, 5462 L, 343 L/h, 506 L/h, 2349 L and 748 L/h, respectively. The goodness-of-fit plots of the final model for acid and lactone form of atorvastatin are presented in

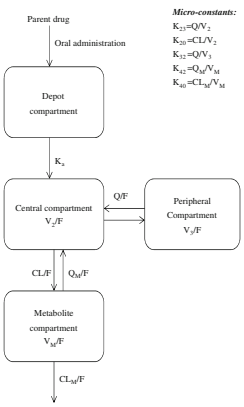

Fig. 1 Compartmental model used in NONMEM

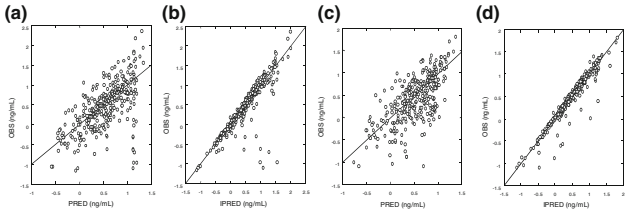

Fig. 2 Observed, individual and population predicted plasma concentrations of the parent (**a** and **b**) and metabolite (**c** and **d**)

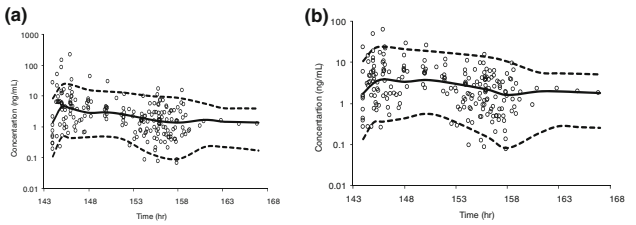

Fig. 3 Bootstrap analysis (**a**) and visual predictive check (**b**)

Fig. 2. It can be depicted from the goodness-of-fit plots that all the points are close to the line of unity indicating good agreement between observed, individual and population predicted plasma concentrations of the parent (Fig. 2a, b) and metabolite (Fig. 2c, d). In this study, we found renal transplantation, LDH (liver enzyme) and gender as the significant covariates for clearance and volume of distribution of lactone metabolite, respectively. Renal transplant recipients had 50 % lower metabolite clearance compared to non-transplant patients. The bootstrap analysis and visual predictive check (Fig. 3a, b) demonstrated robustness of the present population pharmacokinetic model.

Conclusions: In summary, a combined parent-metabolite population pharmacokinetic model of atorvastatin acid was developed. The pharmacokinetic analysis indicated significantly reduced clearance of lactone metabolite in stable kidney transplant recipients. Greater risk of statin-related skeletal muscle toxicity is possibly because of decreased clearance of lactone metabolite [2]. This finding should be taken into account while prescribing atorvastatin treatment in kidney transplant population who have additional co-morbidities and are on multiple interacting medications.

References

[1] Macwan JS, Ionita IA, Dostalek M, Akhlaghi F (2011) Development and validation of a sensitive, simple, and rapid method for simultaneous quantitation of atorvastatin and its acid and lactone metabolites by liquid chromatography-tandem mass spectrometry (LC–MS/MS). Anal Bioanal Chem 400(2):4 23–433

[2] Hermann M, Bogsrud MP, Molden E, Asberg A, Mohebi BU, Ose L, et al (2006) Exposure of atorvastatin is unchanged but lactone and acid metabolites are increased several-fold in patients with atorvastatin-induced myopathy. Clin Pharmacol Ther 79(6):532–539

T-023 Characterizing the Pharmacokinetics of Imatinib in Hard-to-Test Pediatric Population via Physiologically-Based Pharmacokinetic Modeling

Linh M. Van[1*], Ryosei Leo Kawai[1, 2], William Sallas[3], Yanfeng Wang[4]

[1]Novartis, Cambridge, MA, USA; [2]Daiichi Sankyo Co. Ltd, Tokyo, Japan; [3]Novartis, East Hanover, NJ, USA; [4]Novartis, Florham Park, NJ, USA

Objectives: The analysis focused on the application of physiologically-based pharmacokinetic (PBPK) modeling to project imatinib concentration–time profiles in plasma of pediatric patients scaled from adult patient population. The development and evolution of the imatinib PBPK model to support clinical dose recommendation in pediatric patients will be discussed.

Methods: A previously developed PBPK model for imatinib to support first-in-human (FIH) dose projections validated using animal data [1] was subsequently optimized with adult data. Extrapolation to pediatrics was done by scaling clearance range observed in a phase III trial in adults to project imatinib exposure in pediatric population. Particular attention with respect to understanding the PK behavior in hard-to-test age groups, such as 1 year old was explored. Model parameters were modified using growth and maturation database obtained from literature. The effects of body size and blood perfusion on the PK profiles were evaluated in addition to maturation in clearance. The projections of plasma concentrations based on the proposed pediatric body surface area (BSA) normalized dose were compared with available observed concentrations similarly normalized as part of the model evaluation.

Results: The projected plasma concentration–time profiles were generally in good agreements with the observed plasma concentration for most pediatric subjects, except for the youngest, for which the exposure appeared to be over-predicted, especially C_{max} at steady state after multiple doses (Fig. 1).

The differences in predictions of children and adults seemed to be due to mixed results of changing distribution volume and blood circulating flow rate, in addition to clearance maturation with age. Improvement of model prediction could be achieved for young subjects by refining certain model assumptions or parameters, such as assuming different plasma protein maturation in cancer patients from healthy subjects, or a lower extent of oral absorption for those age groups instead of a complete absorption - considering the immaturity of the gastrointestinal tract. Collectively, the prediction was within (<2-fold) of the adult exposure suggesting a useful application of PBPK approach in scaling imatinib clearance down to children at 1 year of age.

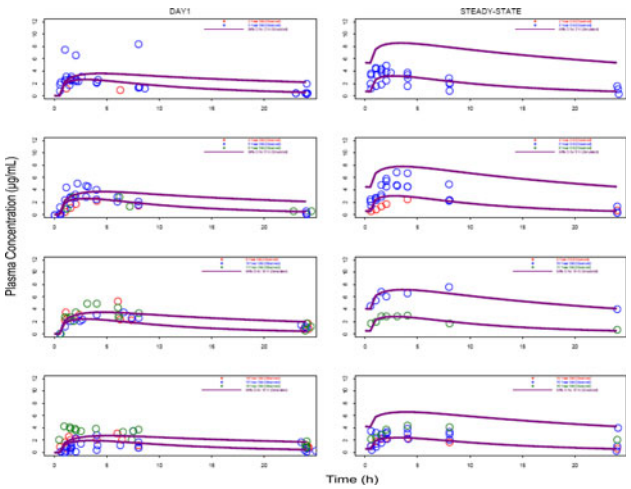

Fig. 1 Imatinib observed plasma concentrations and the predicted range (µg/mL) vs. hours after 1st dose (left panel) and after multiple doses at steady state (right panel) by age groups (top to bottom: 2-3, 4-6, 9-11, and 14-16 years)

Conclusions: With no PK in children less than 2 years of age, the PBPK pediatric simulation provided a scientific rationale to support the dose recommendation of imatinib in children down to 1 year of age. Early development of such mechanistic models allowed seamless integration of preclinical data to predict PK in adults and from adults to pediatrics for clinical dose justification; thereby, an integrative platform evolved to address issues that were raised during the development program for imatinib.

Reference

[1] Tanaka C, Kawai R, Tse FLS (1999) Physiologically-based pharmacokinetic modeling of a protein-tyrosine kinase inhibitor, STI571. AAPS PharmSci 1(4)

T-024 Using Monte Carlo Simulations to Assess Dosing Regimen Adjustments of Piperacillin/Tazobactam in Obese Patients with Varying Renal Functions

Teodora Pene Dumitrescu[1,2*], Rachael Kendrick[1], Heidi Calvin[3], Seth Berry[1]

[1]Quintiles, Overland Park, KS, USA; [2]GlaxoSmithKline, Research Triangle Park, NC, USA; [3]Shawnee Mission Medical Center, Shawnee Mission, KS, USA

Objectives: Piperacillin is a time-dependent antibiotic, for which the time the free-drug concentrations exceed the minimum inhibitory concentration (MIC) is the key pharmacodynamic parameter. The piperacillin/tazobactam (PTZ) label recommends dose adjustments when creatinine clearance (CrCl) is below 40 mL/min. In addition, extended-infusion dosing regimens assessed via Monte Carlo Simulation (MCS) methods were shown to be superior to traditional (short-term) dosing regimens at the same daily dose. With the increased rates of obesity throughout the world, exploring the effects obesity has on antimicrobial disposition and clinical effectiveness is critical. Reports have suggested that dose adjustments may be warranted based on the anticipated alterations in both the volume of distribution (Vd) and clearance (Cl) in the obese population. However, PTZ dosing in obese patients with renal impairment has not been well studied. The objective of this study was, using MCS methods, to compare the probability of target attainment (PTA) of PTZ in normal and obese patients of varying renal functions for traditional and extended-infusion dosing regimens.

Methods: The piperacillin population PK model selected from the literature was a one compartment model with zero-order input, first order elimination, and that included CrCl and body weight (WT) as covariates on Cl and Vd, respectively [1]. Using this model, 30 trials (1000 subjects/trial) were simulated with obese (BMI $>$ 30 and WT $>$ 90 kg; test) and normal weight population (BMI between 18.5 and 25, and WT $<$ 90 kg; control) treatment arms using the Pharsight® Trial Simulator™ 2.2.2 software package, including both population variability and parameter uncertainty. The highly correlated CrCl and WT covariates were obtained by sampling, with replacement, from an existing database of 957 real subjects. Simulations were conducted using the following dosing regimens:

The PTA (for MICs of 16, 32 and 64 mg/L) calculation was stratified by CrCl ($\leq$20 mL/min, 20–40 mL/min, and $>$40 mL/min) for each trial, and summarized across all trials in the obese and normal weight populations.

Results: MCS of the target attainment rates for short- (30 min) and prolonged- (4 h) infusion dosage regimens revealed no differences between the normal and obese populations in any of the CrCl strata. In support to the current dose adjustment recommendations, an inverse relationship was observed between PTA and CrCl for all regimens, in both weight groups. Within the same daily dose level, all extended-infusion PTZ regimens were pharmacodynamically superior to the short-infusion regimens. Simulations showed that all treatment regimens resulted in suboptimal mean PTA for MIC of 64 mg/L. For a 32 mg/L MIC, all regimens resulted in suboptimal mean PTA in the $>$40 mL/min CrCl group, while regimens 7 and 9 were the only two regimens resulting in mean PTA $>$80 % for the $<$20 mL/min and 20–40 mL/min CrCl groups. For MIC of 16 mg/L, the only regimen with a mean PTA $>$80 % in the $>$40 mL/min CrCl group was regimen 9. In addition, regimens 1, 5, 7, and 9 resulted in $>$80 % mean PTA in the $<$20 mL/min and 20–40 mL/min CrCl groups.

Regimen	PTZ dose (g)	Infusion	Time interval (h)	Regimen	PTZ dose (g)	Infusion	Time interval (h)
1	3.375	30 min	Every 6	6	3.375	4 h	Every 12
2	2.25	30 min	Every 6	7	4.5	30 min	Every 6
3	2.25	30 min	Every 8	8	4.5	30 min	Every 8
4	2.25	30 min	Every 12	9	4.5	4 h	Every 8
5	3.375	4 h	Every 8				

Conclusions: In contrast to the theory that obese individuals may require different PTZ dosing regimens, no influence of weight on piperacillin exposure and PTA was observed for any of the simulated dosage regimens. This suggests that no weight-based PTZ dose adjustments are required in obese population. In addition, the MCS results presented here show that prolonged-infusion regimens achieved higher PTAs compared to 30 min infusions, at the same daily dose, thus validating the use of extended-infusion regimens in both the normal weight and the obese individuals. Additional MCSs are required to identify PTZ dosing regimens that achieve PTA $>$80 % for the 32 and 64 mg/L MIC levels, in each of the CrCl strata.

Reference

[1] Li C, Kuti JL, Nightingale CH, Mansfield DL, Dana A and Nicolau DP (2005) Population pharmacokinetics and pharmacodynamics

of piperacillin/tazobactam in patients with complicated intra-abdominal infection. J Antimicrob Chemother 56:388–395

T-025 A Cloud-based Cluster Computing Platform for Pharmacometric Applications

Timothy Bergsma*, William Knebel, Daniel Polhamus, Jeffrey T. Hane, Marc R. Gastonguay

Metrum Research Group LLC, Tariffville, CT, USA

Objectives: The advent of cloud computing creates new opportunities and challenges with respect to the perennial need for a production-quality pharmacometric computing infrastructure. We sought to design a platform that minimizes *cost*, *maintenance*, and *system-dependence* while maximizing *scalability*, *quality assurance*, and *feature support* for two widely-received pharmacometric applications: NONMEM® [1] and OpenBUGS [2].

Methods: OpsCode Chef [3] software was used to develop a machine image for Amazon Web Services [4]. Chef allowed fully scripted hardware abstraction for systematic version control of the image during development. The image itself was deployed simultaneously on an arbitrary number of virtual machines (i.e., a cluster) using StarCluster [5] control software residing on the user's workstation. On the image, the following were pre-installed: NONMEM 7.2.0 (using NMQual 8.1.3 [6] and Intel Fortran compiler 12.0.4 [7]), OpenBUGS 3.2.1, R 2.15.1 [8], Sun Grid Engine 6.2 [9], and RStudio Server 0.96.316 [10]: a full-featured, browser-accessible environment for R. Post-deployment, the R package metrumrg 5.24 [11] was installed to provide NONMEM® connectivity, while the package R2OpenBUGS 3.2-1.4 [12] was installed as the OpenBUGS connector. Pharmacometric applications were accessed as follows (Fig. 1): the user pointed a web browser at RStudio Server, authenticated, and loaded metrumrg and/or R2OpenBugs; NONMEM® or OpenBUGS was then invoked per the package documentation—optionally by means of scripted commands. Features in the packages metrumrg and qapply adequately supported parallelization by means of Sun Grid Engine for NONMEM® and OpenBUGS, respectively. Parallelization was supported across runs, and within runs by individual (NONMEM®) or by Markov Chain (OpenBUGS). Machines were added or removed from the active cluster as necessary.

Results: The resulting platform met our expectations for a production modeling and simulation environment. The use of cloud resources minimized *cost* while maximizing *scalability*: fees were based only on computational time and block storage used; additionally, arbitrary numbers of virtual machines, initiated by any number of individual end-users, could be employed simultaneously without the otherwise-prohibitive costs of full ownership. Use of version-controlled machine images reduced *maintenance* burden while enhancing *quality assurance*: the image, which could be implemented on either fixed persistent or elastic cloud computing (EC2) instances, represented a well-defined management target that could be systematically characterized and readily reproduced with a complete audit trail. Additionally, in the event of a service outage, the image could be efficiently cloned in a different service region. Use of a browser interface with server-hosted software helped homogenize user experience, thereby limiting *system dependency* from the user's perspective. All *features* of the target applications were supported by this paradigm. In particular, access to an arbitrary number of nodes in a cluster environment made within-run parallelization highly practical; run times for representative models under NONMEM® 7.2 dropped substantially with even modest parallelization relative to single-core execution (Table 1). Extensive use of open-source components made this solution easy to adopt: R, RStudio, metrumrg, R2OpenBUGS, NMQual, OpenBUGS, Sun Grid Engine, Chef, StarCluster, and alternative Fortran compilers are freely available.

Fig. 1 A web browser connects to RStudio Server—hosting an R environment in which corresponding packages serve as connectors to pharmacometric applications (NONMEM® and OpenBUGS)

Table 1 Run times (h) under NONMEM® 7.2.0 for two representative models using various numbers of cores (i.e. 'nodes' argument in the 'pnm' file)

Model	Dual absorption	linear/non-linear	PKPD
NONMEM® 7.2.0 subroutine	ADVAN6		ADVAN6
Subjects	1000		70
Cores	Time		
1	80.7		4
8	16.8		1.1
16	8.9		0.66
24	6.2		0.4
48	3.8		.31
96	2.5		

Conclusions: A cloud-based cluster computing solution enabled economical, scalable use of pharmacometric applications in a multi-user environment. Full feature support, ease of maintenance, and superior quality assurance were accommodated. The design made extensive use of off-the-shelf components. When implemented with EC2, this platform practically eliminated the impact of computation time from the critical path of completion for typical pharmacometric projects.

References

[1] Beal S, Sheiner LB, Boeckmann A, Bauer RJ, NONMEM User's guides (1989–2009). icon development solutions, Ellicott City

[2] Lunn D, Spiegelhalter D, Thomas A, Best N (2009). The BUGS project: evolution, critique, and future directions. Stat Med 28:3049–3067

[3] http://www.opscode.com/chef/

[4] Fusaro VA, Patil P, Gafni E, Wall DP, Tonellato PJ (2011). Biomedical cloud computing with Amazon web services. PLoS Comput Biol 7(8): e1002147. http://www.ploscompbiol.org/article/info%3Adoi%2F10.1371%2Fjournal.pcbi.1002147

[5] http://web.mit.edu/stardev/cluster/

[6] http://nmqual.googlecode.com

[7] Knebel W, Bergsma TT, Dagdigian C, Hane J, Gastonguay MR (2010) Utilizing NONMEM 7 and the Intel Fortran compiler in a distributed computing environment. Population Approach Group Europe. http://www.page-meeting.org/pdf_assets/6315-PageNM7IFCposter.pdf

[8] R Core Team (2012) R: a language and environment for statistical computing. R Foundation for Statistical Computing, Vienna. ISBN 3-900051-07-0. http://www.R-project.org/

[9] Gentzsch W (2001). Sun grid engine: towards creating a compute power grid. Proceedings of the 1st international symposium on cluster computing and the grid. IEEE computer society, p 35, Washington, DC. http://dl.acm.org/citation.cfm?id=792378

[10] http://www.rstudio.com/ide/download/server

[11] Bergsma TT, Knebel W, Fisher J, Gillespie WR, Riggs MM, Gibiansky L, Gastonguay MR (2013). Facilitating pharmacometric workflow with the metrumrg package for R. Comput Methods Prog Biomed 109:77–85. http://www.sciencedirect.com/science/article/pii/S0169260712001915

[12] Sturtz S, Ligges U, Gelman A (2005). R2WinBUGS: a package for running WinBUGS from R. J Stat Softw 12(3):1–16. http://cran.r-project.org/web/packages/R2OpenBUGS

T-026 Understanding PK of Coral Snake Envenomation: Torward Improved Antivenom Therapy

Dayanira Paniagua[1*], Lucía Jiménez[1], Camilo Romero[2], Irene Vergara[1], Arlene Calderón[1], Melisa Benard[1], Michael Bernas[3], Carlos Sevcik[4], Marlys Witte[3], Leslie Boyer[5], Alejandro Alagón[1]

[1]Instituto de Biotecnología, Universidad Nacional Autónoma de México, Cuernavaca, México; [2]Departamento de Producción Agrícola y Animal, Universidad Autónoma Metropolitana, Unidad Xochimilco, México, DF, México; [3]Department of Surgery, University of Arizona, Tucson, AZ, USA; [4]Instituto Venezolano de Investigaciones Científicas (IVIC), Caracas, Venezuela; [5]Venom Immunochemistry, Pharmacology, and Emergency Response (VIPER) Institute, University of Arizona, Tucson, AZ, USA

Objectives: Coral snake (*Micrurus fulvius*) is a poison snake endemic from US. The mayor toxins of venom are presynaptic neurotoxins that alter the acetylcholine release in the neuromuscular junction causing a progressive paralysis that can evolve to respiratory arrest, the mayor immediate cause of death. Symptoms may be delayed for 18 h after the bite, making the diagnosis of severe envenomation complicated [1], consequently, when a person is bitten, antivenom is administered by intravenous bolus injection. The selected dose (number of vials) is based in the experience of the treating doctor. Since the PK of coral snake venom has never been described, the aim of this work are: (1) To have a better understanding of coral snake envenomation through the knowledge of the pharmacokinetics of venom administrated subcutaneously and by measuring the contribution of the lymphatic in the absorption and distribution of venom [2]. (2) To analyze the impact of the intravenous antivenom in venom pharmacokinetics. (3) To correlate de above a data with the development of symptomatology and to find biomarkers that could be used as endpoints in future clinical trial designs.

Methods: The absorption and systemic bioavailability of *M. fulvius* venom after SC administration was determined using a central lymph-cannulated sheep model (group 3). As the reference, we also used non-cannulated animals (group 2). Also, the kinetics of the venom was followed after intravenous bolus injection (group 1) (Fig. 1). For antivenom effect, we administrated antivenom in an intravenous bolus injection after 2 h of subcutaneous administration of venom. Each of the three groups included four sheep; experiments lasted 6 h and the animals were kept under anesthesia during the whole experiment. Venom concentrations in serum and lymph were measured by sandwich enzyme-linked immunoassay.

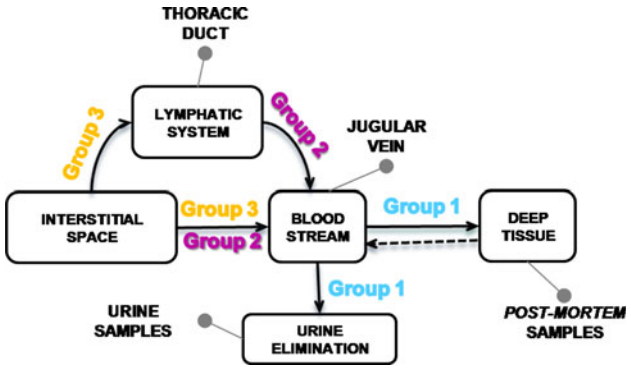

Fig. 1 Experimental design to analyze the absorption, distribution and elimination of the venom administrated SC

Results: The kinetics were determined (Fig. 2) and preliminary non compartmental PK analysis has been made [3], showing that venom injected into blood stayed in systemic circulation for 75 ± 7 min (MRT), with a half-life ($t_{1/2}$) of 25.3 ± 3.2 min, a initial volume of distribution V_D of 3.2 ± 0.5 l equivalent to 7 % of body weight, that increase in steady state to 12 ± 1.8 % (Vss = 5.7 ± 9 l). In contrast, when administered subcutaneously the venom MRT, $t_{1/2}$ and Vss

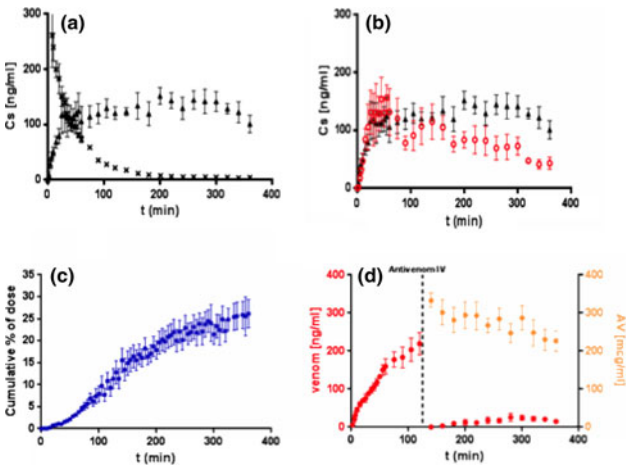

Fig. 2 **a** Serum venom concentrations after one mg IV inyection (×), and SC administration to non-cannulated sheep after SC inyection of 5 mg of *M. fulvius* venom (···). **b** ▲ Serum venom concentration following SC administration in non-canulated (·) and lymph ▲ cannulated sheep (□) after SC inyection of 5 mg of *M. fulvius* venom. **c** Cumulative percentage of the venom dose collected in lymph cannulated sheep after SC inyection of 5 mg of *M. fulvius* venom. **d** Serum venom and antivenom concentration after SC inyection of 5 mg of *M. fulvius* venom in non-cannulated sheep followed by antivenom administration in a bolus intravenous dose 2 h later. Symbols represent the mean ± SEM for $n = 4$ animals per treatment group

increased 5.5, 9 and 5.6-fold, respectively. The absorption of venom to blood was incomplete when the venom was injected SC, with a recovery of 60 ± 5 % of the initial dose during the 6 h of the experiment. Lymph contributed with 39 % of the absorbed venom to blood. When the antivenom is injected, the AUC is impacted decreasing 1.6 fold since the venom concentrations fall immediately to unquantifiable levels.

Conclusions: Preliminary results show a nonlinear pharmacokinetic behavior of venom when is injected subcutaneously. The absorption of venom by the lymphatic system plays a relevant role. The inoculation site functions as a venom depot, which prolongs the absorption and residence time of venom. When the AV is administrated IV, the venom levels fall until undetectable. Further non-linear analysis should been needed to establish a realistic model that can predict the pharmacokinetic and simulate the effect of different doses and administration routes for antivenom therapy.

References

[1] Kitchens CS (1987) LHS Van Mierop: Envenomation by the eastern coral snake (*Micrurus fulvius fulvius*). JAMA 258: 1615–1618

[2] Porter, CJH, SA Charman (2000) Lymphatic transport of proteins after subcutaneous administration. J Pharm Sci. 89: 297–310

[3] AGAH working group pharmacokinetics: collection of terms, symbols, equations, and explanations of common pharmacokinetic and pharmacodynamic parameters and some statistical functions (2004), 3–5

T-027 Target-Mediated Drug Disposition (TMDD) of AMG 145, a Fully Human Anti-Proprotein Convertase Subtilisin/Kexin Type 9 (PCSK9) Monoclonal Antibody after Administration to Non-Human Primates

Anita Grover[1], Maurice G. Emery[1], David Salinger[1], Alex Colbert[1], Megan A. Gibbs[1], Clapton S. Dias[2], Joyce Chan[3], Simon Jackson[3], John P. Gibbs[1,*]

[1]Amgen, Seattle, WA, USA; [2]Amgen, Thousand Oaks, CA, USA; [3]Amgen, South San Francisco, CA, USA

Objectives: AMG 145 is a monoclonal antibody being developed for hypercholesterolemia. AMG 145 binds to PCSK9 with high affinity, preventing its interaction with the LDL receptor (LDLR), restoring LDLR recycling and LDL-C uptake. The objective was to characterize the PK/PD of AMG 145 after single dose administration in nonhuman primates.

Methods: Male, naive cynomolgus monkeys were randomly assigned to placebo ($n = 10$) or one of six treatment groups ($n = 5$/group): 0.05, 0.2, 0.5, 3, 10, or 30 mg/kg. Each subject received a single SC injection. Serum unbound AMG 145 and PCSK9 were measured using ELISA, and LDL-C was measured using a clinical analyzer. Simultaneous PK/PD analyses were performed with NONMEM 7.2.

Results: Nonlinear PK was observed for AMG 145, and dose-dependent decreases in unbound PCSK9 and LDL-C were observed following AMG 145 administration. The quasi-steady-state approximation to the TMDD model described unbound AMG 145 and PCSK9. The model was optimized by allowing the steady state constant (K_{ss}) to increase after a time delay. The linear PK parameters suggested an 11.5 day half life after saturating doses. An indirect response model captured the time course of LDL-C reduction. Suppression of PCSK9 below the estimated IC_{50} of 1.13 nM (inter-subject variability: 58 %) resulted in significant LDL-C reduction. Based on model predictions, a maximal reduction in LDL-C of ~80 % was predicted after the 3 mg/kg dose.

Conclusions: A semi-mechanistic PK/PD model well characterized AMG 145 and LDL-C response in non-human primates. The model included elimination of AMG 145 through its interaction with PCSK9 consistent with the mechanism of action. This model may have applicability to human studies.

T-028 Prediction of Thorough QT Trials based on Population Pharmacokinetic: Pharmacodynamic Analysis of Phase I Study QT Data

Mirjam N. Trame[1,*], Torbjörn Vik[2], Ulrika Wählby Hamrén[3], Karin M. Henriksson[4,5], Lena E. Friberg[1]

[1]Pharmacometrics Research Group, Department of Pharmaceutical Biosciences, Uppsala University, Uppsala, Sweden; [2]AZ ECG Centre, AstraZeneca R&D, Mölndal, Sweden; [3]Clinical Pharmacology&Pharmacometrics, AstraZeneca R&D, Mölndal, Sweden; [4]Department of Medical Sciences, Uppsala, Sweden; [5]Department of Epidemiology, AstraZeneca R&D, Mölndal, Sweden

Objectives: 'Thorough QT (TQT) trials' are expected from regulators in drug development for non-antiarrhythmic drugs, because of the association between QT prolongation and the risk of torsades de pointes. [1] An approach that can make the evaluation of the QT prolongation potential of drugs more cost-effective would be valuable. At AstraZeneca (AZ) high-quality digital electrocardiogram (dECG) measurements are performed as standard in the Phase I single (SAD) and multiple (MAD) ascending dose studies. The aim of this population analysis was (1) to develop a model to quantify possible drug effects on the heart rate corrected QT (Fridericia's correction; QTcF) interval, to be used for prediction of the typical trends and variability of QTcF in TQT trials, and (2) to explore whether constructed 5 min mean QTcF interval data are informative enough, compared to 10 s replicates with 1 min or 30 s intervals over a 5 min period, for QTcF interval measurements in terms of estimation of the underlying diurnal rhythm, estimation of drug effect on QTcF interval, and associated variability.

Methods: The database included drug concentrations and QTcF dECG data for two compounds, which had been investigated in SAD and MAD studies as well as in TQT studies. The SAD/MAD datasets consisted of 14,291 QTcF measurements from 162 subjects for compound 1 and 22,209 QTcF measurements from 128 subjects for compound 2. The PK and QTcF data from the TQT study were blinded for the analysts at Uppsala University up until predictions of the TQT studies had been performed based on the analysis of the SAD/MAD data. Population PKPD-models were developed using non-linear mixed effects modeling in NONMEM7. In the analysis step of the SAD/MAD data, cosine functions were investigated to describe the underlying (placebo) diurnal change in QTcF measurements. Thereafter, linear, E_{max} and sigmoid E_{max} relations between plasma concentrations and drug effect on QTcF were evaluated. Gender and study effects were investigated as covariates. Various sources of variability were evaluated such as IIV (including covariance) and IOV in the parameters (including the residual error), autocorrelation between QTcF measurements, and the sensitivity to the assumption of normally distributed residuals by application of the dynamic transform both sides (TBS) approach. [2] The placebo and drug effect models were evaluated for three different ways of handling the QTcF interval data: (i) 5 min mean QTcF interval data (1 obs per time point), (ii) one 10 s replicate every 30th s over 5 min

(i.e. 10 obs per time point), and, (iii) one 10 s replicate per min (i.e. 5 obs per time point) over 5 min.

Once the QTcF model had been developed based on the SAD/MAD data, the TQT study outcomes were predicted based on the TQT design. To allow for simulation of the drug concentrations in the TQT study without development of a population PK compartment model, a dose-and-time-point specific PK "model" was built from the SAD/MAD PK data for each dose level that was studied in the TQT studies. Typical values and their variability at each time point were estimated, and a covariance between time points was allowed (full BLOCK matrix). The estimates from the PK "model" and the final estimates of the PK-QT model based on SAD/MAD data were applied in the simulations. Simulations were performed as a Visual Predictive Check (VPC), i.e. the median, 5th and 95th percentiles and the 95 % confidence intervals (CI) of the percentiles were computed from the simulated data and after unblinding, the observed QTcF data in the TQT studies were overlaid.

Results: The 1 min and 30 s QTcF interval data showed similar results, while the 5 min mean QTcF interval data did not support the same model complexity (diurnal rhythm, drug effect and variability) and resulted in different parameter estimates. For both drugs, using the 30 s QTcF interval data, the underlying (placebo) baseline was best described by a dual cosine function with periods of 12 and 24 h. Women had typically 20 ms higher QTcF than men while there was no significant difference between studies. Both drugs were found to have a small significant drug effect on QTcF which was best described for compound 1 by an additive linear model (Slope = 0.0034 ms/nM (90 % CI: 0.002–0.0044 ms/nM), IIV(SD) = 0.004 ms/nM) predicting an increase in QTcF of 9.3 ms at the highest observed concentration, and for compound 2 by an additive sigmoid E_{max} model with a low E_{max} (0.0026 ms; 90 % CI: 0.0014–0.0038 ms) for the typical individual but with a relatively high IIV (SD = 11 ms). IIV on the Slope and E_{max} were additive, predicting that the drug increases QTcF in some subjects and reduces QTcF in others. IOV was found to be statistically significant on baseline QTcF for both compounds. Overall the model adequately described the observed SAD/MAD data. After unblinding of the TQT data, it was revealed that the simulations agreed well with the typical trends and variability in the observed QTcF data for both compounds, except for a slight under prediction of the lower percentile of compound 1 (Fig. 1 a) and a slight under prediction of the median and upper percentile at time points <0 h and of the lower percentile at time points >0 h for the 500 mg dose of compound 2 (Fig. 1b). Allowing re-estimation of the QTcF baseline for compound 2 based on the TQT data resulted in a 10 ms higher QTcF baseline compared to the SAD/MAD dataset which explains the under predictions found at time points <0 h.

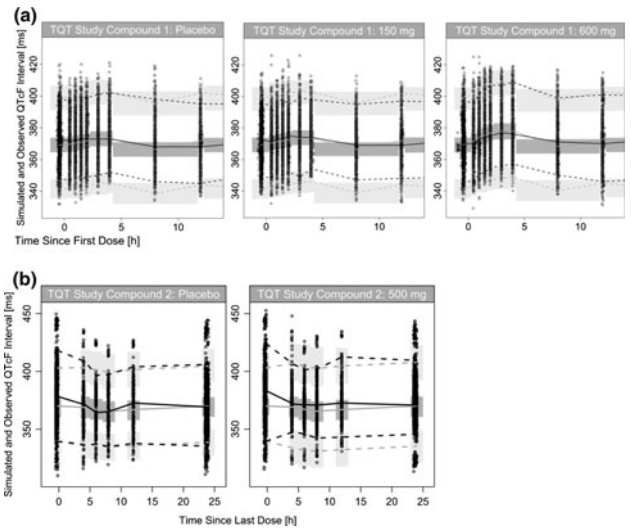

Fig. 1 **a**, **b** VPCs from 500 simulations of the TQT study for compound 1 (A) and compound 2 (B) show the median (*solid black line*), 5th and 95th percentiles (*dashed black lines*) for the observed (*black dots*) and simulated (*solid* and *dashed grey lines*) QTcF interval data with 95 % confidence intervals for the median (*dark grey field*), 5th and 95th percentiles (*light grey fields*) based on the simulations

Conclusions: A model-based approach for quantifying drug effects on QTcF interval was successfully developed based on data collected in SAD/MAD studies. The models were shown to accurately predict the typical trends and variability in the TQT trials. The 30 s and 1 min QTcF interval data resolution resulted in similar predictions, while constructed 5 min mean QTcF interval data could not support all parameters and when modeled under predicted the drug effect. These findings describe a framework to allow for possible predictions of TQT study results based on early QT assessment in Phase I studies.

References

[1] Darpo B, Garnett C (2012) Early QT assessment: how can our confidence in the data be improved? Br J Clin Pharmacol (in press)

[2] Dosne A (2012) A strategy for residual error modeling incorporating both scedasticity of variance and distribution shape. PAGE 21 Abstr 2527. www.page-meeting.org/?abstract=2527

T-029 Population Pharmacokinetic Analysis of the Novel Camptothecin Analogue AR-67 in Phase I Oncology Patients

Eleftheria Tsakalozou[1,*], Susanne Arnold[2], Markos Leggas[1]

[1]Pharmaceutical Sciences, University of Kentucky, Lexington, KY, USA; [2]Markey Cancer Center, University of Kentucky, Lexington, KY, USA

Objectives: AR-67 is a lipophilic camptothecin analogue currently under early stage clinical trials. A favorable toxicity profile and clinical responses observed during a recently completed phase I clinical trial render AR-67 a promising candidate for further clinical development [1]. Moreover, in vitro and in vivo studies suggest that AR-67 elimination is mediated via extensive metabolism in the gut and liver by UDP-*glucuronosyltransferases* (UGTs) [1, 2]. Similarly to other anticancer agents, AR-67 is a narrow therapeutic index drug. Therefore, identifying sources of intersubject variability is warrant to accurately describe the dose-exposure–response relationship and render AR-67 administration safe. The objectives of this study were (1) to quantitatively describe the pharmacokinetics of AR-67 in phase I oncology patients and (2) identify determinants of intersubject variability in this population.

Methods: Data from cancer patients with solid tumors participating in a phase I clinical trial were included in this analysis. Patients received AR-67 daily as a 1-hour intravenous infusion for five consecutive days every 21 days and were monitored for toxicity and response. A complete pharmacokinetic profile of AR-67 was obtained on days 1 and 4 of cycle 1 producing a relatively rich set of data. Population pharmacokinetic analysis was performed using the nonlinear mixed-effects modeling implemented in NONMEM v7.2.0 with PDxPOP. Plasma concentrations versus time data were fitted with a two compartment structural model with first-order elimination from

the central compartment. Inter-occasion variability (IOV) (day 1 vs. day 4) was studied as described by Karlsson et al. [3]. Selected covariates of clinical relevance (age, BSA, gender, indicators of renal and liver function, AR-67 dose levels and hematocrit) were evaluated for their effect on population parameters and were incorporated in the model after being tested for colinearity. Additionally, smoking, obesity and performance status were evaluated as determinants of clearance, exposure and toxicity and body-measures (BSA, Ideal Body Weight, Adjusted Ideal Body Weight, Lean Body Weight and Body Mass Index) were tested for correlation with AR-67 clearance. Model superiority was decided based on visual inspection of diagnostic plots, precision of parameter estimates, model stability and statistically significant ($p < 0.05$) decrease in the Objective Function Value (OFV, −2LL).

Results: A two-compartment model fit the data best. The pharmacokinetic analysis was performed using Expectation–Maximization methods (composite) and the population parameter estimates that were obtained for either lactone or total AR-67 did not differ significantly. Estimated pharmacokinetic parameters (mean, RSE %) for lactone model were: clearance (CL), 25.0 L/h (3.79); volume distribution of central compartment (V1), 3.7 L (1.86); intercompartmental clearance (Q), 29.7 L/h (5.75); volume of distribution of peripheral compartment (V2), 38.1 L (4.92). Clearance was the population parameter associated with the lowest intersubject variability (58.6 %) while V1 was associated with the highest intersubject variability (106 %) base model of the lactone data. Interestingly, inclusion of blood urea nitrogen (BUN) as a covariate explained 23.3 % of intersubject variability of V1 [V1 = EXP(1.35 × (BUN/12.7))] and sex was found to account for 24.3 % of V1 intersubject variability (V1 = 2 L for females and V1 = 5.8 L for males) in the lactone and total AR-67 model, respectively. Smoking and obesity had no effect on AR-67 clearance although they have been reported to interfere with the activity of UGTs [4, 5]. Notably, patients with worst performance statuses were more susceptible to drug-induced toxicity ($p < 0.05$) and body-measures were not identified as determinants of the intersubject variability on CL. Finally, incorporation of IOV in the lactone or total AR-67 model did not decrease the estimated residual variability (32.7 and 27.7 % for the lactone and total AR-67 base model, respectively).

Conclusions: The pharmacokinetic profile of AR-67 in phase I oncology patients with solid tumors was effectively described by a two-compartment model. Although a covariate model was developed for AR-67, intersubject variability associated with population parameter estimates remained >25.1 %; suggesting that genetic polymorphisms of transporters and metabolic enzymes with a role on the AR-67 disposition could contribute to the observed variability. Finally, based on our analysis, flat or fixed dosing of AR-67 warrants further investigation as clearance was found to be independent of body-size measures.

References

[1] Arnold SM, et al (2010) A phase I study of 7-t-butyldimethylsilyl-10-hydroxycamptothecin in adult patients with refractory or metastatic solid malignancies. Clin Cancer Res 16(2):673–680

[2] Horn J, et al (2011) Metabolic pathways of the camptothecin analog AR-67. Drug Metab Dispos 39(4):683–692

[3] Karlsson MO, Sheiner LB (1993) The importance of modeling interoccasion variability in population pharmacokinetic analyses. J Pharmacokinet Biopharm 21(6):35–50

[4] Brill MJ, et al (2012) Impact of obesity on drug metabolism and elimination in adults and children. Clin Pharmacokinet 51(5):277–304

[5] van der Bol JM, et al (2007) Cigarette smoking and irinotecan treatment: pharmacokinetic interaction and effects on neutropenia. J Clin Oncol 25(19):2719–2726

T-030 Optimal Design of Pediatric Studies: Accuracy of Population and Individual Exposure Estimates

Yan Feng*, Eric Masson, Amit Roy

Bristol-Myers Squibb, Princeton, NJ, USA

Objectives: The availability of software tools for optimizing clinical study sampling design for nonlinear-mixed effects models [1–3] have made it convenient to specify informative sampling schemes and assess the precision of population PK (PPK) parameter estimates. Optimal design is of particular importance in pediatric drug development, as the characterization of drug PK is usually based on sparse sampling of PK, given the logistical and ethical challenges in conducting pediatric clinical trials. This is particularly germane to pediatric drug development, as the approval of drugs for pediatric use is increasingly based on extrapolation of adult efficacy data based on a demonstration of similarity of exposure–response in adult and pediatric subjects. We describe the application of optimal sampling design and clinical trial simulation to not only ensure the typical PK parameters of an investigational agent is adequately characterized in each pediatric age group of interest,[4] but also to ensure that the expected accuracy of individual exposure estimates are adequate to support exposure–response analyses.

Methods: Optimal sampling schedules were determined using WINPOPT [1] for a linear two compartment PPK model with zero-order IV infusion and first-order elimination, for an IV administered monoclonal antibody (mAb), assuming allometric coefficients of 0.75 and 1 on clearance and volume of central compartment (CL and VC, respectively). Several alternative sampling scenarios based on the optimal samples were investigated, taking into account that it is most convenient to collect pre-dose and post-infusion samples for this IV administered mAb. PK concentration values and steady-state exposures were simulated with this model for pediatric patients in a planned phase 2 pediatric study, based on body weight values were sampled from the CDC growth charts [5]. The scenarios simulated were as follows: (1) 30 pediatric subjects (target sample size in Phase 2 study) with peak, trough and optimal sample collection (2): 30 pediatric subjects with only peak and trough samples and (3) 30 pediatric subjects combined with 785 adult subjects (from adult clinical studies) with peak and trough samples. The PPK model parameters were then re-estimated with simulated PK data from the simulated virtual subjects PK data, and the precision of the PPK model parameter estimates in each age group was determined for each simulation scenario. The power of clearance (CL) and central volume of distribution (VC) estimation at each adolescent age group were calculated based on simulation results. Furthermore, the accuracy and precision of the estimated typical value of CL and VC in each age group was determined, as well as the accuracy of the individual estimated exposures.

Results: The simulation results suggested that all tested study design scenarios had both ipilimumab CL and VC achieve >80 % power of the 95 % confidence interval within 60 % and 140 % of the point estimate for the geometric mean estimates of CL and VC. The power of CL and VC estimations at all adolescent sub-group are all above 95 %, except that the power of CL estimate at age 12 years group is ~85 % in scenario 2 where only 30 pediatric subjects peak and trough samples were available for trial simulation. In additional, the precision of individual parameter estimate of CL and VC are also greater than 85 % which ensures precision of exposure measurement for future exposure–response analysis.

Conclusions: The clinical trial simulation was used to ensure that there was sufficient power to obtain accurate estimates of typical values of CL and VC for each age group, and also to ensure that individual estimates of exposure were within 20 % of the true values.

References

[1] WinPOPT:Home. Accessed at http://www.winpopt.com/index.htm

[2] PFIM. Accessed at http://www.pfim.biostat.fr/

[3] PopED 2. Accessed at http://poped.sourceforge.net/

[4] Wang Y, Jadhav PR, Lala M, Gobburu JV (2012) Clarification on precision criteria to derive sample size when designing pediatric pharmacokinetic studies. J Clin Pharmacol 52:1601–1606

T-031 Population Pharmacokinetic Modeling of Sparse Data of Tabalumab in Phase II Studies of Rheumatoid Arthritis Patients Using a Bayesian Approach

Yan Ji*, David Radtke, Julie Satterwhite, Pierre-Yves Berclaz

Eli Lilly and Company, Indianapolis, IN, USA

Objectives: To develop a population pharmacokinetic (PK) model to characterize the PK of tabalumab, a human monoclonal antibody that neutralizes membrane-bound and soluble B cell activating factor (BAFF), in patients with active rheumatoid arthritis (RA) in two sparsely sampled Phase II clinical studies, using a Bayesian approach to incorporate prior information.

Methods: The population PK model was developed based on data collected from a total of 183 RA patients over 24 weeks in two Phase II studies. In the intravenous (IV) infusion study, 30 or 80 mg of tabalumab was infused over 30 min at weeks 0, 3, and 6, in a total of 63 patients. In the subcutaneous (SC) injection study, doses of 1, 3, 10, 30, 60, or 120 mg were administered at weeks 0, 4, 8, 12, 16, and 20, in a total of 120 patients. The analyses were performed using NONMEM VI with the ADVAN6 subroutine and first order conditional estimation (FOCE) with interaction. The dataset included 728 tabalumab concentrations from 13 post-dose sampling timepoints scheduled in the IV study and 736 tabalumab concentrations from 8 post-dose sampling timepoints scheduled in the SC study. Due to sparse data during the absorption and distribution phase, a Bayesian approach was employed to inform the analysis, using priors derived from the combined analysis of three previous Phase I and Phase II studies. Patient factors including body weight, age, gender, ethnic origin and baseline BAFF level were evaluated as covariates to tabalumab PK.

Results: The PK of tabalumab were adequately characterized by a 2-compartment open model, with both linear and saturable clearance components. The saturable clearance is believed to be mediated by specific and saturable binding of tabalumab to membrane-bound BAFF. The linear clearance was estimated to be 5.25 (95 % CI: 4.83, 5.57, %SEE = 1.39 %) mL/h, while the saturable clearance was estimated to be 15.5 (95 % CI: 14.0, 17.1, %SEE = 2.13 %) mL/h. The Michaelis–Menten constant was 0.586 (95 % CI: 0.474, 0.717, %SEE = 6.76 %) μg/mL, suggesting that when tabalumab concentration is significantly above this range, the linear clearance predominates. The mean SC bioavailability was estimated to be 56.9 % (95 % CI: 52.0, 62.3 %, %SEE = 2.46 %). The volume of distribution of the central and peripheral compartment was 2.31 and 1.75 L, respectively. The inter-patient variability of tabalumab was moderate (<40 %), except for saturable clearance (83 %). Body weight was found to have a statistically significant effect on the PK of tabalumab, with linear clearance increasing with body weight. However, evaluation of the effect of body weight on the tabalumab concentration profile and area under the concentration–time curve (AUC) suggested that the effect of body weight on tabalumab PK is not clinically relevant and does not warrant dose normalization.

Conclusions: Using a Bayesian approach to incorporate information from previous clinical studies, a population PK model was developed to characterize the PK of tabalumab in two sparsely sampled Phase II clinical studies in RA patients. This approach allowed the characterization of tabalumab in the RA patient population from sparse data, which would not have been possible without application of the Bayesian priors. The results of this analysis were used to aid dose selection for further clinical studies in RA patients.

T-032 Population Pharmacokinetic Modeling and Allometric Scaling of IV ST-246® to Support Optimal Dosing Strategy in Humans

Yali Chen[1,*], Janet M. Leeds[1], T. R. Shanthakumar[1], Kady Honeychurch[1], Dennis Hruby[1], J.F. Marier[2], Li Yan[2], Frederique Fenneteau[2], Mohamad-Samer Mouksassi[2]

[1]SIGA Technologies, Inc. Corvallis, Oregon, USA; [2]Pharsight, A Certara™ Company, Montreal, QC, Canada

Objectives: SIGA is developing an intravenous (IV) formulation of ST-246® for the treatment of pathogenic orthopoxvirus including smallpox virus. An oral formulation of ST-246 has previously been evaluated in cynomolgus monkeys and healthy human volunteers. Human efficacy trials are not feasible because smallpox was eradicated from the earth by 1980; the FDA's animal efficacy rule is being applied to the development of ST-246. The objective of this study was to use pharmacokinetic modeling and simulation to predict the concentration–time profiles of IV ST-246 in humans and ultimately support dose selection for future studies in humans.

Methods: Data from three preclinical studies following single and repeated IV administration of ST-246 in cynomogus monkeys were considered for population pharmacokinetic (popPK) modeling. A popPK model for IV in monkeys was developed using standard techniques: building a base structural model, random effect evaluation, covariate identification with exploratory graphing and formal testing. The final model was evaluated using visual predictive checks. The following software programs were used: NONMEM7.1.0., Phoenix 1.1, S-PLUS 8.1 and R 2.13.0.

The monkey IV model had all PK parameters allometric scaled to a power of 0.75 for clearance terms and to a power of 1 for volumes. The goal of the modeling was to find an IV dosing schedule (dose and infusion duration) in humans that produce similar exposure (AUC, C_{max}, and C_{min}) to the one previously observed after oral administration of ST-246 in healthy humans. The distribution of human body weight from a previous clinical study was used in the simulations. The same relationship between covariates and PK parameters was assumed to hold in humans. The between subject variability on PK parameters after IV administration in humans were assumed to be similar to those after oral dosing (conservative approach). The following scenarios were tested:

Time of Infusion: 1, 2, 3, 4, 5, and 6 h

Doses: BID: 40, 60, 65, 70, 80, 85, 90, 95, 100, 200, and 300 mg

QD: 100, 115, 120, 130, 145, 160, 200, 400, and 600 mg

The treatment duration was 14 days and exposure measures were computed at steady state.

Simulated data were overlaid on PK information from a clinical study with repeated oral administration of ST-246 in healthy human using 400 and 600 mg.

Results: The best structural model describing the disposition of ST-246 following IV infusion in monkeys was a three-compartment model. The final model included the body weight as an allometric scaling factor and dose as a covariate on clearance. This took into account the reduced clearance at higher doses. Model assessment by

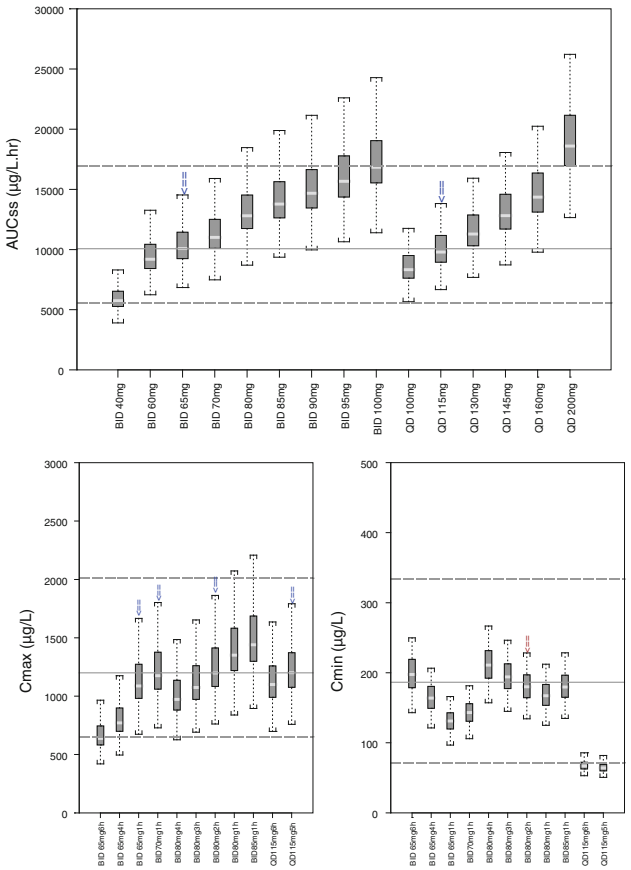

Fig. 1 Predicted AUC, C_{min} and C_{max} relative to the targeted AUC range

goodness-of-fit plots revealed that predicted concentrations of ST-246 were consistent with the observed concentrations. Furthermore, the adequacy of the PK model was verified using a visual predictive check.

The simulation results predicted that, in general, a regimen that could generate equivalent C_{min} would require longer infusion time with higher AUC values than the regimen that generates equivalent AUC and C_{max} or alternately require BID IV infusions. An example of the simulations is shown in Fig. 1.

Overall, repeated IV infusion of 115 mg QD over 5 h or 65 mg BID over 1 h would provide AUC and C_{max} values at steady state very similar to those observed after oral doses of 400 mg. Repeated IV infusion of 80 mg BID over 2 h resulted in C_{min} values at 12 and 24 h similar to those observed following oral administration of 400 mg QD in healthy uninfected humans. Similarly, repeated IV infusion of 145 mg QD over 4 h or 95 mg BID over 1 h would provide AUC and C_{max} values at steady state very similar to those observed after oral doses of 600 mg. Finally, repeated IV infusion of 85 mg BID over 1 h resulted in C_{min} values at 12 and 24 h similar to those observed following oral administration of 600 mg QD in healthy uninfected humans.

Conclusions: The results of popPK modeling and simulation enabled to find dosing regimen of IV ST-246 that will provide exposure within the targeted exposure range determined from observed PK data after oral administration in humans.

Acknowledgment: This project was supported by Contract No. HHSN2722008000 41C.

References

[1] Mandema JW, Verotta D, Sheiner L (1992) Building population pharmacokinetic-pharmacodynamic models. I. Models for covariate effects. J Pharmacokinet Biopharm 20(5):511–528

[2] Tunblad K, Lindbom L, McFadyen L, Jonsson EN, Marshall S, Karlsson MO (2008) The use of clinical irrelevance criteria in covariate model building with application to dofetilide pharmacokinetic data. J Pharmacokinet Pharmacodyn 35(5):503–526

T-033 Modeling and Simulation of Nebivolol to Explore the Impact of Pharmacokinetic Drug Interaction on Expected Blood Pressure Lowering Effect

Chun Lin Chen[1,*], Nathanael Dirks[2], Tatiana Khariton[1], Marc R. Gastonguay[2], Stephan Ortiz[1], Parviz Ghahramani[1]

[1]Forest Research Institute, Jersey City, NJ, USA; [2]Metrum Research Group LLC, Tariffville, CT, USA

Objectives: Nebivolol, a β1-selective β-blocker, is a racemic mixture composed of *d*-nebivolol and *l*-nebivolol for the treatment of hypertension. Valsartan is a nonpeptide, and specific angiotensin II receptor blocker for the treatment of hypertension. With coadminstration of valsartan, reductions were seen in mean *d,l*-nebivolol C_{max} and AUC following single and multiple dose administration. The objective of this work is to predict the expected clinical impact of reduced nebivolol exposure on seated diastolic blood pressure (DBP) lowering in the target population.

Methods: Population pharmacodynamic (PD) analysis of nebivolol effect on DBP was conducted in patients with mild to moderate hypertension using NONMEM, Version VII, FOCEI method. A saturable maximum effect (E_{max}) model best described the relationship between *d,l*-nebivolol concentration and DBP in hypertensive patients. Covariates that were investigated included age, gender, race, CYP2D6 genotype, diabetic status, body mass index, and smoking status. The adequacy of the final model was investigated using posterior-predictive check. Simulations were performed from the joint distribution of bootstrapped fixed effect parameter estimates for typical E_{max} and EC_{50}, over a range of reductions in $C_{ss,max}$ (20–80 %) and $C_{ss,avg}$ (20–50 %) for approved nebivolol doses of 5, 10, and 20 mg.

Results: 760 hypertensive patients were enrolled in the nebivolol group and 69 in the placebo group. The EC_{50} estimate of *d,l*-nebivolol concentrations was 0.0179 ng/mL. The E_{max} for DBP reduction was estimated to be approximately 5 mm Hg after placebo correction. No significant covariate effects were found on the DBP PK-PD relationship. Simulation results for 20 % reduction in $C_{ss,avg}$ at 5, 10, and 20 mg nebivolol doses indicated a median (95 % CI) decrease in the typical DBP treatment effect (mmHg) of 0.049 (0.012, 0.12), 0.026 (0.0063,0.066), and 0.013 (0.0032,0.035), respectively. For 50 % reduction in $C_{ss,max}$ at 5, 10, and 20 mg nebivolol doses indicated a median (95 % CI) decrease in the typical DBP treatment effect (mmHg) of 0.05 (0.012,0.13), 0.025 (0.006,0.069), and 0.013 (0.003,0.035), respectively.

Conclusions: The population PD model adequately characterized the relationship between nebivolol concentrations and DBP response. Despite potential decreases in exposure (50 % of $C_{ss,max}$ and 20 % of $C_{ss,avg}$), the median decrease in blood pressure lowering effect of

nebivolol is ≤0.05 mm Hg. Therefore, no clinically meaningful effect is expected from the PK drug interaction by valsartan.

T-034 Integrated Model of Lopinavir Pharmacokinetics: The Role of α-1-Acid Glycoprotein Binding

Kun Wang[1,*], David Z. D'Argenio[1], Anandi Sheth[2], Jeffrey L. Lennox[2], Edward P. Acosta[3], and Ighovwerha Ofotokun[2]

[1]University of Southern California, Los Angeles, CA, USA; [2]Emory University, Atlanta, GA, USA; [3]University of Alabama at Birmingham, Birmingham, AL, USA

Background and Objectives: The two major binding proteins for most drugs in humans are serum albumin and α-1-acid glycoprotein (AAG). Protease inhibitors (PI) are bound primarily to AAG and with high affinity, thus PI free plasma concentrations are known to be inversely related to AAG concentration. The most important determinants of PI activity in vivo are the sensitivity of the virus and the concentration of free (unbound) drug at the site of action. As an acute phase protein, AAG synthesis rises significantly in response to infections and injuries [1], which is one of the contributing factors to the observed variability in plasma AAG concentrations in HIV infected patients. Given the PIs high binding affinity for AAG, their high plasma concentrations in the presence of ritonavir enhancement, and the low saturation capacity of AAG, it has been speculated that variations in AAG levels could result in clinically important changes in PI pharmacokinetics (PK) or pharmacodynamics (PD). Since the free drug concentration more accurately reflects its availability to the target cell, changes in AAG levels could have important implications in HIV pharmacotherapy.

The aim of this work is to develop an integrated population PK model for lopinavir (LPV) to investigate the role of AAG. The composite model includes the plasma PK of total LPV and ritonavir (RTV), as well as the PK of free plasma LPV incorporating the effect of AAG.

Methods: The model was developed based on the results from two similar studies in treatment-naïve HIV-infected patients initiating antiretroviral therapy with LPV/RTV 400 mg/100 mg PO BID. The study population, design and enrollment criteria have been reported in detail elsewhere [2]. In study 1 (S1), 16 patients had intensive plasma sampling at 2 and 16 weeks following treatment initiation (1, 2, 3, 4, 6, 8, 10 and 12 h post dose). Concentrations of AAG in the plasma were quantified using an enzyme-linked immunosorbent assay (ELISA), while total and free LPV plasma concentrations were measured by high-performance liquid chromatography (HPLC) with ultraviolet (UV) detection and equilibrium dialysis methods, respectively. Total ritonavir plasma concentrations were measured by HPLC. In study 2 (S2) 20 patients had plasma sampling on day 1 and at weeks 2 and 24 following treatment initiation (sample times on each day relative to dose administration: −2, 0, 1, 2, 3, 4 h).

Data from both studies were used in the sequential population modeling of total RTV and total LPV, the latter incorporating the action of RTV on LPV kinetics. A population model relating measured AAG and total LPV on free LPV was developed and then linked to the LPV/RTV model resulting in a composite population model relating LPV and RTV dosing and AAG to total and free LPV. Population modeling was conducted using ADAPT 5 (MLEM algorithm).

Results: LPV and RTV total plasma concentrations were each described by a one-compartment model with an absorption lag time, and an exponential term was used to incorporate the effect of RTV concentration on the clearance of LPV as illustrated in Fig. 1. Body mass index (BMI) was found to be a significant covariate contributing to the interindividual differences in LPV clearance. The population parameter estimates for the LPV/RTV model in Fig. 1 are shown in Table 1. Due to the limited sampling the absorption rate for LPV was fixed. Figure 2 displays the model goodness of fit plots for LPV total plasma concentration (individual—top left; population—top right, conditional residuals versus individual predictions—bottom left, conditional residuals versus time—bottom right). A visual predictive check is shown in the left panel of Fig. 3 for day 1 of S2. The visual predictive check in right panel of Fig. 3 is the combination of week 2 and week 16 for S1, and week 2 and week 24 for S2 (Fig. 4).

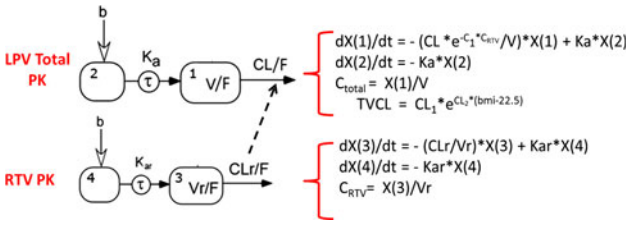

Fig. 1 PK model for total LPV and RTV

Table 1 Parameter estimation results for the LPV/RTV total model

Parameter	Mean (%RSE)	HV (%KSE)
cl/f	–	24 (62)
V/F	55.7 (15.2)	55 (31)
cl	0.624 (47.5)	38.3 (259)
Tau	0.875 (32.7)	60.5 (63)
M	0.325	–
CL_1	5.70 (12)	–
CL_2	0.055 (34.)	–
CLr/F	22.0 (11.9)	50 (18)
Yt/f	177 (29.3)	62 (42)
	0.74 (47.0)	107 (57)
Tiur	1.10	70

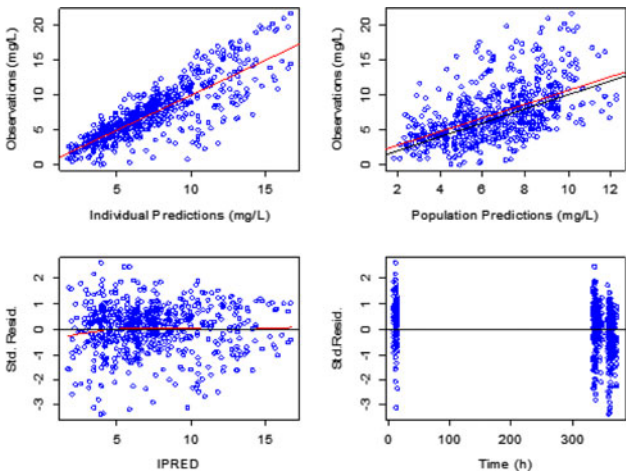

Fig. 2 Goodness of fit plots for LPV total

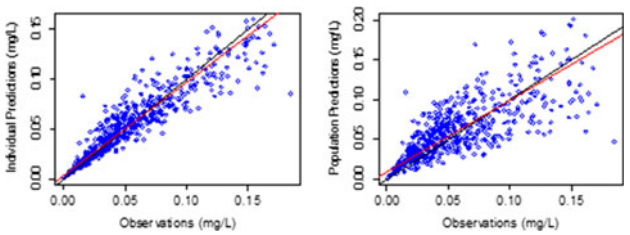

Fig. 3 Selected goodness of fit plots for LPV free

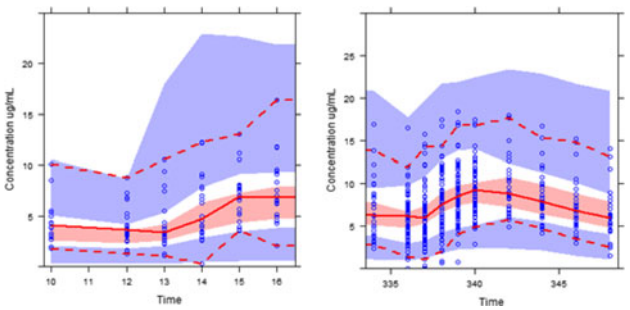

Fig. 4 The red line is median. The dash lines are the 5th and the 95th percentiles of observed data. The shaded areas are the corresponding confidence intervals of simulated data

Table 2 Population estimition results for LPV free model

Parameter	Mean (%RSE)	Nv (%RSE)
fu	0.00733 (6.99)	27.2 (3 5.9)
c2	0.00262 (23.0)	96.2 (36.2)
c3	1.20 (2.22)	8.15 (31.5)

A separate mixed effects analysis relating measured LPV total and AAG concentrations to LPV free concentration was conducted and the following model selected:

$$LPVf_i = fu \cdot e^{(-c2 \cdot AAG_i)}(LPV_i)^{c3} + e_i$$

where $LPVf_i$ and LPV_i are the measured free and total LPV concentrations. The data from S1 and S2 were pooled, along with the associated AAG measurements, to estimate the model parameters as shown in Table 2. Figure 3 displays the model goodness of fit plots for LPV free plasma concentration (individual—left; population—right).

Conclusions: The integrated model developed to describe the PK of LPV, RTV and their interaction, as well as the effect of AAG on LPV binding, found that over the range of AAG values in the studies (23.6–479 mg/dL) there is a significant effect of AAG on binding with effective fraction unbound values ranging from 0.00689 to 0.002, which is consistent with prior protein-free LPV studies.

References

[1] Kushner I (1982) The phenomenon of the acute phase response. Ann NY Acad Sci 389:39–48

[2] Ofotokun I, et al (2011) Immune activation mediated change in alpha-1-acid glycoprotein: impact on total and free lopinavir plasma exposure. J Clin Pharmacol 51(11):1539–1548

T-035 K-PD Modeling of Parathyroid Hormone Response After Calcium Administration in Healthy Subjects

Jae Eun Ahn[1,*], Sangil Jeon[2], Jongtae Lee[2], Seunghoon Han[2], Dong-Seok Yim[2]

[1]College of Pharmacy, Kangwon National University, Chuncheon, Kangwon-do, South Korea; [2]Department of Clinical Pharmacology, Seoul St. Mary's hospital, The Catholic University of Korea, Seoul, South Korea

Objectives: Plasma ionized calcium (Ca^{2+}) levels are tightly regulated in the body; thus it is not feasible to assess the difference in calcium absorption directly from them in normal physiologic conditions. This study aimed: (1) to develop a semi-mechanistic model whose approach is similar to that of K-PD model [1] for parathyroid hormone (PTH)-Ca^{2+} system, and (2) to indirectly compare the difference in Ca absorption after the administration of Ca supplements using PTH responses.

Methods: A total of 108 PTH and 107 Ca^{2+} concentrations were collected from 12 subjects from the clinical trial to evaluate the change in health indexes after the administration of Geumjin hot spring mineral water (thermal water) and calcium supplements in Korean healthy subjects. Six subjects received 240 mL of Geumjin thermal water that contains 200 mg of Ca, 3 subjects, 500 mg of calcium carbonate ($CaCO_3$) tablet (equivalent to 200 mg Ca) with 240 mL of purified water, and 3 subjects, 500 mg $CaCO_3$ tablet with 240 mL of normal saline. Blood samples were collected before and up to 8 h after the administration. While PTH-Ca^{2+} system is very complex, it was simplified with the following assumptions: (1) The net absorbed Ca from each supplement is positive but unobservable due to the Ca-homeostasis; (2) The decrease in PTH is only due to the increased but unobserved Ca^{2+}; (3) Feedback mechanism of PTH drop to Ca^{2+} level is not considered. Indirect response models with zero-order input and first-order output rates (Fig. 1) were fitted to the observed Ca^{2+} and PTH data, respectively. It is known that increased Ca^{2+} levels decrease the secretion of PTH, which was incorporated to the model in the way that unobservable Ca^{2+} increases the output rate of PTH in a linear manner.

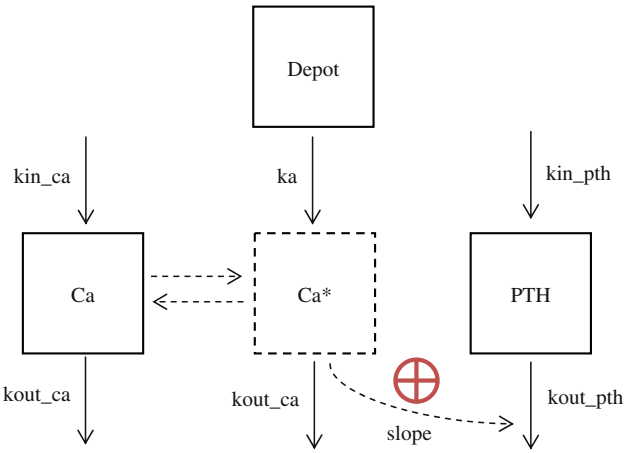

Fig. 1 Schematic of the K-PD model

ka: first-order absorption rate constant for Ca, kin_ca: zero-order input rate for Ca^{2+}, kout_ca: first-order output rate constant for Ca^{2+}, kin_pth: zero-order input rate for PTH, kout_pth, first-order output rate constant for PTH, *: unobserved.

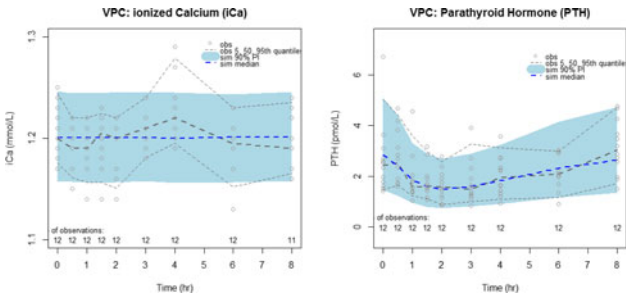

Fig. 2 VPCs of Ca^{2+} (*left*) and PTH (*right*)

The analysis was performed using NONMEM 7.2.0 (ICON Development Solutions, MD) with Pirana 2.6.1 [2] and R 2.15.1 (www.r-project.org) with RStudio version 0.96.330 (http://www.rstudio.com/).

Results: The model predicted the half-life of Ca absorption to be 59.4 min (RSE 39.7 %). The slope parameter was estimated to be 2.84 (RSE 29.15 %), which could be interpreted as the effect of absorbed Ca to PTH response as well as a scale parameter for the hypothetical Ca^{2+} concentration (the initial condition of depot compartment was assumed to be 1). Other parameter estimates for the input and output rate constants for Ca^{2+} and PTH were in similar magnitudes to the findings from the mechanistic PK/PD modeling [3]. The visual predictive checks (VPCs) demonstrated that the model provided reasonable predictions Ca^{2+} and PTH (Fig. 2). The difference in Ca absorption (ka) or its effect (slope) was not found in this study, although the number of subjects is considered insufficient for any meaningful covariate testing.

Conclusions: K-PD modeling was performed to characterize PTH-Ca^{2+} system after the administration of Ca supplements in healthy subjects. With the absence of observable difference in plasma Ca^{2+} levels, PTH responses were used as a surrogate marker for Ca absorption, which did not seem to be significantly different among the Ca supplements in this study.

References

[1] Jacqmin P et al (2007) Modelling response time profiles in the absence of drug concentrations: definition and performance evaluation of the K–PD model. J Pharmacokin Pharmacodyn 34(1):57–85

[2] Keizer RJ, et al (2011) Piraña and PCluster: a modeling environment and cluster infrastructure for NONMEM. Comput Methods Prog Biomed 101(1):72–79

[3] Shrestha RP, et al (2009) Mechanism-based pharmacokinetic/pharmacodynamic model of parathyroid hormone-calcium homeostasis in rats and humans. J Pharmacol Exp Therapeut 330(1): 169–178

T-036 Longitudinal PK-PD Modeling in Support of Phase 3 Maintenance Dose Selection of MK-3222 for Psoriasis

Anthe Zandvliet[1,*], Russ Wada[2], Hanbin Li[2], Kristine Nograles[3], Rich Shames[4], Sandy Allerheiligen[6], Thomas Kerbusch[1], Robin Mogg[6], Bill Hanley[5]

[1]Merck Research Laboratories, Oss, The Netherlands; [2]Quantitative Solutions, Menlo Park, CA, USA; [3]Merck Research Laboratories, Kenilworth, NJ, USA; [4]Merck Research Laboratories, Palo Alto, CA, USA; [5]Merck Research Laboratories, Westpoint, PA, USA; [6]Merck Research Laboratories, Upper Gwynedd, PA, USA

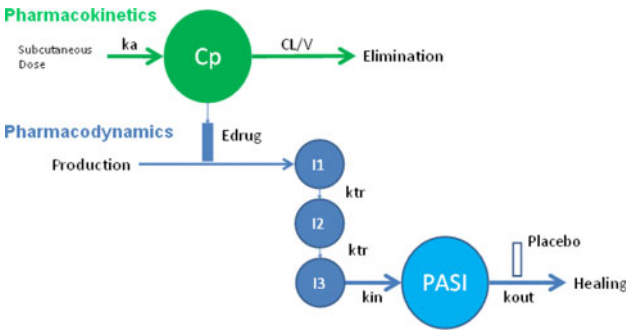

Fig. 1 Semi-mechanistic structural PK-PD model describing MK-3222 concentrations and the PASI fraction of baseline over time

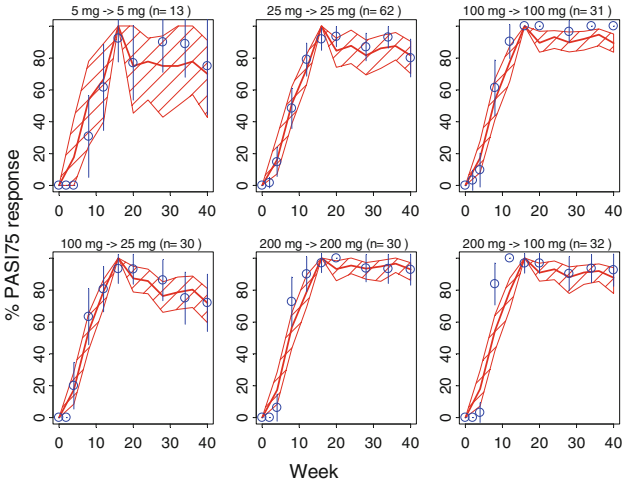

Fig. 2 Visual predictive checks of PASI75 response rate in Week 16 responders

Objectives: MK-3222 is a high affinity humanized anti-IL 23 p19 specific MAb being developed for treatment of psoriasis. A semi-mechanistic model was developed to describe and simulate PASI scores and PASI75/90 response rates over time. The objective of the model-based evaluation was (a) to support maintenance dose selection and (b) to evaluate alternative dosing intervals.

Methods: Data from a Phase 2b dose ranging study (up to week 40), which was carefully designed to establish a dose–response relationship, were used for this analysis [1]. A total of 355 patients was randomized to receive MK-3222 (dose levels 5, 25, 100, 200 mg or placebo) at week 0 and 4 (loading dose). A total of 298 subjects continued treatment from week 16 in a Q12 W dosing regimen. The PASI75 responders at week 16 in the 100 and 200 mg groups were re-randomized in a 1:1 ratio to either continue the current dose (100 $\geq$ 100 mg SC and 200 $\geq$ 200 mg SC) or reduce the dose (100 $\geq$ 25 mg and 200 $\geq$ 100 mg SC).

A semi-mechanistic PK-PD model was developed to describe the PASI fraction of baseline over time. The structural model is depicted in Fig. 1. Clinical trial simulations (100 replicates of 300 patients per cohort) were conducted to explore various maintenance doses and dosing frequencies. These simulations accounted for parameter uncertainty and between-patient variability.

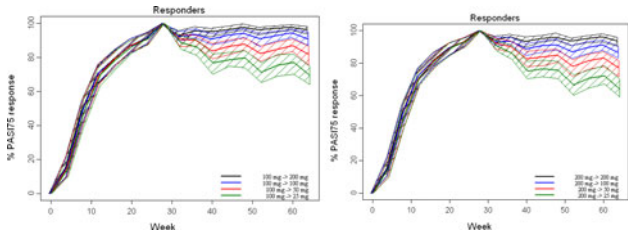

Fig. 3 Clinical trial simulations of PASI75 response rate in week 28 PASI75 responders for patients who are initially treated with 100 mg (left panel) or 200 mg (right panel) SC MK-3222 administered at weeks 0, 4 and 16 for induction of efficacy, followed by maintenance doses (25, 50, 100, 200 mg SC) administered in a 12-week dosing interval

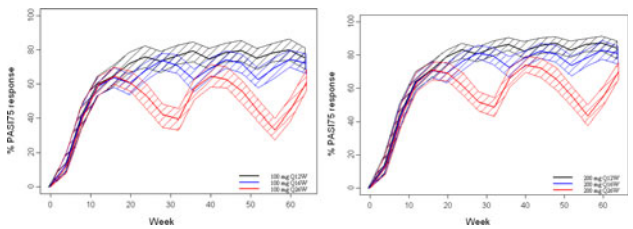

Fig. 4 Clinical trial simulations of PASI75 response rate during treatment with 100 mg (*left*) or 200 mg (*right*) SC MK-3222 administered in 12, 16, or 26-week dosing intervals. Blue symbols: observed results (P05495), Red curves: model-based predictions based on 100 replicates for each cohort (P95, P50, P5) including inter-individual variability for PK and uncertainty for PASI

Key assumptions:

- The Phase 2b patient population is representative of the Phase 3 patient population
- PASI profiles based on Phase 2b data up to week 40 can be extrapolated to later time points and different regimens (16 and 26 weekly dosing)

Results: The model adequately described the observed clinical data from a Phase 2b study P05495 (Fig. 2). Figure 3 demonstrates that PASI75 response rates are predicted to be similar for 100 and 200 mg Q12 W dosing regimens. Loss of efficacy is predicted at lower maintenance doses of 25 or 50 mg Q12 W. Figure 4 shows that the 12-week dosing interval results in a sustained response at the 100 and 200 mg dose levels. In contrast, a sustained PASI75 response rate may not be achieved in a less frequent dosing regimen.

Conclusions: This semi-mechanistic PK-PD model-based analysis demonstrates that a 12-week dosing frequency using 100 or 200 mg doses of MK-3222 is expected to result in optimal efficacy for the treatment of psoriasis.

Reference

[1] Thomas K, et al (2001) Phase 2b dose selection for the treatment of autoimmune disorders leveraging comparator data

T-037 Exposure Response Modeling and Simulations of Naloxegol to Further Evaluate the Dose–Response Relationship

Nidal Al-Huniti*, Khanh Bui, Jaakko Lappalainen, Mark Sostek

AstraZeneca Pharmaceuticals, Wilmington, DE, USA

Objectives: Naloxegol is a selective peripheral opioid receptor antagonist. Its action restricted to organs outside the central nervous system, naloxegol blocks opiate receptors in the gastrointestinal system and reduces the incidence of opioid-induced constipation (OIC) without reversal or reduction of opioid-mediated analgesia. The objectives of this work were (1) to develop an exposure response relationship for the response rate. (2) Model the dropout rate for weeks 1–4 and integrate both response rate and dropout rate to support phase 3 dose selection for naloxegol.

Methods: The analysis dataset included 185 patients with OIC from a Phase II dose-ranging study. The efficacy variable was the proportion of responders (i.e. Patients who showed an increase of $\geq$3 Spontaneous Bowel Movement (sbm)/week and $\geq$1 sbm/week increase over baseline for at least 3 out of 4 weeks). The response rate was calculated as number of responders in a particular treatment group divided by number of Intent- to- treat (ITT) patients in that treatment group. The probability (π_i i) of having sbm $\geq$3/week and $\geq$1 sbm/week increase over baseline was modeled as function of dose. Dropout was modeled with a Weibull distribution for the time to event (dropout). The performances of the models were evaluated using a battery of diagnostic plots and by posterior predictive check. Model-based simulations for phase 3 were conducted to recommend

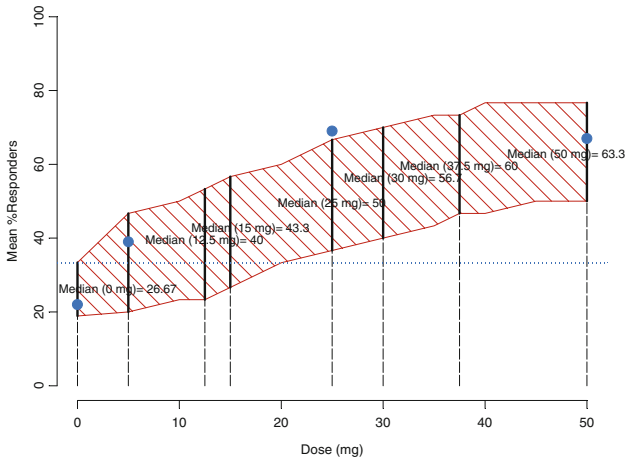

Fig. 1 Simulated Dose Response model incorporating dropout rates for naloxegol (5th–95th percentile). Observed responder rates (blue circles) fall within the model predictions

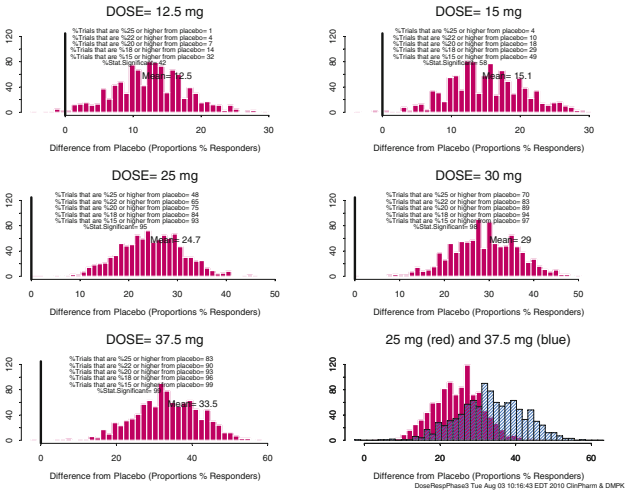

Fig. 2 Distribution of difference from placebo for responder rates based on simulation of 1000 trials

naloxegol doses. All models were developed in both NONMEM VII and Winbugs to compare the parameter estimates across the tow software. Simulations were conducted in NONMEM VII and analyzed using S-Plus/R statistical software.

Results: The integrated model for dropout and responder rate described Phase II data very well. The model predicted median responder rates were 26.67, 31, 50 and 63.3 % for placebo, 5, 25 and 50 mg respectively (Fig. 1). The observed dropout rate for the 25 mg was lower than placebo; therefore the observed responder rate for the 25 mg was outside the model predicted 5^{th}-95^{th} percentile. The dose–response relationship, accounting for dropouts, was simulated and is shown in Fig. 2. Model parameter estimates in Winbugs and NONNMEM VII were very similar.

Further simulations of naloxegol dose–response based on phase III sample size ($n = 200$) for doses up to 40 mg (Fig. 1) showed that 25 mg dose would have a projected success rate of >90 % (15 % benefit over placebo and having a statistically significant p value after adjusting for multiplicity).

Conclusions: The dose–response relationship was well described by proposed integrated model. Model-based simulations suggest that doses of 25 mg and higher provides a promising success rate in phase III. Parameter estimates in NONMEM VII and Winbugs were similar.

T-038 Simulation and Re-estimation Method to Evaluate Sample Size and Study Duration for a Pharmacokinetic Proof of Concept Study

Stefano Zamuner*, Tarjinder Sahota, Daren Austin

GlaxoSmithKline, Clinical Pharmacology Modeling and Simulation, Stockley Park, UK

Objectives: Pharmaceutical companies have developed or acquired technologies for producing improved protein and antibody therapeutics and some have began to develop biobetter biosimilar products.

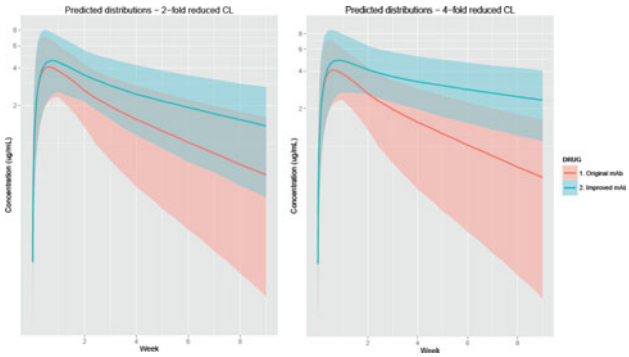

Fig. 1 Predicted pharmacokinetic profiles (90 % percentiles) for original and improved mAbs

Proprietary technologies for producing improved biologics include half-life extension methods, glycoengineering, cell production systems, and drug delivery systems. We consider the case of a hypothetical mAb with a terminal half-life of 14 days, administered subcutaneously every other week that incorporates FcRn protein engineering to reduce clearance. This modification may offer monthly or even every other month dosing, greater patient convenience and a reduction in infusion or injection site reactions. Proof of concept (PoC) for such a mAb is therefore based on a comparison of apparent clearance between the two mAbs, and a suitable trial design should have 80 % power to detect a two-fold reduction in apparent clearance.

Methods: A population pharmacokinetic model was developed based on published data for typical mAbs, with systemic clearance (9–12 L/h), volume of distribution (5–6 L), and bioavailability (0.64). Between-subject variability of 40–50 % was assumed. The new mAb was assumed to have a reduced apparent clearance of between 1.5 and 4-fold, with a minimum of two-fold considered clinically relevant. A suitable PoC study is assumed to test three doses of the modified mAb, plus the original mAb, in a parallel group design with up to nine subjects per treatment group and variable study duration (4–12 weeks).

Two-hundred studies were simulated using NONMEM 7.2 and R software, with uncertainty in the original mAb CL/F incorporated using the PRIOR option in NONMEM. Success (PoC) was defined as the ability to detect a 2-fold reduction in apparent clearance for the simulated design. The proposed model based sample size computation method was also compared with the method proposed by Kang et al. [1], although we have included uncertainty in both apparent clearance and study duration.

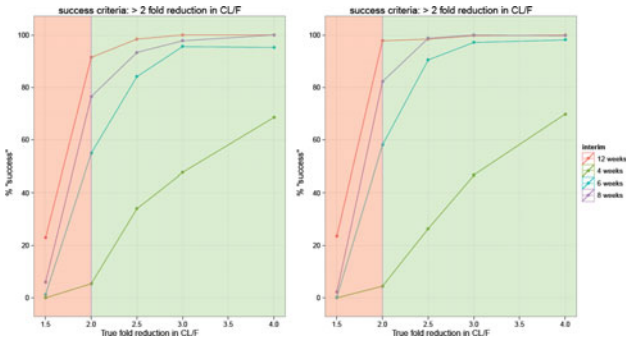

Fig. 2 X-axis represents the hypothesized NBE CL reduction used for simulation of PK data and on the y-axis, the corresponding (*green*) power (%) or (*red*) type I error rate

Results: Simulation profiles for both the original mAb and the one with improved half-life, with two- and four-fold reductions in clearance, are shown in Fig. 1. Probability of success as a function of reduction in clearance and study duration is shown in Fig. 2 (with $N = 6$ and $N = 9$ subjects per group).
Conclusions: An eight-week study provides adequate power to detect a two- to four-fold reduction in clearance of a hypothetical engineered version of the original mAb. Simulation re-estimation methods show that using a model-based population-pharmacokinetic methodology and relatively small cohort sizes controls for Type 1 error, whilst providing acceptable parameter precision.

Reference

[1] Kang D, Schwartz JB, Verotta D (2005). Sample size computations for PK/PD population models. J Pharmacokinet Pharmacodyn 32:685–701

T-039 Global Optimum Search for NONMEM Using Genetic Algorithm

Insook Jung[1,*], Gi-Su Heo[2], Ji-Young Jeon[1], Yong-Jin Im[1], Soo-Wan Chae[1,3], Min-Gul Kim[1]

[1]Clinical Trial Center, Chonbuk National University Hospital, 20, Geonji-ro, Deokjin-Gu, Jeonju-si, Jeollabuk-do, 561-712, South Korea; [2]Electronics and Telecommunications Research Institutes, Daejeon, 305-700, South Korea; [3]Department of Pharmacology, Medical School, Chonbuk National University, 20, Geonji-ro, Deokjin-Gu, Jeonju-si, Jeollabuk-do, 561-712, South Korea

Objectives: NONMEM still uses the local optimization method of BFGS quasi-Newton algorithm. It usually requires initial parameter values to lie within a relatively small neighborhood of the true optimum in order to ensure any desired accuracy. To reduce the sensitivity to the initial values selection for the local search, a global optimization approach is required.
Methods: Genetic algorithm (GA) is very popular due to its simplicity and robust convergence capability of global optimum search. GA is based on the mathematics of evolution/selection and survival of the fittest (Fig. 1). Our search space of GA is restricted to those originally considered during the evaluation of initial values of fixed-effects $THETAs of NONMEM. We propose a global optimum search algorithm called g-NONMEM. It combines the global search strategy of GA and the local estimation strategy of NONMEM (Fig. 2). Firstly, initial values (genomes) are randomly generated, and NONMEM is implemented for each genome to find a local optimum for fixed effects. GA implements NONMEM 7.2 to calculate the fitness by creating g-control codes. g-control codes duplicate a control file of NONMEM, except that it contains special values for $THETA, that are searched for and replaced by GA. And then, g-NONMEM extracts the required fitness (OFV, number of parameters, eigenvalues and success of covariance matrix) directly from the NONMEM xml outputs. g-NONMEM updates the current position with the convergent position of NONMEM for each genome. Model with the lowest fitness carried to the next generation. Then, g-NONMEM employs GA to find a global optimum based on every genome's fitness.
Results: g-NONMEM used the dataset to describe the population PK of vancomycin in Korean pediatric patients [1]. g-NONMEM is performed with NONMEM 7.2 and gfortran on 16 Intel Xeon CPU/HP800 under Ubuntu. Model evaluation uses FOCE estimation with interaction. In the simulation, g-NONMEM was insensitive to initial value selection. Even when the initial values are far away from their global optima, g-NONMEM almost guarantees the global optimization (Table 1).
Conclusions: g-NONMEM leads to a global optimization for fixed-effects of NONMEM (Fig. 3). Furthermore, GA can be implemented directly to optimize the objective function in NONMEM of nonlinear mixed effects models without any local optimization-based estimation.

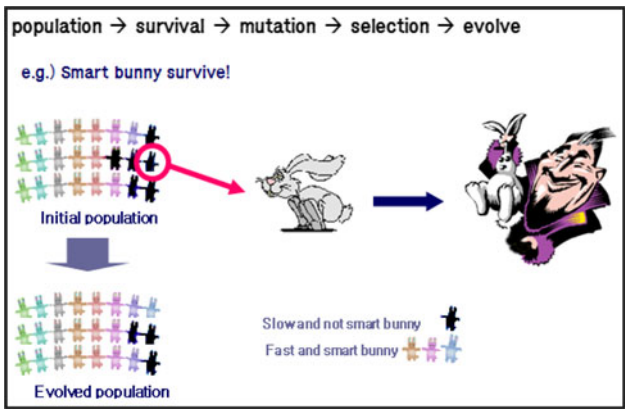

Fig. 1 Pictoral representation of genetic algorithm approach

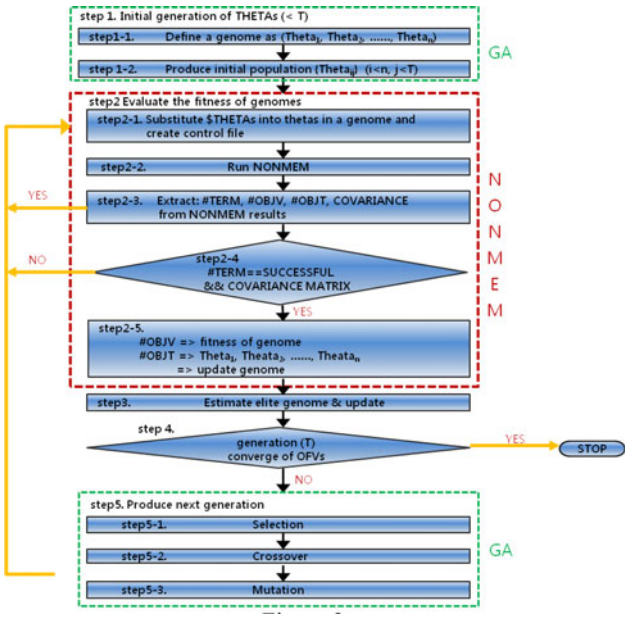

Fig. 2 Flowchart of steps involved in global optimal search in NONMEM using genetic algorithm

Table 1 Comparison of models used in NONMEM

Model	Step (1)	GA 40 Genomes/10 0generations ($0 \leq \theta i \leq 5$)	GA 100 Genomes/300 generations ($0 \leq \theta i \leq 10$)
1 CMPT	606.270	606.271	606.271
1 CMPT	606.270	606.271	606.271
2CMPT	583.782	583.794	583.794

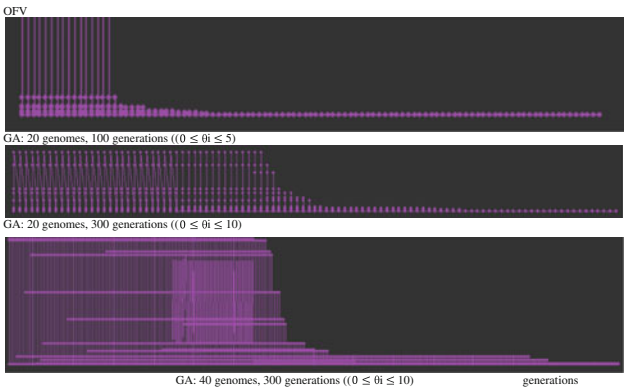

Fig. 3 Global optimization for fixed-effects of NONMEM

References

[1] Jeon J-Y (2008) Population pharmacokinetics of vancomycin in Korean pediatric patients. Master thesis, Seoul National University

[2] Kim S, Li L (2001) A novel global algorithm for nonlinear mixed-effects models using particle swarm optimization. J Pharmacokinet Pharmacodyn 38:471–495

[3] Mentre F (2008) Stochastic EM algorithms in population pharmacokinetic-pharmacodynamic analyses. The American conference on pharmacometrics (ACoP) 2008. March 9.12 Tucs on, Arizona

[4] Oh IS, Lee JS, Moon BR (2004) Hybrid genetic algorithms for feature s election. IEEE Trans Pattern Anal Mach Intell 26(11): 1424–1437

T-040 Model Based Dosing Rationale for Darunavir when Co-administered with Low-dose Ritonavir in Pediatric HIV-1 Infected Patients

Anne Brochot[1,*], Peter Vis[2], Tom Van De Casteele[3], Magda Opsomer[3], Frank Tomaka[4], An Vermeulen[1], Thomas N. Kakuda[4]

[1]Janssen Research & Development, Beerse, Belgium; [2]LAP&P Consultants BV, Leiden, The Netherlands; [3]Janssen Infectious Diseases BVBA, Beerse, Belgium; [4]Janssen Research & Development, Titusville, NJ, USA

Objectives: The HIV protease inhibitor (PI) darunavir, in combination with low-dose ritonavir (DRV/rtv) and other antiretrovirals (ARVs), is approved for the treatment of ARV-naïve and -experienced HIV-1 infected adults and ARV-experienced pediatric patients aged 3 to <18 years. The objectives of this analysis were (1) to adapt a previously developed population pharmacokinetic (PK) model of DRV to integrate data from ARV-naïve pediatric patient from 12 to <18 years old, and (2) to provide dose recommendations for ARV-naïve pediatric patients aged 3 to <12 years.

Methods: Rich sampling data after 2 weeks of oral treatment from two studies performed in adults and three studies performed in children with HIV-1 infection were pooled for this analysis. Studies 1 and 2 included 30 ARV-experienced adult patients (18–66 years) treated with DRV/rtv 600/100 mg b.i.d. Study 3 included 41 ARV-experienced children (6 to <18 years) and explored various DRV/rtv b.i.d. regimen based on body weight (300/50, 375/50, 450/60 and 600/100 mg) [1]. Study 4 included 19 ARV-experienced pediatric subjects (3 to <6 years), treated with DRV/rtv 20/3 mg/kg b.i.d. [2]. Ten patients from study 4 were further included in a substudy in which they were switched to a once daily regimen for 2 weeks and an intensive PK profile was assessed with rich sampling. The dosing consisted of DRV/rtv 40/7 mg/kg q.d. for subjects <15 kg and 600/100 mg q.d. for subjects ≥15 kg. Study 5 included 12 ARV-naïve children (12 to <18 years) treated with DRV/rtv 800/100 mg q.d. [3].

An existing population PK model for DRV was established in adults based on studies 1 and 2 [4]. This was a two-compartment model with first order absorption. Apparent clearance was dependent on the concentration of α_1-acid glycoprotein (AAG). This model was adjusted a priori to take bodyweight into account for both CL/F and V_C/F, and the parameters estimated. Models were developed using NONMEM (version VII) with FOCE. Model selection was based on standard goodness-of-fit plots, precision of parameters estimates and the objective function value. Simulations using the final model were performed for various dosing scenarios in ARV-naïve children 3 to <12 years old and dose recommendations were proposed based on comparable simulated total exposures (AUC) as in ARV-naïve adults receiving the standard oral dose of DRV/rtv 800/100 mg q.d.

Results: All structural parameters were well estimated, and interindividual variability (IIV) could be detected for apparent clearance, apparent inter-compartmental clearance and the first order absorption constant. A visual predictive check showed adequate predictive performance for the influence of bodyweight on exposure. Substantial shrinkage was found for the first order absorption rate constant and for the inter-compartmental clearance. This is probably due to the fact that parameters are estimated at steady-state, yielding relatively little individual information on the distribution of KA and Q/F. However, this has no impact on the exposure simulation and the model was therefore fit for purpose.

The q.d. dose regimens based on simulations for children aged 3 to <12 years should result in exposures close to the target adult exposure after treatment with DRV/rtv 800/100 mg q.d., whilst minimizing the pill burden and allowing to switch from suspension to tablet as early as possible. Based on the typical value of apparent clearance obtained from the population PK model, the expected DRV exposures (AUC) for different q.d. doses were simulated as a function of body weight and AAG concentrations. Since apparent clearance, hence exposure, is dependent on AAG, each regimen was simulated using three different values of AAG which were the 5th, 50th and 95th percentiles of the values observed in studies 4 and 5 and over a weight range of 10–65 kg. The expected exposures with a DRV/rtv once daily dosing regimen of 35/7 mg/kg from 10 to <15 kg, 600/100 mg from 15 to <30 kg, 675/100 mg from 30 to <40 kg and 800/100 mg for 40 kg and higher, most closely matched adult exposure and were therefore recommended.

Conclusions: The population PK model for DRV/rtv in adults was successfully adjusted to describe and predict the pharmacokinetics of DRV in both adults and children, treated with once or twice daily regimen. Simulations of potential once daily dose regimens in children aged 3 to <12 years old were applied to explore the resultant exposures so that, together with efficacy and safety data from previous pediatric and adult trials an optimal dose could be recommended for regulatory approval.

References

[1] Blanche S, Bologna R, Cahn P, Rugina S, Flynn P, Fortuny C, Vis P, Sekar V, van Baelen B, Dierynck I, Spinosa-Guzman S (2009) Pharmacokinetics, safety and efficacy of darunavir/ritonavir in treatment-experienced children and adolescents. AIDS 23(15):2005–2013

[2] Violari A, Bologna R, Kimutai R, et al (2011) ARIEL: 24-week safety and efficacy of darunavir/ritonavir in treatment-experienced

pediatric patients aged 3 to <6 years. 18th CROI. Abstract S-1001

[3] Giaquinto C, Flynn P, Blanche S, et al (2012) Darunavir/ritonavir once daily in treatment-naïve adolescents: 48-week safety, efficacy, tolerability and pharmacokinetic results of the DIONE study. XIX International AIDS Conference. Poster MOPE037.

[4] Vis P, Sekar S, van Schaick E and Hoetelmans R (2006) Development and application of a population pharmacokinetic model of TMC114 in healthy volunteers and HIV-1 infected subjects after administration of TMC114 in combination with low-dose ritonavir. Abstract 964. 15th Annual Meeting of the Population Approach Group in Europe (PAGE), Bruges, 14–16 June

T-041 Incorporating Target Shedding into a Minimal PBPK-TMDD Model for mAbs

Linzhong Li*, Iain Gardner, Rachel Rose

Simcyp Limited, Sheffield, UK

Objectives: The impact of target-mediated drug disposition (TMDD) on PKPD of therapeutic proteins has been well appreciated in recent years. However, target dynamics are more complex than published TMDD models account for. For instance, virtually all structural and functional categories of membrane proteins have been found to be shed from cells [1], and for a large percentage of marketed monoclonal antibody therapeutics (mAb), target shedding has been shown to exist and several clinical studies have also indicated a significant effect of target shedding on mAbs PKPD [2]. The objective of this study is to extend existing TMDD models to take into account the dynamic interaction between a drug and its target in the physiological or pathophysiological condition, where the target is present as both a membrane bound and a shed, soluble form.

Methods: Membrane bound targets can exist in the tissues or on circulating cells in blood, and they are subject to ectodomain shedding to generate soluble target, both of which may coexist in the blood, interstitial space, or both. Furthermore, drugs may modulate the shedding, resulting in a high concentration of soluble target. In order to mechanistically model both target-mediated drug disposition as well as drug-mediated target disposition, we first generalized the existing TMDD models to take account for the ectodomain shedding and interconnection between membrane bound and soluble forms of targets in addition to TMDD at both forms of the target. The left diagram in Fig. 1 schematically shows the shedding model used in this study, where the distribution of shed target from tissue to plasma is characterized by the first-order rate constant λ, and the membrane target shedding is represented by first-order rate constant k_{shed}. Furthermore, we allow the shedding rate to be modified by the drug.

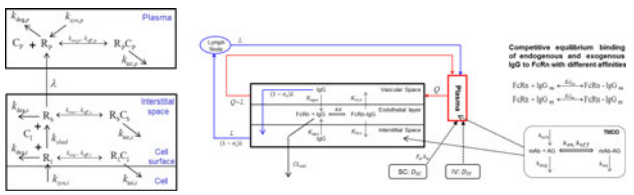

Fig. 1 R_I—free membrane target in interstitial space; R_S—shed soluble target in interstitial space; R_P—shed soluble target in plasma; C_P—drug in plasma; C_P—drug in interstitial space (*left*). The model structure of the minimal PBPK model coupled with the full TMDD model without shedding (*right*) [3]

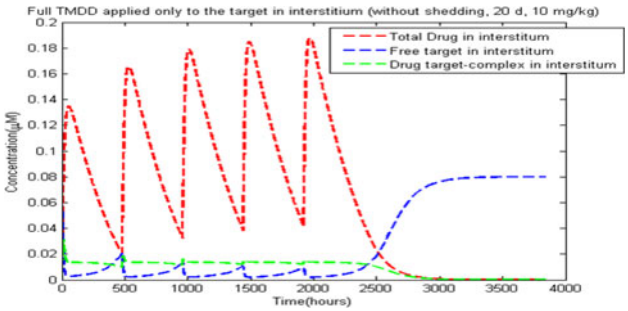

Fig. 2 Simulation of a mAb with 20 days of doing interval, assuming no target shedding

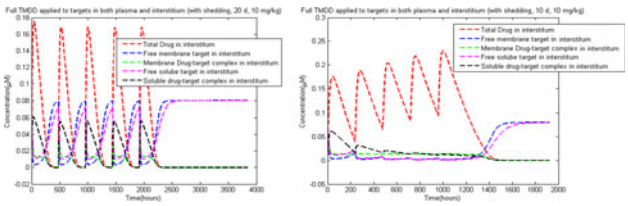

Fig. 3 Simulation of a mAb with 20 days of doing interval, assuming target shedding (*left*). Simulation of a mAb with 10 days of doing interval, assuming target shedding (*right*)

A general simulation algorithm was developed in Matlab, which incorporates TMDD models with and without shedding into a minimal PBPK model for mAbs we developed previously [3], whose model structure is shown in the right diagram of Fig. 1. In general, the integrated model we developed can take account for different target properties, including, but not limited to, (1) membrane bound targets in tissues or on circulating cells in blood without shedding; (2) soluble targets in the circulation; (3) membrane bound targets in tissue interstitial space with shedding and the shed target as a soluble form existing in the interstitial space as well as in the circulation; (4) both membrane bound and soluble forms of targets coexist due to differential splicing.

Simulations were run assuming that in the absence of binding to the target the mAb has typical IgG kinetics (21 day half-life). Simulations were then conducted with the TMDD model with and without shedding occurring. The parameters used for the shedding model are based on a set of parameter values for full TMDD model: $k_{on} = 31.375(\mu M)^{-1}$, $k_{off} = 0.6083\ h^{-1}$, $k_{syn} = 0.002312\ \mu M/h$, $k_{int} = 0.16375\ 1/h$, $R_{max} = 0.08\ \mu M$.

Results: Figures 1, 2 and 3 demonstrate the simulated effect of target shedding on the plasma levels and receptor occupancy of a monoclonal antibody as well as associated drug-mediated free target level for multiple dosing. Specifically, Fig. 2 shows that when it is assumed no shedding happens and a full TMDD model is applied, then a multiple dosing with dosing interval 20 days is sufficient to suppress the level of membrane bound target. When the shedding is considered, then the same dosing interval is not able to suppress the free soluble target level in the interstitial space, as shown in the left plot in Fig. 3, and instead a doing interval of 10 days is needed to control the free soluble target level, as demonstrated in the right plot of Fig. 3.

Conclusions: Published TMDD models have been extended to take into account the effect of target shedding on the behavior of a typical

monoclonal antibody in a minimal PBPK model. This simulation study shows that when a high concentration of soluble target exists due to membrane target shedding, using a TMDD without consideration of the shedding process could be misleading in determining dosing regimen.

References

[1] Zang Y, Pastan I (2008) High shed antigen levels within tumors: an additional barrier to immunoconjugated therapy. Clin Cancer Res 14(24):7981–7986

[2] Kuang B, King L, Wang H (2010) Therapeutic monoclonal antibody concentration monitoring: free or total? Bioanalysis 2(6):1125–1140

[3] Li L, Chetty M, Gardner I, Dostalek M, Grist E, Machavaram K (2012) Development of a minimal-PBPK model for simulating monoclonal antibody pharmacokinetics in human. Poster presentation at AAPS National Biotechnology Conference (21st–23rd May)

T-042 Population Pharmacokinetics of Unbound Hydrocortisone in Critically Ill Infants with Vasopressor-resistant Hypotension

Heather E. Vezina[1,*], Varsha Bhatt-Mehta[2], Chee Ng[1]

[1]The Children's Hospital of Philadelphia, Philadelphia, PA, USA; [2]University of Michigan, Ann Arbor, MI, USA

Objectives: Hydrocortisone (HC) is commonly used to treat vasopressor-resistant hypotension in critically ill infants with relative adrenal insufficiency [1]. HC binds to corticosteroid-binding globulin (CBG) ($\approx$80 %) and albumin ($\approx$10 %) [2]. Only 5–10 % is unbound and biologically active [2]. The pharmacokinetics (PK) of unbound HC in critically ill infants receiving HC treatment are unknown. The objectives of the present work were to determine the plasma PK of unbound HC in this unique pediatric population and identify patient-specific characteristics associated with PK variability.

Methods: Each subject had a single, random, baseline endogenous HC sample drawn. Stress and maintenance doses of HC (45 or 15 mg/m^2/day divided every 6 h) were administered as a bolus according to a standard neonatal intensive care unit protocol. For each subject, the baseline endogenous plasma sample and residual plasma from up to 3 random, post-dose samples drawn for routine clinical laboratory tests were analyzed for unbound HC concentrations using LC/MS/MS [2]. Several structural models were evaluated including one- and two-compartment models with baseline endogenous HC modeled as a constant and as a circadian rhythm function. Model parameter estimates were obtained using the first order conditional estimation with interaction (FOCE-I) method in NONMEM version 7.2. Available covariates (median, range) were weight (1.2, 0.5–4.4 kg), postnatal age (0.7, 0.1–9.3 weeks), gestational age (27, 23–41 weeks), and postconceptual age (28, 24–41 weeks). Covariate models were developed based on visual inspection of covariate-parameter relationships and likelihood ratio testing during stepwise forward inclusion and backward elimination where a change in the objective function value of 10.8 units ($p < 0.001$, $df = 1$) was defined as significant. Stability of the final model and precision of the parameter estimates were evaluated by a bootstrap re-sampling procedure with 1000 runs.

Results: 194 unbound HC concentrations from 62 infants less than 3 months old were used in the population PK analysis. 4 baseline endogenous HC concentrations drawn during exogenous HC administration were excluded from the analysis. A one-compartment model with first-order elimination best described the data. Baseline endogenous HC was modeled as a constant and added to the individual predictions. Interindividual variability was modeled exponentially for clearance (CL) and baseline endogenous HC (BL) but was fixed to zero for volume of distribution. Postconceptual age (PCA) modeled by a centered exponential function was a significant shared covariate on CL and V. PCA accounted for 41.5 % of the interindividual variability in CL. There were no covariate effects on BL. Eta-shrinkages were 11.7 and 12.1 % for CL and BL, respectively. Final parameter estimates, relative standard errors (RSE) and 95 % confidence intervals (CIs), as well as bootstrap estimates and 95 % CIs are in the table below. Successful estimation and covariance steps were achieved in 100 % of the bootstrap runs.

Parameter	Final estimate	RSE (%)	95 % CI	Bootstrap estimate	Bootstrap 95 % CI
CL (L/h)	0.827	10.4	0.659–0.995	0.839	0.666–1.03
PCA effect	0.196	9.74	0.159–0.233	0.197	0.160–0.239
V(L)	3.75	17.3	2.48–5.02	4.03	2.68–6.50
BL (ng/mL)	1.36	21.8	0.778–1.94	1.38	0.887–2.12
Interindividual variability in CL (CV %)					
Interindividual variability in BL (CV %)	0.296		(54.4 %)	26.9	0.140–0.452
0.290			0.137–0.507		
Residual variability by proportional error model (CV %)	2.42		(156 %)	11.7	1.87–2.97
2.36	1.78–2.92				
Residual variability by additive error model	0.330		(57.4 %)	13.3	0.244–0.416
	0.324		0.239–0.420		
0.049	16.6		0.033–0.065	0.047	0.033–0.064

RSE(%) 100 % $\times$ SE/estimate; *CV*(%) coefficient of variation; *SD* standard deviation

Conclusions: Our findings represent the first population PK report of unbound HC in critically ill infants with vasopressor-resistant hypotension. The typical half-life value for unbound HC was 3.14 h. The PK were well described by a one-compartment model that incorporated baseline endogenous HC into the predictions. The CL of unbound HC was faster in infants with an older PCA. After accounting for PCA, the remaining interindividual variability in CL was large and additional covariates such as sex, measures of hepatic and renal function, and host genetics associated with HC metabolic pathways should be examined in future studies.

References

[1] Higgins S, Friedlich P, Seri I (2010) Hydrocortisone for hypotension and vasopressor dependence in preterm neonates: a meta-analysis. J Perinatol 30:373–378

[2] Bhatt-Mehta V and Barks JD (2011) Relationship between free and total cortisol concentrations in the serum of newborn infants. J Neonatal-Perinatal Med 4:247–252

T-043 Pharmacometric Modeling of Clinical ADAS-cog Assessment Data using Item Response Theory

Sebastian Ueckert[1,*], Elodie L. Plan[1,2], Kaori Ito[3], Mats O. Karlsson[1], Brian Corrigan[3], Andrew C. Hooker[1]

[1]Pharmacometrics Research Group, Uppsala University, Uppsala, Sweden; [2]Metrum Research Group, Tariffville, CT, USA; [3]Primary Care Business Unit, Pfizer Inc., Groton, CT, USA

Objectives: Several publications have demonstrated the potential value of modeling and simulation for drug development and the resulting increased application of pharmacometric methods throughout the development process. In the therapeutic area of Alzheimer's Disease (AD), the ADAS-cog score is an endpoint of particular importance and models are developed in order to describe the longitudinal change of this response. Generally, these models treat the ADAS-cog score as a continuous variable, therefore ignoring the underlying discrete nature of the score [1]. In a separate communication, we present the benefits of an item response theory (IRT) based analysis of ADAS-cog assessments by linking the subscores of the ADAS-cog subtests to the non-observable variable "cognitive disability". The objectives in this part of the work, were to demonstrate how this approach can be extended to longitudinal Alzheimer's Disease trial data. Our aim was to investigate the potential benefits of this approach in terms of description of the score distribution, drug effect detection power and flexibility of clinical trial simulations.
Methods: *Data*: The modeling analysis was based on data from the placebo arm of a phase III study with mild to moderate AD patients [2]. The data utilized consisted of item level ADAS-cog assessment data from 322 patients with 7 scheduled assessments over a time range of 18 month. A total of 84,907 data entries were available for the analysis.
Model: The basis for this work was an ADAS-cog IRT model (presented separately) describing the responses of individual test items from an ADAS-cog assessment as a function of the hidden variable cognitive disability. All test specific parameters in the baseline model were fixed and the longitudinal change of cognitive disability was characterized through a linear function with subject specific slope and intercept (model structure as published by Ito et al. [1]). Model adequacy was assessed through visual predictive checks (VPCs) both on the ADAS-cog score level and on the item level.
Clinical Trial Simulations: The power to detect a drug effect using either the ADAS-cog IRT or the summary score model was compared through clinical trial simulations (CTSs) for various study sizes. First, 500 clinical trials were simulated from the longitudinal IRT model assuming a placebo controlled trial (mild-moderate AD patients, 18 months duration) for a disease modifying agent (20 % reduction in disease progression rate, introduced on the hidden variable). Subsequently, the resulting datasets were separately analyzed with the IRT and the summary score models. Drug effect detection power with each approach was calculated as the fraction of trials for which the drug effect was statistically significantly different from zero (assessed through log-likelihood ratio test).
Additionally, the possibility to perform CTSs for different patient populations and different ADAS-cog variants was demonstrated by repeating the outlined procedure with baseline parameter values for a mild cognitively impaired and a mild AD patient population as well as for an ADAS-cog assessment with and without the delayed word recall test.
Results: All parameters were estimated with satisfactory precision from the available data (relative standard error between 4.2 and 10.1 %). The typical baseline ADAS-cog value was found to be 22.2 points and the typical yearly increase, 3.5 points. VPCs indicated satisfactory data description on the summary score level and for most items (subscores). Some items of the "naming objects and fingers" and the "remembering test instructions" components presented discrepancies between model simulations and observations, but were judged marginal for the overall model performance.
Analysis with the ADAS-cog IRT model resulted in a considerably higher power to detect a drug effect in the CTSs. In order to reach 80 % power the summary score analysis needed more than 600 individuals, whereas the IRT-based analysis achieved the same power with about 400 individuals, corresponding to a reduction of 33 % in sample size. CTSs in different patient populations revealed a slightly higher power to detect a drug effect in the mild cognitively impaired population than in the mild AD population. Removing the "delayed word recall" component decreased the power in both populations.
Conclusions: By using an IRT ADAS-cog model, we combined ADAS-cog data from a longitudinal clinical trial with information characterizing the relationships between the individual items of a cognitive assessment as obtained from clinical trial databases. The resulting longitudinal ADAS-cog accurately describes the underlying distribution of the summary score by considering the inherent discrete and bounded nature of the data. In the CTSs, the IRT model showed considerably higher power to detect drug effects than the continuous summary score model. An additional feature of this approach is the separation of test, patient population and drug specific parameters, increasing the flexibility of CTS and thus providing additional tools for planning future trials.

References

[1] Ito K, Corrigan B, Zhao Q, French J, Miller R, Soares H, Katz E, et al (2011) Disease progression model for cognitive deterioration from Alzheimer's disease neuroimaging initiative database. Alzheimer's Dementia 7(2): 151–160. doi:10.1016/j.jalz.2010.03.018.

[2] Feldman HH, Doody HS, Kivipelto M, Sparks DL, Waters DD, Jones RW, Schwam E, et al (2010) Randomized controlled trial of atorvastatin in mild to moderate Alzheimer disease: LEADe. Neurology 74(12):956–964. doi:10.1212/WNL.0b013e3181d6476a

T-044 Semi-Mechanistic Population Pharmacokinetic Modeling of Cefadroxil: An Example of PEPT2-Mediated Renal Tubular Reabsorption

Yehua Xie[1,*], David E. Smith[1], Yongjun Hu[1], Hong Shen[2], Meihua R Feng[1]

[1]Department of Pharmaceutical Sciences, College of Pharmacy, University of Michigan, Ann Arbor, MI, USA; [2]Department of Pharmaceutical Candidate Optimization, Bristol-Myers Squibb Research and Development, Princeton, NJ, USA

Objectives: PEPT2, a proton-coupled oligopeptide transporter, plays a primary role in the renal tubular reabsorption of some drugs including the antibacterial agent cefadroxil which is essentially excreted unchanged in the urine of mice. The systemic clearance of cefadroxil is significantly higher in PEPT2 null mice than in wild-type

mice due to depletion of this protein [1]. The aim of this study was to characterize the pharmacokinetics of cefadroxil in wild-type and PEPT2 null mice using non-linear mixed effects modeling (NONMEM).

Methods: Pharmacokinetic data of cefadroxil in wild-type and PEPT2 null mice following intravenous administration (doses ranged from 1 to 100 nmol/g) were analyzed using NONMEM v7.2. Different models with linear and/or nonlinear elimination kinetics were then examined. The final model was selected based on the likelihood ratio test and visual inspection of diagnostic plots.

Results: The pharmacokinetic profile of cefadroxil was best described by a two-compartment model with linear renal elimination (i.e., filtration and tubular secretion) and nonlinear tubular reabsorption (mediated by PEPT2) in wild-type mice, whereas, only linear renal elimination (i.e., filtration and tubular secretion) was considered in PEPT2 null mice (Fig. 1). The nonlinear kinetics of PEPT2-mediated tubular reabsorption was well characterized by the Michaelis–Menten parameters $V_{max} = 0.08 \pm 0.03$ nmol/min/g and $K_m = 9.1 \pm 4.0$ μM (Table 1). These results are consistent with previously reported PEPT2 transport kinetics (i.e., $K_m = 10$ to 40 μM).

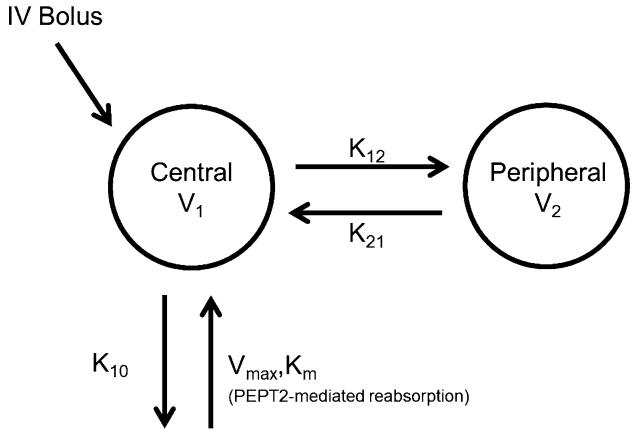

Fig. 1 Schematic structural model of cefadroxil after intravenous (IV) bolus input. ($K_{12} = Q/V_1$, $K_{21} = Q/V_2$)

Table 1 Pharmacokinetic parameter estimates of cefadroxil using a two-compartment model with parallel linear elimination and nonlinear reabsorption in wild-type and PEPT2 null mice

Parameter	Mean population value (% RSE)	Between subjects variability (% RSE)
V_1 (mL/g)	0.173 (7)	34 (11)
V_2 (mL/g)	0.359 (14)	34 (11)[b]
Q (mL/min/g)	0.039 (28)	–
K_{10} (min^{-1})	0.152 (12)	18 (21)
V_{max} (nmol/min/g)	0.08[a] (38)	–
K_m (μM)	9.1[a] (44)	–
Residual (Proportional)	0.101 (7)	–

[a] This pharmacokinetic parameter was estimated in wild-type mice and set to zero in PEPT2 null mice

[b] Shared ETA between V_1 and V_2

Conclusions: In the present study, we demonstrated that the pharmacokinetics of cefadroxil was well characterized by a model that incorporated linear renal elimination along with nonlinear PEPT2-mediated tubular reabsorption in mice. This population pharmacokinetic model may help to provide mechanistic insight into the predominant role of PEPT2 in renal tubular reabsorption of cefadroxil and facilitate the prediction of cefadroxil disposition in human.

Reference

[1] Shen H, et al (2007) Impact of genetic knockout of PEPT2 on cefadroxil pharmacokinetics, renal tubular reabsorption, and brain penetration in mice. Drug Metab Dispos 35(7):1209–1216

T-045 Meta-Analysis of Malignancies, Serious Infections, and Serious Adverse Events with Tofacitinib or Biologic Treatment in Rheumatoid Arthritis Clinical Trials

Sima Ahadieh[1,*], Tina Checchio[1], Thomas Tensfeldt[1], Jonathan French[2], Jamie Geier[3], Richard Riese[1], Sujatha Menon[1], Mary Boy[1], Sriram Krishnaswami[1]

[1]Pfizer Inc., Groton, CT, USA; [2]Metrum Research Institute, Tariffville, CT, USA; [3]Pfizer Inc, New York, NY, USA

Objectives: Patients with rheumatoid arthritis (RA) experience adverse events (AEs) attributed to both the disease and its treatment. Tofacitinib is a novel oral Janus kinase inhibitor being investigated as a targeted immunomodulator and disease-modifying therapy for RA. To contextualize events within the tofacitinib clinical trial program, a meta-analysis of published data sources was completed in patients with RA receiving biologic drug therapy within a randomized clinical trial (RCT) setting to quantify safety endpoints of: malignancies excluding non-melanoma skin cancer (NMSC), serious infections (SIs), and serious AEs (SAEs).

Methods: Medline, Embase, PubMed, and summary basis of approvals from regulatory submissions were searched to identify RCTs for abatacept, rituximab, etanercept, infliximab, certolizumab, golimumab, adalimumab, and tocilizumab in RA. The search identified >300 papers from which data from 80 RCTs, representing more than 31,000 subjects, were extracted for analysis for the three endpoints. Non-RCTs, long-term extensions, and observational studies were excluded from the literature results. Tofacitinib results from five RCTs (Phase 3 [P3]) are presented. The dependent variable for the analysis was the incidence rate (IR) of an event/100 patient-years (pt-yrs). Data were analyzed using a random effects meta-analysis model. The IR data were log transformed to avoid negative confidence intervals (CIs). An imputation methodology was applied to account for IRs of zero and a sensitivity analysis was performed to assess the effects of adjustment on the individual and overall mean, as well as the impact on the estimated variance surrounding each study arm.

Results: Estimated IRs for endpoints of malignancies, SIs, and SAEs revealed similar rates among biologic therapies for treatment of RA. Across all biologic therapies, point estimates ranged from 0.8 to 1.4 events/100 pt-yrs for malignancies; 2.5–6.5 for SIs; and 10.7–22.0 for SAEs. Event rates for tofacitinib were 0.62 (95 % CI 0.36, 1.07) events/100 pt-yrs for malignancies (Fig. 1); 2.91 (2.27, 3.74) events/100 pt-yrs for SIs; and 10.3 (9.00, 11.78) events/100 pt-yrs for SAEs, all in P3. The 95 % CIs for tofacitinib were contained within the range of published estimates.

Conclusions: This RCT meta-analysis provides a quantitative assessment of the incidence of important safety events reported with therapies for the treatment of RA. Overall, tofacitinib event rates for

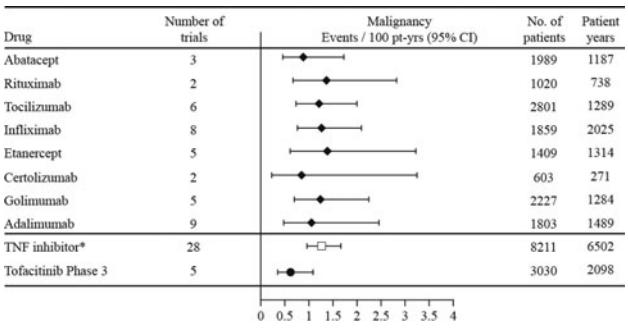

Fig. 1 Weighted mean IRs (95 % CI) of malignancies (excluding NMSC) for tofacitinib or biologic therapies used to treat moderate-to severe RA. *Estimate from 28 TNF inhibitor studies

malignancies, SIs, and SAEs were comparable to published rates for approved biologic therapies. Future analyses are warranted to estimate relative effects (treatment comparisons), model studies with no events (IR = 0), and account for study population differences.

Reference

[1] Ahadieh et al (2012) Arthritis Rheum; 64(10 Suppl): S726, Abst 1697

T-046 Approaches to Detect Non-Compliant Patients and Obtain Unbiased Estimates of Population PK Model Parameters in a Population with Prevalent Non-compliance

Leonid Gibiansky[1,*], Ekaterina Gibiansky[1], Valerie Cosson[2], Nicolas Frey[2], Franziska Schaedeli Stark[2]

[1]QuantPharm LLC, North Potomac, MD, US; [2]Hoffmann-La Roche Ltd, Basel, Switzerland

Objectives: To propose and evaluate methods for detection of non-compliance using concentration–time data and for obtaining unbiased estimates of population pharmacokinetic (PK) model parameters in a population with prevalent non-compliance.

Methods: Datasets that emulated three studies with different duration, sampling schemes and different levels of non-compliance were simulated. A two-compartment model with relatively fast first-order absorption (with 1–2 h absorption half-life), relatively long terminal half-life (1–2 days), and significant drug accumulation during 4-weeks to 4-months treatment period of once-a-day dosing was used. Non-compliance was simulated as drug holidays (of several days) preceding some observations in 20–80 % of subjects. For each dataset, the model without accounting for non-compliance was fitted first to evaluate bias of the parameter estimates. Then, two methods accounting for non-compliance were tested.

In the first method (referred to as the ETA-on-epsilon method), a random effect on the magnitude of the residual error was introduced. High magnitude of the residual error estimated for some subjects was thought to be associated with non-compliance in these subjects. The same model was fitted to the simulated datasets where increasing fractions of subjects with the highest residual errors were commented out. Association of non-compliant subjects with high-residual-error subjects was investigated. Parameter estimates of these models were compared with the true (used for simulations) parameters and the parameters of the model that did not account for non-compliance.

The other method (referred to as the "profiles" method) was developed for the data with a specific sampling pattern that included an outpatient (non-compliant) part with several trough samples followed by the rich profile after the inpatient (compliant) dose. The method is the generalization of the idea proposed in [1] that relies only on the doses known to be administered (e.g., inpatient doses). In this method, all concentration measurements during the outpatient part of the study (except the trough value immediately preceding the inpatient dose) are removed from the dataset and an additional parameter (relative bioavailability of the outpatient doses) is introduced. This allows decoupling of the unreliable (outpatient) and reliable (inpatient) dosing and concentration data. In case of a one-compartment drug, the method reduces to that proposed in [1]. The parameter estimates obtained using this method were compared with the true parameters. Association of the individual estimate of relative bioavailability during the outpatient part of the study with the compliance status during this period was investigated. The ETA-on-epsilon method was also tested on the data used for the profiles method.

Results: Investigation of the ETA-on-epsilon method indicated that the parameter estimates of the model that did not account for non-compliance could be significantly biased, especially for the datasets that included high fraction of non-compliant patients. Introduction of the ETA-on-epsilon parameter significantly reduced the bias. Individual ETA-on-epsilon values allowed identification of non-compliant subjects. When subjects with high magnitude of the residual error were removed from the dataset, bias due to non-compliance was further reduced. During incremental removal of the subjects with the highest ETA-on-epsilon values the population parameter estimates converged to the true values until bias disappeared. At the same time, variance of the ETA-on-epsilon random effect became smaller and then disappeared indicating that the ETA-on-epsilon random effect indeed was caused by non-compliance. However, precision of the obtained parameter estimates decreased
for the datasets with high fraction of non-complaint subjects that needed to be removed from the dataset to obtain unbiased parameter estimates. Investigation of the profiles method indicated that it allowed for the unbiased estimates of the model parameters in the datasets with any fraction of non-compliant patients. However, the method heavily relied on the availability of rich data following the inpatient dose. Simulated non-compliant subjects were estimated to have low bioavailability during the outpatient part of the study. Thus, the estimates of bioavailability can be used as an indication of compliance during time preceding the inpatient dose.

The proposed methods allowed identification of subjects with non-compliance and reduced or completely eliminated bias in the parameter estimates for the simulated datasets with various sampling schemes and fractions of non-complaint patients. Applications of these methods to real data are ongoing.

The two proposed methods can be viewed as complimentarily tools, each with its own advantages and limitations. The profiles method should provide unbiased parameter estimates for any non-compliance pattern but it can be applied only for the specific sampling schemes that include relatively rich data following the inpatient (fully compliant) dose. The ETA-on-epsilon method is not based on any assumptions about the sampling schemes but it is unlikely to account for the completely random non-compliance if it is present in the majority of patients.

Conclusions: For a number of simulated datasets with various sampling schemes and various fractions of non-compliant patients, the proposed ETA-on-epsilon and profiles methods allowed to identify subjects with compliance problem and to obtain the unbiased estimates of model parameters. Even without additional modifications, inclusion of the inter-individual random effect on the residual error resulted in a significant reduction of the

estimation bias. The proposed methods offer a way to evaluate the influence of compliance on the population PK parameter estimates.

Reference

[1] Gupta P, Hutmacher MM, Frame B, Miller R (2008) An alternative method for population pharmacokinetic data analysis under noncompliance. J Pharmacokinet Pharmacodyn 35(2): 219–233

T-047 Population Pharmacokinetic-Pharmacodynamic Modeling of Intrathecal Ropivacaine in Orthopedic Patients

Francois Gaudreault[1,*], Pierre Drolet[2], Michel Fallaha[3] and France Varin[1]

[1]Faculty of Pharmacy, Université de Montréal, Montréal, QC, Canada; [2]Department of Anesthesiology, Maisonneuve-Rosemont Hospital, Montréal, QC, Canada; [3]Department of Orthopedic Surgery, Maisonneuve-Rosemont Hospital, Montréal, QC, Canada

Objectives: Spinal ropivacaine has been shown to provide effective anesthesia and pain relief in surgical outpatients, but is currently not licensed for intrathecal use [1–2]. This study was designed to develop a population pharmacokinetic-pharmacodynamic (PK-PD) model for optimizing the clinical use of this drug.
Methods: Ropivacaine (17.5 mg) was administered intrathecally (L2) to ten orthopedic patients. Current perception thresholds (CPT) in response to a gradual increase (20 μA every 3 s) in transcutaneous electrical stimulation (primary endpoint) as well as clinical assessment (ice-cold testing) were conducted in the thigh area while ropivacaine plasma concentrations were determined up to 24 h after the administration of the local anesthetic. Two parallel first-order absorption rate constants were used to characterize the biphasic release of ropivacaine from its site of injection (absorption compartment). An equilibrium rate constant (ke0) between the absorption and hypothetical effect compartments was added. Effect compartment concentrations were fitted to the simultaneously acquired CPT data using a sigmoid E_{max} model in NONMEM.
Results: Ropivacaine maximal response (E_{max}: 1860 ± 736 μA) was observed within 10.8 ± 3.2 min of dosing, with a subsequent return to baseline (E_0: 127 ± 33.1 μA) 4.1 ± 0.7 h after the administration of the local anesthetic. The increase and decrease in CPT correlated well with the loss and recovery of ice-cold sensation, respectively. Mean effect compartment equilibrium half-life ($T_{1/2}$ ke0) was 8.1 ± 1.1 min. Interindividual variability (IIV) for the pharmacodynamic model parameters (E_{max}, E_0 and ke0) were 96, 80 and 35 %, respectively. The effect-site amount producing 50 % of the E_{max} (AE_{50}) was 7.9 ± 1.5 mg (IIV = 33 %), which is accordance with the ED_{50} (8.41 mg, 95 %CI: 7.15–9.67 mg) obtained from a previous pharmacodynamic study after spinal injection of ropivacaine in patients [3]. None of the model parameters, including apparent clearance (Cl/F: 16.6 ± 2.3 L/h, IIV = 41.9 %) and volume of distribution (V/F: 83 ± 4.1 L, IIV = 25 %) showed sex, age or body weight dependency.
Conclusions: A population PK-PD model was developed that quantitatively describes the time-course of sensory blockade during intrathecal anesthesia in orthopedic patients. The model may be useful to optimize ropivacaine dosing regimen.

References

[1] CNS Drugs 2006; 20(11):917–933
[2] Drug Safety 2004; 27(14):1093–1114
[3] Anesth Analg 2009; 109(4):1331–1334

T-048 Fisher Information Matrix Compared with Decision Analytics for Optimizing Clinical Trials

Hodge Lee*

qPharmetra LLC, Andover, MA, USA

Objectives: This presentation will compare the key differences, advantages, disadvantages, and thus best context for use of the Fisher Information Matrix and a Decision Analytic objective function for optimizing clinical trial design. The Fisher Information Matrix (FIM) has been used as a metric to guide analyses seeking more informative, and thus more optimal clinical trial designs. It seeks to demonstrate which alternative sampling strategies, sample sizes, etc., reduce the uncertainty in the conclusions from a trial's result, as manifested in the standard errors from a maximum likelihood model of the results. Among the alternatives to the FIM is expected Net Present Value (eNPV), one of the commonly used metrics from the field of Decision Analysis. eNPV has also been used for years to guide pharmaceutical decision-making, enabling the overt calculation of how valuable any additional information gleaned will be using Value of Information (VoI) analysis. VoI integrates the costs and benefits of alternative outcomes with their probability of occurring, and the ramifications of learning. Given its history of usage in the field of Modeling and Simulation (M&S) FIM will be more familiar to most in that field, while eNPV will not. Thus the types of problems each is best suited to may not be clear to many M&S practitioners.
Methods: The presentation will illustrate how FIM and eNPV fare in a variety of decision types by way of a fictitious drug development example (this example mimics actual experiences the presenter has in applying the methods). In it, proprietary data has been used to predict how a new drug will fare in later stage development given the results in earlier trials and with similar drugs, and given alternative designs for a PoC (proof of concept) study. Both FIM and eNPV will be computed using simulated PoC outcomes. For eNPV, the VoI will be calculated given the impact on the cost, time to market, and value to patients and prescribers. The results will be illustrated across types of decisions (e.g., drivers in the trial, such as observation times, trial duration, choice of primary endpoint, and sample size). This will be compared against the "true" underlying simulated outcome for each drug to gauge which conditions each objective function fares best at yielding a decision that best benefits patients and the decision-makers.
Results: The example demonstrates under what conditions (e.g., whether a the design alternatives impact the time to market, cost of development, the "option pricing" value of delaying decisions until more is learned, the ability to design a better trial downstream, informing communications with regulators), each objective function performs best. Although fictitious to protect proprietary information, the example cites real-life experiences applying such techniques. Finally, a discussion of the practical realities of employing each method will be provided.

Conclusions: Both the Fisher Information Matrix and Decision Analytic objective functions are helpful at informing decisions. However, the context of when each is better suited to inform truly optimal decisions is different, with decisions the drivers of time, patient value, and decision-maker information each being important to consider when designing a trial. Finally, the practical realities of both methods, given their technical backgrounds and analytic burden will be discussed.

References

[1] Clemen RT (1996) Making hard decisions: an introduction to decision analysis, 2nd edn, Duxbury Press, Pacific Grove

[2] Hodge FL, Dykstra K (2001) Value of information: embedding the power of modeling and simulation into strategic decisions. Poster Presentation, ACoP

[3] Hooker AC, Ueckert S, Andrew M, Karlsson M, Ito K, Corrigan C (2011) Model-based trial optimization for phase II and III designs in Alzheimer's disease, Presentation, ACoP

[4] Grabowski H (1997) The effect of pharmacoeconomics on company research and development decisions. Pharmacoeconomics 11(5):389–397

[5] Groenendaal H, Bush M, Hodge FL, Dykstra K, Mudd P, Rajapakse A, Zagmutt F, Quantitative risk analysis: improving decision making by quantifying uncertainty. AAPS Newsmagazine, April

[6] Hughes DA, Walley T (2001) Economic evaluations during early (phase II) drug development: a role for clinical trial simulations? Pharmacoeconomics 19(11):1069–1077

[7] Julious S, Swank D (2005) Moving statistics beyond the individual clinical trial: applying decision science to optimize a clinical development plan. Pharm Stat 4:37–46

T-049 Population Pharmacokinetics Modeling of Anastrozole (Arimidex) in Female Pediatric Subjects with McCune: Albright Syndrome (MAS)

Felix Agbo

AstraZeneca LP, Wilmington, DE, USA

Objectives: (1) To describe the PK of anastrozole in pediatric girls (age ≤10 years) with gonadotropin-independent precocious puberty due to McCune-Albright Syndrome; (2) To identify the influence of covariates on anastrozole disposition; (3) To estimate the interindividual and residual variability of anastrozole PK; and (4) To compare the PK of anastrozole in female pediatric patients suffering from MAS with adolescent boys with gynecomastia.

Background: McCune Albright Syndrome (MAS) is a rare disorder characterized by precocious puberty, polyostotic fibrous dysphasia, and café au lait spots. Traditional therapy of precocious puberty in this disorder has been characterized by problems with both efficacy and compliance. Preliminary data suggest that anastrozole may be useful in suppression of estrogen action in precocious puberty subjects with MAS. Although well studied in adults, the pharmacokinetics of anastrozole has not previously been studied in this pediatric population.

Methods: Anastrozole concentration time data from two clinical trials were used in this analysis. Study 0046 was an open-label, multicenter, multi-national trial evaluating the safety and efficacy of a daily oral dose regimen 1 mg anastrozole in 28 female pediatric (age ≤10 years) patients with MAS. The study was prospectively designed to include sparse blood sampling strategy for the evaluation using population PK techniques. Four blood samples were taken from each subject. Study 0001 was an open-label, PK and PD study of anastrozole 1 mg in 36 pubertal boys aged 11–18 years inclusive with gynecomastia of recent onset. Rich data from the adolescent boy's study (14 samples per subject) were included in the analysis to determine the structural PK for anastrozole and for comparison of pediatric girls and adolescent boys anastrozole pharmacokinetics. The data set for analysis contained 504 anastrozole concentrations from 36 adolescent male subjects and 111 concentrations from 28 pediatric female subjects.

Base model development: Models were built using NONMEM software (Version V Level 1.1). One- and two-compartment models with first-order absorption and elimination were fit to the anastrozole concentration–time data. The models were parameterized in terms of CL, V and Ka. Interindividual variability for all parameters was described using exponential error models. Random residual error was expressed using the proportional model. First order conditional estimate with interaction (FOCEI) method was used for all analyses. *Covariate model building:* Statistical significance of each covariate-parameter relationship was tested individually in a step-wise parameter addition method in NONMEM. Significance of parameters was assessed at the $p < 0.01$ level (decrease in the objective function of at least 6.63 units for 1 *df* for Chi square distribution.). Covariates tested included RACE, AGE, WT, HT, BSA, BMI, and LBM. *Final model development:* Statistical significance of each covariate-parameter relationship was tested individually in a stepwise deletion method. Significance of parameters was assessed at the $p < 0.005$ level (increase of objective function value of at least 7.88 units for 1 *df* for Chi square distribution). *Model evaluation:* Final model was evaluated graphically by comparing the individual and population predictions with the observed concentration and by bootstrap analysis.

Results: The results are summarized in the table and figures. A two-compartment model with first-order absorption and elimination adequately described anastrozole PK following a 1-mg once daily oral dose regimen in female pediatric and male adolescent subjects. Model parameters were estimated with good precision. Goodness of fit plots indicated the model described the data well. The model indicated low to moderate IIV on clearance (37.8 %) and central volume of distribution (28.9 %). Of the covariates tested SEX and BSA were significantly influential on CL/F and V/F, respectively. The

Table 1 Summary of typical anastrozole population pharmacokinetic parameters of the final model

Model parameters	Estimate (SE); CV %	95 % confidence interval
Apparent oral clearance, CL/F (L/h)	1.83 (0.163)	1.51 to 2.15
Volume of distribution, V/F(L)	58.9 (3.20)	52.6 to 65.2
Inter-compartmental clearance, Q/F (L/h)	2.72 (0.321)	2.09 to 3.35
Steady-state volume of distribution, V_{ss}/F(L)	194 (25.8)	143 to 245
Absorption rate constant, ka (1/h)	2.80 (0.334)	2.15 to 3.45
Effect of body surface area on V/F $V/F = \theta(2) + \theta(6)*(BSA-1.58)$	52.3 (4.22)	44.0 to 60.6
Effect of sex on CL/F $CL/F = \theta(1)*(1 + \theta(7)*SEX)$	−0.466 (0.0654)	−0.594 to −0.338
Inter-individual variability CL/F	0.143 (0.0336); 37.8 %	0.0771 to 0.209
Inter-individual variability V/F	0.0838 (0.0232); 28.9 %	0.0383 to 0.129
Residual variability	0.0187 (0.00295); 13.7 %	0.0129 to 0.0245

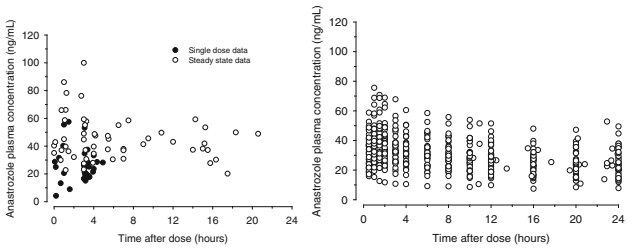

Fig. 1 Anastrozole plasma concentration—time after dose for girls (*left*) and boys (*right*)

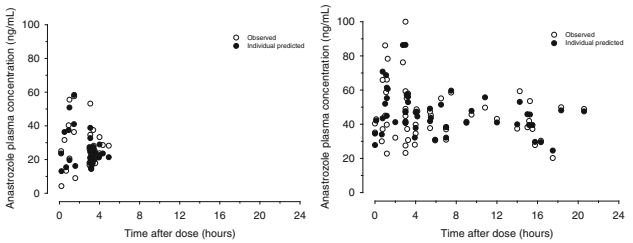

Fig. 2 Individual-predicted and observed anastrozole plasma concentration—time after dose for girls—single dose (*left*), steady-state (*right*) (final model)

unexplained residual variability was low (13.7 %). The model indicated that girls had a lower predicted CL/F than boys, 0.977 versus 1.83
L/h, a 46.6 % decrease. Anastrozole exposure C_{max} and AUC was 70 and 34 %, respectively, higher for girls than boys. Model-predicted values for steady-state C_{max} and AUC were 63.1 ng/mL (range: 35.8–108 ng/mL) and 941 ng h/mL (range: 608–1770 ng h/mL) for the girls and 37.2 ng/mL (range: 14.5–67.6 ng/mL) and 701 ng h/mL (range: 236–1330 ng h/mL) for the boys, respectively. The younger girls (3–6 year old) had the highest exposure to anastrozole, with mean C_{max} and AUC values of 68.2 ng/mL (range: 43.3–108 ng/mL) and 943 ng h/mL (range: 608–1770 ng h/mL), respectively, which were 83 and 34 % higher than in boys (Table 1).
Conclusions: The final two-compartment model with first-order absorption and elimination adequately described the concentration data well with low to moderate inter-subject variability. Overall, the exposure of anastrozole was higher in girls than boys (Figs. 1, 2).

T-050 Prediction of Shrinkage of Individual Parameters Using Bayesian Information Matrix in Nonlinear Mixed Effect Models with Evaluation in Pharmacokinetics

François Combes[1,2,3], Sylvie Retout[2], Nicolas Frey[2], France Mentré[1,*]

[1]INSERM, UMR 738, Univ Paris Diderot, Sorbonne Paris cité, Paris, France; [2]Pharma Research and Early Development, Clinical Pharmacology, F. Hoffmann-La Roche ltd, Basel, Switzerland; [3]Institut Roche de Recherche et Médecine Translationnelle, Boulogne-Billancourt, France

Objectives: In population pharmacokinetics (PK), precision of population parameter estimates depends on design and are evaluated using Fisher information matrix. Individual parameters are usually estimated by the maximum a posteriori (MAP) and precision of individual estimates can be evaluated using the Bayesian fisher information matrix (M_{BF}) [1]. Shrinkage of individual parameters towards the mean occurs when information is sparse and can be quantified as a reduction of variance of the estimated random effects (RE) [2]. This study aims at (1) exploring the relationship between BM_F and shrinkage in order to propose a prediction of shrinkage and (2) evaluating by simulation the prediction of individual parameter precision and shrinkage.
Methods: We first derived the expression of M_{BF} for additive RE and constant residual error and then extended it for exponential RE and/or combined residual error, using first order approximation of the model. Using the formula of shrinkage in linear mixed effects models, we derived a prediction of shrinkage from M_{BF}. Regarding the evaluation by simulation, we simulated data from sparse and rich design for two PK examples: a simple one (one compartment) with six different scenarios (additive or exponential RE, with low and high variabilities, additive or combined residual error); a more complex example derived from a real case study [3] (two compartment, dual linear and non-linear elimination). We used NONMEM 7.2 and MONOLIX 4.0 to perform individual estimation via MAP assuming known population parameters and fixed to their exact value. We also recorded individual standard errors (SE). We then compared predicted and estimated individual SE for each scenario and example as well as the predicted and estimated shrinkage, evaluated using the formula with ratio of variances.
Results: For the simple example, considering all scenarios and designs, predicted SE of the two parameters using M_{BF} were close to the estimated SE with both software and varied as expected with the richness of the design and the variabilities. There were also a very good agreement (almost identity line) between estimated shrinkage (which varies from 0 to 70 %) and predicted shrinkage. Similar results were observed for all the parameters of the real example.
Conclusion: The Bayesian Information Matrix allows to evaluate impact of design on precision of individual parameters and to predict shrinkage. It can be used for design optimization and will be implemented in PFIM.

References

[1] Merlé Y, Mentré F (1995) Bayesian design criteria: computation, comparison and application to a pharmacokinetic and a pharmacodynamic model. J Pharmacokinet Biopharm 23(1):101–125
[2] Savic R, Karlsson M (2009) Importance of shrinkage in empirical Bayes estimates for diagnostics: problems and solutions. The AAPS J 11(3):558–569
[3] Frey N, Grange S, Woodworth T (2010) Population pharmacokinetics analysis of tocilizumab in patients with rheumatoid arthritis. J Clin Pharmacol 50(7):754–766
[4] Results in this abstract have been previously presented in part at PAGE 2012, Venice, Italy, June 2012 and published in the conference proceedings as Abstract 2442.

T-051 Enantioselective Pharmacokinetics of Indobufen, an Inhibitor of Platelet Aggregation

Sangmin Choe[1], Kyun-Seop Bae[2], Yook-Hwan Noh[2,*], Jin-Ah Jung[3], Seok-Joon Jin[2], Jin A Jung[2], A-reum Kim[2], Hyeong-Seok Lim[2]

[1]Division of Clinical Pharmacology, Clinical Trials Center, Pusan National University Hospital, Busan, Republic of Korea; [2]Department of Clinical Pharmacology and Therapeutics, Asan Medical Center, Ulsan University College of Medicine, Pungnap-2-dong, Seoul,

Republic of Korea; [3]Department of Clinical Pharmacology and Therapeutics, Samsung Medical Center, Seoul, Republic of Korea

Objectives: Ibutstrin® (Indobufen), a reversible inhibitor of platelet aggregation is effective in the prophylaxis of thromboembolic events at risky patients [1]. Ibutstrin® exists in two enantiometric forms and S-indobufen is known to be more potent [2]. This study was performed to characterize the pharmacokinetics (PK) of each enantiomer of indobufen and its association with genetic polymorphisms of UDP glucuronosyltransferases (UGT).
Methods: Serial blood samples were collected from 12 Korean healthy adult male volunteers after single oral administration of ibustrin®, 200 mg, to characterize the PK of indobufen. Plasma concentrations of S- and R- enantiomer of indobufen were measured by validated high performance liquid chromatography, respectively. Six common *UGT1A* genotypes were determined by SNaPshot or real-time PCR method. PK was analyzed by non-compartmental (NCA) methods using WinNonlin® 5.2 (Pharsight Corporation, Mountain View, CA), and by compartmental modeling using NONMEM® 7.2 (ICON Development Solutions, USA).
Results: Mean AUC_{inf} and C_{max} of R-indobufen (319.7 h*mg/L, 27.8 mg/L) were higher than those of S-indobufen (222.4 h*mg/L, 22.5 mg/L). Both of S- and R-indobufen were best fitted by two compartment disposition model. The absorption was complex and weibull model with first order kinetics (Ka) and mixed zero (D1) and with absorption lag (ALAG1) best described the concentration–time data in the absorption phase. There was no significant association between the PK and *UGT1A* genotypes in both of S- and R-indobufen.
Conclusions: This study provided us the basic phasic PK information comparing both form of indobufen enantiomers. This result could be useful for the optimal drug therapy, and for the development of enantioselective, novel indobufen formulation.

References

[1] Bhana N, McClellan KJ (2001) Indobufen: an updated review of its use in the management of atherothrombosis. Drugs Aging 18:369–388

[2] Glowka FK, Karazniewicz M (2004) Resolution of indobufen enantiomers by capillary zone electrophoresis. Pharmacokinetic studies of human serum. J Chromatogr A 1032:219–225

T-052 Model-Based Meta-Analysis in Rhematoid Arthritis: Correlation of DAS28 and ACR50 Treatment Effects

Rui Zhu[1,*], Yehong Wang[1], Jingjing Sun[1], Zheng Su[1], John C. Davis[1], Jaap W. Mandema[2], Meina Tang[1], John D. Davis[1], Jim Xiao[1], Jin Yan Jin[1]

[1]Genentech, Inc., South San Francisco, CA, USA; [2]Quantitative Solutions, Menlo Park, CA, USA.

Objectives: ACR20/50/70 and DAS28 are clinical efficacy endpoints for rheumatoid arthritis (RA) studies. Studies powered for ΔΔDAS28 (i.e., DAS28 change compared to baseline and control) require smaller sample sizes than those powered for ΔACRs (i.e., ACRs change from control), while ACRs are ultimately required for drug approval in the US. Thus quantitative understanding of the correlation between the two endpoints could aid interpretation of earlier-stage study results and provide justification for study designs powered for ΔΔDAS28 assessment.
Methods: Data were obtained from published randomized controlled RA trials in patients with minimum treatment duration of 12 weeks. Paired data on DAS28 and ACR50 (logit transformed) at the predetermined primary time point (ranged from 12 to 54 weeks) for each trial were analyzed using a nonlinear regression model implemented in S-PLUS 8.2. Numerous covariates were also tested in the model.
Results: Data used in the analysis were from 26 trials, representing over 11,000 patients and 7 drug classes, including anti-TNF (infliximab, adalimumab, certolizumab, golimumab), anti-IL17 (ixekizumab), anti-CD28 (abatacept), anti-CD20 (rituximab), anti-IL6R (tocilizumab), DMARD (methotrexate), and glucocorticoids. The correlation of ΔΔDAS28 and ΔACR50 was well described by the model. The estimated mean scaling factors (SC) between ΔΔDAS28 and ΔACR50 were significantly different across drug classes, i.e., −1.46, −0.95, −1.25 for anti-TNF, anti-IL6R, and other drug classes combined, respectively. In addition, trials with higher baseline DAS28 were more likely to show lower ΔACR50 than trials with lower baseline DAS28. However, the effects of DAS28 in control groups, ΔΔDAS28, and treatment duration on SC were not statistically significant.
Conclusions: Treatment effects of DAS28 and ACR50 are moderately correlated. The correlation can be affected by drug class and baseline DAS28. The model may be applied to aid clinical trial designs with the sample size powered based on target ΔΔDAS28.
The results in this abstract have been previously presented at the ASCPT 2013 Annual Meeting. Indianapolis, Indiana, March 5–9, 2013 and published in the conference proceedings.

T-053 Clinical Trial Simulation to Evaluate Concentration-controlled Regimens and Probability of Trial Success for Tofacitinib in Kidney Transplant

Jonathan French[1,*], Matt Hutmacher[2], Manisha Lamba[3], Sriram Krishnaswami[3], Mark Peterson[4], Gary Chan[3], and Michael Tortorici[5]

[1]Metrum Research Group, Tariffville, CT, USA; [2]Ann Arbor Pharmacometrics Group, Ann Arbor, MI, USA; [3]Pfizer, Inc., Groton, CT, USA; [4]Pfizer, Inc., Cambridge, MA, USA; [5]Pfizer, Inc., Collegeville, PA, USA

Objectives: Tofacitinib is a novel, oral Janus kinase inhibitor being investigated as a targeted immunomodulator. Tofacitinib achieved similar rates of biopsy-proven acute rejection and improved renal function compared with cyclosporine (CsA) in a Phase 2b study in de novo kidney transplant (KT) patients. Using data from this study, time-to-event models, driven by subject-specific two-hour post-dose concentrations (C2) were developed for four endpoints: biopsy-proven acute rejection (BPAR), cytomegalovirus disease (CMVD), serious infection (SI), and post-transplant lymphoproliferative disease (PTLD) [1]. The objective of this investigation was to evaluate, through simulation, several real-world therapeutic drug monitoring (TDM) regimens and two dose-adjustment algorithms with respect to their predicted twelve-month BPAR, CMVD, SI and PTLD incidence rates. The purpose was to assess the probability of success for an active-control Phase 3 study of tofacitinib in kidney transplant patients. In this case, successful optimization of the tofacitinib TDM/dose-adjustment algorithm was defined as demonstrating non-inferiority to active control in Month 12 BPAR incidence under the proposed trial design.
Methods: Each simulated trial was a parallel group, active controlled trial with 225 patients per arm. The clinical trial simulations were comprised of the following steps. First, longitudinal C2 values conditional on the TDM regimen and dose-adjustment algorithms were simulated. Conditional on the simulated C2 values, the four clinical endpoints of interest were simulated. The proposed Phase 3 program consists of an active comparator arm of the standard-of-care agent tacrolimus. Therefore, for each simulated clinical trial in this analysis,

the tacrolimus BPAR rates were simulated. The TDM/dose-adjustment regimens that were evaluated in this investigation included three concentration-controlled regimens (for which the target concentration window and target duration in the window varied over time) and two hybrid regimens (which combined elements of concentration-controlled and fixed-dose regimens). For the concentration-controlled regimens, two dose selection algorithms were evaluated. The 'Simple' algorithm selects the dose using a simple decision-tree based on the most recent C2 value. The alternative was a novel Bayesian algorithm that maximizes the probability of placing the patient in the target concentration range based on the aggregate subject-specific C2 data. In total, there were 8 combinations of TDM regimen and dose adjustment algorithms.

TDM regimen type	TDM regimen name	Dose adjustment algorithms evaluated
Concentration-controlled	High exposure (HE)	'Simple' and Bayesian
	Low exposure (LE)	'Simple' and Bayesian
	Gradual decline	'Simple' and Bayesian
Hybrid (concentration-controlled to fixed dosing)	Hybrid high exposure	Bayesian
	Hybrid gradual decline	Bayesian

For the active comparator, the posterior predictive distribution for twelve-month BPAR rates was obtained by fitting a Beta-binomial model to the summary-level data from Ekberg [2], and an estimate of the between-study variability in twelve-month BPAR rates was obtained from a random effects meta-analysis model fit to data from five tacrolimus trials using regimens similar to those which are planned for the Phase 3 study [2–6].

All simulation was done in R, version 2.14.1. Uncertainty in the exposure–response models was incorporated using bootstrap distributions, which were generated using the metrumrg R package [7] and NONMEM version 7.2.0.

Results: In the assumed patient population, the expected twelve-month BPAR rates for tofacitinib ranged from 16.5 to 19.7 % across the 8 regimens/algorithms, as compared to 13.1 % for tacrolimus. The expected CMVD infection rates ranged from 1.6 to 5.9 %; the expected SI rates ranged from 28.4 to 31.4 %; and the expected PTLD rates ranged from 1.1 to 1.6 %. In general, regimens/algorithms with lower exposures had lower CMVD, SI and PTLD rates and higher twelve-month BPAR rates.

Comparing the dose adjustment algorithms, the Bayesian algorithm performed better than the Simple algorithm (Fig. 1). The Bayesian algorithm placed 10–20 % more patients in the target concentrations ranges, and the Simple algorithm placed 5–20 % more patients above the target concentration ranges, resulting in higher median C2 values.

Using a non-inferiority margin for a difference in twelve-month BPAR rates of 20 %, 6 of 8 regimens/algorithms have a probability of achieving non-inferiority, or probability of technical success (PTS) of greater than 80 %, with the concentration-controlled regimen that targeted the highest concentrations achieving ≈90 % PTS. However, the PTS drops considerably as the non-inferiority margin is decreased (Fig. 2).

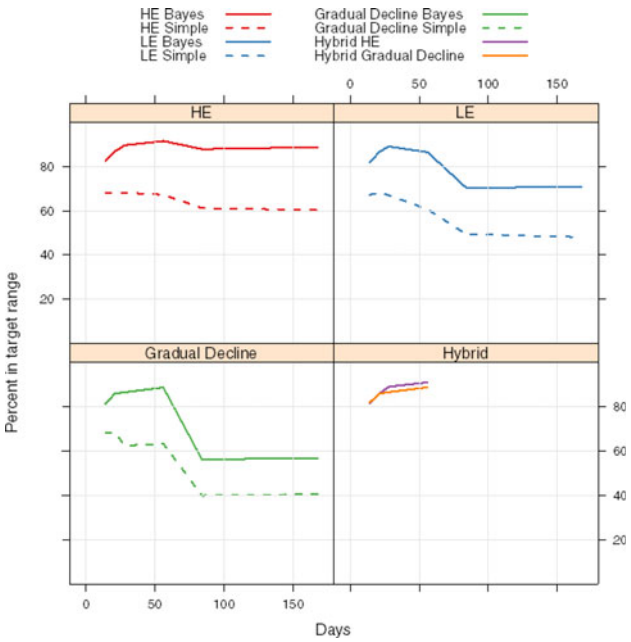

Fig. 1 Comparison of dose adjustment algorithms for placing patients in the target concentration range

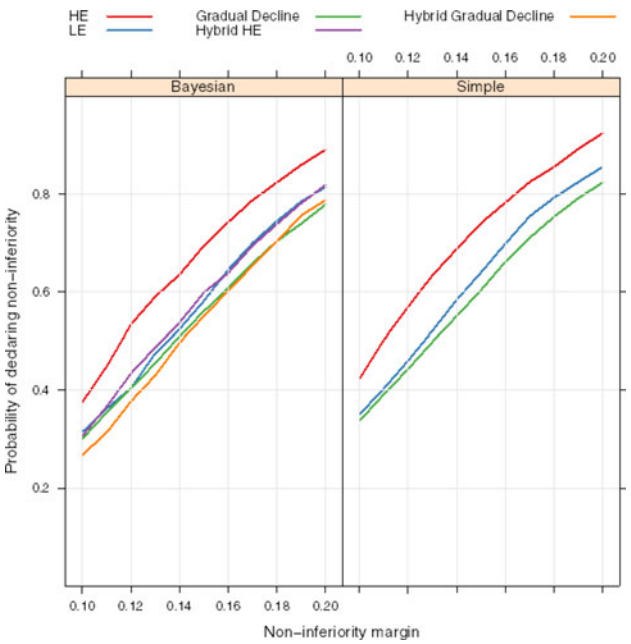

Fig. 2 Comparison of algorithms for probability of declaring non-inferiority

Conclusions: For the three concentration-controlled regimens, the majority of patients can be put into the target concentration ranges using either the Bayesian or Simple dose selection algorithm. However, in these simulations the Simple algorithm results in a larger fraction of patients above the target ranges than the Bayesian algorithm. These higher average exposures lead to corresponding higher infection rates and lower BPAR with the Simple algorithm. Further, use of real-world simulation scenarios and TDM/dose adjustment schedules has the potential to achieve improved outcomes in clinical trials.

References

[1] Krishnaswami S, Lamba M, Hutmacher MM, French J, Harnisch L, Meier-Kriesche U, Budde K, Cibrik DM, Weimar W, Cohney S, Chan G (2010) First application of exposure–response modeling to optimize clinical outcomes of tasocitinib (CP-690,550). In: Kidney transplant patients: preliminary results. P15.01, TTS Congress, New Immunosuppressive Agents, Vancouver

[2] Ekberg H, et al (2007) N Engl J Med 357:2562–2575

[3] Hernández D, et al (2007) Transplantation 84:706–2514

[4] Silva Jr., HT et al (2007) Am J Transplant 7:595–608

[5] Ciancio G, et al (2004) Transplantation 77:244–251

[6] Ciancio G, et al (2005) Transplantation 8:457–465

[7] Bergsma T, et al (2012) Metrumrg: pharmacometric tools for data preparation, modeling, simulation, and reporting. R package version 5.17. URL:http://CRAN.R-project.org/package=metrumrg

T-054 Preliminary Mechanistic Pharmacokinetic Model for the Quantitative Determination of Ropivacaine Systemic Absorption during Femoral Nerve Block in Anesthetized Rabbits

Fady Thomas[1,*], Pierre Drolet[2], France Varin[1]

[1]Faculté de pharmacie, Université de Montréal, Montréal, QC, Canada; [2]Département d'anesthésie et réanimation, Hôpital Maisonneuve-Rosemont, Montréal, QC, Canada

Objectives: Peripheral nerve block represents the best balance between analgesia and side effects as a choice of postoperative analgesic technique for major knee surgery [1]. Current recommendations on the use of local anesthetics (LA) do not take into account factors such as the varying local disposition at different sites of administration. To provide the most appropriate and safe peripheral nerve block, a characterization of local disposition is highly needed [2]. In order to thoroughly describe in a quantitative manner, the systemic absorption of LA during a femoral nerve block, we developed a mechanistic pharmacokinetic model in rabbits by simultaneously fitting unbound ropivacaine plasma and perineural concentrations.

Methods: A femoral nerve block guided by neurostimulation was performed under isoflurane anesthesia in seven New Zealand male rabbits. Adequate placement was confirmed when a motor response was elicited with a current less than 0.3 mA. A microdialysis probe was concomitantly implanted at the injection site (depot) and left to equilibrate [3]. Ropivacaine 0.5 % (6 mg in 4 min) was then injected. Dialysates and plasma samples were collected for up to 12 h and subsequently analyzed for ropivacaine concentration using a previously developed HPLC–UV method [4]. Unbound plasma and local concentration–time profiles were obtained and simultaneously fitted using NONMEM® (version VII). The absorption rate (k_{13}) estimated by our mechanistic model was compared with that obtained using Loo-Riegelman method, a deconvolution technique often used in clinical settings where local concentrations are ethically unobtainable. For this purpose, we used ropivacaine disposition parameters previously obtained after intravenous administration in three rabbits.

Results: After testing different pharmacokinetic models, the following mechanistic model was identified to best describe local and systemic unbound ropivacaine concentration–time data following a femoral nerve block.

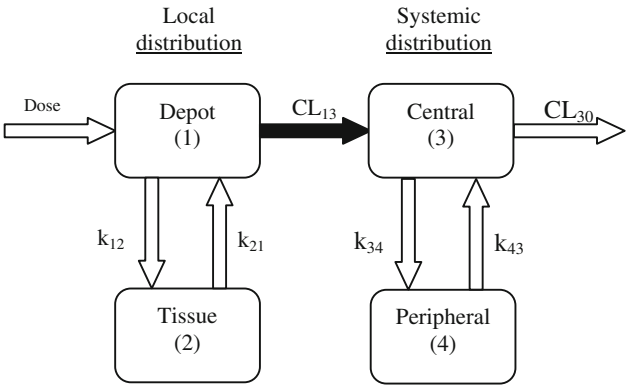

Table 1 Preliminary parameter estimates with interindividual variability (CV %) using the mechanistic pharmacokinetic model for local and systemic unbound ropivacaine concentrations after femoral nerve block with a dose of 6 mg during 4 min in anesthetized rabbits

Parameter	Unit	Estimate	(CV %)
k_{12}	min^{-1}	0.0288	(42.5)
k_{21}	min^{-1}	0.0077	(25.5)
CL_{13}	mL min^{-1}	0.0268	(17.5)
V_1	mL	0.996	(42.3)
CL_{30}	mL min^{-1}	101.3	(20.4)
V_3	mL	27100	(22.2)
k_{34}	min^{-1}	0.022	(47.4)
k_{43}	min^{-1}	0.0072	(41.9)
k_{13}	min^{-1}	0.027	–
k_{30}	min^{-1}	0.0037	–

CV % coefficient of variation of parameter estimates

It consisted essentially of two local compartments: deposit (1) and tissue (2) and two systemic compartments: central (3) and peripheral (4). Intercompartmental rate constants from tissue to depot compartment (k_{21}), from depot to the tissue compartment (k_{12}), from central to peripheral (k_{34}) and from peripheral to central compartment (k_{43}) were obtained. Parameters such as clearances from the depot (CL_{13}) and central (CL_{30}) compartments, and their respective volumes of distribution (V_1 and V_3) were also estimated. Preliminary parameter estimates with their interindividual variability are presented in Table 1. Systemic absorption ($k_{13} = CL_{13}/V_1$) and elimination ($k_{30} = CL_{30}/V_3$) first-order rate constants were calculated.

Deconvolution results indicate that only 60.5 % of the dose was absorbed after 12 h with a slow absorption rate constant of 0.004 min^{-1}. This value is almost tenfold slower than that estimated in our model ($k_{13} = 0.027$ min^{-1}) but not significantly different from that of k_{21} (0.0077 min^{-1}).

Conclusions: This study represents the first mechanistic pharmacokinetic model for LA after a peripheral nerve block. It suggests that the rate-limiting step for ropivacaine disposition after a femoral nerve block is the rate of release from the surrounding nerve tissues and not that of systemic absorption. This knowledge will provide support to the assumptions made during the development of a pharmacokinetic/

pharmacodynamic model that would predict LA analgesic effect in patients receiving a femoral nerve block.

References

[1] Fowler SJ, et al (2008) Br J Anaesth 100(2):154–164
[2] Rosenberg P, et al (2004) Reg Anesth Pain Med 29(6):564–575
[3] Thomas F, et al (2011) Vet Anaesth Analg 38(6):576–579
[4] Gaudreault F, et al (2009) Ther Drug Mon 31(6):753–757

W-001 Simulation Study of a Sildenafil Survival Trial in Adults with Pulmonary Arterial Hypertension (PAH) Using a Time Varying Hazard Model to Characterize the Exposure–Response Observed in Children

Pascal Chanu[1], Xiang Gao[2], Rene Bruno[1], Laurent Claret[1], Lutz Harnisch[3,*]

[1]Pharsight Consulting Services™, A division of Certara™, St. Louis, MO, USA; [2]Pfizer, Clinical Pharmacology, Groton, CT, USA; [3]Pfizer, Pharmacometrics, Global Clinical Pharmacology, Sandwich, UK

Objectives: Sildenafil (REVATIO®), 20 mg TID, received approval for the treatment of adult PAH in US and Europe. A pediatric study had been performed in patients (1–17 years) [1] and sildenafil (REVATIO®) was subsequently approved in Europe for the treatment of pediatric PAH, with a dose regimen of 10 mg for children ≤20 kg body weight, and 20 mg for children above 20 kg. The long-term extension of the pediatric study revealed very good overall survival results with 84 % of patients still alive after 4 years of treatment. However, an increase in mortality with higher doses was also observed [2]. The objectives of this analysis were to adequately characterize the exposure-mortality relationship by accounting for longitudinal changes of potential covariates on mortality and to utilize the resulting model to assess the design of a mortality trial in adults for its interpretability [3].
Methods: During the extension of the pediatric trial ($n = 234$, 1–17 years), patients were randomized to a Low, Medium or High dose group with nominal doses ranging from 10 to 80 mg depending on patients body weight, with dose adjustments according to body weight changes. A survival analysis using a time varying hazard model was performed in NONMEM7 to characterize the relationship between survival, etiology, and baseline or time varying covariates, body weight and WHO functional class, and drug exposure. Clinical trial simulations were performed in R to assess a survival trial in adults using three dose levels, 5/20/80 mg TID, to quantify the impact of confounding factors such as add-on therapy on its readout.
Results: Survival in pediatrics was found to be mainly impacted by etiology in addition to sildenafil exposure: a hazard ratio of about 2 was estimated for primary versus secondary PAH patients at the same exposure level. The higher mortality with higher doses was adequately described using average steady state concentration as a time varying variable which integrated sildenafil clearance and dose, and body weight changes over time. Simulations revealed, that if the exposure-mortality response observed in children would apply to adults, the risk of wrongly concluding non-inferiority of 80 mg versus 5 mg is predicted to be very low. But this risk could significantly increase if the trial conduct is impacted by longitudinally confounding factors especially their combination.
Conclusions: The adequate characterization of survival drivers made it possible to assess the outcome of a non-inferiority survival trial in adults and the potential impact of external confounding factors during the study conduct. This work contributes to the design of an adult mortality trial and the assessment of its interpretability.

References

[1] Barst R, et al (2012) A randomized, double-blind, placebo-controlled, dose-ranging study of oral sildenafil citrate in treatment-naive children with pulmonary arterial hypertension, Circulation 125(2):324–334
[2] FDA sildenafil REVATIO® drug label. http://www.accessdata.fda.gov/drugsatfda_docs/label/2012/203109s000lbl.pdf
[3] FDA Drug Safety Communication. Aug 30th, 2012. http://www.fda.gov/Drugs/DrugSafety/ucm317123.htm

W-002 Population Pharmacokinetic Modeling of a Novel Delayed-Release Formulation of Metformin (MetDR)

Adekemi Taylor[1,*], Emmanuel Chigutsa[1,2], Jonathan Monteleone[1], Mark Fineman[3]

[1]Pharsight, a Certara company, St. Louis, MO, USA;
[2]University of Cape Town, Cape Town, South Africa;
[3]Elcelyx Therapeutics, Inc., San Diego, CA, USA

Objectives: EFB0027 (MetDR; Elcelyx Therapeutics, Inc., San Diego, CA) is a delayed-release (DR) metformin tablet formulated to target delivery of metformin to the lower gut to promote incretin-like effects while decreasing systemic exposure. MetDR has been demonstrated in Phase I studies to provide similar glucose reduction to metformin immediate-release (MetIR), despite lower metformin exposures. The decreased systemic exposure of metformin should reduce accumulation, resulting in improved safety, especially in subjects with declining renal function, while maintaining efficacy. Thus, this formulation may overcome current contraindications and tolerability issues with approved formulations of metformin in type II diabetes mellitus (T2DM) patients. The objective of this analysis was to characterize the pharmacokinetics of MetDR and compare the absorption and bioavailability to MetIR.
Methods: Data from a four-period randomized cross-over Phase I study in 21 middle-aged and elderly male and female T2DM patients with normal renal function were used to construct a dataset for population pharmacokinetic (popPK) modeling. In each period, MetIR and/or MetDR was administered with food for 5 days according to one of the following treatments: (A) 2000 mg MetIR daily given as 1000 mg twice daily (BID), (B) 2000 mg MetDR daily given as 1000 mg BID, (C) 1000 mg MetDR daily given as 500 mg BID, or (D) 1000 mg MetIR + 2000 mg MetDR daily given as 500 mg BID MetIR + 1000 mg BID MetDR. Plasma samples were collected on Day 4 immediately prior to and 120 min after the evening (PM) dose and on Day 5 immediately prior to and up to 11 h after the morning (AM) dose. Data from Treatments A, B, and C were used for modeling. NONMEM® (version 7.2.0) with the FOCE-I estimation method was used to develop the popPK model. Selection of the final metformin model was based on goodness-of-fit plots, the minimum value of the objective function as a statistical evaluator, and parameter estimate precision as measured by the percent relative standard error (%RSE). To assess the predictive ability of the popPK model, a visual predictive check (VPC) was done. Model- and non-compartmental analysis- (NCA) derived areas under the concentration–time curves from the time of dosing to the time of the last quantifiable concentration ($AUC_{0\text{-}t}$) were also compared.

Results: A one-compartment model with linear elimination characterized the disposition of both metformin formulations. MetIR was well described by a first-order absorption model with no lag time. To describe the complex concentration–time profiles following MetDR administration, a number of different absorption models were investigated for MetDR that explored first-order and saturable absorption, time-of-dose and dose dependent bioavailability, and circadian variations in the absorption process. MetDR absorption was best described by a model with saturable absorption, with a maximum absorption rate that follows a circadian rhythm, an absorption lag time, and a bioavailability relative to 1000 mg BID MetIR (F_{rel}) that is dependent on dose and time of dose administration (AM vs. PM). Between-subject variability was identified on CL/F and on the amount of drug at the absorption site at which the absorption rate is half-maximal. Between-occasion variability was identified on the circadian rhythm phase shift for MetDR and the bioavailabilities of MetIR and MetDR. A proportional residual error model was applied. Most fixed effect parameters were well estimated, as was the residual error. F_{rel} of 500 mg BID and 1000 mg BID MetDR following the AM dose were estimated as 82.0 % (20 % RSE) and 56.6 % (14 % RSE), respectively. MetDR bioavailability was predicted to be higher following the PM dose than the AM dose, although additional sampling at night will be required to accurately quantitate the difference. The lag time for MetDR absorption was estimated to be 3.86 h (0.8 % RSE). The model was also able to adequately capture concentration–time profiles following administration of MetIR and both doses of MetDR. VPC results also indicated good model performance for the different treatments. The model-derived $AUC_{0\text{-}t}$ values corresponded well to those calculated by NCA.
Conclusions: A popPK model was developed that described the absorption and disposition of IR and DR metformin formulations, capturing the unique absorption properties of the MetDR formulation. The results are consistent with saturable absorption of metformin [1] and current understanding of gastrointestinal function associated with circadian rhythms [2]. This popPK model will be updated as more data become available and will serve as a framework for performing simulations to understand metformin accumulation in T2DM patients in order to determine safe and effective doses of MetDR.

References

[1] Sambol NC, Chiang J, O'Conner M, Liu CY, Lin ET, Goodman AM, Benet LZ, Haram JH (1996) Pharmacokinetics and pharmacodynamics of metformin in healthy subjects and patients with noninsulin-dependent diabetes mellitus. J Clin Pharmacol 36(11):1012–1021

[2] Konturek PC, Brzozowski T, Konturek SJ (2011) Gut clock: implication of circadian rhythms in the gastointestinal tract. J Physiol Pharmacol 62(2):139–150

W-003 A Physiologically Based Pharmacokinetic-Pharmacodynamic Model to Quantify Uricosuric Activity in the Isolated Perfused Rat Kidney

Yogesh T. Patel[1,*], Kevin R. Sweeney[2], David R. Taft[1]

[1]Long Island University, Brooklyn, NY, USA; [2]Pfizer Inc., Groton, CT, USA

Objectives: Although preclinical evaluation of uricosuric agents is limited due to presence of uricase enzyme in small animals, the isolated perfused rat kidney model (IPRK) is a potentially useful tool to evaluate the disposition and activity of novel uricosuric compounds. The objectives of this research are: (1) To develop a PBPK model for uric acid disposition in the IPRK. This PBPK model was used to predict baseline uric acid excretion for evaluation of uricosuric activity of the test compound. (2) To develop a PBPK-PD model to characterize the renal disposition and uricosuric effect of test compound in the IPRK. The test compound is a novel chemical entity with demonstrated high affinity for the rat URAT1 transporter. The compound also exhibits relatively high protein binding.
Methods: IPRK experiments were conducted using male Sprague–Dawley rats (250–350 g). Baseline uric acid excretion data were obtained over a range of initial uric acid concentrations (1–7 mg/dL). Uricosuric activity was evaluated at two different concentrations of test compound (50 and 100 μg/mL), at 1 mg/dL uric acid concentration. In order to increase filtration fraction of the compound, experiments were performed at low perfusate albumin level (0.25 % W/V). Urine samples were collected for 10 min interval with perfusate sample withdrawn at midpoint. Drug and uric acid concentrations in perfusate and urine samples were analyzed using HPLC. GFR was determined as inulin clearance. As shown in Figs. 1 and 2, PBPK models for baseline uric acid excretion (Fig. 1) and uricosuric activity (PBPK-PD model, Fig. 2) were developed through modification of a published model [1]. Performance of PBPK model to predict baseline uric acid excretion in the IPRK was evaluated by simulating 1000 replicates of data set (result not shown). Population PK-PD analysis was performed by NONMEM VII using FOCE-I method. Goodness of fit was assessed by visual inspection of diagnostic plots, uniform distribution of random errors, standard errors of parameter estimates and parameter plausibility.
Results: Viability of kidney preparations was monitored throughout experiments and found acceptable for all IPRK experiments though performed at low perfusate albumin level. %FEUA (percentage of

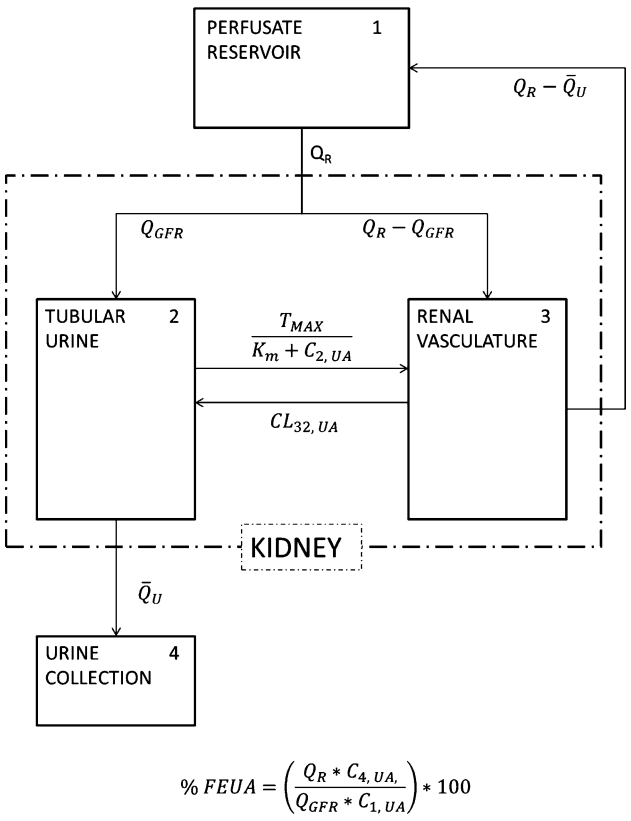

Fig. 1 PBPK model for uric acid disposition in the IPRK

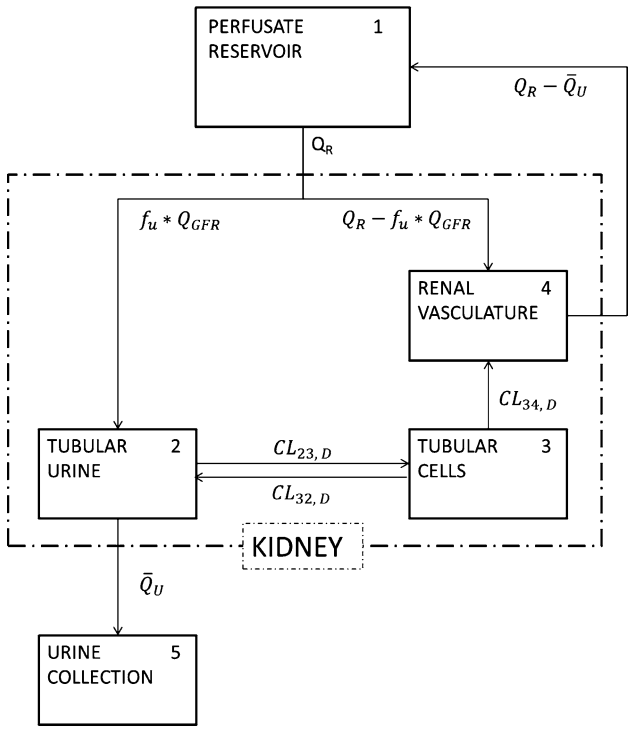

Fig. 2 PBPK-PD model for disposition and uricosuric activity of test compound in the IPRK

filtered uric acid excreted in urine) was directly related to uric acid reabsorption, and the parameter was used as a biomarker to quantify uricosuric activity of test compound. %FEUA was found to increase with perfusate uric acid concentration, and this nonlinear behavior of uric acid excretion was best described by incorporating Michaelis–Menten kinetics for URAT1-mediated uric acid reabsorption into the model (Fig. 1). Due to the absence of experimental data at higher uric acid concentrations that could achieve maximum reabsorption capacity (i.e., saturation), maximum transport rate (T_{MAX}) for uric acid could not be estimated, and its value was fixed at 110 μg/mL based on best-fitting of data observed in diagnostic plots. The PBPK model for uric acid disposition in the IPRK fitted individual profiles well (Fig. 3). Final population estimates of K_M, $CL_{32,UA}$, $V_{1,UA}$ and $V_{2,UA}$ for the model were 505 μg/mL, 0.228 mL/min, 83.1 mL and 0.639 mL, respectively. Interindividual variance implemented on T_{MAX} and $V_{1,UA}$ were estimated as 18.3 and 11.0 %. The model-generated estimate of K_M was higher compared to the value obtained in vitro using membrane vesicles ($K_M \sim 190$ μg/mL) [2]. The PBPK model for uric acid disposition was used to predict baseline %FEUA in perfusion experiments evaluating uricosuric activity of test compound. Activity was quantified as an increase in %FEUA from predicted baseline, and correlated with concentration of test compound in the tubular urine using an E_{max} model (Fig. 2). Concentrations of test compound as well as uricosuric effect were well characterized by the proposed PBPK-PD model (Fig. 4). Final population estimates of $CL_{23,D}$, $CL_{32,D}$, $CL_{34,D}$, $V_{1,D}$, E_{max} and EC_{50} for the test compound were 6.24 mL/min, 0.0751 mL/min, 0.0169 mL/min, 76.2 mL, 22.8 and 16.6 μg/mL, respectively whereas interindividual variance on $CL_{23,D}$ was estimated to be 36.3 %. Relative standard errors for all parameters estimates ranged from 1.9 to 80 %.

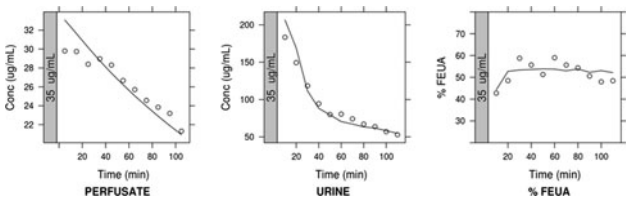

Fig. 3 PBPK model for uric acid disposition in the IPRK: Observations and individual predictions of perfusate concentration, urine concentration and %FEUA versus time for a representative perfusion experiment (*solid line*, predicted PK profile; *open circles*, observed data)

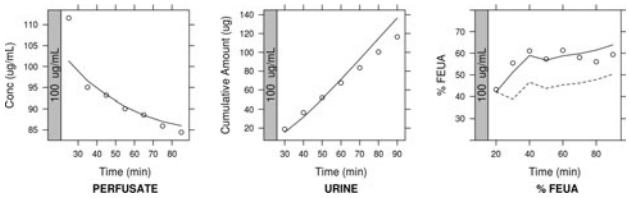

Fig. 4 PBPK-PD model for disposition and uricosuric effect of test compound in the IPRK: Observations and individual predications of perfusate concentration, cumulative amount excreted in urine and FEUA versus time for a representative perfusion experiments (*dotted line*, baseline %FEUA predicted from PBPK model; *solid line*, predicted PK and PD profile for test compound; *open circles*, observed data)

Conclusions: The PBPK model for uric acid disposition developed in this research successfully predicts baseline uric acid excretion in the IPRK model. Likewise, the PBPK-PD model allowed for precise characterization of the disposition of test compound and its uricosuric activity in the system. However, caution must be used when extrapolating these results in humans, as species differences in URAT1 transporter activity may prevent successful correlation to the clinical setting.

References

[1] Hekman P, van Ginneken CA (1982) J Pharmacokinet Biopharm 10:77–92

[2] Sato M, et al (2010) Biochim Biophys Acta 1808:1441–1447

W-004 AODware: A Model-based Application for Optimal and Adaptive Optimal Experimental Design Exploration

Mattia Veronese[1], Stefano Zamuner[2,*], Andrea Loreggia[3], Alessandra Bertoldo[4]

[1]Department of Neuroimaging, Institute of Psychiatric, King's College London, London, UK; [2]Clin. Pharm. Modelling and Simulation, GlaxoSmithKline, Stockley Park, UK; [3]Department of Mathematics, University of Padova, Padova, Italy; [4]Department of Information Enginering, University of Padova, Padova, Italy.

Objectives: Optimal experimental designs have been successfully applied to increase the efficiency and minimize cost of PK/PD clinical trials by optimizing dose allocation and sampling schedules [1, 2].

These techniques rely on the maximization of the information content which can be extract from a particular experiment, allowing to improve precision and accuracy of parameter estimates.
Typical optimal design (OD) algorithms use the model description of the investigated system to set the experimental variables by minimizing the estimation error of model parameter estimates [3]. However, OD requires detailed information about the model of the investigated system and reliable prior values for its parameters.

On the contrary, Adaptive optimal designs (AOD) have been proposed for the sequentially optimization of the design in population studies [4, 5]. These are sub-optimal approaches which combine the information gathered from previous experiments with model-based prediction of the investigated system. Differently from OD, AOD allows to refine the choice of experimental variables while the experiment is still running. This approach could provide greater robustness in the presence of prior parameter misspecifications compared to OD. On the other hand, change of experimental design may represent a cost and it cannot be always performed. Thus, the type of experimental design strategy to be used should be evaluated case by case, considering all the experimental constraints of the system.

In this work we present AODware, an integrated package for experimental design evaluation via model-based simulations.
Methods: *The software*. AODware consists of three independent functional blocks: simulation, estimation and optimization (Fig. 1). The *simulation block* generates simulated data based on a particular model of system, including population parameter values (fixed and random effects), measurement error variance and experimental setting considered by the user. From simulated data, the *estimation block* provides the corresponding nonlinear mixed effect model estimates. The estimates are computed automatically using NONMEM [6]. The *optimization block* provides optimal doses and sample times given a certain model and a set of parameter priors. The optimization block is based on the POPED package [7] a software tool specifically developed for optimal design in population kinetics. The integration of these elements allows the user to easily quantify and to compare the performance of different experimental designs. AODware has been designed with particular attention to some structural elements: (1) a multi-level architecture, (2) the presence of expandable libraries and (3) the use of external software automatically driven by the program. This choice was done to maximize the robustness and efficacy of the program.
The simulation studies. We applied AODware in three cases of interest: oral dosing of Cadralazina [8], oral dosing of Theophylline [9], and receptor occupancy PET studies [5]. For each case different experimental designs (optimal and adaptive optimal) were tested and the estimates of population PK/PD model parameters were compared with the corresponded true values. Prior parameter misspecification was considered to evaluate the robustness of AOD performance respect to OD. Parameter %biases and RMSE error were used as performance indexes.
Results: The presence of a unique environment for both data simulation and parameter estimation has allowed AODware to easily compare the performances of different experimental design algorithms (adaptive and non-adaptive) in different PKPD contexts, by providing a direct indication about the advantages of a specific experimental design respect to others. In the Cadralizina case, for example, the application of optimal design with uncorrected hypothesis about the drug kinetic demonstrated to be almost comparable to the optimal non-misspecified design (Fig. 2), with the only exception of the distribution volume which resulted significantly biased. In the case of PET receptor binding model, instead, AODware showed the possibility to use adaptive optimization to recover from the application of an initial uninformative dose (Fig. 3). This use of AODware allows also to perform a sensitivity

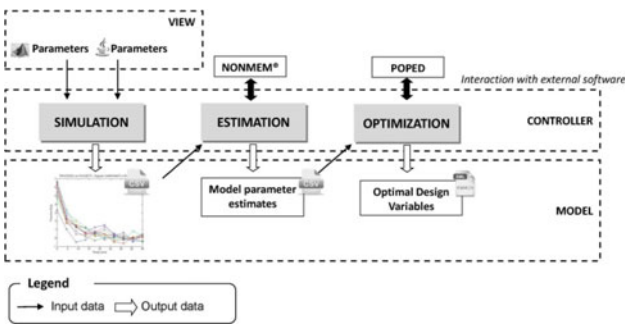

Fig. 1 AODware hierarchical organization. The scheme shows the organization of the functional blocks and the data flow adopted in the program. The program architecture follows the model-view-controller design pattern

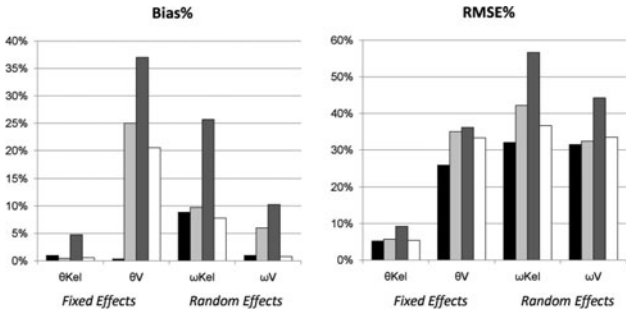

Fig. 2 Comparison between optimal and adaptive optimal designs in Cadralazine. Bias % and RMSE % are reported for all the population parameters and all the tested designs. Kel and V indicate respectively Caladrazine drug elimination and distribution volume. Black bars refer to OD applied without misspecification (D-optimality criteria); *light-gray bars* refer to OD applied with misspecification (+150 % per parameter); *dark-gray* and *white bars* indicate AOD results respectively after first and second iteration, starting with a misspecified hypothesis

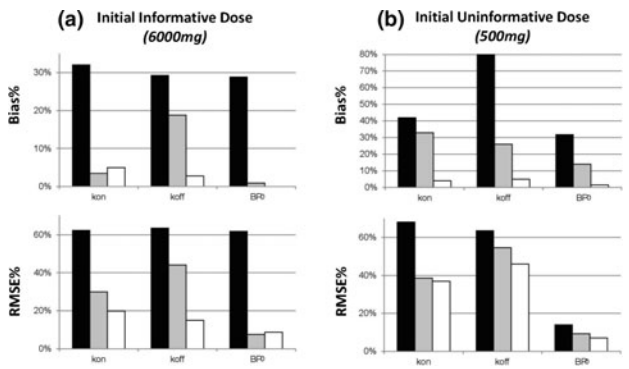

Fig. 3 AOD in receptor occupancy PET studies. Bias % and RMSE % are evaluated after 3 following iterations of the algorithm (*black*, *gray* and *white bars* respectively). Optimization was performed over both time sampling and administered drug dose. **a** The results obtained with initial informative dose. **b** The results achieved starting with uninformative dose. The same initial time setting was applied to both scenarios. In both cases, independently from the starting conditions, adaptive optimization produced a significant decrease of estimate precision and accuracy

analysis, by quantifying the variability of precision and accuracy of model parameter estimates to a particular experimental variable.

Conclusions: AODware represents an integrated solution for experimental design evaluation, generally applicable to a wide range of PKPD studies. The use of simulations and subsequent estimations allows evaluating the effects of experimental variables (i.e., doses, number of subjects, sampling time, …) on the model parameter estimation. Moreover, it offers the possibility to evaluate the impact that biased initial parameter assumptions have on the experiment definition. In light of these results, AODware may represent a useful tool to guide the experiment settings in PKPD studies.

References

[1] Mentrè F, Mallet A, Baccar D (1997) Optimal design in random-effects regression models. Biometrika

[2] Duffull SB, Mentre F, Aarons L (2001) Optimal design of a population pharmacodynamic experiment for ivabradine. Pharm Res

[3] Hooker AC, Foracchia M, Dodds MG, Vicini P (2003) An evaluation of population D-optimal designs via pharmacokinetic simulations. Ann Biomed Eng

[4] Ogungbenro K, Dokoumetzidis A, Aarons L (2009) Application of optimal design methodologies in clinical pharmacology experiments. Pharm Stat

[5] Zamuner S, Di Iorio VL, Nyberg J, Gunn RN, Cunningham FJ, Gomeni R, Hooker AC. Adaptive-optimal design in PET occupancy studies. Clin Pharmacol Ther

[6] Beal S, Sheiner LB (1998) NONMEM User Guides, Nonmem Project Group

[7] Foracchia M, Hooker AC, Vicini P, Ruggeri A (2004) POPED, a software for optimal experiment design in population kinetics. Comput Methods Prog Biomed

[8] Haglund K, Dahlqvist R, Emilsson H, Englund G (1998) Cadralazine pharmacokinetics: a pilot study. Eur J Clin Pharmacol

[9] Beal S, Sheiner L (1992) NONMEM's User's Guide, Technical Report. University of California, San Francisco

W-005 Predicting Combinatorial Efficacy of Rituximab and Doxorubicin in Non-Hodgkin Lymphoma Xenografts

Xiaochen Zhao[1,*], John M. Harrold[1], Leonid Kagan[1], Robert M. Straubinger[1,2], and Donald E. Mager[1]

[1]Department of Pharmaceutical Sciences, University at Buffalo, State University of New York, Buffalo, NY, USA; [2]New York State Center of Excellence in Bioinformatics and Life Sciences, 701 Ellicott St., Buffalo, NY, USA

Objectives: Non-Hodgkin's lymphoma (NHL) is a B cell neoplasm and the most common hematological cancer in adults. Rituximab, a CD20-targeting monoclonal antibody, induces death of B cells through immune-mediated effector functions, direct effects on tumor cells, and sensitization to chemotherapy [1, 2]. One possible mechanism of cellular sensitization to cytotoxic drugs by rituximab is the inhibition of the NFκB pathway with subsequent downregulation of the mitochondrial anti-apoptotic protein Bcl-xL as shown in Ramos cells [3]. Although rituximab-based therapies are standard treatment for NHL, design of combination regimens remains empirical. An integrated systems pharmacodynamic model, linking molecular mechanisms of rituximab action to tumor responses, has been developed to predict synergistic antitumor effects of rituximab administered with fenretinide or rhApo2L in NHL xenografts [4]. Such an approach might facilitate the design and optimization of new combination regimens. This study aims to assess the predictive performance of this model for a second rituximab-based chemotherapy in a xenograft system of NHL.

Methods: Our prior model [4] was modified to predict the combinatorial efficacy of rituximab and doxorubicin in Ramos lymphoma xenografts in mice. Pharmacokinetics of rituximab and doxorubicin drive the subsequent pharmacodynamics. Binding of rituximab to CD20 on the cell surface triggers tumor growth inhibition, direct apoptosis, and intracellular signal transduction. The cytotoxic effect of doxorubicin is sensitized through modified signaling when used in combination with rituximab (Fig. 1). Parameters associated with single-drug disposition and efficacy were identified separately from literature sources and a pilot study, and the system-specific parameter, natural tumor growth, was determined from a control group in this xenograft study. Ramos human B lymphoma cells were injected subcutaneously into severe combined immunodeficiency (SCID) mice. Once tumors were palpable, three groups of mice received rituximab (once dose weekly), doxorubicin (three doses weekly), or their combination. Tumor volumes were monitored over time, and four tumor samples from each treatment group were excised at the end of the experiment for biomarker measurement. Expression of anti-apoptotic protein Bcl-xL was quantified by western blot, and the relative changes of Bcl-xL/β-actin levels in treated tumors were compared with the controls. Unperturbed tumor growth was estimated from fitting control tumor volume profiles in ADAPT 5. Simulations were performed in Berkeley Madonna to predict preclinical combinatorial efficacy of rituximab and doxorubicin on Ramos cell tumor progression.

Results: Mice treated with doxorubicin alone showed minimal tumor inhibition at the 2nd week of therapy. Rituximab alone produced a moderate tumor growth delay that was significantly greater than control and doxorubicin treatment groups on the last day. Inhibition of tumor progression by combination therapy was detectable in the 1st week of treatment, and was significantly more effective during the 2nd week. A two-way ANOVA revealed a significant effect of treatment ($p < 0.01$) and time ($p < 0.01$), with no significant interaction between treatment and time variables. Tumor growth in the control group was well described by a linear function with a zero-

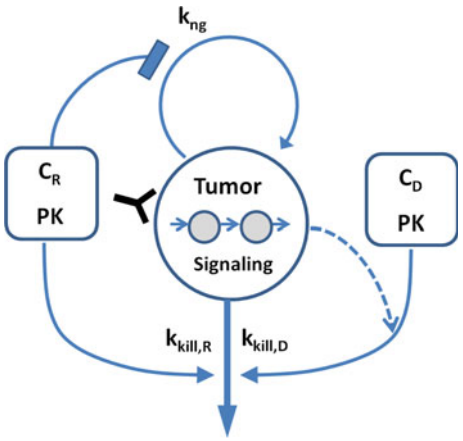

Fig. 1 Schematic of PK/PD model describing combination therapy with rituximab and doxorubicin in mice bearing Ramos B cell lymphoma xenografts

order growth rate constant of 11.2 mm^3 h^{-1} (CV % = 5.16 %). Only unperturbed tumor growth was estimated, and the integrated systems pharmacodynamic model accurately described tumor growth kinetics in all treatment groups. In addition, tumor biomarker expression (Bcl-xL) was slightly decreased after two-weeks of treatment with rituximab alone, which agreed well with model prediction. Tumors treated with doxorubicin alone also exhibited a minor decrease in Bcl-xL, whereas the combination was associated with statistically significant Bcl-xL inhibition that correlated well with in vivo antitumor efficacy. **Conclusions:** A systems pharmacodynamic model of rituximab combination treatment of NHL was extended to capture the enhanced efficacy with a second cytotoxic drug (doxorubicin), thereby expanding model conditions and supporting its use for exploring novel rituximab-based combination regimens in NHL.

References

[1] Bezombes C, Fournie JJ, Laurent G (2011) Direct effect of rituximab in B cell-derived lymphoid neoplasias: mechanism, regulation, and perspectives. Mol Cancer Res 9(11):1435–1442

[2] Smith MR (2003) Rituximab (monoclonal anti-CD20 antibody): mechanisms of action and resistance. Oncogene 22(47): 7359–7368

[3] Jazirehi AR, et al (2003) Rituximab (anti-CD20) selectively modifies Bcl-xL and apoptosis protease activating factor-1 (Apaf-1) expression and sensitizes human non-Hodgkin's lymphoma B cell lines to paclitaxel-induced apoptosis. Mol Cancer Ther 2(11):1183–1193

[4] Harrold JM, Straubinger RM, Mager DE (2012) Combinatorial chemotherapeutic efficacy in non-Hodgkin lymphoma can be predicted by a signaling model of CD20 pharmacodynamics. Cancer Res 72(7):1632–1641

W-006 Semi-mechanistic Multiple-analyte Population Model of Antibody-drug-conjugate Pharmacokinetics

Dan Lu[1,*], Chee Ng[2,3], Priya Agarwal[1], Sandhya Girish[1], Dongwei Li[1], Saileta Prabhu[1], Denise Nazzal[1], Ola Saad[1], Randy Dere[1], Neelima Koppada[1], Jin Yan Jin[1]

[1]Genentech, South San Francisco, CA, USA; [2]Children Hospital of Philadelphia, Philadelphia, PA, USA; [3]School of Medicine, University of Pennsylvania, Philadelphia, PA, USA

Objectives: Monomethyl auristatin E (MMAE) containing antibody–drug-conjugates (ADCs) are being developed in patients for treating various types of cancers. ADCs are complex mixtures, therefore their pharmacokinetics are assessed by evaluating multiple analytes including total antibody (TAB), antibody-conjugated MMAE (acMMAE) and unconjugated MMAE after dosing. Both TAB and acMMAE concentrations represent mixtures of various drug-to-antibody ratio (DAR) species. The objective of this analysis is to develop a semi-mechanistic multiple-analyte population model to better understand the major pathways of ADC elimination and unconjugated MMAE formation after ADC administration. The pharmacokinetic (PK) and toxicokinetic (TK) data in cynomolgous monkeys were used for this analysis.

Methods: The PK data of multiple analytes for anti-CD79b ADC was quantified at single dose of 0.3, 1, 3 mg/kg in PK study and 1, 3, 5 mg/kg every-three-week for 4 doses in a TK study in cynomolgous monkeys. The PK data of MMAE after intravenous administration of unconjugated MMAE at single dose of 0.03 and 0.063 mg/kg were also obtained in monkeys from a separate study. The data from these 3 studies were used for modeling. Multiple semi-mechanistic integrated models were explored to describe the PK of TAB, acMMAE and unconjugated MMAE simultaneously. Parallel hybrid ITS-MCPEM estimation algorithm was used for parameter estimation in S-ADAPT 1.57. The observed below quantification limit data were modeled using M3 method. The best model was chosen based on log likelihood ratio test or Schwarz criterion.

Results: ADC elimination clearance pathways are comprised of both deconjugation and proteolytic degradation pathways (Fig. 1). A multiple-compartment PK model which assumes a sequential deconjugation from high DAR species to low DAR species adequately described the PK data of TAB and acMMAE. A Weibull model was found to best describe the deconjugation rate constant change with the DAR. The proteolytic degradation clearance is modeled with Michaelis–Menton kinetics. The unconjugated MMAE exposure in plasma is mainly contributed by the FcRn and target-mediated proteolytic degradation pathway but not the deconjugation pathway. The fraction of conversion from the proteolytic degradation pathway to form the unconjugated MMAE is estimated to be ~66 % by the model, while the fraction of conversion from the deconjugation pathway is only ~2 %.

Conclusions: The final integrated model well described the observed TAB, acMMAE and unconjugated MMAE PK data in cynomolgous monkeys. The best model structure suggested that the ADC is eliminated via both the deconjugation pathway and the FcRn and target-

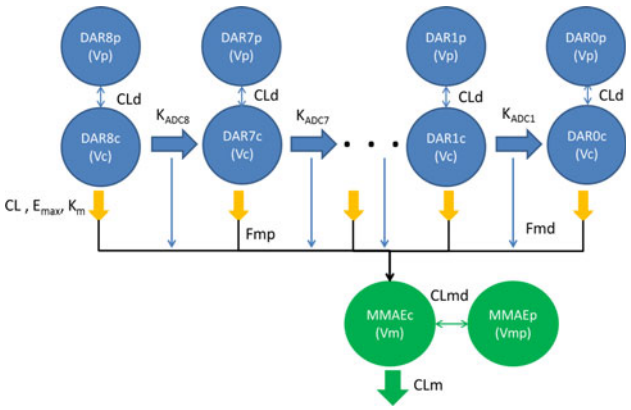

Fig. 1 Final model structure of semi-mechanistic multiple-analyte population model for MMAE containing ADCs. DAR8c, DAR7c, …, DAR1c, DAR0c: concentrations of anti-CD79b ADC in the central compartment with DAR = 0–8. DAR8p, DAR7p, …, DAR1p, DAR0p: concentrations of anti-CD79b ADC in the peripheral compartment with DAR = 0–8. MMAEc: concentration of unconjugated MMAE in the central compartment. MMAEp: concentration of unconjugated MMAE in the peripheral compartment. K_{ADC8}, K_{ADC7}, …, K_{ADC1}: deconjugation rate constants for each DAR species (DAR = 8, 7, …, 1) of the ADC. Vc: central volume of distribution for ADC; Vp: peripheral volume of distribution for ADC; Vm: central volume of distribution for unconjugated MMAE; Vmp: peripheral volume of distribution for unconjugated MMAE; CL: non-specific proteolytic degradation clearance of ADC; E_{max}: maximal target-mediated proteolytic degradation rate of ADC; Km: concentration of ADC to reach half of the maximal E_{max}; CLd: distributional clearance of ADC; Fmpp: fraction of formation to unconjugated MMAE in the central compartment from the proteolytic degradation pathway of ADC (mediated by FcRn and targets); Fmd: fraction of formation to unconjugated MMAE in the central compartment from the deconjugation pathway of ADC; CLmd: distributional clearance of unconjugated MMAE; CLm: systemic clearance of unconjugated MMAE from the central compartment

mediated proteolytic degradation pathway. However, the unconjugated MMAE is formed mainly via the degradation pathway. This finding suggested that the unconjugated MMAE level generated after ADC dosing might be modulated by modifying the binding affinity of the ADC to FcRn and/or target and consequently the rate of FcRn and/or target-mediated proteolytic degradation.

W-007 Model-Based Meta-Analysis for Time Courses of Percent Responders in Diabetic Peripheral Neuropathy, Postherpetic Neuralgia and Fibromyalgia Pain Trials

Chih-Wei Lin*, Wei Liu, Walid Awni, Sandeep Dutta

Clinical Pharmacology and Pharmacometrics, AbbVie, North Chicago, IL, 60064, USA

Objectives: The objective of this work was to characterize the time courses of percent responders and relative efficacy of medications evaluated in clinical trials for neuropathic pain including diabetic peripheral neuropathy (DPN), postherpetic neuralgia (PHN) and fibromyalgia (FM) using a model-based meta-analysis (MBMA).

Methods A database was developed by a systemic search for all publicly available efficacy and safety information on drugs evaluated for treatment of neuropathic pain including DPN, PHN or FM. The initial database included summary-level efficacy and safety data for 82 trials. Based on efficacy endpoints, imputation methods and medications of interest, the final analyzed data contained $\sim$13000 subjects within 31 trials with 4 medications approved by FDA for treating neuropathic pain: duloxetine, pregabalin, gabapentin, and milnacipran. A MBMA was conducted to describe the time courses of the 30 or 50 % pain reduction responder rate over the treatment period and the dose–response relationship for the drugs used in the trials. The effect of using baseline observation carried forward (BOCF) or last observation carried forward (LOCF) imputation on responder rates was also evaluated.

In the final model the number of responders was described by a binomial distribution. The responder rates for different times and doses were described by a function combined an inverse logit E_{max} mixed function to characterize the dose–response relationships, and a cumulative exponential function to describe the time course of the responder rate for each indication.

$$N_{responder}(t,d) \sim \text{binomial}\left(P_{\%Responder}(t,d), N(t,d)\right)$$

$$P_{\%Responder}(t,d) = \text{logit}^{-1}\left(E_{0,endpt} + \eta_{trial} + I_{LOCF} + \frac{(E_{max}\cdot d)}{d + \exp\left(LNED_{50,drug}\right)}\right)\cdot\left(1-\exp(-k\cdot t)\right)$$

where the probability of binomial distribution is described by $P_{\%responder}(t, d)$, where t represents time and d represents dose. $P_{\%responder}(t, d)$ is described as a product of an inverse logit E_{max} function and a cumulative exponential function. $E_{0,endpt}$ is placebo response for 3 or 50 % responder rate in the logit domain. η_{trial} is random effect to account for between trial variability in the placebo response. I_{LOCF} is the effect of LOCF imputation over BOCF. The drug effect was described by a E_{max} function, where E_{max} is the maximum pain reduction effect and $ED_{50,drug}$ is the dose to achieve 50 % maximum response. *k* is the rate constant for the accumulation of pain reduction effect. The correlation between observations within an arm was evaluated by a compound symmetry correlation structure. Analyses were performed in S-PLUS.

Results: The placebo response rate for 30 % pain reduction (BOCF) was estimated to be 34, 22 and 26 %, and for 50 % pain reduction was estimated to be 22, 12 and 15 % for DPN, PHN and FM, respectively. LOCF provided 7.8, 7.0 and 4.3 % higher response than BOCF for DPN, PHN and FM, respectively. Evaluated drugs provide an additional 10–17 % increase in 30 % responder rate and 8–13 % increase in 50 % responder rate for DPN, an additional 16–24 % increase in 30 % responder rate and 11–16 % increase in 50 % responder rate for PHN, and an additional 8–11 % increase in 30 % responder rate and 7–8 % increase in 50 % responder rate for FM over placebo effect. The times to achieve drug effect plateau (calculated as 5 half-lives from k) for DPN, PHN and FM were estimated to be 5.0, 8.4, and 8.4 weeks. At approved maximum doses, duloxetine gave the highest responder rate in DPN with estimated rates of 51 and 35 % to achieve 30 % and 50 % pain reduction. Pregabalin gave the highest responder rate in PHN with estimated rates of 46 and 28 % to achieve 30 and 50 % pain reduction. Duloxetine gave the highest responder rate in FM with estimated rates of 37 and 23 % to achieve 30 and 50 % pain reduction (Table 1).

Table 1 Parameter estimate from the efficacy endpoint models

Model parameter	DPN	PHN	FM
E0_30 % reduction	−0.65	−1.3	−1.1
E0_50 % reduction	−1.3	−2.0	−1.7
E_{max}	0.79	1.8	0.55
LNED50 Duloxetine	2.2	–	1.4
LNED50 Pregabalin	5.6	5.2	4.8
LNED50 Gabapentin	–	7.7	–
LNED50 Milnacipran	–	–	4.2
LOCF effect	0.37	0.44	0.25
k	0.69	0.41	0.41
ωBT (SD)	0.25	0.27	0.21
ρ (Within arm correlation)	0.60	0.47	0.02

Conclusions: These results suggest the trial durations for DPN, PHN and FM of at least 5–8 weeks would be required to observe clinically meaningful separation of pain response between drugs included in this analysis from placebo. Duloxetine was most efficacious in DPN and FM, while pregabalin was most efficacious in PHN.

W-008 Population Analysis Characterizing the Relationship between Citalopram Exposure and QTc Interval

Timothy J Carrothers[2,*], Tatiana Khariton[1], Antonia Periclou[1], Michelle Green[2], Parviz Ghahramani[1]

[1]Forest Research Institute, Jersey City, NJ, USA; [2]Pharsight, Sunnyvale, CA, USA

Objectives: To develop a population PK-QTc model for citalopram (CIT) to evaluate the relationship between drug concentrations and the time-matched drug-placebo differences for heart rate corrected change in QT interval for citalopram doses ranging 20–60 mg/days.

Methods: Data from 119 healthy volunteers from a dedicated Phase IV TQT study were used in the population pharmacokinetic and, subsequently, PK-QTc analysis of CIT. The primary goal of the population PK modeling was to predict individual plasma concentrations of S-CIT, R-CIT and their metabolites S-demethyl-CIT and R-demethyl-CIT at times matching the ECG measurements (collected by Holter monitoring). The population PK analyses for all four moieties were developed using the first-order conditional estimation (FOCE) method with interaction in NONMEM^{TM} (version VI).

For S-demethyl-CIT and R-demethyl-CIT, a strategy was applied where-
by the metabolites' concentrations were each modeled using a standard disposition model, parameterized with clearances and volumes, with first order absorption. Under this approach, S-CIT and R-CIT doses were assumed to drive the S-demethyl-CIT and R-demethyl-CIT models. The doses for S- and R-demethyl-CIT were set to 0.3 and 0.5 times of the dose of S and R-CIT, respectively, based on the observed ratio between the mean steady state concentrations for demethyl-CIT vs. CIT. The exposure–response analysis examined the relationship between individual corrected QT interval (QTcNi) and the individual predicted plasma concentrations of S-CIT, R-CIT, S-demethyl-CIT and R-demethyl-CIT following exposure to 20 and 60 mg/day doses of citalopram. The measured QT intervals were corrected for heart rate using individualized heart rate correction, wherein a linear regression model was applied to the baseline QT data to derive the individual correction (QTcNi). A non-linear mixed-effects model for QTcNi was developed in S-PLUS® v.6.2 for Windows and consisted of additive effects of baseline, placebo, drug effect, and a normally distributed residual error: QTcNi = Baseline + Placebo + Drug Effect + Error. The influence of citalopram on QTcNi drug effect was modeled using either individual predicted plasma concentrations of each moiety alone, or the sum of the predicted plasma concentrations of the moieties scaled by their respective molecular weights. Drug effect was modeled either as a linear or an E_{max} relationship. Inter-individual variability terms were added on each model parameter but were removed if either numerical convergence was not achieved by the estimation algorithm, or no significant improvement ($p > 0.001$) in the fit was achieved. To assess mean QTc change at 20 and 60 mg/day doses of citalopram, QTcNi associated with drug effect was simulated for typical steady-state C_{max} values at the 20 and 60 mg/day doses allowing for PK-QT model uncertainty.

Results: The population PK models were based on 1893 observations for each of the 4 moieties, collected from 112 subjects. A 2-compartment model, parameterized on clearance and volume of distribution, with linear elimination and dose-dependent bioavailability best described the plasma concentration–time data of S-CIT. One-compartment models, parameterized on clearance and volume of distribution, with linear elimination best described the plasma concentration–time data of R-CIT, S-demethyl-CIT and R-demethyl-CIT. The QTcNi exposure–response model was based on 27,262 QT observations collected from 119 subjects during baseline and active-treatment visits. Baseline, placebo, and drug effects for CIT were well estimated (Table 1). For a male subject, typical baseline QTcNi was estimated at 392 ms, with inter-individual variability of 16 ms. Mean baseline QTcNi for a female was 13 ms higher. As expected, baseline measurements also followed a strong diurnal pattern; a typical study subject experienced up to a 10 ms range of fluctuation in QTcNi over the course of the full 24-h day. After accounting for baseline and diurnal pattern, placebo effect was found to reduce the QTcNi by 1 ms. A modest diurnal pattern was present in placebo effect as well. After exploration of different linear combinations of R-CIT and S-CIT, the sum of S-CIT and R-CIT concentrations was chosen as the most appropriate moiety for use as a predictor in the model. The relationship between QTcNi and S-CIT + R-CIT concentrations was best described by an E_{max} model. The maximal QTcNi change (E_{max}) attributed to the sum, (S-CIT + R-CIT) was estimated to be 26 ms. Between-subject variability in E_{max} was estimated at 51 %. No evidence of hysteresis in the S- and R-CIT exposure-QTc effect relationship was found. After accounting for baseline, placebo, citalopram, and moxifloxacin effects, a 9 ms residual variability in QTcNi measurements remained. Residuals from the final citalopram QTcNi model were explored for their association with individually predicted S- and R-demethyl-CIT concentrations; however, no evidence of any association was detected. Hence, the QTcNi increases observed after repeated administration of citalopram can be described by the sum of S- and R-CIT moieties alone. The estimated typical maximum QTc increase following administration of citalopram, was 26 compared to the 17 ms estimated for S-CIT alone (reported in a separate study on, see the adjoining abstract [1]). This additional 9 ms QTc increase observed following administration of citalopram is concluded to be related to R-citalopram. An independent analysis was also performed assuming a linear relationship between the natural logarithm of the observed PK concentrations and time-matched, placebo-corrected changes in QTcF following 20 and 60 mg/day doses and interpolated for the 40 mg/day dose [2] (Fig. 1).

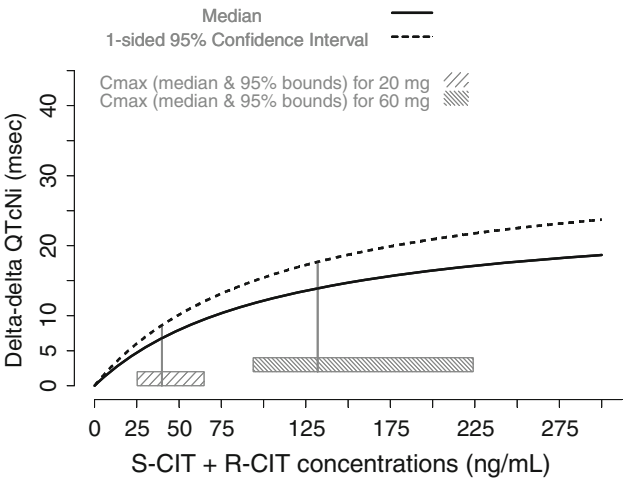

Fig. 1 Time-matched and placebo-subtracted QTcNi associated with drug effect at a range of predicted concentrations for the sum of S-CIT and R-CIT

Table 1 Final parameter estimates for QTcNi-plasma exposure model with bootstrap standard errors

Main model parameters	Population mean		Additive inter-individual variability	
	Estimate	SE, %CV	Estimate	SE
Baseline for males (msec)	392.1	0.6	15.9	6.1
Increase in baseline for females (msec)	13.0	23	–	–
Placebo (msec)	−0.78	47	–	–
Log (E_{max}, msec) for S-CIT + R+CIT effect	3.24	4.4	0.51	9.1
Log (EC_{50}, ng/mL) for S-CIT + R+CIT effect	4.7	5.4	–	–
Residual variability (as st. dev.), msec	8.5	1.7	–	–

Conclusions: From the final PK-QT model of citalopram, simulations estimated a placebo-corrected 8.2 ms (95 % 1-sided upper bound of 10.4 ms) QTcNi increase at typical C_{max} at steady-state following a 20 mg/day dose and a 15.5 ms (95 % 1-sided upper bound of 19.7 ms) increase at typical C_{max} at steady-state following a 60 mg/day supra-therapeutic dose. This is compared to 5.2 and 11.2 ms increases estimated at typical steady-state C_{max} at 10 mg/day and supratherapeutic 30 mg/day doses of escitalopram alone, respectively (see adjoining abstract [1]). Given the fact that the pharmacologic effect of citalopram in depression is primarily due to S-citalopram, the outcome of this study suggests a higher risk of QTc prolongation with citalopram treatment compared with escitalopram without additional clinical benefit. The independent analysis using linear model and observed concentrations provided comparable estimates with a mean increase in QTcF of 12.6 ms (with 95 % UCI of 14.3 ms) for a 40 mg/day dose of citalopram [2].

References

[1] Population Exposure–Response Analysis for an Escitalopram Thorough-QT Study. ACOP, 2013

[2] Prescribing Information for Celexa® (citalopram hydrobromide) tablets/oral solution, last modified on 12/2012. http://www.frx.com/pi/celexa_pi.pdf. Accessed on January 24, 2013

W-009 Additional Features and Graphs in the New NPDE Library for R

Emmanuelle Comets, Thi Huyen Tram Nguyen, France Mentré*

INSERM, UMR 738, Paris, France; Univ Paris Diderot, Sorbonne Paris Cité, Paris, France

Objectives: Over the last few years, several new approaches including Visual Predictive Check (VPC), prediction discrepancies (PD) [1] and normalised prediction distribution errors (NPDE) [2, 3] have been proposed to evaluate nonlinear mixed effect models. In the new library of npde, includes methods to handle data below the limit of quantification (BQL) [4] and new diagnostic graphs with prediction bands [5]. We also develop a new method to re-scale the NPDE in the original observations scale.

Methods: The prediction discrepancy (PD) for an observation yij is obtained as the quantile of yij within its predictive distribution. Normalised prediction distribution errors (NPDE) are obtained using a similar approach but after decorrelation of both the observed and simulated values used to obtain the predictive distribution. Visual assessment of the fit is usually performed through scatterplots of PD/NPDE versus time or model predictions, which are akin to residual plots. Under the null hypothesis of model adequacy, PD are expected to follow a uniform distribution while NPDE should follow a normal distribution.

Several new features are implemented already in the NPDE library version 2.0 (released in October 2012, available at www.npde.biostat.fr). S4-class programming provides a more user-friendly interface, and the library includes new graphical diagnostics, with prediction intervals which can be added to each graph, and diagnostic graphs for covariate models [7]. Tests can be performed to compare the distribution of the NPDE relative to the expected standard normal distribution.

We have proposed methods to impute the PD for a BQL observation by sampling in U(0,pLOQ) where pLOQ is the model-predicted probability of being BQL, and the NPDE by imputation methods: censored observations are first imputed from the imputed PD, using the predictive distribution function obtained by simulations, then NPDE are computed for the completed dataset [4].

We also develop new plots for PD/NPDE which preserves the observation shape using predicted profiles from the model. For unbalanced designs, where binning is applied, this is performed for each bin, with an option to choose a reference class for the typical profile.

Results: We illustrate the new library on data simulated using the design of the COPHAR3-ANRS 134 trial. In the trial, viral loads were measured for 6 months in 34 naïve HIV-infected patients after initiation of a tri-therapy, and up to 50 % of data were BQL. The decrease in viral loads was modelled assuming a biexponential decline and parameters estimated using MONOLIX. In the simulation study, the same model and design points were used as for the original data; simulated datasets were generated using the estimated parameters and five evaluation datasets were generated either with the same set of parameters or by modifying the value of the second slope or its variability, to illustrate the new diagnostics for models under the null or under alternative hypotheses. For the NPDE and PD, the new re-scaled graphs yield pattern close to VPC, with the added advantage that PD/NPDE naturally handle design heterogeneity.

Conclusions: The new graphs for PD/NPDE allow to preserve the shape of the process being modelled, while preserving the statistical properties of PD/NPDE which are particularly valuable in unbalanced designs, and distinguish these metrics from VPC and their many flavors (pcVPC [8]). They will be available in the new version of NPDE.

References

[1] Mentré F, Escolano S (2006) Prediction discrepancies for the evaluation of nonlinear mixed-effects models. J Pharmacokinet Biopharm 33:345–367

[2] Brendel K, Comets E, Laffont C, Laveille C, Mentré F (2006) Metrics for external model evaluation with an application to the population pharmacokinetics of gliclazide. Pharm Res 23:2036–2049

[3] Comets E, Brendel K, Mentré F. Computing normalised prediction distribution errors to evaluate nonlinear mixed-effect models: The NPDE add-on package for R. Comput Meth Prog Biomed 90:154–166

[4] Nguyen THT, Comets E, Mentré F (2012) Extension of NPDE for evaluation of nonlinear mixed effect models in presence of data below the quantification limit with applications to HIV dynamic model. J Pharmacokinet Pharmacodyn 39:499–518

[5] Comets E, Brendel K, Mentré F (2010) Model evaluation in nonlinear mixed effect models, with applications to pharmacokinetics. J-SFdS 1:106–128

[6] Brendel K, Comets E, Laffont C, Mentré F (2010) Evaluation of different tests based on observations for external model evaluation of population analyses. J Pharmacokinet Pharmacodyn 37:49–65

[7] Bergstrand M, Hooker AC, Wallin JE, Karlsson MO (2011) Prediction-corrected visual predictive checks for diagnosing nonlinearmixed-effects models. AAPS J 13:143–151

Acknowledgments: The research leading to these results has received support from the Innovative Medicines Initiative Joint Undertaking

under grant agreement no. 115156. This work was part of the DDMoRe project but does not necessarily represent the view of all DDMoRe partners.

W-010 Cellular Pharmacodynamic Model of Bortezomib Effects on U266 Myeloma Cells

Vaishali L Chudasama*, Donald E Mager

University at Buffalo, SUNY, Buffalo, NY, USA

Objectives: Bortezomib, a reversible proteasome inhibitor, is commonly used in the treatment of multiple myeloma alone and in combination with other chemotherapeutic agents [1, 2]. However, mechanisms underlying bortezomib signal transduction pathways are poorly understood [3–6]. Understanding the mechanisms of bortezomib, and how it influences the behavior of intracellular proteins involved in regulation of cell cytotoxicity is necessary to optimize bortezomib mono- or combination regimens. A Boolean network model was previously developed [7] to identify critical proteins involved in bortezomib-mediated signal transduction pathways [8]. The Boolean network could not account for complete temporal profiles of proteins and cell dynamics. Therefore, the objective of this study is to develop a cellular pharmacodynamic model to characterize the time-course of bortezomib-mediated cell cytotoxicity in U266 human myeloma cells.

Methods: Relative expressions of pNFκB, Bcl-xL, and cleaved parp were measured using immunoblotting after exposure to bortezomib (20 nM) at various time points from 0 to 33 h. Cell proliferation was measured at 0, 24, 48, 72, and 96 h using WST-1 reagent assay kit after exposure to a range of bortezomib concentrations (0.001–1000 nM). Different model structures were evaluated for describing protein dynamics and cell proliferation profiles. Linear functions were used to define stimulation or inhibition mechanisms. The final model was selected based on AIC, precision of parameter estimates, and visual inspection. All data were fitted simultaneously using MATLAB (2011). The final model was used to predict the overall bortezomib dose–response curve, which was compared to experimental data.

Results: The final cell-based pharmacodynamic model (Fig. 1) captured the data well (Fig. 2). The model includes a precursor pool with a transit compartment to describe pNFκB (NFKB) dynamics, indirect effects with two transit compartments to describe Bcl-xL dynamics, a transit compartment series to describe cleaved parp (CL_PARP), and an exponential growth model to describe cell proliferation (Cell). Fold-change in NFκB expression was used to stimulate Bcl-xL precursor production, whereas fold-change in CL_PARP was used to stimulate Bcl-xL degradation. Cell killing was regulated by Bcl-xL-mediated inhibition and CL_PARP induced stimulation of cell death (k_{kill}). All parameters are estimated with good precision (%CV <50 %), except for the Bcl-xL degradation rate constant (127 % CV). The final model predicted bortezomib potency after 48 h of drug exposure (3.80 nM) was comparable to the experimentally observed value (1.51 nM).

Conclusions: Bortezomib exposure was successfully linked to cell proliferation via protein dynamics as a driver (Fig. 2). The model accurately describes cellular proteins and cell proliferation after bortezomib exposure simultaneously and is able to reasonably predict the in vitro IC_{50}. The model could serve as a basis for development of bortezomib regimens in combination with other anti-myeloma agents such as curcumin. Furthermore, this type of model holds great promise for optimizing bortezomib single-agent and combination regimens, predicting interaction potency of anti-myeloma agents, and potential scaling from in vitro to in vivo systems.

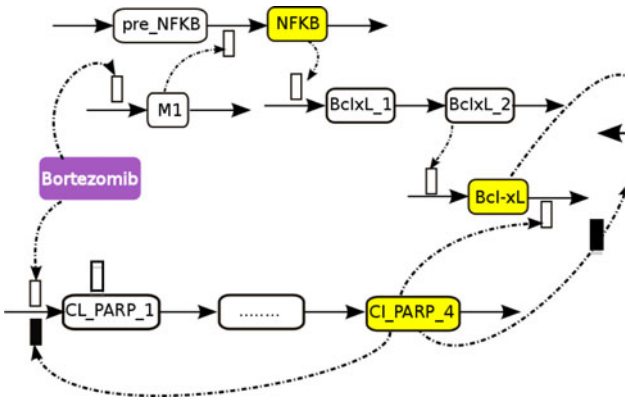

Fig. 1 Schematic of proposed cellular model of bortezomib effects on U266 cells. Inhibition Stimulation

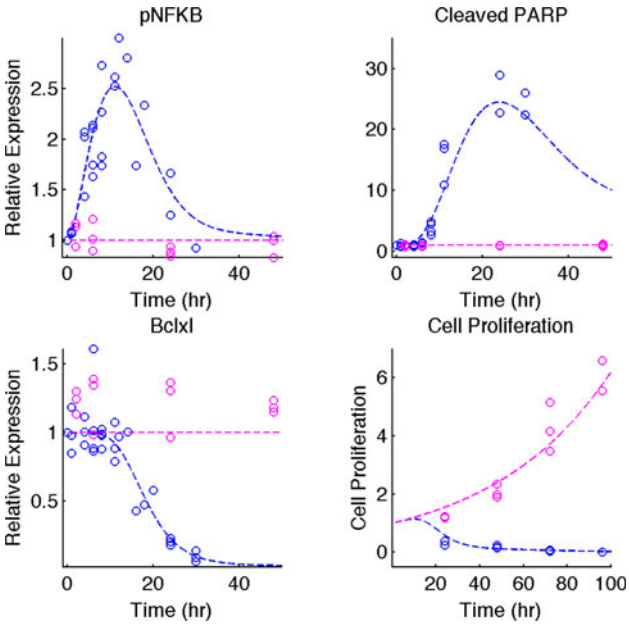

Fig. 2 Observed (*circle*) and model fitted (*dashed line*) protein dynamics and cell proliferation. Bortezomib 20 nM (*blue*), Control (*magenta*)

References

[1] Richardson PG, Barlogie B, Berenson J, Singhal S, Jagannath S, Irwin D, Rajkumar SV, Srkalovic G, Alsina M, Alexanian R, et al. (2003) **A** phase 2 study of bortezomib in relapsed, refractory myeloma. N Engl J Med 348(26):2609–2617

[2] San Miguel JF, Schlag R, Khuageva NK, Dimopoulos MA, Shpilberg O, Kropff M, Spicka I, Petrucci MT, Palumbo A, Samoilova OS, et al (2008) Bortezomib plus melphalan and prednisone for initial treatment of multiple myeloma. N Engl J Med 359(9):906–917

[3] Hideshima T, Chauhan D, Richardson P, Mitsiades C, Mitsiades N, Hayashi T, Munshi N, Dang L, Castro A, Palombella V, et al (2002) NF-kappa B as a therapeutic target in multiple myeloma. J Biol Chem 277(19):16639–16647

[4] Hideshima T, Ikeda H, Chauhan D, Okawa Y, Raje N, Podar K, Mitsiades C, Munshi NC, Richardson PG, Carrasco RD, et al.

(2009) Bortezomib induces canonical nuclear factor-kappaB activation in multiple myeloma cells. Blood 114(5):1046–1052

[5] Hideshima T, Mitsiades C, Akiyama M, Hayashi T, Chauhan D, Richardson P, Schlossman R, Podar K, Munshi NC, Mitsiades N, et al. (2003) Molecular mechanisms mediating antimyeloma activity of proteasome inhibitor PS-341. Blood 101(4):1530–1534

[6] Hideshima T, Richardson P, Chauhan D, Palombella VJ, Elliott PJ, Adams J, Anderson KC (2001) The proteasome inhibitor PS-341 inhibits growth, induces apoptosis, and overcomes drug resistance in human multiple myeloma cells. Cancer Res 61(7):3071–3076

[7] Chudasama VL, Mager DE Logic-based modeling of bortezomib mediated cellular responses in U266 human myeloma cells. BMC Syst Biol (Under review).

[8] Ovacik A, Mager DE (2012) Reduction of Rituximab-mediated Cell signaling using boolean network modeling. Poster presentation. AAPS 2012, Chicago

W-011 Using Qualitative Modeling in Drug Development

Rebecca Baillie*, Christina Friedrich, Michael Reed

Rosa & Co, San Carlos, CA, USA

Objectives: Qualitative modeling, creating a graphical and precise representation of known and hypothesized biological relationships, is used to systematically compare and integrate disparate data, link disease mechanisms to clinical outcomes, and prioritize drug targets. Feedback from the users of qualitative models indicated that additional benefits may derive from those models that are different than originally expected. This study was undertaken to objectively identify and quantify results derived from qualitative modeling projects, both pre-specified targets and additional outcomes that were identified during the course of the project. A secondary objective was to determine if project targets or additional outcomes were related to the drug development stage or biology of the drug compounds being modeled.

Methods: We retrospectively compared the results from eight qualitative modeling projects with each modeling effort having a different decision focus and different goals for that decision. Statement of work contracts were used to identify the disease area, drug development stage at the start of the project, and specified deliverables, i.e., pre-specified targets, while final project reports were used to identify outcomes. The two lists were compared and outcomes were defined as pre-specified targets or additional outcomes. Additional outcomes fell into categories: improving experimental design, facilitating communication, identifying data gaps, or clarifying mechanisms of action. Disease areas were defined as immunology, oncology, metabolism, or neurology. The drug development stages were preclinical (5 projects) or clinical (3 projects).

Results: All projects met pre-specified targets, and five projects had additional outcomes that were identified during the model development. Some outcomes were clearly related to the drug development stage of the project, while others, such as clarifying mechanism of action, occurred in both preclinical and clinical development. In 3 preclinical projects, additional outcomes included improving experimental design and identification of data gaps in addition to the expected targets. Facilitating communication across multidisciplinary teams occurred in projects in both preclinical and clinical development. No effect of disease area was found on project outcomes.

Conclusions: In this analysis, we found that a majority (5/8) of qualitative modeling projects had additional outcomes. While some of these outcomes were correlated to the stage of the drug development; others occur in both preclinical and clinical development stages. Some additional outcomes, such as facilitated communication, may be difficult to quantify in terms of impact on the development program. Other outcomes, such as optimized experimental design and identification of data gaps, may have clear and quantifiable impact. Further research is needed to evaluate the impact of these additional outcomes on the drug development programs.

W-012 Population Analysis of Total Kidney Volume, a Prognostic Marker of Disease Progression in Patients with Autosomal Dominant Polycystic Kidney Disease: Effect of Genotype and Imaging Modalities

Mohamad-Samer Mouksassi[1,*], Jean-Francois Marier[1], Lamia Sid-Otmane[2], Fredrik Jonsson[1], Klaus Romero[2]

[1]Pharsight, a Certara Company, Montreal, QC, Canada;
[2]Critical Path Institute, Tucson, AZ, USA

Objectives: Autosomal dominant polycystic kidney disease (ADPKD) is the most common hereditary kidney disease affecting 1:400–1:1000 individuals. The development and growth of cysts over time causes increased kidney size leading to interstitial fibrosis and renal failure. ADPKD patients suffer from increasing morbidity due to their enlarging kidneys including severe pain, increasing abdominal girth, hypertension, hematuria, renal stones and renal infection. End stage renal disease (ESRD) has been shown to develop in approximately 50 % of affected patients by age 53. Quantitative radiological imaging can be used to measure total kidney volume (TKV) as prognostic markers for monitoring the rate of disease progression and response to therapy. The goal of this project was to characterize the rate of growth of TKV in patients with ADPKD and assess potential sources of between subject variability.

Methods: TKV data collected by the Consortium for Radiologic Imaging Studies of Polycystic Kidney Disease (CRISP), as well as multiple, longitudinal, well-characterized research registries maintained over decades by leading institutions conducting clinical investigation in ADPKD (University of Colorado - Denver, Emory University, and Mayo Clinic) were used. Longitudinal TKV data from ultrasonography (US), computer assisted tomography (CT) scan and magnetic resonance imaging (MRI) were included. Nonlinear mixed-effect (Phoenix NLME 1.2) modeling was used to assess longitudinal TKV data. Patients with a least two TKV measurements separated by at least 6 months apart were included in the analysis. Various kidney volume growth models were evaluated. Sources of variability such as age, sex, race, ethnicity, weight, height, mutations (PKD1, PKD2, No Mutation or unknown), eGFR, creatinine clearance (CrCL), and serum creatinine (Scr) were analyzed. A separate model was fit to each imaging modality (US, CT, MRI).

Results: A total of 1140 (US), 868 (MRI) and 832 (CT) patients with ADPKD were included in the analysis. The total number of observation was 2664 (US), 2164 (MRI), 1053 (CT). Overall median (range) values of age of first TKV measurement was 40 (0-93.05). TKV was best described with the following exponential growth model:

$$TKV_i(t) = TKV_{0,i} \times e^{[(0.693 * Time)/HLi]}$$

where $TKV_i(t)$ = TKV (mL) at time t for i^{th} individual, $TKV_{0,i}$ = baseline TKV for i^{th} individual, HL_i = half-life of disease progression (half-life to doubling of TKV) for i^{th} individual. The model was qualified using visual predictive check and goodness of fit plots (Fig. 1). The effect of imaging modality was significant. Based on US

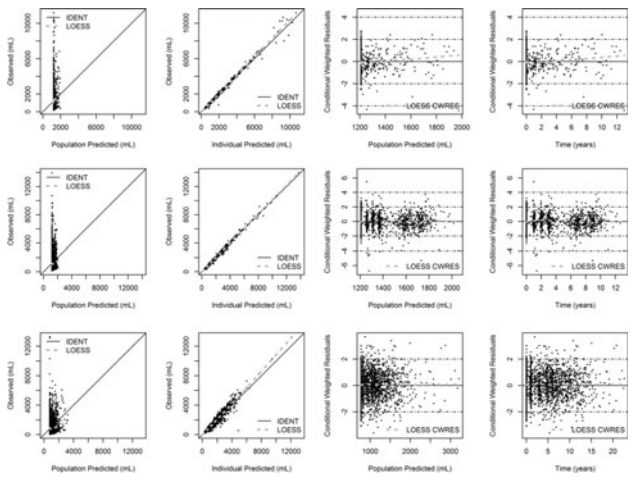

Fig. 1 Goodness of fit for the MRI (*first row*), CT (*second row*) and US (*third row*) models

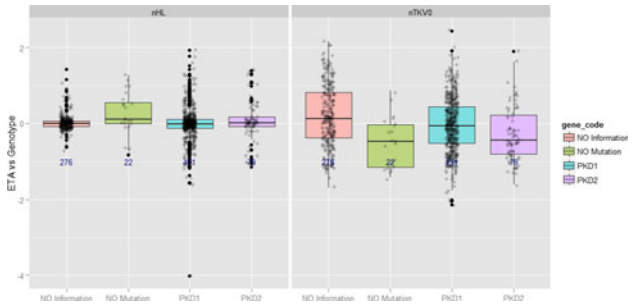

Fig. 2 Random effects versus mutation (MRI model shown)

data, typical population values of TKV_0 and HL were 772 mL and 11.0 years, respectively. MRI and CT data gave similar typical population values of TKV_0/HL: 1207.8 mL/17.1 years and 1210.3/18.3 years, respectively. Yearly growth rate of the kidney volumes were estimated to be: 6.5 % (US), 4.1 % (MRI) and 3.8 % (CT). The best residual error was a proportional one with a CV % of: 19.3, 7.3 and 13.1 % for US, MRI and CT respectively. Using observed baseline TKV did not improve the models. On the other hand, height was identified as a covariate explaining the variability in TKV_0. The HL was an intrinsic characteristic of each individual patient and it was not related to genetic mutations (Fig. 2).

Conclusions: A population analysis of TKV was performed to characterize disease progression in patients with ADPKD and identify sources of variability. The typical half-life of disease progression (based on MRI/CT) was approximately 18 years which translate to a yearly growth rate of 4 %. This is in line of literature information on this disease. As expected, TKV data measured with US imaging modality was associated to a higher variability and higher estimated growth rate due to the limitations of this imaging method. Data sources using MRI or CT modalities could be potentially combined into future analyses since no significant differences were observed. The above model may be used to monitor and longitudinally predict the long term behavior of TKV growth in patients with ADPKD. Future work will attempt to link the growth of TKV over time as a biomarker to predict clinically relevant negative outcomes of ADPKD, such as worsening of renal function, ESRD and mortality. The ultimate goal will be to construct a "drug-biomarker (TKV)-disease outcome (ADPKD-ESRD, mortality,…)" model that can support the use of TKV as a drug development tool to help enrich trials for new therapies.

W-013 Hemoglobin and Red Blood Cell Modeling After Chronic Oral Administration of GSK1278863 to Cynomolgus Monkeys

Aline Barth[1,*], Brendan Johnson[2], Herbert Struemper[2], David Adams[3]

[1]University of Florida, Gainesville, FL, USA;
[2]GlaxoSmithKline, Research Triangle Park, NC, USA;
[3]GlaxoSmithKline, Upper Merion, Pennsylvania, PA, USA

Objectives: To evaluate models that can be used to describe the erythropoietic effects of GSK1278863 after chronic administration to cynomolgus monkeys with future application to modeling and simulation to support Phase 2 dose selection.

Methods GSK1278863 is in development for the treatment of anemia in patients with chronic kidney disease. A 9 month toxicology study with 24 male and 24 female cynomolgus monkeys was performed with 4 dose groups: 0 (vehicle), 3, 10 and 50 mg/kg once per day via oral gavage. Blood samples were withdrawn at: −3, −1, 4, 13, 26 and 39 weeks (the beginning of the treatment was at week 0). The recovery phase of the study included 4 males and 4 females (2/sex at 0 and 50 mg/kg/day dose levels) from the previous main study. The dosing in these animals was suspended at week 39 and a blood sample was taken at week 45. All studies were conducted in accordance with the GSK Policy on the Care, Welfare and Treatment of Laboratory Animals and were reviewed the Institutional Animal Care and Use Committee either at GSK or by the ethical review process at the institution where the work was performed.

The impact of GSK1278863 on the red blood cell (RBC) count and hemoglobin (Hgb) concentration was modeled through different approaches. Instead of using the full pharmacokinetic profile, the dose was used to drive the pharmacodynamic (PD) response, i.e., a K-PD approach [1]. It uses a virtual compartment (biophase) in which the concentration is in equilibrium with the observed effect. The model depends only on the dosing information and PD data for the estimation of all parameters. For the PD portion of the model, cell lifespan and transit compartment models were evaluated, both with and without a precursor compartment. Cell lifespan models assume that the cells are produced, survive for a certain amount of time and then are eliminated due to senescence [2]. The transit compartment approach uses a series of transit compartments to describe the aging and elimination of RBC and Hgb, effectively reflecting a varying cell lifespan within a population of cells, in contrast to the assumptions of the cell lifespan models [3].The data was modeled using the software NONMEM 7.1.2. Initial parameter estimates and model characteristics were explored with the software Berkeley Madonna and the diagnostic plots were generated with the software R, including the package Xpose.

Results: The evaluation of transit models with and without precursor and lifespan model with precursor resulted in poor relative standard errors (RSE), as high as 158 % for RBC models and 342 % for Hgb models and also inadequate visual predictive check plots. Analysis of the data with the basic life span model provided appropriate baseline, SC50 (50 % of the maximum response), Smax (maximal stimulation) and KDE (elimination rate constant from the virtual compartment) estimates for both the RBC and Hgb models. Fixing the cell life span parameter to a literature value was also evaluated. For the RBC model the use of the physiological literature value was adequate. In order to fit the Hgb data, estimation of the life span parameter provided an

overall better fit. With these models, the fixed-effect parameter estimates were in accordance with the observed data and with low RSE (<26 %). Random-effect parameters were also well estimated; inter-individual variability RSE <56 % for RBC model and <39 % for Hb model, and additive residual error RSE of <15 % for both models.
Conclusions: The basic life span model without precursor provided better results when fitting the observed hemoglobin and red blood cell data. Therefore it is likely to be a useful model for the evaluation of pharmacodyamic effects after chronic administration of GSK1278863 in clinical trials.

References

[1] Jacqmin P, et al (2007) Modelling response time profiles in the absence of drug concentrations: definition and performance evaluation of the K-PD model. J Pharmacokinet Pharmacodyn 34(1):57–85
[2] Perez-Ruixo J, et al (2005) Population cell life span models for effects of drugs following indirect mechanisms of action. J Pharmacokinet Pharmacodyn 32(5–6):767–793
[3] Hamren B, et al (2008) Models for plasma glucose, HbA1c, and hemoglobin interrelationships in patients with type 2 diabetes following tesaglitazar treatment. Clin Pharmacol Ther 84(2):228–235

W-014 Population Pharmacokinetics of the Ofatumumab in Combination with Chemotherapy in Relapsed or Refractory Aggressive Lymphoma

Rajendra P. Singh[1,*], Herbert Struemper[2], Bela R. Patel[1], Roxanne C. Jewell[2]

[1]CPMS GlaxoSmithKline, King of Prussia, PA, USA; [2]CPMS GlaxoSmithKline, RTP, NC, USA

Objectives: Ofatumumab is a human monoclonal IgG1κ-antibody targeting a distinct CD20 epitope. It is active against B cell lymphoma cell lines and chronic lymphocytic leukemia, including cell lines with low CD20-antigen density and an increased expression of complement inhibitory molecules. The present work aims to characterize the pharmacokinetics (PK) of ofatumumab after three cycles of intravenous (IV) infusions in combination with ICE (ifosfamide, carboplatin, etoposide) or DHAP (dexamethasone, cytarabine, cisplatin) chemotherapy in subjects with relapsed or refractory CD20-positive aggressive lymphoma (diffuse large B cell lymphoma, transformed lymphoma, or grade 3b follicular lymphoma).
Methods: Data were obtained from 61 subjects with relapsed or refractory aggressive lymphoma who received ofatumumab in combination with ICE or DHAP chemotherapy (NCT00823719). Ofatumumab was given as 2 weekly doses in the first cycle, followed by an infusion on Day 1 of two subsequent 21-day cycles. The first ofatumumab infusion was initially 300 mg, which was increased to 1000 mg by protocol amendment; all other infusions were 1000 mg. Nonlinear mixed-effects modeling was performed for the population pharmacokinetic analysis, using NONMEM program version 7.1.2 (ICON, Ellicott City, MD). A two-compartment structural model with linear first-order elimination was selected as the structural model after evaluation of linear and nonlinear two-compartment models to describe the pharmacokinetic data. Final model selection was based on evaluation of goodness-of-fit plots, biological plausibility, precision of parameter estimates, and the minimum objective function value. Nonparametric bootstrap and visual predictive checks were implemented for final model evaluation.
Results: The pharmacokinetics of ofatumumab in relapsed or refractory aggressive lymphoma in combination with chemotherapy was adequately described by a two-compartment model with linear first-order elimination. The typical value for CL was 9.1 mL/h. The typical value for the population volume of central compartment was 3.81 L. The inter-compartment clearance (Q) was 57.4 mL/h and peripheral volume was 3.95 L. Body surface area was found to be a covariate for clearance, volume of the central compartment, and volume of the peripheral compartment. Sex was found to be a predictor of volume for the central compartment, with females having approximately 20 % smaller volume than males.
The inclusion of a target-mediated clearance component in the model was not required for this analysis in subjects with aggressive lymphoma including DLBCL, unlike prior population analyses combining subjects with chronic lymphocytic leukemia (CLL), follicular lymphoma (FL), and rheumatoid arthritis (RA) [1,2]. As previously noted [2], the relative contribution of target-mediated clearance was highest for CLL, where circulating B-cell counts are typically very high, and was smaller in FL and RA; like FL and RA, DLBCL typically has lower numbers of circulating B cells than CLL. Other factors that may have reduced the need for target-mediated clearance in the model include the effect of concomitant chemotherapy in reducing tumor cells in the peripheral blood and the sparse sampling schedule.
Conclusions: The two-compartment population pharmacokinetic model with linear elimination developed following IV infusion in combination with ICE or DHAP chemotherapy in subjects with aggressive lymphoma including DLBCL adequately characterized the pharmacokinetics of ofatumumab in this study.

References

[1] Sale M, Jewell RC, Patel BR (2011) Ofatumumab population pharmacokinetic analysis in patients with chronic lymphocytic leukemia (CLL), follicular lymphoma (FL), and rheumatoid arthritis (RA). ACoP 2011
[2] Struemper H, Sale M, Patel BR, Jewell RC (2012) Target-mediated clearance of ofatumumab: a tale of different disease states. PAGE 2012

W-015 A Semi-Mechanistic Transit Compartment Model to Describe Variable Absorption of Mycophenolic Acid in Pediatric Patients after Renal Transplantation

Min Dong[1,*], Tsuyoshi Fukuda[1,3], Jens Goebel[2,3], Alexander A. Vinks[1,3]

[1]Division of Clinical Pharmacology, Cincinnati Children's Hospital Medical Center, Cincinnati, Cincinnati, OH, USA; [2]Nephrology and Hypertension Division, Cincinnati Children's Hospital Medical Center, Cincinnati, OH, USA; [3]Department of Pediatrics, University of Cincinnati, Cincinnati, OH, USA

Objectives: Mycophenolic acid (MPA) is a broadly used immunosuppressive drug to prevent allograft rejection in pediatric kidney transplantation. Large inter- and intra-individual variability in drug exposure especially in the absorption phase has been observed [1]. The purpose of this study was to develop a population pharmacokinetic (PK) model of MPA with an emphasis on characterizing the absorption phase, and to identify covariate factors to predict exposure variability in the early post-transplant period (days 4–9) in pediatric renal transplant recipients.

Methods: A total of 224 MPA plasma concentration–time data points from 25 pediatric renal transplant patients between ages 2–20 years were available for model development. Population PK analysis was performed using nonlinear mixed effect modeling by NONMEM 7.2 with first-order conditional estimation with interaction (FOCE-I). Multiple absorption models, including first-order with lag time, zero-order with lag time, first-order and zero-order parallel, Weibull function, and a transit compartment model, were explored to describe the variable absorption phase. Patients' demographics and laboratory data were included in the covariate analysis. The final model was evaluated by non-parametric bootstrap analysis and prediction-corrected visual predictive check (PC-VPC) [2].
Results: A two-compartment with a transit absorption model best described the data. Allometric scaling using normal fat mass and estimated creatinine clearance were identified as significant predictors of apparent clearance. A non-linear relationship between dose and MPA exposure was observed and was well described by the model. The final population parameter estimates were: CL/F, 37.9 L/h/70 kg; Vc/F, 31.6 L/70 kg; Q/F, 38.8 L/h/70 kg and Vp/F, 980 L/70 kg.
Conclusions: The final model successfully described MPA PK data in the population studied. The transit compartment model may provide a better approach than traditional absorption models in describing MPA absorption.

References

[1] Fukuda T, Goebel J, Thøgersen H, Maseck D, Cox S, Logan B, Sherbotie J, Seikaly M, Vinks AA (2011) Inosine monophosphate dehydrogenase (IMPDH) activity as a pharmacodynamic biomarker of mycophenolic acid effects in pediatric kidney transplant recipients. J Clin Pharmacol 51(3):309–320

[2] Bergstrand M, Hooker AC, Wallin JE, Karlsson MO (2011) Prediction-corrected visual predictive checks for diagnosing nonlinear mixed-effects models. AAPS J 13(2):143–151

W-016 Non-Parametric Reduced Sampling Algorithm (NPRSA) for Pharmacokinetic Sample Reduction

Pavan Vaddady[1,*], Martin Johnson[2], Pravin Jadhav[3], John Clements[1], Bharath Kumar[1], Prajakti Kothare[4]

[1]Merck Sharp & Dohme Corp., Kenilworth, NJ, USA; [2]Merck Sharp & Dohme B.V., Oss, The Netherlands; [3]Merck Sharp & Dohme Corp., Upper Gwynedd, PA, USA; [4]Merck Sharp & Dohme Corp., West Point, PA, USA

Objectives: Phase I clinical pharmacology studies contribute a significant cost of early clinical development and employ rich PK sampling schemes. Typically serial PK sampling schemes are not substantially altered after initial studies in man despite greater available pharmacokinetic knowledge. Therefore, there exists an opportunity to reduce cost and blood draws for trial participants.
A non-parametric sampling reduction algorithm was developed with a user friendly interface for this purpose. The algorithm leverages existing dense sampling PK schemes for a compound to propose a reduced sampling scheme that balances having the fewest number of time-points with obtaining adequate characterization of non-compartmental PK parameters (C_{max} and AUC).
Methods: This is an R-language based algorithm adapted and expanded in scope from a previously developed sample reduction algorithm developed by Reyderman et al. The algorithm creates scenarios reflecting all possible permutations of time points based on the user supplied minimum and maximum time points and presents

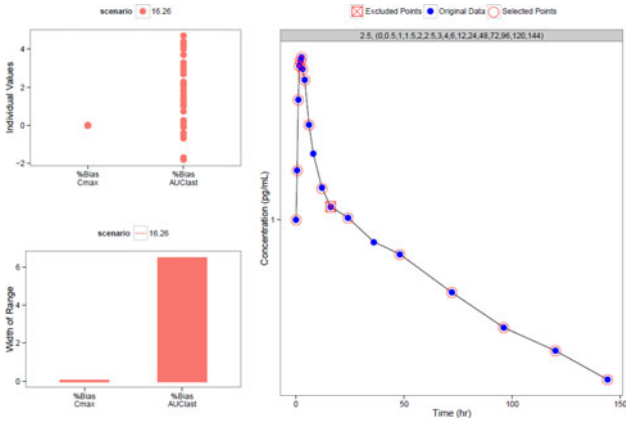

Fig. 1 Representative figure for evaluation of a scenario (16.26)

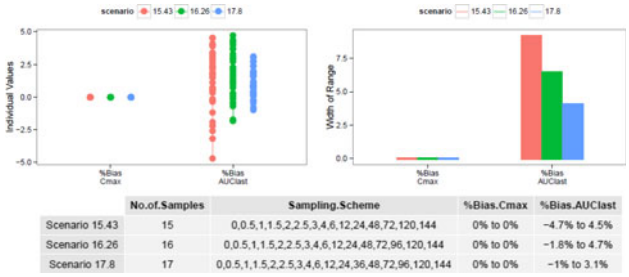

	No.of.Samples	Sampling.Scheme	%Bias.Cmax	%Bias.AUClast
Scenario 15.43	15	0,0.5,1,1.5,2,2.5,3,4,6,12,24,48,72,120,144	0% to 0%	−4.7% to 4.5%
Scenario 16.26	16	0,0.5,1,1.5,2,2.5,3,4,6,12,24,48,72,96,120,144	0% to 0%	−1.8% to 4.7%
Scenario 17.8	17	0,0.5,1,1.5,2,2.5,3,4,6,12,24,36,48,72,96,120,144	0% to 0%	−1% to 3.1%

Fig. 2 Representative figure for comparison of three scenarios (15.43, 16.26 and 17.8)

the % bias from observational data in AUC and C_{max} for each scenario. It selects a list of possible scenarios that satisfy the pre-specified criteria. Based on the user's choice, the algorithm can further evaluate a given scenario or compare multiple scenarios or evaluate a modified sampling scheme. Some of the features included in this algorithm are removing/including pre-defined time points in the final selection of time points, linear and linear-up/log-down AUC trapezoidal rule implementation, steady state versus non-steady state differentiation, AUC0-inf, AUC0-last, AUCall and AUCextrapolated calculations, scoring functions to rank the schemes that satisfy the user defined selection criteria, compare multiple selected scenarios, summary tables and figures for each of the evaluations.
As a representative example, a case study is demonstrated using a hypothetical example of sampling scheme for Study X based on prior dense pharmacokinetic profiles from historical studies A and B. The original full sampling schedule from studies A and B consisted of a total number of 19 unique sample times (0, 0.5, 1, 1.5, 2, 2.5, 3, 4, 6, 8, 12, 16, 24, 36, 48, 72, 96, 120 and 144 h). The following pre-specifications were applied: the last time point would be 144 h, a 16 h sample would not be included and each scenario would have at least 10 time points: 0, 0.5, 1, 1.5, 2, 2.5, 3, 4, 6, 144 h. The remaining 8 time points were subject to additional selection. The maximal % bias of the individual C_{max} and AUC values were set at <5 % for AUC0-last and <5 % for C_{max}.
Results: Based on application of the above selection criteria, 8 scenarios with 11 samples, 28 scenarios with 12 samples, 56 scenarios with 13 samples, 70 scenarios with 14 samples, 56 scenarios with 15 samples, 28 scenarios with 16 samples, 8 scenarios with 17 samples and 1 scenario with 18 samples were evaluated. Based on the scoring function: 0.75*(Number of Samples) + 0.25*(Sum of Range of % Bias for C_{max} & AUC), 8 scenarios that satisfied the selection criteria

were identified. This included 1 scenario with 15 samples, 2 scenarios with 16 samples, 4 scenarios with 17 samples and 1 scenario with 18 samples. Based on comparisons of summary tables/figures, a scenario was chosen that had the lowest score based on the scoring function and the minimum number of samples (15) (Figs. 1, 2).

Conclusions: This novel algorithm can be applied for designing PK sampling schemes for phase I studies such as single ascending dose studies after 1st PK break, multiple ascending dose studies, control drug arms of clinical pharmacology studies. It directly reduces patient and study design burden due to a smaller number of blood draws and decreases bioanalytical costs. Some of the limitations are it can be applied only when studies with similar design criteria are planned (such as sampling time points, no. of subjects). However, this is offset by the consideration that the algorithm can be applied relatively quickly and is useful when compartmental modeling is not yet in place.

W-017 Exposure–Response Analysis of the Effect of Trametinib, a MEK inhibitor, on Tumor Size in Patients with V600 BRAF Mutation Positive Melanoma

Joannellyn Chiu*, Daniele Ouellet

GlaxoSmithKline, Research Triangle Park, NC, USA

Objectives: Trametinib is a reversible, highly selective, allosteric inhibitor or mitogen-activated extracellular signal regulated kinase 1 (MEK1) and 2 (MEK2) that is currently under development for treatment of patients with metastatic BRAF V600 mutation-positive melanoma. The objectives of this analysis were to characterize the relationship between trametinib exposure and tumor size over time, and to identify covariates that may influence response.

Methods: Tumor size (TS) data (sum of longest diameter) were pooled from 348 patients with V600 BRAF mutation positive melanoma enrolled in Phase II and Phase III studies. Patients included in the analysis received either 2 mg of trametinib once daily ($N = 257$) or chemotherapy (i.e. dacarbazine (DTIC) 1000 mg/m^2 or paclitaxel 175 mg/m^2) ($N = 91$). TS over time was described based on the model by Claret et al. [1] with estimates of baseline (BSL), tumor growth (KL), drug effect (KD), and resistance/progression (λ); random effects were explored on all 4 parameters using NONMEM VII. Different measures of exposure and covariates were investigated in the model building. A drop out model based on RECIST criteria was used for visual predictive check (VPC) to simulate clinical data ($n = 1000$). Simulated TS data from subjects who have progressive disease (PD) were retained up to the time point when the subject first becomes progressive. Progressive disease (PD) is defined as when the sum of the total lesions increase by 20 % and demonstrates an absolute increase of at least 5 mm. Simulations ($n = 200$) were performed to better understand the effect of different exposure levels on tumor kinetics.

Results: Median baseline TS was 64.0 mm. More lesions, high level of lactate dehydrogenase (LDH), and Eastern Cooperative Oncology Group (ECOG) performance status of >1 were associated with higher baseline TS, and inclusion of these covariates decreased between-subject variability in BSL from 74 to 45 %. In a typical patient receiving chemotherapy, a median increase of 3.1 mm in TS is predicted after 6 weeks (+5 %). LDH was a significant predictor of disease progression with patients with high LDH levels progressing 2.46 times more rapidly in chemotherapy arm (+12 % increase in TS at 6 weeks). In a typical patient receiving trametinib, rate of tumor shrinkage (KD) is estimated to be 0.00801/day resulting in a median decrease in TS of 23 % after 6 weeks, while resistance/progression (λ) develops at a rate of 0.0343/day. Trametinib exposure was significant on the parameter describing progression (λ), suggesting that progression is delayed with higher trametinib concentrations (C_{min}). There was no difference in response between BRAF V600E and V600 K mutations.

The median TS over a 6-month period is shown below assuming patients received either chemotherapy or trametinib doses of 1.0, 1.5, or 2.0 mg once-daily. Simulation results are shown assuming that patients remained on study despite increases in TS, i.e. no drop-out, (left panel) and after accounting for drop out (right panel)

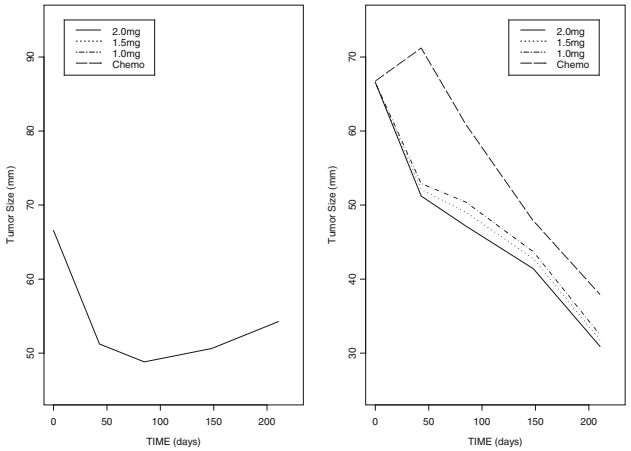

Conclusions: Change in tumor size was related to trametinib exposure, with more sustained response with higher trametinib C_{min}. Total number of lesions, LDH, and ECOG performance status were significant covariates on baseline TS, and patients with high LDH levels progressed more rapidly.

References

[1] Claret L, Girard P, Hoff PM, Van Cutsem E, Zuideveld KP, Jorga K, Fagerberg J, Bruno R (2009) Model-based prediction of phase III overall survival in colorectal cancer on the basis of phase II tumor dynamics. J Clin Oncol. doi:10.1200/JCO.2008.21.0807

[2] Eisenhauer EA, Therasse P, Bogaerts J, Schwartz LH, Sargent D, Ford R, Dancey J, Arbuck S, Gwyther S, Mooney M, Rubinstein L, Shankar L, Dodd L, Kaplan R, Lacombe D, Verweij J (2009) New response evaluation criteria in solid tumours: revised RECIST guidelines (version 1.1). Eur J Cancer 45:228–247

W-018 Whole Body Physiologically-Based Pharmacokinetic Model for Colistin and Colistimethate Sodium (CMS) in Six Different Species: Mouse, Rat, Rabbit, Baboon, Pig and Human

Salim Bouchene[1,*], Sandrine Marchand[2,3], Lena E. Friberg[1], Sven Björkman[1], William Couet[2,3], Mats O. Karlsson[1]

[1]Department of Pharmaceutical Biosciences, Uppsala University, Uppsala, Sweden; [2]INSERM U-1070, Poitiers, France; [3]Laboratoire de Toxicologie et de Pharmacocinétique, CHU de Poitiers, Poitiers, France

Table 1 Typical estimates for CMS and colistin PK parameters

Species	$CL_{r\text{-}CMS}$ (mL/min/kg)	$CL_{r\text{-}col}$ (mL/min/kg)	$CL_{nr\text{-}col}$ (mL/min/kg)	$V_{ss\text{-}CMS}$ (mL/kg)	$V_{ss\text{-}col}$ (mL/kg)
Mouse	17.1	0.043	3.4	171.9	444.9
Rat	6.4	0.019	6.6	382.8	537.1
Rabbit	5.62	0.017	0.1	79.6	391.6
Baboon	1.62	0.048	5.4	167.8	468.3
Pig	3.45	0.018	14.4	80.9	416.7
Human	2.96	0.0092	2.36	167.4	212.0

Objectives: Colistin is used to treat MDR GNB infections and administered as a prodrug, CMS [1, 2]. Characterizing colistin tissue distribution is important in order to optimize bacteria kill and to reduce toxicity. Whole Body Physiologically-Based Pharmacokinetic (WBPBPK) models are valuable tools to predict tissue drug disposition [3]. The aim of this work was to develop a WBPBPK model describing plasma PK of CMS and colistin in six animal species simultaneously and predicting their tissue distribution.

Methods: 40 mice (1 per time point), 6 rats, 3 rabbits, 3 baboons, 2 pigs and 12 healthy volunteers were included in the study. A single dose of 15 mg/kg CMS was administered to mice (SC), rats and rabbits (IV bolus). Single doses of 32, 160 and 80 mg CMS were administered to baboons (10 min-infusion) pigs and humans (1 h-infusion), respectively. Venous blood was collected between 0 and 4 h after administration for mice, 0 and 3 h for rats, 0 and 7 h for rabbits, 0 and 9.16 h for baboons, 0 and 8 h for pigs and 0 and 18 h for humans. CMS and colistin were assayed at each time point [4].

CMS is eliminated renally and via hydrolysis into colistin whereas colistin is mainly eliminated non-renally [1, 2]. Hydrolysis of CMS to colistin is assumed to occur in all tissues [5] with the same rate in all species. A WBPBPK model was developed describing each tissue as a single, perfusion limited and well-stirred compartment. Specific tissue volumes and blood flows for each species were used in the model. All clearances and Kp factors of CMS and colistin were estimated sequentially using the prior functionality in NONMEM 7. Prior information was from literature [1–3], physiological description of tissues [6] and in vitro experiments.

Results: The CMS to colistin hydrolysis half-life was estimated to 0.92 h. PK parameter estimates are summarized in Table 1.

Conclusions: The model reasonably well described CMS and colistin PK profiles in all studied species. The PK parameters were scaled across species with respect to the physiological differences. This model may be a valuable tool for PKPD scaling across species to predict bacteria kill in target tissues.

References

[1] Couet et al (2011) Clin Pharmacol Ther
[2] Mohamed et al (2010) Antimicrob Agents Chemother
[3] Hall et al (2012) J Pharm Sci
[4] Gobin et al (2010) Antimicrob Agents Chemother
[5] Bouchene et al (2012) ICAAC
[6] Björkman et al (2001) J Pharm Sci

W-019 A New Mechanism-based PK/PD Model for Antimicrobial Combinations of Colistin and Doripenem against *Pseudomonas aeruginosa*

Neang S Ly[1*], Brian T Tsuji[1], Gauri G Rao[1], Pamela A Kelchlin[1], Patricia N Holden[1], Alan Forrest[1], Phillip J Bergen[2], Roger L Nation[2], Jian Li[2], Jurgen B Bulitta[1,2]

[1]School of Pharmacy and Pharmaceutical Sciences, SUNY Buffalo, Buffalo, NY, USA; [2]Monash Institute of Pharmaceutical Sciences, Monash University (Parkville campus), Melbourne, Australia

Objectives: The rapid emergence of resistant gram-negative bacteria such as *P. aeruginosa* and a severe lack of antibiotics against these pathogens are causing a global health crisis. There is an urgent need to rationally optimize dosage regimens of available antibiotics in mono- and combination therapy. While current antibiotic combination regimens have only been designed empirically, quantitative approaches for optimizing antibiotic combinations are very promising to combat multidrug-resistant bacteria. Colistin, an old antibiotic, has been resurfaced owing to its activity against multidrug-resistant gram-negatives; however, emergence of resistance during colistin monotherapy occurs and colistin combination therapies with other agents are beneficial to prevent the emergence of colistin resistance and ensure good therapeutic outcome. Previous models accounted for two bacterial subpopulations quantified on antibiotic-free and antibiotic-containing agar plates, but described antibiotic monotherapy and did not model multiple drug plates [1]. Our primary objective was to develop a mechanism-based pharmacodynamic model to characterize the rate and extent of bacterial killing and suppression of resistance and to identify and evaluate the mechanisms of synergy of colistin and doripenem. Secondly, we sought to develop a new approach to model data from multiple drug-containing agar plates.

Methods: Three *P. aeruginosa* strains, including a reference strain (colistin hetero-resistant ATCC 27853, MIC to colistin and doripenem are 1.0 and 0.25 mg/L) and two clinical isolates (colistin hetero-resistant C390, MIC to colistin and doripenem are 1.0 and 1.0 mg/L) and colistin resistant 19147, MIC to colistin and doripenem are >128 and 1.0 mg/L) were employed in in vitro hollow fiber infection models over 10 days with an initial inoculum of 10^9 colony forming units per mL (CFU/mL). Six clinically relevant dosage regimens of colistin and doripenem alone and in combination were simulated against all strains. The dosage regimens were growth control, colistin given as continuous infusion with steady state concentrations of 2 mg/L or 5 mg/L, doripenem given as C_{max} of 25 mg/L every 8 h (half-life of 1.5 h), colistin 2 mg/L and doripenem C_{max} 25 mg/L, and colistin 5 mg/L and doripenem C_{max} 25 mg/L. The total bacterial population and resistant subpopulations were quantified over 10 days. The colistin resistant subpopulations were quantified on agar plates containing 0.5, 1, 2, 3, 4, 6, 8 and 10 mg/L colistin. All viable counts were modeled simultaneously using the MCPEM importance sampling algorithm (S-ADAPT, pmethod = 4, v1.57) via SADAPT-TRAN. The bacterial concentrations on colistin containing agar plates were modeled as time-dependent functions of the different subpopulations. An additive residual error model on $\log_{10}$ scale was used for high bacterial concentrations and a Poisson error was included for low colony counts per agar plate.

Results: For ATCC 27853 and C390, three subpopulations were identified; including a colistin susceptible/doripenem susceptible, colistin intermediate/doripenem resistant, and colistin resistant/doripenem susceptible subpopulation. Two subpopulations were needed for colistin resistant strain 19147 (colistin resistant/doripenem intermediate and colistin resistant/doripenem resistant) as displayed in Fig. 1. A life cycle growth model [2] was able to describe the viable count profiles over 10 days for all strains with mean generation times

of 1.77, 2.50, and 12.5 h for ATCC 27853, C390, and 19147. A previously described colistin target site model was used [3]. Killing by colistin was modeled as a second-order process, and net killing by doripenem was model as a first order saturatable killing. To characterize the time course of synergy between colistin and doripenem, two models were developed: 'subpopulation synergy' mechanism (whereby antibiotic A kills the resistant subpopulation of antibiotic B and vice versa) [4] and 'mechanistic synergy' (i.e. antibiotic A enhances the activity of antibiotic B). Mechanistic synergy in addition to subpopulation synergy was needed to adequately describe killing by the combination. Modeling suggested that colistin enhanced killing by doripenem and that killing by colistin was not affected by doripenem. Doripenem alone was inactive against the doripenem-resistant subpopulation. However, in the presence of colistin, modeling suggested that colistin enhanced the killing activity by doripenem against its resistant subpopulation with a maximum rate (KmaxR) of 0.239 1 h for strain ATCC 27853 and 1.08 1 h for C390. In colistin resistant strain 19147, doripenem did not elicit any activity; however, in combination, colistin increased the maximum killing by doripenem for the doripenem-intermediate subpopulation from 0 to 0.3951 h without altering activity against the colistin resistant and doripenem resistant subpopulation. The population fits of all strains were reasonably precise and unbiased both for the total population and bacteria growing on colistin containing agar plates (Figs. 2, 3, 4).

Conclusions: Colistin combined with doripenem displayed rapid killing and suppressed emergence of resistance over 10 days in a dynamic hollow fiber infection model at clinically relevant drug concentrations. Colistin and doripenem achieved both subpopulation synergy and mechanistic synergy with colistin enhancing the rate of killing by doripenem. This is one of the first mechanism-based models to simultaneously characterize the time course of synergy and quantify multiple resistant subpopulations. This new approach holds great promise to rationally optimize innovative polymyxin combination regimens in patients and may serve as a framework to advance combination modeling for other infections.

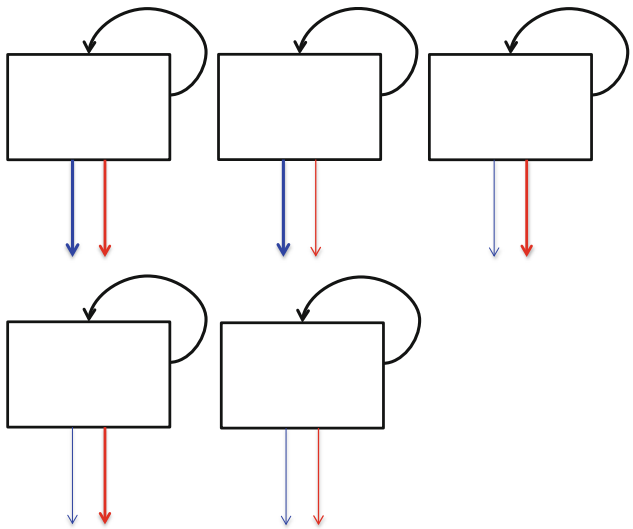

Fig. 1 Sup-population model including a colistin susceptible (Col^S), colistin intermediate (Col^I), colistin resistant (Col^R) and the respective doripenem (Dor) populations for strains: a) ATCC 27853 and colistin hetero-resistant C390, and b) colistin resistant 19147

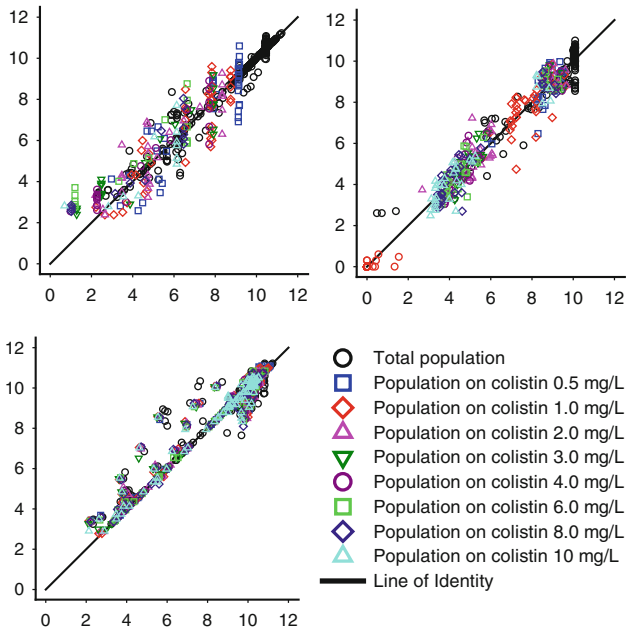

Fig. 2 Observed vs. population fitted $\log_{10}$ CFU/mL on antibiotic free and colistin containing agar plates for **a** ATCC27853, **b** colistin hetero-resistant C390, and **c** colistin resistant 19147

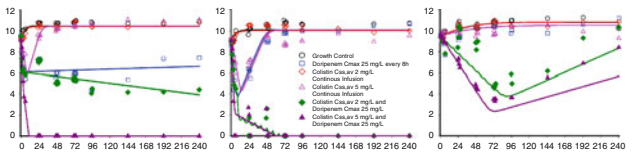

Fig. 3 Observed and population fitted log10 CFU/mL for strains **a** ATCC 27853, **b** colistin hetero-resistant C390, and **c** colistin resistant 19147

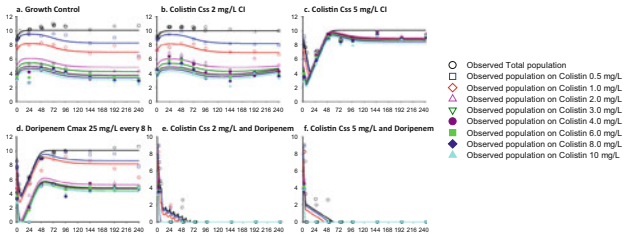

Fig. 4 Observed and population fitted $\log_{10}$ CFU/mL for colistin hetero-resistant C390 on antibiotic free agar plates and agar plates with different concentrations of colistin

References

[1] Jumbe N, Louie A, Leary R, et al (2003) J Clin Invest 112:275–285

[2] Bulitta JB, Ly NS, Yang JC, et al (2009) Antimicrob Agents Chemother 53:46–56

[3] Bulitta JB, Yang JC, Yohonn L, et al (2010) Antimicrob Agents Chemother 54:2051–2062

[4] Bulitta JB, Li J, Poudyal A, et al (2009) Abstract A1-573, 49th ICAAC, San Francisco

W-020 Physiologically-based Pharmacokinetic Modeling of Atorvastatin Acid and Major Metabolites in Stable Kidney Transplant Recipients with Diabetes Mellitus

Joyce S. Macwan[1*], Michael B. Bolger[2], Fatemeh Akhlaghi[1]

[1]Clinical Pharmacokinetics Research Laboratory, Department of Biomedical and Pharmaceutical Sciences, University of Rhode Island, Kingston, RI, USA; [2]Simulations Plus, Inc., 42505 10th Street West, Lancaster, CA 93534, USA

Objectives: To develop a whole-body physiologically-based pharmacokinetic (PBPK) model describing an oral absorption of atorvastatin acid and the formation of its major metabolites in stable kidney transplant recipients with diabetes mellitus using in silico and experimentally measured input parameters.

Methods: A clinical study was conducted in stable kidney transplant recipients with diabetes mellitus. Following a single oral administration of 40 mg atorvastatin calcium (Lipitor®, Pfizer Pharmaceuticals, NY, USA), several blood samples were collected at various time points 12 h post-dose. Quantitative determination of atorvastatin acid and its metabolites in plasma samples were performed using previously described validated liquid chromatography-tandem mass spectrometry method [1]. The absorption and pharmacokinetics of atorvastatin acid and three metabolites (atorvastatin lactone, *ortho*-hydroxy atorvastatin acid and *ortho*-hydroxy atorvastatin lactone) were simulated using GastroPlus™ 8.0 (Simulations Plus, Inc., Lancaster, CA, USA) simulation and modeling software. The program's Advanced Compartmental and Transit (ACAT™) model coupled with its generic PBPK™ module and Population Estimates of Age-Related Physiology (PEAR™) feature were used to predict systemic exposure of parent drug and its metabolites. The kinetic parameters of cytochrome P450 3A4 mediated metabolic clearance of atorvastatin acid and atorvastatin lactone measured using diabetic liver microsomes [2] were integrated in the model. *In vitro* dissolution studies of Lipitor® were carried out in different pH media to assess pH dependent acid-lactone inter conversion and release profile. The essential input parameters to construct PBPK model of atorvastatin acid were determined experimentally, in silico predicted and/or obtained from the literature. Tissue/plasma partition coeff-i cients were calculated using Berezhkovskiy and modified Rodgers algorithm for permeability (liver) and perfusion-limited (non hepatic) tissues, respectively. Parameter sensitivity analysis feature of GastroPlus™ was utilized to assess the sensitivity of predicted disposition parameters to key input parameters. Part of the validation process included virtual trial simulations to evaluate the combined effects of inter-individual variability in population physiology and the predicted disposition parameters along with formulation/compound specific properties using a whole-body PBPK model linked with Monte Carlo simulation.

Results: The predicted plasma concentration–time profiles of atorvastatin acid and three metabolites were in a good correlation with mean plasma concentration–time curves observed in study patients (Fig. 1a, b). Berezhkovskiy algorithm utilized to determine tissue distribution of permeability-limited tissues as it successfully estimated observed large volume of distribution of atorvastatin acid. Atorvastatin acid (BCS and BDDCS class II drug) was completely dissolved in dissolution medium with high pH such as ≥6.8 (Fig. 2a). However, dissolution studies performed in low pH medium including 1.2 and 3 indicated poor dissolution and simultaneous formation of lactone metabolite which is in accordance with results reported by Kearny et al. [3]. The formation of lactone form was higher at very low pH (pH 1.2) as compared to pH 3 (Fig. 2b) and its absence at higher pH reflected instability in basic medium. The systemic exposure of atorvastatin acid was under-predicted when measured in vitro dissolution *vs* time data were integrated in dissolution model could be because of significant differences between its aqueous and biorelevant solubility. The model under-predicted the observed plasma concentration–time profile when in vitro metabolism data measured using non diabetic livers were incorporated. The stochastic simulation performed using virtual trail feature of the software showed that the observed mean plasma concentration–time curve of atorvastatin acid lie between 90 % confidence interval, maximal and minimal simulated concentrations of ten virtual patients (Fig. 3). Parameter sensitivity analysis revealed that systemic exposure of atorvastatin acid is most sensitive to change in intestinal transit time. The predicted peripheral tissue distribution of atorvastatin acid was highest in muscle tissue that possibly explains higher incidences of myotoxicity in diabetic population [4].

Conclusions: A whole-body PBPK model was constructed to simulate systemic exposure of an orally administered atorvastatin acid and formation of major metabolites in stable kidney transplant recipients

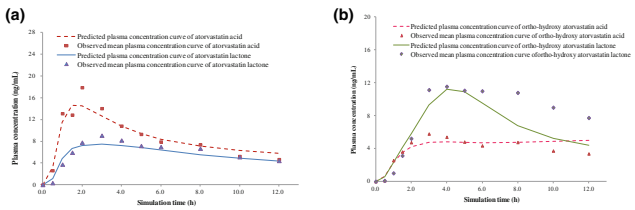

Fig. 1 **a** Predicted vs observed plasma concentrations: atorvastatin and atorvastatin lactone. **b** Predicted vs observed plasma concentrations: ortho-hydroxy atorvastatin acid and ortho-hydroxy atorvastatin lactone

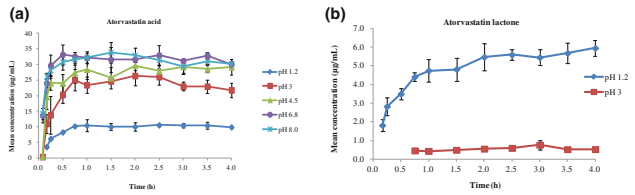

Fig. 2 **a** Atorvastatin acid over time by pH. **b** Atorvastatin lactone over time by pH

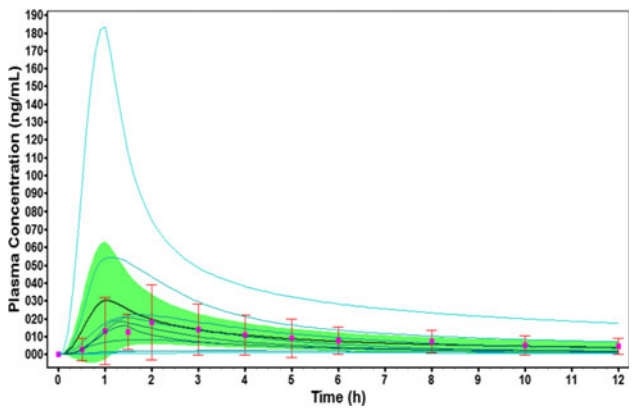

Fig. 3 Observed and simulated storvastatin concentration vs. time

with diabetes mellitus. This study also demonstrated that disease specific in vitro metabolic clearance data are superior for the appropriate prediction of systemic exposure of a drug that undergoes extensive metabolism, which might changed due to altered activity of drug metabolizing enzymes in specific disease state [5].

References

[1] Macwan JS, Ionita IA, Dostalek M, Akhlaghi F (2011) Anal Bioanal Chem 400(2):423–433

[2] Dostalek M, Sam WJ, Paryani KR, Macwan JS, Gohh RY, Akhlaghi F (2012) Clin Pharmacokinet 51(9):591–606

[3] Kearney AS, Crawford LF, Mehta SC, Radebaugh GW (1993) Pharm Res 10(10):1461–1465

[4] Graham DJ, Staffa JA, Shatin D, Andrade SE, Schech SD, La Grenade L, et al (2004) JAMA 292(21):2585–2590

[5] Dostalek M, Court MH, Yan B, Akhlaghi F (2011) Br J Pharmacol 163(5):937–947

Solid line shows the mean of simulated concentrations of ten subjects. Square with error bar represents the mean of observed clinical plasma concentrations. The green highlighted area represents 90 % confidence interval of simulated concentrations data around mean. The solid blue, dashed, and dotted lines represent individual simulated results that incorporate 100, 95, 90, 75, 50, 25, and 10 % of the range of simulated data.

W-021 Keep on Walking: Pharmacokinetic-Pharmacodynamic (PK-PD) Analysis and Dose Selection Support for Ataluren in the Treatment of Nonsense Mutation Duchenne–Becker Muscular Dystrophy (nmDBMD)

Scott Van Wart[1,*], Murad Melhem[1], Jay Barth[2], Christopher Rubino[1], Gary Elfring[2], Valerie Northcutt[2], John Babiak[2], Paul Ambrose[1]

[1]Institute for Clinical Pharmacodynamics, Latham, NY, USA; [2]PTC Therapeutics, Inc., South Plainfield, NJ, USA

Background and Objectives: nmDBMD is a childhood disease caused by a genetic mutation resulting in the lack of production of functional dystrophin protein required to stabilize muscle cell membranes. Ataluren can enable ribosomal readthrough of premature stop codons and is under development for the treatment of nmDBMD. Despite increased production of the missing dystrophin protein in vitro, there was an attenuation of response at higher ataluren concentrations resulting in a bell-shaped concentration–response relationship. The goals here were to: (A) develop an integrated population PK-PD and disease progression model to characterize the impact of ataluren therapy on ambulation in pediatric and adolescent nmDBMD patients, and (B) use the integrated model to assess the potential impact of ataluren on disease progression of nmDBMD.

Methods: Data were obtained from a randomized, multicenter, double-blind, placebo-controlled, dose-ranging Phase 2b study conducted by PTC Therapeutics in 173 pediatric nmDBMD patients ages 5–17 years. Patients were randomized (1:1:1 ratio) to one of three thrice daily (morning/midday/evening) treatment regimens to receive placebo or ataluren at either 10/10/20 mg/kg or 20/20/40 mg/kg for 48 weeks. At the completion of blinded treatment, patients were eligible to receive open-label ataluren (20/20/40 mg/kg) for an additional 48 weeks. Blood samples were collected on multiple occasions to determine plasma ataluren concentrations. Patient height (HTCM) and weight was recorded, and ambulation was assessed using a modified American Thoracic Society (ATS) 6-min walk test (6MWT) to determine 6-min walking distance (6MWD), at screening, at baseline and every 6 weeks during treatment for up to 96 weeks. The approach used to develop the integrated nmDBMD disease-progression and ataluren PK-PD model, as well as the process used to support ataluren dose selection, is highlighted in Fig. 1. All analyses were conducted using NONMEM 7.

Results: In Stage 1, a 2-compartment (CMT) population PK model was shown to best describe the ataluren PK data from healthy adults. The adult ataluren PK model was subsequently bridged to the pediatric and adolescent nmDBMD patient data using body weight and disease-state indicators as covariate effects (ISoP 2013 abstract by Murad Melham). For each patient, a steady-state area under the plasma concentration–time curve over 24 h was calculated and divided by 24 to obtain an average steady-state ataluren concentration (C_{ave}) for use in PK-PD analyses. In Stage 2, a sigmoidal Hill-type model best characterized the expected increase in 6MWD (GROW) as a function of HTCM in healthy children using a naïve pooled modeling approach and data obtained from literature studies by Lammers

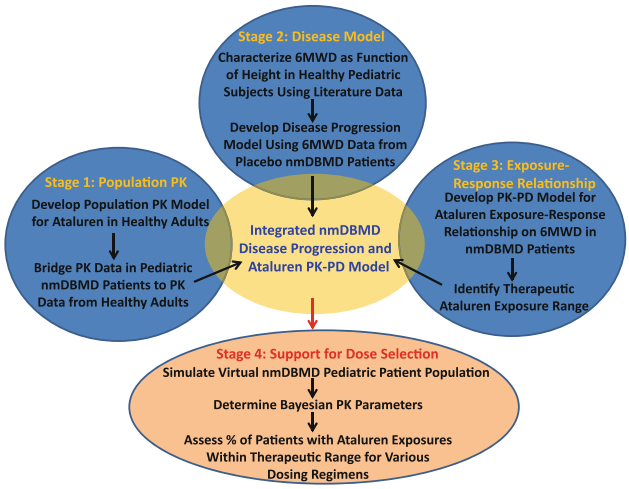

Fig. 1 Development of integrated nmDBMD disease progression and ataluren PK-PD model to support dose selection

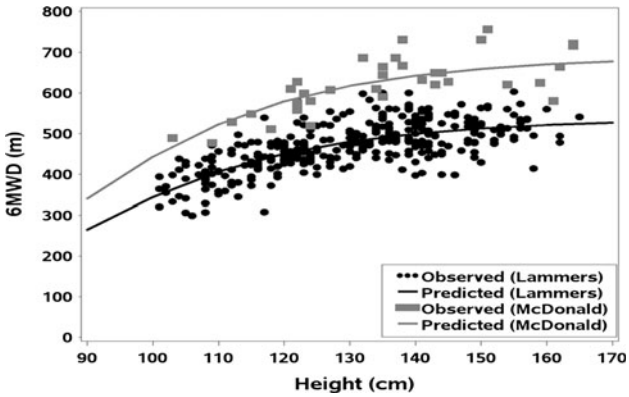

Fig. 2 Sigmoidal Hill-type model for the relationship between 6MWD and HTCM in healthy children

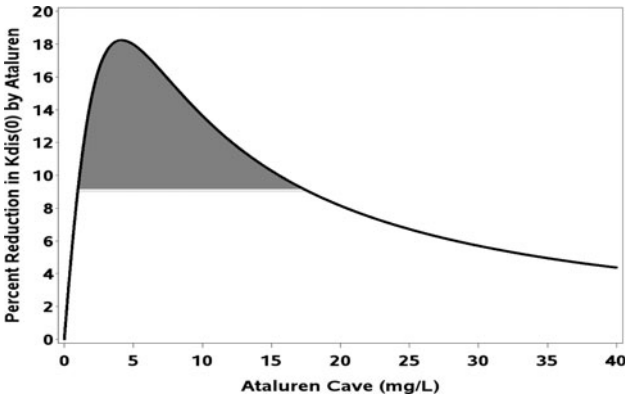

Fig. 3 %Reduction in $k_{dis(0)}$ as a function of ataluren C_{ave}; shaded area depicts C_{ave} producing ≥50% maximal effect

et al. [1] and McDonald et al. [2]. Statistically significant differences in $6MWD_{max}$ were detected between studies (Fig. 2), while $HTCM_{50}$ and γ were similar. The equation for the McDonald data (Eq. 1) was used to project 6MWD in nmDBMD patients as HTCM increased during the study, since this investigator used the same modified ATS 6MWT as did PTC Therapeutics.

$$GROW_{(t)} = \frac{696 \cdot HTCM_{(t)}^{5.72}}{90.7^{5.72} + HTCM_{(t)}^{5.72}} \quad (1)$$

An indirect response (IDR) model was used to characterize the time-course of 6MWD in nmDBMD patients receiving placebo for 48 weeks. The maximum possible zero-order growth rate [$k_{in,max(t)}$] was determined as the product of GROW(t) and k_{out} (estimated to be 0.520 $week^{-1}$). The core underlying assumption for the disease model was that nmDBMD patients function at some fraction (FUNC) of the 6MWD expected for a HTCM-matched healthy child. The initial starting 6MWD was the product of $GROW_{(t)}$ and FUNC, which was significantly related to age (Eq. 2) suggesting older children at same HTCM are more debilitated. Individual FUNC estimates were constrained between 0 and 1 using a logistic transform. Examination of the placebo nmDBMD patient data showed the onset of disease progression may be delayed or even non-existent during the study. A 3-CMT transduction model featuring a first-order disease progression rate [$k_{dis(0)}$, which was parameterized as a function of baseline 6MWD as shown in Eq. 3] was used to allow FUNC to decline to FUNC2 to account for continued and potentially delayed disease progression in the IDR model (Eq. 4).

$$FUNC = 1 - \frac{Age}{11.1 + Age} \quad (2)$$

$$k_{dis(0)} = 0.0106 \cdot \left(\frac{Baseline6MWD}{350}\right)^{-3.06} \quad (3)$$

$$\frac{d6MWD}{dt} = FUNC2 \cdot k_{in,max(t)} - k_{out} \cdot 6MWD, \quad IC = GROW \cdot FUNC \quad (4)$$

In Stage 3, both sigmoidal Hill-type and bell-shaped [3] PK-PD models were evaluated to characterize the reduction in $k_{dis(0)}$ (slowing nmDBMD disease progression) as a function of ataluren C_{ave} using data from both placebo and on-treatment groups. The bell-shaped model (estimating $K_D = 9.29$ mg/L and $K_2 = 0.540$ mg/L as shown in Eq. 5) provided the better fit to the data. As shown in Fig. 3, the maximum reduction in $k_{dis(0)}$ was 18.2 %; ataluren C_{ave} between 0.97 and 17.6 mg/L produced ≥50 % of the maximum reduction and served as the targeted therapeutic ataluren exposure range.

$$k_{dis} = k_{dis(0)} - \left(\frac{k_{dis(0)} \cdot C_{ave}}{9.29 + C_{ave} + 0.540 \cdot (C_{ave})^2}\right) \quad (5)$$

In Stage 4, Monte Carlo simulations were performed to generate 5000 virtual pediatric nmDBMD patients having similar demographic distributions as the studied nmDBMD patients. The virtual nmDBMD patients were administered various ataluren dosing regimens and Bayesian ataluren PK parameters and C_{ave} values were obtained. A greater number of nmDBMD patients treated with 10/10/20 mg/kg ataluren (98.3 %) were predicted to have ataluren C_{ave} in the targeted therapeutic exposure range as compared to the 20/20/40 mg/kg ataluren (65.2 %), supporting use of the 10/10/20 mg/kg ataluren treatment regimen.

Conclusions: An integrated nmDBMD disease progression and ataluren PK-PD model, incorporating data across multiple studies and data sources, was developed and used to support ataluren dose selection for this indication.

References

[1] Lammers AE, Hislop AA, Flynn Y, Haworth SG (2008) Arch Dis Child 93:464–468

[2] McDonald CM, Henricson EK, Han JJ, et al (2010) Muscle Nerve 41:500–510

[3] Adair GS (1925) J Biol Chem 63:529–545

W-022 Exposure–Response Analysis to Assess the Proposed Starting Dose of Pasireotide for the Treatment of Cushing's Disease

Jing-yu Yu[1,*], Sang Chung[2], Immo Zadezensky[2], Nitin Mehrotra[1]

[1]Division of Pharmacometrics, Office of Clinical Pharmacology, CDER, FDA, Silver Spring, MD, USA; [2]Division of Clinical Pharmacology 2, Office of Clinical Pharmacology, CDER, FDA, Silver Spring, MD, USA

Objectives: On December 14 2012, FDA approved pasireotide for the treatment of adult patients with Cushing's disease for whom pituitary surgery is not an option. Cushing's disease is a rare endocrine disease caused mostly by histologically benign ACTH-secreting pituitary tumors. Currently there are ~17,000 patients living with Cushing's disease in United States. The registration trial included two arms with two different dosing regimens, 0.6 mg b.i.d. and 0.9 mg b.i.d., but the trial was not powered to compare the efficacy and safety between two dose regimens. At Month 6, the percentages of responders for the primary efficacy endpoint were 15 and 26 % in the 0.6 mg b.i.d. and 0.9 mg b.i.d. groups, respectively. Only 0.9 mg b.i.d dose met the pre-specified primary end point. The objective of this analysis is to compare the efficacy and safety profile for the two dosing regimens from exposure–response (E–R) perspective.

Methods: A multivariate logistic regression was conducted to assess the E–R relationship for efficacy and safety endpoints and identify the covariates that predict response. The exposure metric used in E–R analysis was observed steady state pre-dose C_{min} (or average C_{min}) of each individual at a corresponding time of interest (e.g., Month 3 or 6). The efficacy assessment was based on mean of urinary free cortisol (mUFC) values. The primary efficacy variable was defined as the proportion of responders in each dose arm. A responder was defined as a patient who attained mUFC ≤ ULN (145 nmol/day) at Month 6 and whose dose was not increased relative to the randomized dose

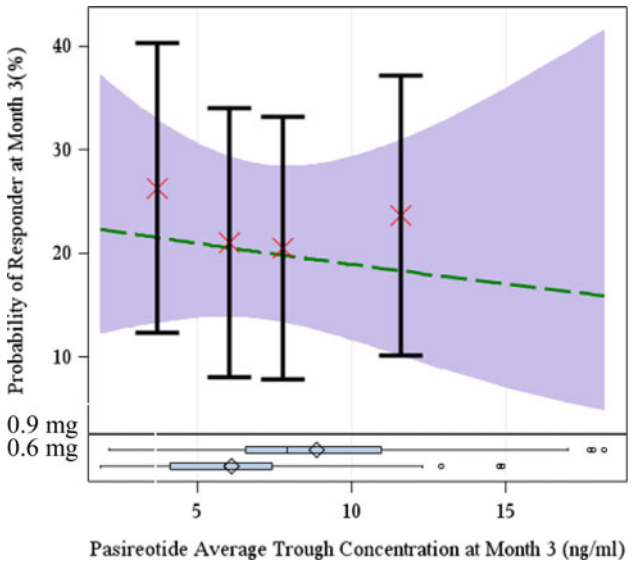

Fig. 1 No evident relationship between exposure and response rate after adjusting for baseline mUFC. Logistic regression model includes the probability of responder at month 3 as a function of average pasireotide concentration at month 3 after controlling for baseline mUFC (Ctrough p value = 0.65; Baseline mUFC p value = 0.046). The mean and 95 % CI of the observed response rate versus the median of observed trough concentration quartile is represented by black bars while dashed green line and purple band represent the model predicted mean and 95 % interval of response rate. The box plots at the bottom represent the distribution of trough concentration in each dose group

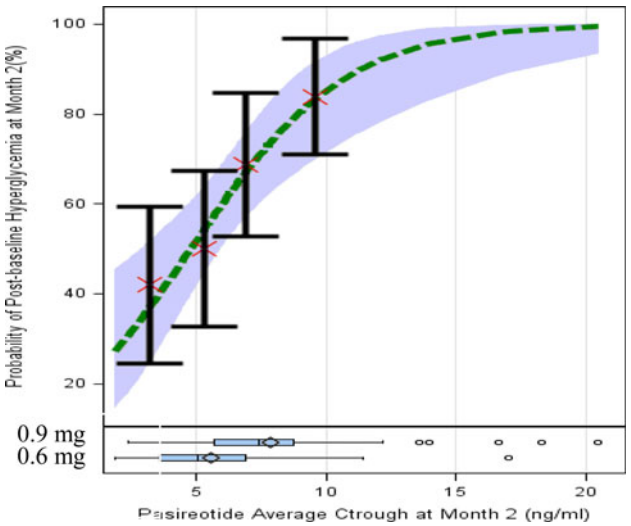

Fig. 2 Increase in probability of developing post-baseline hyperglycemia (>1% HbA1c increase from baseline) at month 2 with the Increase of Exposure in all Patients after adjusting for baseline HbA1c. Logistic regression model includes the probability of post-baseline hyperglycemia at month 2 as a function of average pasireotide concentration at month 2 after controlling for baseline HbA1c (Ctrough p value = 0.0004; baseline HbA1c p value = 0.045). The mean and 95 % CI of the observed response rate versus the median of observed trough concentration quartile is represented by black bars while dashed green line and purple band represent the model predicted mean and 95 % interval of probability of post-baseline hyperglycemia. The box plots at the bottom represent the distribution of trough concentration in each dose group

prior to Month 6. Since the main adverse event associated with the pasireotide therapy was hyperglycemia, the E-R analysis for safety focused on the proportion of the patients who had post-baseline increase of more than 1 % in HbA1C. The following covariates were evaluated in the analysis: baseline mUFC, baseline HbA1C, baseline ALT, prior medication, prior pituitary irradiation, prior pituitary surgery, gender, race, age, and BMI.

Results: Despite the fact that the median trough concentration is 50 % higher in 0.9 mg b.i.d. dose group compared to 0.6 mg b.i.d. dose group, there is a substantial overlap in exposures between these two dose groups due to the high inter-subject variability in pharmacokinetics. We did not find a clear relationship between exposure (i.e., average trough concentration) and probability of response at Month 3 (Fig. 1), suggesting no significant additional benefit of 0.9 mg b.i.d. over 0.6 mg b.i.d. The results are consistent if response at Month 6 is used as the response variable and average steady state concentration over 6 months as the exposure variable. In addition, exposure–response analysis was also conducted using mUFC as a continuous variable for efficacy and conclusions regarding the E-R relationship for efficacy remain the same. E-R analysis for safety indicated that there is a clear trend toward increasing probability of experiencing $\geq$1 % post-baseline increase of HbA1C with the increasing exposures (Fig. 2), suggesting that 0.9 mg b.i.d. may result in a higher probability of post-baseline hyperglycemia than the 0.6 mg b.i.d. dosing regimen.

Conclusions: Overall, exposure–response analysis suggests that 0.6 mg b.i.d. may be as effective as 0.9 mg b.i.d., and will provide better hyperglycemia-related safety profile than 0.9 mg b.i.d. for all patients. However, due to the high unexplained variability in response, 0.9 mg b.i.d. may be beneficial for some patients as a starting dose or for whom not responding to 0.6 mg b.i.d. and should be allowed as an option. Even though 0.6 mg b.i.d dose did not meet the primary end point, both 0.6 mg and 0.9 mg b.i.d were approved as starting doses with an option of titrating based on response and tolerability. Exposure–response analyses were pivotal in enhancing our understanding of the adequacy of the proposed starting dose for Pasireotide.

References

[1] Pasireotide label: http://www.accessdata.fda.gov/drugsatfda_docs/label/2012/200677lbl.pdf

[2] Pasireotide approval letter: http://www.accessdata.fda.gov/drugsatfda_docs/appletter/2012/200677Orig1s000ltr.pdf

W-023 Population Pharmacokinetic (PK) Analyses to Bridge Ataluren Disposition Between Healthy Adults and Patients with Nonsense Mutation Duchenne–Becker Muscular Dystrophy (nmDBMD)

Murad Melhem[1], Scott Van Wart[1,*], Christopher Rubino[1], Paul Ambrose[1], Gary Elfring[2], Valerie Northcutt[2], Jay Barth[2]

[1]Institute for Clinical Pharmacodynamics, Latham, NY, USA; [2]PTC Therapeutics, Inc., South Plainfield, NJ, USA

Objectives: nmDBMD is a childhood disease caused by a genetic mutation resulting in the lack of production of functional dystrophin protein required to stabilize muscle cell membranes. Ataluren can enable ribosomal readthrough of premature stop codons and is under development for the treatment of nmDBMD. The objectives of this analysis were to: (a) characterize ataluren PK in both healthy subjects and the intended patient population of pediatric and adolescent patients with nmDBMD, bridging any potential PK differences among age groups or between healthy subjects and patients; and (b) generate ataluren exposure measures to facilitate the exploration of efficacy PK-PD relationships in pediatrics and adolescents with nmDBMD.

Methods: Data for the development of a population PK model for ataluren were derived from two Phase 1 studies in healthy adult volunteers (ages 18–30 years) and four Phase 2 studies conducted in nmDBMD patients (ages 5–17 years). All subjects had at least one PK sample and the majority (approximately 70 %) had 35 or more samples following single or multiple dose administration of ataluren. Structural population PK compartmental models were evaluated using data from healthy adult volunteers. The 2-compartment model was parameterized using a first-order absorption rate constant (k_a), apparent clearance (CL/F) and central volume of distribution (Vc/F), and the apparent distribution clearance (CLd/F) and peripheral volume of distribution (Vp/F). The impact of food on the rate and extent of absorption, and the impact of diurnal variation on CL/F were also assessed. The model parameters were re-estimated after pooling the data from both the healthy adults and nmDBMD patients to allow testing for potential differences between healthy adults and nmDBMD patients, as required. To explore subject covariates as predictors of PK parameters, a formal covariate analysis was conducted using forward selection ($\alpha = 0.01$) followed by backward elimination ($\alpha = 0.001$) procedures. The final model was evaluated/qualified using a prediction-corrected visual predictive check (pcVPC) [1]. All population PK analyses were conducted using NONMEM®, Version 7, level 1.2 [2].

Results: A two-compartment model with first-order absorption and linear elimination (Table 1) best described ataluren plasma concentration–time profiles in pooled data from healthy adults ($N = 61$) and nmDBMD patients ($N = 211$). Interindividual variability in parameters were estimated using exponential error models, while residual error was modeled as an additive error structure in the logarithmic domain. The population PK model estimated a higher relative bioavailability (1.91-fold higher) for healthy adults relative to that of nmDBMD patients. Diurnal variation for the ataluren CL/F was also included in the final model to account for higher observed drug concentrations following evening doses. The model estimated a 39.2 % higher ataluren CL/F following morning or mid-day doses relative to the CL/F following evening doses. Body weight was also identified as a statistically significant predictor of both CL/F and Vc/F; k_a was predicted to decrease with increasing dose using a power function. No statistically significant effect of food was detected on either the rate or extent of ataluren absorption ($p = 0.103$ and 0.109, respectively).The results of the pcVPC (Fig. 1) suggested negligible prediction bias. Generally, the bulk of the prediction-corrected observed data are contained within the prediction interval and the central tendencies in corrected observed data were adequately captured with corrected predictions.

Conclusions: A two-compartment population PK model was developed to describe ataluren disposition in healthy volunteers and patients pediatric/adolescent with nmDBMD. The model estimated a 39.2 % higher ataluren CL/F following morning or mid-day doses relative to the CL/F following evening doses. A higher relative bioavailability was estimated in healthy adults relative to nmDBMD patients. Body weight was identified as a statistically significant predictor of both apparent oral clearance and apparent oral central volume of distribution. Ataluren absorption rate was predicted to decrease with increasing dose. The final population PK model was qualified and was subsequently used for generating ataluren exposures in nmDBMD patients in order to assess the pharmacokinetic-pharmacodynamic relationships for efficacy.

Table 1 Parameter estimates and associated standard errors from the final population PK model fit to the pooled data from healthy adults and nmDBMD patients

Parameter	Final parameter estimate	%SEM
CL/F for evening (PM) dosing (L/h)[a]	5.63	3.27
V_c/F(L)[b]	38.9	8.46
V_p/F(L)	1.28	29.5
CL_d/F (L/h)	0.0668	51.5
Power coefficient from the relationship between ataluren dose (in mg) and ka[c]	16.8	78.0
Power exponent from the relationship between ataluren dose (in mg) and k_a	−0.436	32.8
Proportional shift in CL/F for morning or mid-day dosing (AM)	0.392	12.2
Fold increase in F for healthy subjects relative to nmDBMD patients	1.91	10.1
Power coefficient from the relationship between weight and CL/F	0.438	20.8
Power coefficient from the relationship between weight and V_c/F	0.299	62.9
$\omega^2_{CL/F}$	0.139 (37.28 %CV)	10.9
Covariance (CL/F, V_c/F)	0.123	16.4
$\omega^2_{Vc/F}$	0.202 (44.99 %CV)	22.4
$\omega^2_{Vp/F}$	0.168 (40.99 %CV)	40.1
Residual variability (log SD)	0.606	3.57

[a] Population mean CL/F (L/h) = $[5.63\bullet(1 + 0.392\bullet AM)]\bullet(WTKG_j/31.4)^{0.438}$, where AM = 0 for an evening dose and 1 for either morning or mid-day doses

[b] Population mean $V_c/F(L) = 38.9\bullet(WTKG_j/31.4)^{0.299}$

[c] Population mean ka (h^{-1}) = $16.8\bullet Dose^{-0.436}$

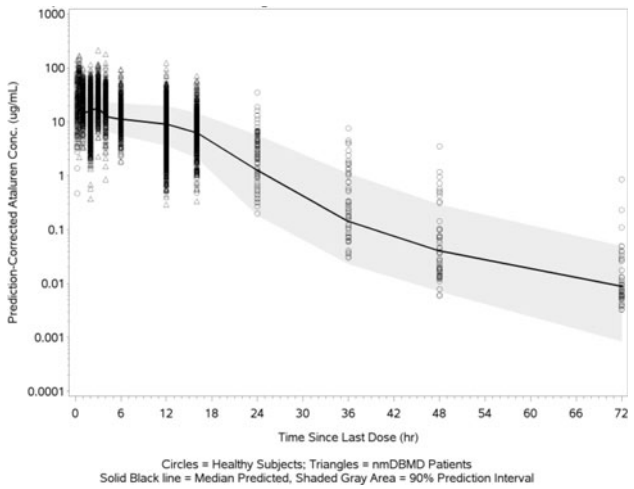

Fig. 1 Prediction-corrected visual predictive check for the final population PK model for ataluren in pooled data from healthy adults and nmDBMD patients

References

[1] Bergstrand M, Hooker AC, Wallin JE, Karlsson MO (2011) Prediction-corrected visual predictive checks for diagnosing nonlinear mixed-effects models. AAPS J 13(2):143–151

[2] Beal SL, Sheiner LB (1992) NONMEM® Users Guides.: Globomax, LLC, Hanover

W-024 Handling of Inter Occasion Variability (IOV) in Individual Optimal Design (OD) of a Colistin PK Sampling Schedule

Anders N. Kristoffersson*, Lena E. Friberg, Joakim Nyberg

Department of Pharmaceutical Biosciences, Uppsala University, Uppsala, Sweden

Objectives: The aim of individual optimal design with a population prior (inter individual variability, IIV) is to optimize the experimental design with respect to the precision of the maximum a posteriori (MAP) estimated individual parameters. Methods of individual optimal design have been investigated by Merlé and Mentré [1] and a variant of the Bayesian information matrix termed FIM maximum a posteriori (FIM_{MAP}) has been applied by, e.g. Hennig et al. [2]. Frequently in mixed effect models inter occasion variability (IOV) is present, but how to handle this additional variability in individual optimal design has not been investigated. This work aims to explore additions to the previously described FIM_{MAP} to handle the presence of IOV in terms of individual parameter precision and calculation runtimes for the design of a colistin PK study.

Methods: To calculate the FIM_{MAP} the prior population model is transformed to an individual model which is integrated over all possible individual values, i.e. the prior population variance, Ω (Eqs. 1 and 2). The expected variance of the individual parameters may then be minimized by maximizing the determinant of the FIM_{MAP}.

$$p_{i,k} = \theta_k * e^{\eta_{ik}} \overset{\eta_{ik} \to \theta_{ik}}{\Rightarrow} \theta_k * e^{\theta_{ik}}, \theta_{ik} \sim N\left(0, \omega_k^2\right) \quad (1)$$

where $p_{i,k}$ is the k^{th} parameter for individual i, θ_k is the k^{th} typical population parameter, η_{ik} is the individual deviation from θ_k for individual i in the population model, θ_{ik} is the deviation from θ_k in the individual model and ω_k^2 is the population variance of η_k

$$FIM_{MAP} = E_\Omega[FIM(X, \Theta)] + \Omega^{-1} \approx \frac{1}{n}\sum_{i=1}^{n} FIM(X, \Theta_i) + \Omega^{-1} \quad (2)$$

where n is the number of individual parameter sets sampled, X is the design, Θ_i is the parameter vector for individual i, and Ω the population prior IIV covariance matrix

Three strategies to include IOV in the FIM_{MAP} were investigated: (i) Inflate—The prior was inflated with the IOV through model re-estimation (Eq. 3) (ii) Random—The IOV variability was included in the individual FIM as a population occasion random effect parameter. (Eq. 4) (iii) MAPocc—The occasion variability was added to the individual FIM as fixed effect occasion parameter sampled per occasion from the prior IOV distribution (Eq. 5). As comparison the optimization was performed without IOV included, termed Ignore below.

$$\text{Inflate:} FIM_{MAP,i} = FIM\left(X, \left\{\Theta_\theta, \Theta_{\eta i}\right\}\right) + \Omega^{*-1} \quad (3)$$

where Θ_θ is the vector of population parameters, $\Theta_{\eta i}$ is the vector of deviations from the typical population parameters for individual i, and Ω^* is the population prior covariance matrix inflated to include IOV

$$\text{Random:} FIM_{MAP,i} = FIM\left(X, \left\{\Theta_\theta, \Theta_{\eta i}, \Pi\right\}\right) + \text{diag}\left(\Omega^{-1}, 0_{p,p}\right) \quad (4)$$

where Π is the covariance matrix for the IOV, $0_{p,p}$ is a zero matrix of dimension p*p and p is the number of occasion effects in the population model.

$$\text{MAPocc } FIM_{MAP,i} = FIM\left(X, \left\{\Theta_\theta, \Theta_{\eta i}, \Theta_{\kappa 1,i}, \Theta_{\kappa 2,i} \ldots, \Theta_{\kappa K,i}\right\}\right) + \text{diag}\left(\Omega, \Pi_1, \Pi_2 \ldots, \Pi_K\right)^{-1} \quad (5)$$

where $\Theta_{\kappa j,i}$ is the vector of occasion deviations for the jth occasion of the ith individual, K is the number of occasions and $\Pi_j = \Pi$

The investigated Colistin PK model included IIV and IOV variability [3], with the optimization focused on precision of the individual deviations of colistin and CMS clearance (η_{CL}), intercompartmental CL of CMS (η_Q) and colistin residual error (η_{RE}). The design was based on a dosing regimen of 9 MU (720 mg) CMS as load (30 min infusion), followed by a maintenance dose of 4.5 MU q12 with one occasion per dose interval. Schedules of 3 or 6 sampling times over 36 h (three occasions) were investigated with sampling prohibited during or up to 15 min post infusion.

The optimization was performed by the ED_s criteria in combination with a prior FIM in the PopED optimal design software [4] based on 45 samples per FIM evaluation with the individual deviation parameters (η_{CL}, η_Q, η_{RE}) set as interesting.

The designs were evaluated based on 300,000 individual simulations and MAP re-estimations in NONMEM7 for which the expected standard deviation (SD) of the parameter Empirical Bayes estimates (EBE:s) were obtained as well as the observed Root Median Squared Error (RMSE). These were compared with the expected SD as calculated from the expectation of the PopED inverse FIM_{MAP}.

Results: The results from the design optimization and evaluation are summarized in Table 1. The methods MAPocc and Random place all samples in the first occasion (first 12 h) whereas methods Ignore and Inflate provide identical designs and populate all three occasions. The PopED and NONMEM expected SD corresponds well for methods MAPocc and Random whereas the PopED expected η_{Cl} SD is severely underpredicted for methods Ignore and Inflate. The designs for methods MAPocc and Random improves the NONMEM expected SD for parameter η_Q and the NONMEM simulated RMSE for parameters η_Q and η_{ER}. The design is saturated (addition of more samples result in replicates) at three samples for methods

Table 1 The optimal sampling times (3 or 6) for the three IOV inclusion methods, Inflate, MAPocc and Random, as well as the comparator, Ignore, are summarized below along with the expected (expressed in SD) and simulated (expressed as RMSE) uncertainty for the individual EBE:s. Sampling points in the first occasion are coded in blue, in the second purple and in the last red

	Method	Sampling time (h)						PopED Exp. SD			NONMEM Exp. SD			NONMEM Sim. RMSE		
		1	2	3	4	5	6	ηCL	ηQ	ηER	ηCL	ηQ	ηER	ηCL	ηQ	ηER
3 samples	Ignore	1.2	21.8	27.5				0.06	0.90	0.32	0.19	1.08	0.32	0.14	0.71	0.78
	Inflate	1.2	21.8	27.5				0.06	1.30	0.39	0.19	1.08	0.32	0.14	0.71	0.78
	MAPocc	0.8	4.3	9.9				0.21	0.86	0.32	0.19	0.70	0.32	0.14	0.56	0.46
	Random	0.8	2.9	6.4				0.21	0.82	0.39	0.23	0.75	0.32	0.16	0.55	0.41
6 samples	Ignore	0.8	0.8	0.8	0.8	23.9	31.8	0.05	0.67	0.25	0.18	1.05	0.25	0.13	0.69	0.33
	Inflate	0.8	0.8	0.8	0.8	23.9	31.8	0.05	0.89	0.29	0.18	1.05	0.25	0.13	0.69	0.33
	MAPocc	0.8	0.8	0.8	4.3	9.3	11.3	0.19	0.79	0.25	0.17	0.67	0.25	0.11	0.45	0.26
	Random	0.8	0.8	0.8	0.9	5.0	11.3	0.17	0.74	0.29	0.18	0.71	0.25	0.12	0.47	0.26

Ignore and Inflate and at four samples for methods MAPocc and Random.

The runtimes for one FIM calculation in PopED were 0.06, 0.06, 0.11 and 2.3 s for methods Ignore, Inflate, MAPocc and Random respectively for the 3 sample design.

Conclusions: Methods MAPocc and Random that directly include the IOV in the FIM_{MAP} improve on ignoring IOV both with respect to the correspondence between PopED and NONMEM predicted EBE SD as well as the overall NONMEM predicted and simulated EBE imprecision and bias. Methods Ignore and Inflate resulted in identical designs and similar PopED predicted parameter SD, possibly due to the small difference between the prior and the IOV inflated relative to the FIM. Here methods MAPocc and Random place all samples in the first occasion which minimize the contribution of IOV to the FIM. Method MAPocc is in this case faster and results in slightly improved predicted and simulated EBE SD and RMSE compared to method Random. In conclusion, three methods to include IOV in individual optimal design were tested. It was found that including the IOV directly in the FIM was superior to either ignoring IOV or inflating the prior to include IOV.

References

[1] Merlé, Y, Mentré F (1995) Bayesian design criteria: computation, comparison, and application to a pharmacokinetic and a pharmacodynamic model. J Pharmacokinet Pharmacodyn 23(1):101–125

[2] Hennig S, et al (2012) Application of the optimal design approach to improve a pretransplant drug dose finding design for Ciclosporin. J Clin Pharmacol 52(3):347–360

[3] Mohamed AF, et al (2012) Application of a loading dose of colistin methanesulphonate (CMS) in critically ill patients: population pharmacokinetics, protein binding and prediction of bacterial kill. Antimicrob Agents Chemother 56(8):4241–4249

[4] Nyberg J, et al (2012) PopED: an extended, parallelized, nonlinear mixed effects models optimal design tool. Comput Methods Prog Biomed 108(2):789–805

W-025 Physiologically Based Pharmacokinetic (PBPK) Modeling of Amoxicillin in Neonates and Infants

Viera Lukacova*, Michael B. Bolger, Walter S. Woltosz

Simulations Plus, Inc., Lancaster, CA, USA

Objectives: An amoxicillin PBPK model was previously developed and validated in typical healthy adults as well as adults with altered renal function. The purpose of this study was to explore the utility of the model in describing amoxicillin pharmacokinetics (PK) in neonates and infants.

Methods: An absorption/PBPK model for amoxicillin was previously developed [1] using GastroPlus™ 8.0 (Simulations Plus, Inc., Lancaster, CA). The program's Advanced Compartmental Absorption and Transit (ACAT™) model described the absorption of the drug, while PK was simulated with its PBPKPlus™ module. Intestinal absorption and tissue distribution included components of both passive diffusion and carrier-mediated transport. Total clearance consisted of renal (major) and hepatic (minor) components. Physiological parameters were generated by the program or obtained from literature. Certain drug-dependent parameters were obtained by fitting against reported plasma concentration–time (Cp-time) profiles and amounts secreted in urine after amoxicillin *i.v.* and *p.o.* administration in healthy volunteers. The model was further validated by predicting amoxicillin PK in different adult populations [2]. Physiologies for infants and neonates were based on information collected from literature. Aside from body weight, height and individual tissue sizes and blood flows, the parameters with a large effect on amoxicillin pharmacokinetics include changes in extracellular water in very young infants, glomerular filtration rate, and renal transporters. Fraction unbound in plasma and blood-to-plasma concentration ratio were also adjusted to account for infant plasma protein levels and hematocrit. Literature information on ontogeny of relevant renal transporters was not found. The PBPK model, along with observed amoxicillin Cp-time profiles after *i.v.* administration was used to estimate the expression of renal transporters in different groups of infants.

Results: The previously developed adult PBPK model for amoxicillin correctly predicted amoxicillin volume of distribution in neonates and infants after incorporating physiological parameters relevant for this population, i.e., tissue sizes, extracellular water volume, and slow passive diffusion across tissue membranes. In adults, the renal clearance consisted of contributions from both passive glomerular filtration and active tubular secretion. In the current model, the glomerular filtration rate (GFR) was incorporated as reported in the literature for different ages of full-term and pre-term infants [3-4]. Transporter expression levels in kidney were fitted against observed Cp-time profiles from some studies and validated by using the final model to simulate amoxicillin PK in subjects of similar age from different studies. Results for the youngest group (1–3-day-old neonates born on average 11 weeks premature) are shown in Fig. 1. The data after 25 mg/kg *i.v.* administration [5] was used to scale the renal transporters (Fig. 1a). The final model was used without any further changes to predict amoxicillin PK after 50 mg/kg *i.v* administration (Fig. 1b) from a different study [6].

Both GFR estimated from literature data [3–4] and fitted renal transporter levels were very low for these premature neonates: estimated GFR was ~10 % of the adult value (when expressed per 1.73 m^2), fitted renal transporter levels per g of tissue were 1 % of adult levels. The differences in scaling for GFR and renal transporter levels are in line with the reported different rates of maturation of GFR and active tubular secretion [5]. The final model was used to explore potential sources of observed variability in amoxicillin PK in infants.

Conclusions: Amoxicillin is eliminated primarily by renal secretion with a minor contribution from liver clearance (metabolism and biliary secretion). A physiological model that included relevant distribution and clearance mechanisms was previously fitted and validated against data for different adult populations. In the current work the model was applied to simulations of amoxicillin PK in neonates and infants: (1) to fill-in missing pieces of physiological

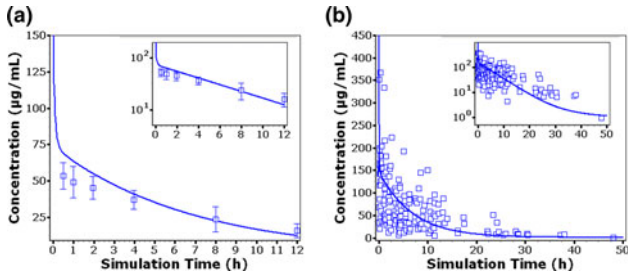

Fig. 1 Simulated (*lines*) and observed (*points*) PK profiles of amoxicillin after *i.v.* administration in preterm neonates (average gestational age 29 weeks). **a** 25 mg/kg dose on day 3 after birth (observed data are from [5]), **b** 50 mg/kg dose on days 1–3 after birth (observed data are from [6])

information (scaling of renal transporter expressions) using available in vivo data which could be used to predict PK of similar drugs; and (2) to explore sources of variability in amoxicillin PK in young children and provide useful insights into the drug's behavior in populations where large scale clinical studies are not feasible.

References

[1] Lukacova V (2012) Poster presentation (#6366), AAPS Annual Meeting, Chicago
[2] Lukacova V (2012) Poster presentation (#6367), AAPS Annual Meeting, Chicago
[3] DeWoskin RS (2008) Regul Toxicol Pharmacol 51:66–86
[4] Arant BS (1978) J Pediatr 92:705–712
[5] Huisman-de Boer JJ (1995) Antimicrob Agents Chemother 39(2):431–434
[6] Charles BG (1997) J Pharm Sci 86(11):1288–1292

W-026 PK/PD Index Versus Mechanism-Based PKPD Modeling to Describe Antibacterial Efficacy of Ciprofloxacin and Colistin

David Khan, Lena E. Friberg, Elisabet I. Nielsen

Department of Pharmaceutical Biosciences, Uppsala University, Uppsala, Sweden

Objectives: PK/PD indices are generally used when deciding on dosing regimens for antibiotic drug treatment. The PK/PD indices are based on the assumption that the antibacterial drug efficacy is correlated to one of the three PK/PD indices; maximum unbound drug concentration over MIC (fC_{max}/MIC), area under the unbound drug concentration–time curve over MIC (*f*AUC/MIC), or the percentage of a 24 h time period where the unbound drug concentration exceeds the MIC ($fT > MIC$). For both ciprofloxacin and colistin, *f*AUC/MIC has been reported to be the best PK/PD index [1–3].

By using the PK/PD indices as endpoint, there is a risk of losing information as the indices only reflect the efficacy at a single time point, typically at 24 h. Mechanism-based PKPD models developed from in vitro time-kill curve experiments consider the whole time span of the experiment rather than just the 24 h time point. It has previously been shown that PKPD models can predict the PK/PD indices for several different antibiotics [4]. The aim of this project was to evaluate recently developed mechanism-based PKPD models for ciprofloxacin and colistin for prediction of the PK/PD indices and to consider advantages/disadvantages of using PK/PD indices vs. mechanism-based PKPD models for dose optimization, for optimizing across half-lives and varying degree of resistance.

Methods: We have previously developed PKPD models for *E.coli* exposed to ciprofloxacin and *P. aeruginosa* exposed to colistin [5, 7]. These models were developed with static time-kill curve data for wild type and well characterized mutans of *E.coli*, and wild type and resistant clinical isolate of *P. aeruginosa*. Both model structures include sensitive growing and resting non-growing bacteria. The model for *E.coli* also includes pre-existing resistant bacteria while the *P. aeruginosa* model features an adaptive resistance mechanism.

In this simulation study, human or mice PK was driving the PKPD models to predict the change in bacterial count following different dosing regimens. For ciprofloxacin, a two compartment PK model was used for human PK while a one compartment model was used for mouse PK. PK parameters were taken from the literature, with terminal half-lives of 4 h for man and 46 min for mouse [4, 5]. Predictions were also made for longer and shorter half-lives (8 h and 1 h) in man.

A PK model for CMS and colistin in patients and an in vitro PKPD model for colistin [6, 7] were combined to predict PK/PD index for colistin. A typical colistin half-life of 18 h was studied as well as a 4.5 h half-life. Dosing regimens with tau of 24, 12, 8 and 4 h were studied for both colistin and ciprofloxacin and a wide range of doses were studied. The best predicted PK/PD index was assessed by fitting the different indices to an E_{max} model and calculating the R^2 value. The influence of PK and resistance on the choice of PK/PD index and target magnitude was investigated.

Results: For normal ciprofloxacin plasma half-life of 4 h, the model predicted *f*AUC/MIC to be the best PK/PD index in humans, however $fT > MIC$ was nearly as good. A *f*AUC/MIC of 50 was predicted to be required for 3 log kill. When the half-life increased, *f*AUC/MIC remained the best PK/PD index. For the shorter ciprofloxacin half life of 1 h, $fT > MIC$ was however shown to be the most predictive PK/PD index while the *f*AUC/MIC index was predicted to not be as good (R^2 0.90 from 0.99). In concordance with the short half-live in mice for ciprofloxacin, $fT > MIC$ was predicted to be the best PK/PD index in this species. When excluding 24 h dosing in mice, *f*AUC/MIC and $fT > MIC$ were both predicted to be good PK/PD indices. For colistin, both fC_{max}/MIC and *f*AUC/MIC correlated well with the antibacterial efficacy when assessed after 24 h of treatment, for the two evaluated half-lives.

Conclusions: As earlier found in clinical studies [3, 5], *f*AUC/MIC was identified by the mechanism-based model to be the best PK/PD index for ciprofloxacin when allowing the human PK profile to drive the killing effect on the bacteria. With a shorter ciprofloxacin half-life, $fT > MIC$ was predicted to be more closely related to the effect than *f*AUC/MIC. This indicates that the selection of the PK/PD index for a drug is sensitive to the PK characteristics in the studied population and hence there is a risk of not using the optimal dosing regimen if strictly dosing after an established PK/PD index. For colistin both fC_{max}/MIC and *f*AUC/MIC were predicted to have good correlations to the 24 h efficacy for all evaluated half-lives. *f*AUC/MIC has previously been shown to be the best PKPD index for colistin in mice [8]. A colistin *f*AUC/MIC of 5 was predicted to achieve a 3 log kill in humans. In mice, a *f*AUC/MIC of 55 has been reported to achieve a 3 log kill for the same *P. aeruginosa* strain

(ATCC 27853) [1]. In summary, the mechanism-based PKPD models were shown to predict PK/PD indices for ciprofloxacin and colistin as earlier been shown for other antibiotics [1]. As illustrated for ciprofloxacin, PK/PD indices may not extrapolate well to all patient-populations or between animals and humans. This study provides further support that mechanism based models based on in vitro data is a useful tool to improve dosing regimens and clinical outcome within the infectious disease area.

References

[1] Dudhani RV, Turnidge JD, Coulthard K, Milne RW, Rayner CR, Li J, Nation RL (2010) Elucidation of the pharmacokinetic/pharmacodynamic determinant of colistin activity against *Pseudomonas aeruginosa* in murine thigh and lung infection models. Antimicrob Agents Chemother 54:1117–1124

[2] Khachman D, Conil JM, Georges B, Saivin S, Houin G, Toutain PL, Laffont C (2011) Optimizing ciprofloxacin dosing in intensive care unit patients through the use of population pharmacokinetic–pharmacodynamic analysis and Monte Carlo simulations. J Antimicrob Chemother. doi:10.1093/jac/dkr22

[3] MacGowan A, Bowker K (2002) Developments in PK/PD: optimising efficacy and prevention of resistance. A critical review of PK/PD in in vitro models. Int J Antimicr Agents 19:291–298

[4] Nielsen EI, Cars O, Friberg LE (2011) Pharmacokinetic/pharmacodynamic (PK/PD) indices of antibiotics predicted by a semimechanistic PKPD model: a step toward model-based dose optimization. Antimicrob Agents Chemother 55(10):4619–4630

[5] Khan D, Lagerbäck P, Gullberg E, Cao S, Malmberg C, Cars O, Hughes D, Andersson DI, Nielsen EI, Friberg LE (2012) External evaluation of a mechanism-based PKPD model: predicting in vitro resistance selection in competition experiments 52nd ICAAC, A-1966, Poster Presentation. San Francisco

[6] Sullivan MC, Cooper BW, Nightingale CH, Quintiliani R, Lawlor MT (1993) Evaluation of the efficacy of ciprofloxacin against *Streptococcus pneumoniae* by using a mouse protection model. Antimicrob Agents Chemother 234–239

[7] Mohamed AF, Karaiskos I, Plachouras D, Karvanen M, Pontikis K, Jansson B, Papadomichelakis E, Antoniadou A, Giamarellou H, Armaganidis A, Cars O, Friberg LE (2012) Application of a loading dose of colistin methanesulfonate in critically ill patients: population pharmacokinetics, protein binding, and prediction of bacterial kill. Antimicrob Agents Chemother 56(8):4241–4249

[8] Plachouras D, Karvanen M, Friberg LE, Papadomichelakis E, Antoniadou A, Tsangaris I, Karaiskos I, Poulakou G, Kontopidou F, Armaganidis A, Cars O, Giamarellou H (2009) Population pharmacokinetic analysis of colistin methanesulfonate and colistin after intravenous administration in critically ill patients with infections caused by gram-negative bacteria. Antimicrob Agents Chemother 53(8):3430–3436

W-027 Gestational Age-Dependent Trends in Maternal-Fetal Glyburide Pharmacokinetics in Pregnant Mice

Diana Shuster*, Linda Risler, Jason Liang, Ken Thummel, Mary Hebert, Danny Shen, and Qingcheng Mao

University of Washington, Seattle, WA, USA

Objectives: Physiological and biochemical changes that occur during pregnancy often alter the pharmacokinetics of drugs, thus affecting their safety and efficacy for the mother and fetus. Glyburide is an oral anti-diabetic agent that has been increasingly used to treat gestational diabetes mellitus. The oral clearance of glyburide was increased by 2-fold in pregnant women compared to non-pregnant controls [1]. The mechanism by which pregnancy changes glyburide pharmacokinetics remains largely unknown. In vivo and in vitro studies suggest that glyburide is extensively metabolized in the liver by CYP3A and CYP2C9 [2], and hepatic CYP3A activity is significantly induced during pregnancy [3]. Therefore CYP3A induction might be one possible mechanism for decreases in maternal glyburide exposure during pregnancy. Since the levels of hepatic Cyp3a content in pregnant mice and its activity are also significantly increased compared with non-pregnant controls [4], we have used the pregnant mouse as an appropriate animal model to study gestational age-dependent effects on glyburide disposition during pregnancy. Thorough characterization of pregnancy-induced changes in the disposition of glyburide (including fetal exposure) will be important for optimizing dosing regimens for use in pregnant women. In this study, we determined gestational age-dependent changes in maternal glyburide pharmacokinetics in pregnant mice. While the maternal disposition of glyburide has been studied in humans, due to ethical and logistical reasons, no data is available regarding fetal exposure, particularly during early gestation, which ultimately determines the toxicity of the drug to the developing fetus. Thus, we also determined fetal exposure to glyburide throughout gestation in pregnant mice.

Methods:

Timed mating and sample collection: Male and female FVB wild-type mice, aged 7–10 weeks, were mated overnight. Under anesthesia, pregnant (Gd 7.5, 10, 15, and 19) or non-pregnant (Gd 0) mice were administered 20 μg glyburide by retro-orbital injection. At various times (0.5, 5, 10, 20, 40, 60, 120, 180, and 240 min) after glyburide administration, animals ($n = 3$–4 per time point) were sacrificed and maternal plasma and fetuses were collected.

Maternal plasma and fetal extraction of glyburide: For every 100 μL of maternal plasma, 450 μL of methanol and 20 μL of internal

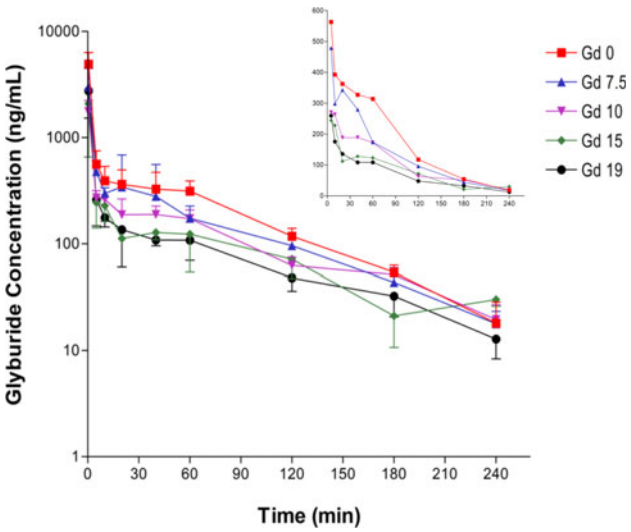

Fig. 1 Maternal plasma concentration–time profiles of glyburide in FVB-wild-type mice. Data from gestation day (Gd) 0 (*red squares*), Gd 7.5 (*blue triangles*), Gd 10 (*purple upside-down triangles*), Gd 15 (*green diamonds*), and Gd 19 (black circles) are shown. Mice were administered 20 μg of glyburide by retro-orbital injection. Smaller concentration–time profiles in the upper right-hand corner were plotted using a linear scale. Shown are mean ± S.D. ($n = 3$–4 mice per time point)

Table 1 Pharmacokinetic parameters of glyburide in FVB wild-type pregnant mice

Parameter	Gd 0	Gd 7.5	Gd 10	Gd 15	Gd 19
$AUC_{0\text{-}240\ min}$ (min*ng/mL)	50,090	43,917	31,755	24,467	23,137
CL (mL/min)	0.40	0.46	0.63	0.82	0.86
V_{ss} (mL)	25.0	32.3	49.7	53.1	63.4
Fetal $AUC_{0\text{-}240\ min}$ (min*ng/g)	8,637	5,341	10,632	9,357	
$AUC_{fetal}/AUC_{maternal}$	0.20	0.17	0.43	0.40	

standard (0.5 ng/μL glyburide-*d11*) were added. Fetal samples were homogenized in 1.25–2.5 mL of PBS using an Omni bead ruptor homogenizer. For every 500 μL of fetal homogenate, 50 μL of 2 M HCl, 4 mL of 60:40 (v/v) n-hexane:methylene chloride, and 20 μL of internal standard (0.5 ng/μL glyburide-d11) were added. Samples were briefly vortexed and centrifuged at 14,000 rpm for 10 min at 4 °C. Supernatants were evaporated using nitrogen gas. Maternal samples were reconstituted in initial mobile phase (57.5 % 5 mM ammonium formate, pH 6.0 and 42.5 % methanol containing 5 mM ammonium formate). Fetal samples were reconstituted in 75 μL of 1 % formic acid in methanol. 2 μL were injected per sample for LC/MS analysis.

LC/MS Analysis: An Agilent HPLC/MS series 1100 G1956B with a single quadrupole mass spectrometer and an Ace 3 C8 column (150 mm x 2.1 mm) were used for the separation and analysis of glyburide (494 m/z). The mobile phases consisted of methanol (B) and water (A), both containing 0.5 mM ammonium formate at pH 6.0. The flow rate was 0.4 mL/min. The gradient was 42.5 % methanol for the first 5 min, then increased linearly to 90 % for 5.1 min, and finally decreased back to 42.5 % for the remainder of the 11 min run time. The mass spectrometer was run in API-ES ionization mode using a capillary voltage of 3500 V and a fragmentation voltage of 115 V.

Pharmacokinetic and Statistical Analysis: The following maternal pharmacokinetic (PK) parameters were estimated using the pseudo-profile-based bootstrap method and R programming language as previously described: $AUC_{0–240min}$, CL, and V_{ss}. The confidence intervals of PK parameters from Gd 7.5, 10, 15, and 19 data were compared to Gd 0 to determine statistical significance. Fetal $AUC_{0–240\ min}$ was calculated by non-compartmental analysis using WinNonlin Pheonix software.

Results: In this study we characterized gestational age-dependent changes in maternal-fetal glyburide pharmacokinetics in FVB wild-type mice. Preliminary results are shown below (Fig. 1; Table 1). Maternal glyburide exposure ($AUC_{0–240\ min}$) steadily decreased throughout gestation by as much as 50 % on Gd 15 and 19 compared to Gd 0. In addition, maternal glyburide CL and V_{ss} nearly doubled by Gd 15, and remain increased on Gd 19 by 2-fold. Fetal exposure to glyburide appeared consistent throughout gestation. It is important to note that while individual fetuses were assayed on Gd 15 and 19, the entire fetal-placental unit had to be assayed on Gd 7.5 and Gd 10 because the fetus is not visibly distinguishable at earlier gestational ages. Therefore, the actual embryonic exposure may be slightly smaller on Gd 7.5 and Gd 10. The fetal:maternal plasma $AUC_{0–240\ min}$ ratio was similar between Gd 7.5 and 10 ($\sim$0.20) but doubled on Gd 15 and 19 ($\sim$0.40). This increase seems to be due to decreases in maternal glyburide exposure throughout gestation.

Conclusions: The largest alterations to glyburide pharmacokinetics occur during mid-late gestation. Maternal glyburide CL and V_{ss} steadily increased throughout pregnancy and doubled by mid-late gestation in pregnant FVB wild-type mice. Increased CL has also been observed in pregnant women taking glyburide to treat gestational diabetes mellitus, therefore increased dosages of glyburide may be necessary during the latter part of human pregnancy to achieve euglycemia. In FVB wild-type mice, fetal exposure to glyburide increased as gestation progressed, and was as much as 40 % of maternal exposure levels. One clinical study found that the mean ratio of umbilical cord:maternal plasma glyburide concentrations was 0.7 ± 0.4 (70 % of maternal plasma levels). The FVB mouse seems to adequately model maternal-fetal glyburide disposition during human pregnancy. Fetal exposure to glyburide is most concerning during late gestation.

References

[1] Hebert MF, Ma X, Naraharisetti SB, Krudys KM, Umans JG, Hankins GD, Caritis SN, Miodovnik M, Mattison DR, Unadkat JD, Kelly EJ, Blough D, Cobelli C, Ahmed MS, Snodgrass WR, Carr DB, Easterling TR, Vicini P (2009) Are we optimizing gestational diabetes treatment with glyburide? The pharmacologic basis for better clinical practice. Clin Pharmacol Ther 85, 607–614

[2] Zhou L, Naraharisetti SB, Liu L, Wang H, Lin YS, Isoherranen N, Unadkat JD, Hebert MF, Mao Q (2010) Contributions of human cytochrome P450 enzymes to glyburide metabolism. Biopharm Drug Dispos 31:228–242

[3] Hebert MF, Easterling TR, Kirby B, Carr DB, Buchanan ML, Rutherford T, Thummel KE, Fishbein DP, Unadkat JD (2008) Effects of pregnancy on CYP3A and P-glycoprotein activities as measured by disposition of midazolam and digoxin: a University of Washington specialized center of research study. Clin Pharmacol Ther 84:248–253

[4] Zhang H, Wu X, Wang H, Mikheev AM, Mao Q, Unadkat JD (2008) Effect of pregnancy on cytochrome P450 3a and P-glycoprotein expression and activity in the mouse: mechanisms, tissue specificity, and time course, Mol Pharmacol 74:714–723

W-028 Evaluating Backup Compound Development Strategies Using Simulation

Bill Poland*

Pharsight, A Certara™ Company, Sunnyvale, CA, USA

Objectives: To illustrate how to evaluate and optimize among strategies for developing backup compounds in conjunction with a lead compound, accounting for cross-compound learning, development costs, and value of speed to market. This is important to manage risk and improve productivity in drug development.

Methods: The approach is illustrated with the following compounds (Table 1), in a therapeutic area in which competition is high, so speed to market is a key factor (such as Hepatitis C treatments). The lead compound (L) has low but positive expected market value, e.g., due to

Table 1 Compound stage and market characteristics

Compound	Next stage	Efficacy (uncertainty: ? = Low ??? = High)	Tolerability (uncertainty)	Expected net market value[a] (uncertainty)	Correlation with lead compound
L (Lead)	Phase 2B	Moderate (??)	Moderate (??)	Low (??)	
B1	Phase 1	Moderate (???)	High (???)	Low (???)	High: same MoA, similar chemistry
B2	Phase 1	High (???)	Moderate (???)	Moderate (???)	Low: different MoA & chemistry

[a] Expected value before further study: a function of efficacy, tolerability, and time to market (value declines over time due to competition). Value is also reduced if multiple compounds reach the market due to "cannibalism" of market share

disappointing POC results, raising the question of whether and how the backup compounds (B1 and B2) should be advanced.
Alternative strategies were compared through Monte Carlo simulation with random draws of the unknown true efficacy and tolerability levels and Bayesian learning about these from additional random draws of Phase 1-3 study outcomes. Strategies included: develop each compound on its own (terminate the others), develop L and B1 in parallel, develop L and B2 in parallel, and develop all three in parallel. Each compound initially had positive expected net value after development costs, but was stopped if this value fell negative when updated by the simulated trial results. Development costs by phase were included in the value measure, so that simulations recognized that early stop decisions save money relative to later stop decisions. To keep the example easily tractable, normal models of efficacy and tolerability were assumed with learning in each phase summarized by equivalent sample sizes, and dosing decisions were left implicit.
Results: Simulation results showed that a high correlation of B1 with L makes B1 not worth developing: if L fails, cross-compound learning makes B1′s net value negative, while if L succeeds, B1 would likely be too similar to L to be worthwhile. However, a lower correlation would make B1, like B2, worth developing in parallel with L (re-evaluating at each stage). B2′s independence, with higher expected efficacy offsetting its earlier position in development, make it worth developing further as long as it appears to be sufficiently superior to L.
Conclusions: Pharmacometricians typically build detailed exposure–response models for efficacy and sometimes tolerability of individual compounds, using Monte Carlo simulation to test and optimize dosing, sample sizes, and other trial design factors. These models can provide input into more strategic Monte Carlo simulation models for designing development programs, and in particular for supporting decisions about whether and how to advance backup compounds. Many factors complicate these decisions, including the potential to learn from lead compound results to a correlated backup, the risk that a backup is so correlated with the lead compound that it will perform no better, the value of speed to market (which may give the lead compound an insurmountable advantage), differing remaining development costs (ignoring sunk costs), and the loss of value when a second successfully developed compound must share market with the first. However, strategy simulations can account for such issues and properly weigh alternative strategies—and may even be critical to making and justifying difficult backup decisions. To evaluate many backups simultaneously, optimization techniques [1, 2] can be combined with simulation, though diminishing returns are expected from multiple backups [3].

References

[1] Bickel JE, Smith JE (2006) Optimal sequential exploration: a binary learning model. Decision Anal 3(1):16–32

[2] Poland B (2009) Optimal sequencing of interdependent drug development programs. American College of Clinical Pharmacology (ACCP) 38th Annual Meeting, San Antonio. Also presented at 2nd ACoP, 2009, Mashantucket, CT. http://2009.go-acop.org/sites/all/assets/webform/ACoP%202009%20Poster%20-%20Bill%20Poland.pdf

[3] Stock DA, Molinoff PB (2002) The value of backup compounds to drug development programs. Drug Inf J 36:95–113. http://www.diahome.org/productfiles/8357/diaj_11547.pdf

W-029 Pharmacometric Analyses of the Pharmacokinetic, Target-Receptor Occupancy, Biomarker and QTcF Data to Guide Dose Selection for a Phase 2 Proof-of-Concept Study

Amit Khatri[1,*], Wei Liu[1], Earle Bain[2], Beatrice Rendenbach-Mueller[2], Sandeep Dutta[1]

[1]Clinical Pharmacology and Pharmacometrics, AbbVie, Abbott Park, IL, USA; [2]Global Pharmaceutical R&D, AbbVie, Abbott Park, IL, USA

Objectives: Drug-A is a potent and selective antagonist for Receptor-X, which may contribute to its clinical efficacy and is currently under clinical development. Phase-I clinical pharmacology studies in healthy volunteers showed that Drug-A binds to its target Receptor-X; however, it was also observed that it results in mechanism based increase in the release of Biomarker-Y, which is not considered clinically desirable for its target indication. Additionally the Drug-A also prolongs QTcF. Greater than 75 % receptor occupancy (RO) at C_{max} and at least 50 % RO at C_{trough} at steady state were considered to be required for clinical efficacy. The objective of current analyses was to perform pharmacometric analyses of the pharmacokinetic, target RO, Biomarker-Y and QTcF data to guide dose selection for a Proof of concept (PoC) or Phase-II study.
Methods: Data from three studies: Phase-I single ascending dose (SAD) study ($N = 56$), multiple ascending dose (MAD) study ($N = 36$) and single dose Positron Emission Tomography (PET) imaging study ($N = 9$) were used for the analyses. In the SAD study, doses up to 1200 mg, in the MAD study, doses up to 400 mg QD for 7 days, and in the PET imaging study, doses up to 1000 mg were orally administered to healthy volunteers. Drug-A concentrations in plasma were measured intensively up to 96 h in the SAD study, on day 1 and day 7 up to 96 h post dose in the MAD study, and during PET scans in the PET imaging study. Biomarker-Y levels were

measured at 0, 2, 4, 6, 8 and 12 h post dose in the SAD and at baseline (day −1) and on day 7 in the MAD study. QTcF was measured at 0, 2, 4, 6, 9, 12 and 24 h post dose in the SAD and at 0, 2, 4, 6, 12 and 24 h post dose on day 1 and 7 in the MAD studies. In the PET imaging study, two PET scans were obtained per subject, and target Receptor-X occupancy was calculated as % of receptors bound to Drug-A in the region of interest.

The population PK and PD models for Drug-A concentrations, Biomarker-Y, QTcF and RO were developed sequentially using FOCE-I method in NONMEM 7 (Ver 1.0). First, the Drug-A PK model was developed. The delay in absorption was modeled using transit compartments. Compartment models with up to 3 compartments for drug disposition were tested during model building. Next, QTcF model was developed using a single cosine function to capture the diurnal changes in QTcF values. Linear and E_{max} models were tested to incorporate the effect of Drug-A on QTcF during model development. Baseline QTcF (at time = 0) was also evaluated as a covariate during QTcF model development. Next, the PD model for Biomarker-Y was developed. During biomarker model development, both plasma concentrations of Drug-A, as well as dose in the form of K-PD model were explored to describe the time course of Biomarker-Y [1]. Finally, the RO model was developed. Sigmoid E_{max} and simple E_{max} models were tested to describe the relationship between RO and average plasma concentration during the duration of the PET scan.

Inter-individual variability in the PK and PD parameters was described by a log normal distribution. Proportional and combined error models were tested to describe the residual variability in the data. Model comparison was performed by likelihood ratio test at α level of 0.05 as well as goodness-of-fit plots. Model evaluation was performed by visual predictive check by simulating 500 datasets.

Following the development of population PK and PD models, simulations were performed to predict the distribution of RO at C_{max} and C_{trough}, QTcF increase, and Biomarker-Y levels at C_{max} at doses 50–800 mg at steady state. Simulations were performed under two scenarios. In scenario I, one trial of 1000 subjects was simulated to provide information about the population distribution of the RO, QTcF increase and Biomarker-Y levels at various dose levels. In scenario II, 200 trials were simulated with 50 subjects at each dose level and distribution of mean RO, QTcF increase and Biomarker-Y levels at trial level were generated. In selection of doses for a PoC study, a mean QTcF increase of 10 ms and peak levels of Biomarker-Y greater than 5× upper limit of normal (ULN) were considered undesirable, while mean RO of greater than 75 % at C_{max} and 50 % at C_{trough} were considered desirable .

Results: Data from 69 subjects with 1193 Drug-A, 330 Biomarker-Y concentrations, 494 QTcF and 17 RO measurements were used to build the PK and PD models. A 2-compartment model with extravascular administration and 4 transit compartments to describe the delay in absorption best described the Drug-A plasma concentration–time data. Diurnal changes in QTcF measurements were best described by a single cosine function. A linear model best described the effect of Drug-A concentrations on QTcF prolongation. The time course of Biomarker-Y was adequately described by the K-PD model with a linear model to describe the effect of Drug-A on Biomarker-Y levels. The RO data was optimally described by an E_{max} model. A proportional error model best described the residual variability in Drug-A and Biomarker-X measurements, while an additive error model best described the residual variability in QTcF and RO measurements. The visual predictive checks did not provide any apparent evidence of model misspecification.

During simulations, doses ≤300 mg were associated with mean QTcF increase of ≤10 ms; doses ≥250 mg were needed to achieve mean RO of ≥75 % at C_{max} and ≥50 % at C_{trough}; and doses ≤300 mg were associated with <2xULN increase in Biomarker-Y levels. Hence, based on the above results doses in the range of 250–300 mg were recommended for the Phase 2 development of Drug-A.

Conclusions: In the present work, we integrated information predictive of efficacy, as well as safety, and provided recommendation about the doses (250–300 mg) at which we can attain success in the proof of concept study while minimizing the risk based on our current knowledge about the therapy.

Reference

[1] Jacqmin P, Snoeck E, van Schaick EA, Gieschke R, Pillai P, Steimer JL, Girard P (2007) Modelling response time profiles in the absence of drug concentrations: definition and performance evaluation of the K-PD model. J Pharmacokinet Pharmacodyn 34(1):57–85

W-030 Relative Bioavailability of Fosphenytoin Sodium Injection Compared to Phenytoin Sodium Injection, Both Given Orally to Healthy Volunteers

Gauri G Rao[1,*], Alan Forrest[1], Neang S Ly[1], Vidya Perera[1], Brian T Tsuji[1], Kevin A. Kaucher[2], Curtis E. Haas[3]

[1]SUNY School of Pharmacy & Pharmaceutical Sciences, Buffalo, NY, USA; [2]Denver Health and Hospital Authority, Denver, CO, USA; [3]University of Rochester Med-i-cal Center, Rochester, NY, USA

Objectives: Phenytoin (PHT) sodium injection, a narrow therapeutic index antiepileptic, administered through nasogastric tube in conjunction with enteral nutrition supplements, has been associated with suboptimal PHT absorption. Fospheny-toin (FPHT), a prodrug of PHT, has better solubility. The oral bioavailability FPHT injectable is unknown. The primary objective of this study was to determine the relative oral bioavailability (F_{REL}) of FPHT compared to PHT, in healthy adult volunteers, based on pharmacokinetic (PK) modeling.

Methods: 10 healthy volunteers were studied in an open-label, randomized, single-dose, 2-period crossover design, with a minimum 7 day washout between periods. Both drugs were administered orally at doses equivalent to 400 mg of PHT acid. Blood samples were collected at pre-dose and at 0.5, 1, 2, 4, 6, 12, 24, 48 and 72 h after dosing. Serum PHT concentrations were determined by fluorescence polarization immunoassay (LOQ 0.5 ng/mL, interday CV <10 %). Since PHT exhibits non-linear PK and as these doses do not generally achieve concentrations needed for precise estimates of the maximum rate of elimination (V_{max}) and the Michaelis constant (K_m), the MAP-Bayesian algorithm in ADAPT5 (1) was used to fit candidate models to the data (2 stage analysis); model discrimination was by the Generalized Information Criterion; Bayesian priors, for V_{max} and K_m, were obtained from the literature (2); non-informative priors were used for the rest of the model parameters. PHT pro-files, from the 2 periods, were co-modeled with no interoccasion variability; the residual error model included additive and pro-por-tional components; the Beal M3 was used to accommodate observations that were < LOQ. The areas under the curves (AUC_{PHT} & AUC_{FPHT}) were determined by numerical integration and the AUC_{RATIO} was also computed (AUC_{FPHT}/AUC_{PHT}).

Results: The study subjects included 8 females and 2 males with an average ± sd age of 37.1 ± 16.3 years, weight of 91.8 ± 38.9 kg and height of 144 ± 45.8 cm. PHT doses showed irregular absorption profiles; the C_{max} values, following FPHT doses, were significantly higher than after PHT [median (range) 10.7 (9.00–19.4) vs. 5.00 (3.20–8.90) mg/L, $p = 0.002$]; and the T_{max}, for FPHT doses was faster [1.00 (0.500–2.00) vs. 6.00 (2.00–24.0) h, $p = 0.008$). The final PK model (Fig. 1; Table 1) included 2 distributional volumes (Vc and Vp), linear distributional clearance (CLd) & parallel

non-linear (K_m and V_{max}) & linear clearance (CL). PHT absorption was modeled with 2 phases (Fr_1 is the fraction of the dose absorbed in phase 1), each with a fit-ted ka, and T_{Lag} delaying absorption in phase 2; FPHT had 1 absorption phase, with T_{Lag}, ka and a fitted relative bio-avail-ability (F_{REL}). The model fit the data well [median (range) r^2 for PHT 0.94 (0.89–0.99) and 0.98 (0.95–1.0) for FPHT]. FPHT bio-availability is greater than that of PHT (F_{REL} mean was 1.21 and 95 % CI was 1.07–1.35). The fitted F_{REL} differed from AUC_{RATIO} overall ($p = 0.0051$), due to indi-vid-uals with differences in C_{max}, between drugs (Fig. 2).

Conclusions: FPHT was absorbed to a greater extent and more rapidly than PHT. Relative bioavailability of drugs with non-linear clearance should not be quantified by AUC ratios, unless both formulations achieve a similar C_{max}. The data should, instead, be co-modeled with relative bioavailability as a fitted parameter.

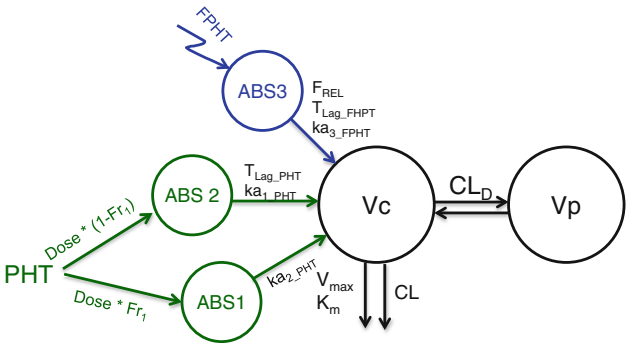

Fig. 1 PK model structure of PHT following administration of oral PHT and FPHT

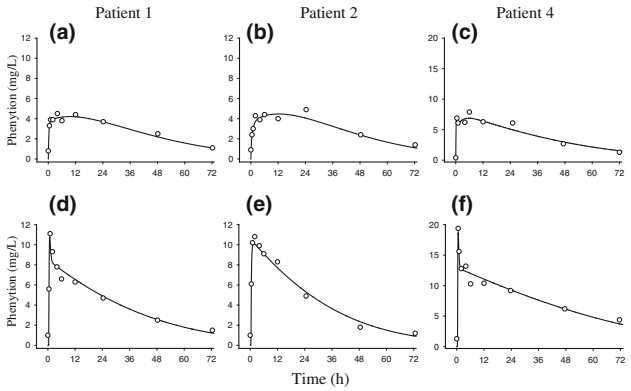

Fig. 2 Example fitted PK profiles of phenytoin following oral administration of parenteral phenytoin (**a–c**) and fosphenytoin (**d–f**)

References

[1] D'Argenio DZ, Schumitzky A, Wang X (2009) ADAPT 5 User's Guide:Pharmacokinetic/Pharmacodynamic Systems Analysis Software. Biomedical Simulations Resource, Los Angeles

[2] Grasela TH, Sheiner LB, Rambeck B, Boenigk HE, Dunlop A, Mullen PW, Wadsworth J, Richens A, Ishizaki T, Chiba K, et al. (1983) Steady-state pharmacokinetics of phenytoin from routinely collected patient data. Clin Pharmacokinet 8:355–364

Table 1 Fitted and derived PK parameter estimations

Parameters	Unit	Minimum	Maximum	Median	Arithmetic Mean	% CV
K_m	mg/L	6.06	9.59	7.67	7.83	14.6
V_{max}	mg/h	13.1	17.2	15	15	9.54
Fr_1	–	0.217	0.678	0.407	0.428	33.6
Vc	mL	8.96	27.9	19.9	19.9	28.4
Vp	mL	27.3	34.3	31	31.1	7.83
V_{ss}	mL	40.1	60.8	50.4	50.8	14.0
CL_D	mL/h	35.7	64.8	61.8	59.4	14.7
CL	mL/h	0.00	0.42	0.013	0.116	161
CL_{int}	mL/h	1.40	2.80	1.86	1.98	23.5
ka_{1_PHT}	h^{-1}	0.494	4.39	1.57	1.86	60.9
ka_{2_PHT}	h^{-1}	0.0334	0.376	0.0642	0.104	106
ka_{3_FPHT}	h^{-1}	1.85	5.39	3.36	3.38	36.4
T_{Lag_PHT}	H	0.00	1.00	0.389	0.351	87.9
T_{Lag_FPHT}	H	0.00	0.786	0.412	0.388	49.1
F_{REL}	–	1.04	1.64	1.15	1.21	15.8
AUC_{PHT}	mg•h/mL	197	364	238	263	22.8
AUC_{FPHT}	mg•h/mL	277	665	327	373	31.7
AUC_{RATIO}	–	1.19	2.00	1.34	1.42	18.8

$CL_{int} = V_m/K_m$; $V_{ss} = Vc + Vp$

W-031 A Pharmacokinetic Evaluation of Tobramycin Administered One, Two, and Three Times Daily to Children with Cystic Fibrosis

Catherine M.T. Sherwin[1,2,*], Chris Stockmann[1,2], Jeffery T. Zobell[3,4], Bradley McCrory[5], Millie Wisdom[6], David C. Young[7,8], Jared Olson[1,3], Krow Ampofo[1], and Michael G. Spigarelli[1,2]

[1]Department of Pediatrics, University of Utah School of Medicine, Salt Lake City, UT, USA; [2]Department of Pharmacology and Toxicology, University of Utah College of Pharmacy, Salt Lake City, UT, USA; [3]Pharmacy, Intermountain Primary Children's Medical Center, Salt Lake City, UT, USA; [4]Intermountain Cystic Fibrosis Pediatric Center, Salt Lake City, UT, USA; [5]University of Cincinnati, Cincinnati, OH, USA; [6]Phoenix Children's Hospital, Phoenix, AZ, USA; [7]Intermountain Cystic Fibrosis Adult Center, Salt Lake City, UT, USA; [8]Pharmacotherapy Outcomes Research Center, University of Utah College of Pharmacy, Salt Lake City, UT, USA

Objectives: Tobramycin is frequently used in the treatment of acute pulmonary exacerbations of cystic fibrosis. Debate surrounds the optimal dosing scheme and the frequency of tobramycin administration. The objective of this study was to characterize the pharmacokinetics of tobramycin administered one, two, or three times daily and to develop an optimal dosing scheme for children with cystic fibrosis.

Methods: Therapeutic drug monitoring data were obtained from children <18 years of age, who were hospitalized from January 2005 through December 2012 at three academic medical centers. Population pharmacokinetic models were constructed using NONMEM 7.2 and pharmacokinetic parameters were compared for each dosing regimen. Dosing schemes were developed and evaluated against optimal aminoglycoside pharmacodynamic targets in Matlab R2012b.

Results: The pharmacokinetic analysis involved 257 patients (193 dosed once per day, 49 two times per day, and 15 three times per day). Overall, the median age was 8.1 years [interquartile range (IQR): 4.6–13.9]. Clearance was highest among children dosed once per day (5.90 L/hr/70 kg) and declined with more frequent dosing (5.11 and 4.96 L/h/70 kg for two and three times per day, respectively). The volume of distribution was smallest among children who received tobramycin once per day (17.6 L/70 kg). Children dosed two and three times per day had volumes of distribution of 20.3 and 21.1 L/70 kg, respectively. Mean (±SD) peak concentrations were highest among patients dosed once per day (56.6 ± 12.3 mg/mL) and were lower among patients dosed two and three times per day (37.7 ± 6.4 and 23.9 ± 5.4 mg/mL, respectively).

Conclusions: This is the first study to evaluate the pharmacokinetics of tobramycin administered one, two, and three times per day to children with cystic fibrosis. Once daily tobramycin dosing resulted in increased clearance and a lower volume of distribution when compared to multiple-daily dosing. This suggests that once daily dosing may be preferable based on its pharmacokinetic profile, however further clinical evaluation is needed to establish the safety and efficacy of this dosing regimen.

W-032 Application of Model-Based Meta-Analysis (MBMA), Population PK/PD, and Exposure–Response (E–R) Analysis to Evaluate the PD Drug–Drug Interaction (DDI) in an Oncology Phase Ib trial

Tong Lu*, Dan Lu, Gillian Smelick, Ray Lin, Steven Gendreau, Gallia Levy, Mark Dresser, Joseph Ware, Jin Yan Jin

Genentech Inc., South San Francisco, CA, USA

Objectives: To determine whether neutropenia observed in an oncology Phase Ib dose-escalation study (GDC4629 g) [1] of GDC0941 in combination with 90 mg/m^2 QW Paclitaxel (PAC) with or without Bevacizumab is comparable to historical PAC monotherapy, and whether an E-R relationship exists for GDC0941 and neutropenia in this study.

Methods: Three pharmacometrics approaches were utilized to evaluate the effect of GDC0941 on neutropenia:

1) *MBMA*: A literature database of PAC mono-therapy in cancer patients was constructed to better understand its PK, efficacy, and safety, and to better design/interpret combination trials. PAC dose–response relationship was developed for neutropenia based on summary-level data for 1886 patients from 35 dosing arms in 24 trials using Logistic regression [2]. The investigators reported neutropenia event rate in the GDC0941 combination study was compared with the predicted median and 90 % CI of the MBMA dose–response, to evaluate whether GDC0941 magnifies PAC's effect on myelosuppression.
2) *Population PK/PD*: A historical population PK/PD model for the effect of PAC mono-therapy on myelosuppression [3] was applied to evaluate the neutrophil count-time profiles in the Phase Ib study. The semi-mechanistic model incorporated the drug-sensitive proliferating compartment, three transit compartments that represented cell maturation, and a compartment of circulating neutrophils. Visual predictive check (VPC) was used to compare the simulated neutrophil count-time profiles based on PAC monotherapy with the observed Phase Ib profiles in combination with GDC0941 ($n = 35$).
3) *E–R*: E–R relationship for GDC0941 exposure and the worst neutropenia grade or the nadir of neutrophil counts was evaluated for patients with both PK and safety data available ($n = 31$).

Results: (1) From the MBMA which included PAC QW and Q3 W regimens, neutropenia event rate was found best correlated with administered PAC dose (mg/m^2) with saturable dose response relationship, but not correlated with average dose (mg/m^2/wk). This result implied that PAC safety may be better correlated with C_{max} than AUC. Observed neutropenia event rate in the Phase Ib study was consistent with the prediction from PAC mono-therapy, suggesting GDC0941 did not magnify PAC's effect on myelosuppression. (2) Based on the VPC, the observed neutrophil count-profiles from 35 patients in the combination setting were in line with the PK/PD model prediction for PAC mono-therapy. The mean neutrophil count-profiles stratified by GDC0941 dosage also showed no dose related pattern.

(3) In the E-R analysis, no effect of GDC0941 exposure was observed on the worst neutropenia grade and the nadir of neutrophil counts.
Conclusions: Evaluation of the DDI potential in cancer therapeutics is of critical importance in the development of targeted agents, which are added to standard of care chemotherapy to treat cancer. Neutropenia is a common adverse event that is associated with PAC. For this Phase Ib dose-escalation study, three modeling approaches have been utilized to evaluate the effect of GDC0941 on neutropenia when given in combination with PAC. Overall, the neutropenia observation in this Phase Ib study was consistent with PAC mono-therapy with no E–R relationship for GDC0941, suggesting no decreased tolerability for the combination therapy.

References

[1] Schöffski P, De Benedictis E, Gendreau S, Gianni L, Krop IE, Levy G, Ware J, Wildiers H, Winer EP. http://cancerres.aacrjournals.org/cgi/content/meeting_abstract/71/24_MeetingAbstracts/PD09-04

[2] Jin JY, Lu D, Li H, Zhang N, Wada R, Joshi A (2012) Model-based meta-analysis for the efficacy and safety of PAC in cancer patients. http://www.page-meeting.org/default.asp?abstract=2417

[3] Friberg LE, Henningsson A, Maas H, Nguyen L, Karlsson MO (2002) Model of chemotherapy-induced myelosuppression with parameter consistency across drugs. J Clin Oncol 20(24): 4713–4721

W-033 Population Pharmacokinetics of Vancomycin Used in the Treatment of Pediatric Cystic Fibrosis Pulmonary Exacerbations

Chris Stockmann[1,2,*], Catherine M.T. Sherwin[1,2], Jeffery T. Zobell[3,4], Lisa Lubsch[5], David C. Young[6,7], Jared Olson[1,3], Blakeslee E. Noyes[8], Krow Ampofo[1], and Michael G. Spigarelli[1,2]

[1]Department of Pediatrics, University of Utah School of Medicine, Salt Lake City, UT, USA; [2]Department of Pharmacology and Toxicology, University of Utah College of Pharmacy, Salt Lake City, UT, USA; [3]Pharmacy, Intermountain Primary Children's Medical Center, Salt Lake City, UT, USA; [4]Intermountain Cystic Fibrosis Pediatric Center, Salt Lake City, UT, USA; [5]Southern Illinois University Edwardsville School of Pharmacy, Edwardsville, IL, USA; [6]Intermountain Cystic Fibrosis Adult Center, Salt Lake City, UT, USA; [7]Pharmacotherapy Outcomes Research Center, University of Utah College of Pharmacy, Salt Lake City, UT, USA; [8]Department of Pediatrics, St. Louis University School of Medicine and SSM Cardinal Glennon Children's Medical Center, St. Louis, MI, USA

Objectives: Vancomycin is the drug-of-choice for the treatment of methicillin-resistant *Staphylococcus aureus* (MRSA) infections in children with cystic fibrosis. However, no studies have characterized the pharmacokinetic profile of vancomycin among children with cystic fibrosis. This study evaluated the pharmacokinetics of intermittent vancomycin administration in children with cystic fibrosis and characterized the covariates that significantly influence vancomycin efficacy and safety.
Methods: Therapeutic drug monitoring data were obtained from two cystic fibrosis care centers that identified children <18 years of age who received vancomycin for the treatment of an acute pulmonary exacerbation from January 2005 through December 2012. Trough and peak serum concentrations were determined before and after the third or fourth dose. Nonlinear mixed effects models were developed to evaluate the population pharmacokinetics of vancomycin using NONMEM 7.2.
Results: Sixty-seven children were identified with a mean (±SD) of 12.1 ± 5.3 years of age. The mean vancomycin dose was 17.4 ± 4.4 mg/kg. The mean trough concentration was determined to be 10.3 ± 3.8 mg/L. The mean area under the serum concentration time curve (AUC) was 282.5 ± 816.9 mg*h/L. A one-compartment model with first-order elimination best described the data. Weight significantly influenced vancomycin clearance ($P < 0.001$). In the final model, clearance was estimated as 5.57 (95 % CI: 5.11–6.03) L/h/70 kg and the volume of distribution was 44.1 (95 % CI: 38.5–49.7) L/70 kg. The between subject variability for clearance was 27 CV % and 40 CV % for the volume of distribution.
Conclusions: This is the first study to investigate the pharmacokinetics of vancomycin among children with cystic fibrosis. Vancomycin pharmacokinetics were well described with a one-compartment model, which identified a strong relationship between vancomycin clearance and increasing weight. Additional pharmacodynamics studies are needed to define an optimal vancomycin dosing regimen for the treatment of cystic fibrosis pulmonary exacerbations in children.

W-034 Population Pharmacokinetics of Foretinib in Adult Asian Subjects with Hepatocellular Carcinoma

Rajendra P. Singh[1,*], Bela Patel[1], Howard Kallender[2], Lone Ottesen[3], Donna Cox[1]

[1]Clinical Pharmacology Modeling Simulation, GlaxoSmithKline, King of Prussia, PA, USA; [2]Oncology Clinical Development, GlaxoSmithKline, Collegeville, PA, USA; [3]Oncology Clinical Development, GlaxoSmithKline, Stockley Park, UK

Objectives: Foretinib is an investigational, oral, multikinase inhibitor that inhibits multiple receptor tyrosine kinases with growth promoting and angiogenic properties with potential for treatment of solid tumors. The primary targets of foretinib are c-MET, RON, AXL, TIE-2 and VEGFR. Hepatocellular carcinoma (HCC) pathogenesis is associated with over-expression c-MET and inhibition of c-MET activation by agents such as foretinib may be of therapeutic benefit in this patient population. Studies conducted in vitro have shown that foretinib undergoes nicotinamide adenine dinucleotide phosphate (NADPH)-dependent oxidative metabolism by CYP3A4 in human liver microsomes. However, physiologic changes in the liver in HCC patients may decrease metabolism by CYP3A4 resulting into increase in the systemic exposure of foretinib. The objective of this analysis was to characterize the population pharmacokinetics (Pop PK) of foretinib based on HCC and non-HCC cancer studies, identify covariates influencing foretinib PK and to evaluate the differential impact of tumor type (HCC versus other tumor type) and formulations on exposure.
Methods: Data from 4 phase I/II studies (1 HCC study in Asia and 3 non-HCC cancer studies in the US) were used for the population pharmacokinetic analysis. A total of 89 advanced-cancer patients (1556 observations) were included in the model development dataset. The subjects were dosed with an oral solution formulation, but were later switched to a bisphosphate salt capsule and free-base tablet formulation. Nonlinear mixed-effects modeling was performed for the population pharmacokinetic analysis, using NONMEM program version 7.1.2 (ICON, Ellicott City, MD). All models were analyzed using first-order conditional estimation (FOCE) with or without interaction. Once the base model was identified, covariates were included in the model and tested for improvement in objective function value using the likelihood ratio. Final model selection was

based on evaluation of goodness-of-fit plots, biological plausibility and precision of parameter estimates. Nonparametric bootstrap and visual predictive checks were implemented for final model evaluation.
Results: A two-compartment PK model with linear elimination and lag time in absorption was used to describe foretinib pharmacokinetics. Inter-occasion variability (IOV) was estimated on clearance, volume of central compartment and rate of absorption (ka). The bioavailability of the formulations was scaled to that of solution. The population estimate of apparent clearance (CL/F) was 79.3 L/h, apparent central volume (Vc/F) was 2150 L, inter-compartmental clearance (Q/F) was 238 L/h, and apparent peripheral volume (Vp/F) was 2,340 L. The absorption rate was 0.56 h with a lag time of 0.36 h. Age and AST levels were found to be predictors of foretinib clearance and weight was found to be the predictor of central volume of distribution. The inter-individual variability on CL/F and Vc/F was 19.2 and 13.9 % with IOV's of 31 and 29.5 % respectively. HCC patients showed ~13.6 % lower clearance as compared to non-HCC cancer patients at equivalent doses. The volume of the central compartment (Vc) was ~21 % lower in HCC patients when similar formulations were compared.
Conclusions: The two-compartment Pop-PK model adequately characterizes the difference in the pharmacokinetics of foretinib in HCC versus non-HCC cancer patients and identified an effect of formulations on bioavailability. HCC patients showed lower clearance which could be a result of differences in metabolism in HCC patients or differences between Asian and American cancer patients.

W-035 Assessment of Actual Significance Levels for Covariate Effects of Monte-Carlo Parametric Expectation–Maximization Algorithm

Chee M. Ng[1,2], Heather E. Vezina[1*,]

[1]The Children's Hospital of Philadelphia, Philadelphia, PA, USA; [2]University of Pennsylvania, School of Medicine, Philadelphia, PA, USA

Background and Objectives: Monte-Carlo parametric expectation–maximization (MCPEM) method has been increasingly used in analyzing population PK/PD data. Due to the inherent sampling noise from the Monte-Carlo random samples that are used to evaluate the expectation steps of the MCPEM, objective function (−2LL) variability is always observed at the final stationary phase and never converged to a single final objective function value like in the FOCE method. This variability in objective function introduces an additional level of uncertainty for using the standard likelihood ratio test for nested model selection. Therefore, the objective of this study was to assess the differences between actual and nominal significance levels, as judged by the likelihood ratio test, for hypothesis tests regarding covariate effects using the MCPEM algorithm in NONMEM.
Methods: Pharmacokinetic (PK) data without covariate relationships were simulated from a one compartment IV bolus model for 50 and 100 individuals. The typical values for CL and V were 0.1 L/h and 1 L, respectively. The inter-individual variability in the parameters was described by a lognormal distribution and variances were set to 0.1 for both CL and V. The proportional error with a variance of 0.1 was used to describe the residual error model. PK data collected at 0.5, 1, 2, 4, 6, 8, 12, and 24 h after single IV bolus doses of 1000 units were used for the analysis. Two nested models were used to analyze the simulated data. The reduced model is the same model (without covariate relationships) that was used to simulate the data and the full model differed from the reduced model in that covariate relationships influencing model parameters were introduced and several covariate distributions were included in the analysis [1]. MCPEM algorithm in NONMEM version 7.3 (beta) with AUTO option for METHOD = IMP INTERACTION (with the exception of NITER which was set to 100 instead of 500) was used to generate the final results. The standard NONMEM setting for MCPEM convergence (CTYPE = 3, CITER = 10, and CALPHA = 0.05) was used. Monte-Carlo random samples (ISAMPLE) of 300 (default setting in NONMEM), 600, and 1000 were used to assess the effect of random sample size on the significant levels for hypothesis testing. Both reduced and full models were then fitted to the simulated data ($N = 2000$) and the differences in the objective function values (ΔOFV) between the reduced and full models were calculated, and actual significance levels ($p = 0.01$, 0.05 and 0.10) were determined and compared to nominal significance levels. Two different objective functions were selected to compute the ΔOFV: the last objective function and the average of the objective

Table 1 Results from Simulation Study

Changes from Default	Actual level[c] corresponding nominal 0.05	ΔOFV[d] for actual level 0.05	Actual level corresponding nominal 0.01	ΔOFV for actual level 0.01
ISAMPLE = 300 (NONMEM Default)				
Covariate Characteristics[b]				
Model 1A: 5:95	0.030	2.76	0.005	5.65
Model 1B: 10:90	0.026	2.88	0.005	5.28
Model 1C: 25:75	0.028	2.84	0.006	5.21
Model 1D: 50:50	0.034	3.01	0.006	5.39
Model 1E: Normal	0.026	2.86	0.007	5.77
ISAMPLE = 600				
Covariate Characteristics				
Model 2A: 5:95	0.063	4.22	0.011	6.73
Model 2B: 10:90	0.053	3.90	0.011	6.81
Model 2C: 25:75	0.055	3.98	0.011	6.87
Model 2D: 50:50	0.063	4.11	0.014	7.13
Model 2E: Normal	0.047	3.74	0.011	7.10
ISAMPLE = 1000				
Covariate Characteristics				
Model 3A: 5:95	0.062	4.23	0.010	6.63
Model 3B: 10:90	0.055	3.94	0.011	6.81
Model 3C: 25:75	0.054	3.95	0.012	6.82
Model 3D: 50:50	0.062	4.11	0.014	7.05
Model 3E: Normal	0.048	3.77	0.011	7.02

[a] The results were obtained using the ΔOFV computed from the last objective function in MCPEM run. Number of subject in the data = 50. Number of replicates = 2000. The results were very similar for data with 50 and 100 subjects

[b] Covariate model is described as $P = \theta_1 *(1 + \theta_2*COV)$. P is the model parameter; COV is individual-specific covariate that assumes the value 0 and 1. Each individual in the data set is randomly assigned one of these values according to different distribution probability and function. For models A, a probability of assigned value of 1 is 5 % and for 0 is 95 %. In model E, normal distribution (zero mean, unit variance) was used to assign the individual-specific value. [c] The fractions of the ΔOFV from 2000 simulated datasets showing a difference of more than 3.84 ($p = 0.05$) and 6.64 ($p = 0.01$). [d] Based on the estimated percentile from 2000 replicates

function from the last 10 iterations that were used to assess MCPEM convergence.

Results/Conclusions: In this simulated study with a rich PK data design, all MCPEM runs achieved model convergence and terminated before the maximum iteration was reached. When NONMEM default ISAMPLE = 300 was used, the actual significance levels for including a covariate relationship in a model were lower than the nominal significance level (Table 1). However, the use of ISAMPLE = 600 or 1000 resulted in close agreement between actual and nominal significance levels. This finding suggested that the selection of the ISAMPLE (the Monte-Carlo random samples used for expectation-step calculation) can affect the actual significance levels of the likelihood ratio test and ISAMPLE higher than the default NONMEM setting (>300) is needed to achieve more reliable likelihood ratio test results for covariate model selection. Further study is ongoing to investigate other potential factors (frequency of PK sampling, residual error magnitude and structure, magnitude of population variability and others) that may influence the actual significance level of the likelihood ratio test in MCPEM to confirm the findings in this study.

Table 1 Population parameter estimates for the structural model

Parameter	Estimate	(%RSE)	IIV [CV %]	(%RSE)
V_{max} (mg/h)	30.7	(15.9)	28.1	(20.7)
K_m (mg/L)	2.56	(35.8)	72.3	(9.9)
V_2 (L)	25.1	(17.7)	101	(56.8)
V_3 (L)	123	(6.1)	30.4	(37.5)
Q (L/h)	33.8	(10.5)	49.1	(47.3)
F1	0.879	(2.8)	24	(30.3)
Ka (h^{-1})	0.561	(11.2)	55	(24.6)
Alag (h)	0.205	(6.2)	NE	NE

IIV inter-individual variability; *NE* not estimated due to numerical difficulties with the first order conditional estimation with interaction (FOCE + I) algorithm

References

[1] Wahlby R, Jonsson EN, Karlsson MO (2001) Assessment of actual significance levels for covariate effects in NONMEM. J Pharmacokin Pharmacodyn 28:231–252

[2] Beal SL (2001) Commentary on significance levels for covariate effects in NONMEM. J Pharmacokin Pharmacodyn 29:403–410

W-036 Voriconazole Population Pharmacokinetics

Michael Dolton[1*], Gerd Mikus[2], Johanna Weiss[2], John Ray[3], Andrew McLachlan[1,4]

[1]Faculty of Pharmacy, University of Sydney, Sydney, NSW, Australia; [2]Clinical Pharmacology Study Centre, Heidelberg University Hospital, Heidelberg, Baden-Württemberg, Germany; [3]SydPath, St Vincent's Hospital, Sydney, NSW, Australia; [4]Centre for Education and Research on Ageing, Concord Repatriation General Hospital, Sydney, NSW, Australia

Objectives: The azole antifungal voriconazole is widely used as a first-line agent in the treatment of life-threatening invasive fungal infections (IFIs) [1]. Voriconazole is known to display non-linear pharmacokinetics and high inter-individual variability, primarily due to saturable metabolism via CYP2C19 [2, 3]. Coupled with the narrow therapeutic index observed with voriconazole, with low concentrations (<2 mg/L) associated with treatment failure and high concentrations (>5 mg/L) with neurotoxic adverse events [4], these factors complicate voriconazole dose selection and adjustment. Despite its widespread use, relatively few population pharmacokinetic analyses are available for voriconazole in adults [5–7]; linear [5], non-linear [7] and mixed linear and non-linear elimination [6] have been used to describe voriconazole elimination in these analyses. Importantly, the effects of clinical covariates (drug–drug interactions in particular) on the disposition of voriconazole are yet to be comprehensively investigated in a population model.

The objectives of this analysis were to develop an integrated population pharmacokinetic model for voriconazole incorporating multiple sources of data, as well as investigating a range of important demographic and clinical covariates that may affect voriconazole pharmacokinetics. Table 1

Methods: Four studies undertaken in a total of 63 healthy volunteers with rich pharmacokinetic sampling were included [8–11] in addition to sparsely sampled data from 146 patients receiving voriconazole for the treatment of IFIs [4]. A total of 3024 voriconazole concentrations were included in the analysis. Non-linear mixed effects modeling was carried out with NONMEM 7.2. Studies were added in a stepwise manner and a base model developed from the richly sampled data; sparsely sampled patient data was then incorporated into the model [12]. Goodness-of-fit criteria such as significant decreases in the objective function value (OFV; $p < 0.05$) and goodness-of-fit plots such as conditional weighted residuals vs. time and conditional weighted residuals vs. population-predicted concentration plots, as well as visual predictive checks (VPCs) were used to guide model selection and development. The confidence intervals of the parameter estimates and visual improvement of the individual plots were also used to evaluate the models. Covariate relationships were tested against several criteria including a significant reduction in OFV, reduction in the inter-individual variability (eta) of the associated structural parameter, and the precision of the additional estimated parameter.

Results: A two compartment model with an absorption lag time and Michaelis–Menten elimination adequately described the dataset; a model incorporating linear elimination resulted in a significant increase in OFV whereas models incorporating mixed linear and non-linear elimination did not improve goodness-of-fit over non-linear elimination alone. Voriconazole elimination was significantly faster following a single dose than at steady state due to auto-inhibition of metabolism [6]; for single dose studies in the model a parameter incorporated on V_{max} estimated a 255 % higher V_{max} (95 % CI 137–373 %) over a single dose than at steady state.

Covariate screening identified significantly higher voriconazole exposure in participants with one or more *CYP2C19* alleles that are associated with a poor metabolizer (PM) phenotype (*CYP2C19*2*) compared to participants without these alleles (*CYP2C19*1/*1*, extensive metabolizer phenotype) (Fig. 1). Participants with a CYP 2C19 heterozygous extensive metabolizer phenotype (*CYP2C19*1/*2*) or poor metabolizer phenotype (*CYP2C19*2/*2*) had a 57 % (95 % CI 42–72 %) lower V_{max} compared to homozygous extensive metabolisers (*CYP2C19*1/*1*).

A number of concomitant medicines were found to significantly affect voriconazole pharmacokinetics. Co-administration of the CYP3A4 inhibitor ritonavir decreased V_{max} by 44 % (95 % CI 36–51 %) whereas co-administration of St John's wort increased V_{max} by 108 % (95 % CI 82–134 %). The strong CYP450 inducers phenytoin and rifampicin increased V_{max} 207 % (95 % CI 144–270 %). Co-administration of a glucocorticoid (prednisolone, methylprednisolone or dexamethasone) increased V_{max} by 31 % (95 % CI 13–49 %). Internal validation of the final model using VPCs verified that the model adequately describes the observed voriconazole concentrations (Fig. 2).

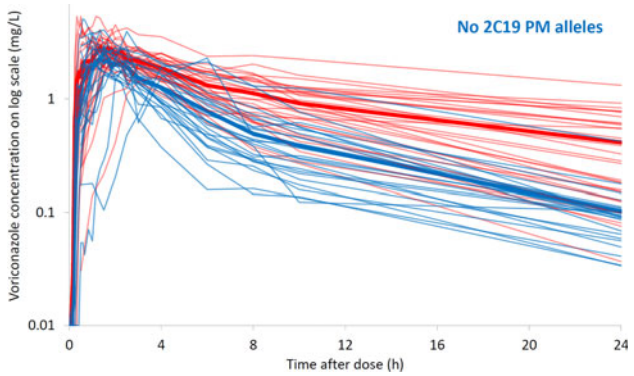

Fig. 1 Voriconazole concentration–time profiles for participants with ≥1 *CYP2C19* poor metabolizer alleles (*red*, $n = 30$) and without (*blue*, extensive metabolizers, $n = 25$) following a 400 mg oral dose. The *bold lines* show the median concentration–time profiles

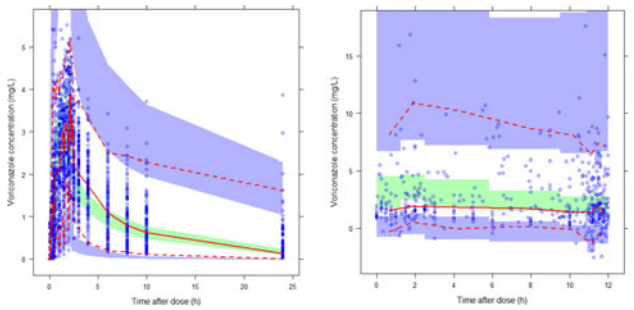

Fig. 2 Prediction-corrected visual predictive checks (pcVPCs) for single dose studies (*left*) [8–10] and multiple dose studies (*right*) [11, 12]. Open circles represent the prediction-corrected observed concentrations. The red solid and dashed lines represent the median and 5th and 95th percentiles of the observed prediction-corrected concentrations, respectively. The green and blue shaded areas around the lines represent the simulation-based 95 % confidence intervals for the median and 5th and 95th percentiles, respectively

Conclusions: A two-compartment model of oral and intravenous voriconazole pharmacokinetic data was developed from five studies and resulted in good precision in parameter estimates and predictive performance. *CYP2C19* genotype is an important intrinsic determinant of voriconazole disposition while a number of drug–drug interactions lead to clinically significant changes in voriconazole exposure. Future work will utilize this model in dosing simulations to target the narrow therapeutic range recommended for voriconazole therapeutic drug monitoring (trough concentration of 2–5 mg/L [4]), and investigate the utility of this model in a Bayesian dose forecasting tool to aid clinicians in voriconazole dose selection and adjustment.

References

[1] Walsh T, et al (2008) Clin Infect Dis 46(3):327–360
[2] Theuretzbacher U, et al (2006) Clin Pharmacokinet 45(7): 649–663
[3] Andes D, et al (2009) Antimicrob Agents Chemother 53(1): 24–34
[4] Dolton M, et al (2012) Antimicrob Agents Chemother 56(9):4793–4799
[5] Pascual A, et al (2012) Clin Infect Dis 55(3):381–390
[6] Friberg L, et al (2012) Antimicrob Agents Chemother 56(6):3032–3042
[7] Hope W, et al (2012) Antimicrob Agents Chemother 56(1):526–531
[8] Scholz I, et al (2009) Br J Clin Pharmacol 68(6):906–915
[9] Mikus G, et al (2006) Clin Pharmacol Ther 80(2):126–135
[10] Rengelshausen J, et al (2005) Clin Pharmacol Ther 78(1):25–33
[11] Katzenmaier S, et al (2011) Clin Pharmacol Ther 90(5): 666–673
[12] Svensson E, et al (2012) Br J Clin Pharmacol 74(3):465–476

W-038 Confirmatory Population Pharmacokinetic Analysis of Bapineuzumab in Subjects with Mild to Moderate Alzheimer's Disease in Two Phase 3 Studies (ELN115727-301 and ELN115727-302)

Omoniyi Adedokun[1], Ming Lu[1*], Kaori Ito[2], Sangeta Raje[3], Mahesh Samtani[4], Steven Xu[4], Brian Corrigan[2], Chuanpu Hu[1]

[1]Janssen Research & Development, LLC, Spring House, PA, USA; [2]Pfizer, Inc., Groton, CT, USA; [3]Pfizer, Inc., Collegeville, PA, USA; [4]Janssen Research & Development, LLC, Titusville, NJ, USA

Objectives: PK data were obtained from two phase 3 trials in APOE ε4 allele carriers and non-carriers with mild-moderate Alzheimer's disease (AD) following multiple IV doses of bapineuzumab ranging from 0.5 to 2 mg/kg. A prior population PK model built from subjects with AD from earlier phase clinical studies with both IV and SC administrations was also available. The structural model was a two-compartment model with first-order absorption, with body weight as the only covariate affecting bapineuzumab PK. The confirmatory population PK approach [1] was applied to estimate bapineuzumab pharmacokinetics for the phase 3 study population and to assess the influence on bapineuzumab exposure for all covariate factors, such as demographics or baseline disease characteristics, that the data can be expected to support in a prospective manner.
Methods: A total of 8,040 serum bapineuzumab concentration measurements from 1,458 subjects with AD (787 subjects from Study 301, and 671 subjects from Study 302) who received multiple IV doses of bapineuzumab ranging from 0.5 to 2 mg/kg were included in the population PK analysis. The population PK base model was pre-specified based on a prior population PK model built from subjects with AD from earlier phase clinical studies, along with the phase 3 study design. The covariate list, assessed on only CL, was pre-specified based on only the individual covariate values. More specifically, the covariate list was determined with the criteria: (1) there were at least 20 subjects for each parameter to be estimated; and (2) covariates were not highly correlated (>0.5).
Results: The typical population values for CL and Vc in a Caucasian subject with a standardized body weight of 70 kg were 0.17 L/day [95 % confidence interval (CI): 0.15–0.18 L/day) and 3.13 L (95 % CI: 1.45–3.18 L)], respectively. The BSV in terms of %CV was 28.1 % for CL and 33.0 % for Vc. Covariate analysis confirmed that bapineuzumab CL and Vc increased with body weight. In addition, CL was 15 % higher in non-Caucasian subjects compared to Caucasian subjects; however, this was not considered clinically relevant. None of the other assessed covariates had a meaningful impact on bapineuzumab CL. The median terminal elimination half-life of bapineuzumab was estimated to be approximately 29 days. Additional sensitivity analyses along with goodness of fits suggest that the model adequately described the data.

Conclusions: A robust population PK model was developed for bapineuzumab following multiple IV administration in subjects with mild to moderate AD. The population PK analysis confirmed that body weight was a significant covariate affecting the systemic exposure to bapineuzumab and may need to be taken into account when bapineuzumab is administered to subjects with AD.

Reference

[1] Hu C, Zhang J, Zhou H (2011) Confirmatory analysis for phase III population pharmacokinetics. Pharm Stat 10(1):14–26

W-039 A Population PK Model for Cariprazine and the Metabolites

Tatiana Khariton[1*], Luann Phillips[2], Sebastien Bihorel[2], Jill Fiedler-Kelly[2], Margit Kapás[3], Antonia Periclou[1], Parviz Ghahramani[1]

[1]Forest Research Institute, Jersey City, NJ, USA; [2]Cognigen Corporation, Buffalo, NY, USA; [3]Gedeon Richter Plc., Budapest, Hungary

Objectives: To develop population pharmacokinetic (PK) models of cariprazine (CAR) and its two main metabolites, desmethyl-cariprazine (DCAR) and didesmethyl-cariprazine (DDCAR) in patients with schizophrenia or bipolar mania following once daily dosing with CAR; and to evaluate the influence of selected demographic characteristics, renal function, CYP2D6 genotype and certain classes of concomitant medications.

Methods: Data from 12 studies (3 Phase 1, 3 Phase 2, and 6 Phase 3) in patients with schizophrenia and bipolar manic or mixed episodes associated with Bipolar I disorder were used to develop the population PK models for CAR, DCAR and DDCAR. The three Phase 1 studies used rich PK sampling schemes, while 9 others (placebo-controlled efficacy and safety studies as well as open-label long-term safety studies) collected sparse PK samples. All of the studies included dose titration with target dose levels ranging from 0.5 to 24 mg/day and treatment periods of up to 48 weeks. The 3 population PK models were fitted sequentially, with individual PK parameters for CAR fixed and serving as input to the DCAR population PK model, and with individual PK parameters for CAR and DCAR fixed and serving as input to the DDCAR population PK model. The base population PK models were developed using the data from the 3 Phase 1 studies and were then updated with the addition of the Phase 2 and 3 studies. Covariate analysis was performed on PK parameters with measurable variability. The influence of demographic, hepatic and renal characteristics of interest was explored on each PK parameter separately using a step-wise generalized additive model (GAM) procedure in SAS and S-Plus. The direction of each step-wise search was both forward and backward. The final model for each PK parameter obtained from GAM analysis was then fit to the data in NONMEM. Univariate step-wise backward elimination of covariates in NONMEM proceeded until all the remaining covariates were significant ($p < 0.001$). Next, the effects of the concomitant medication classes (CYP2D6 inhibitors, CYP3A4 inhibitors, and general CYP inducers) on apparent clearance (CL/F) were added simultaneously to the model for each moiety. The backward elimination procedure ($p < 0.001$) was then followed to determine which concomitant medication covariates were statistically significant. As a last step of the covariate analysis, the effect of CYP2D6 genotype status on the clearance of CAR, DCAR and DDCAR was evaluated. This was done using the data solely from four clinical studies in which blood samples were tested for CYP2D6 genotype status identifying subjects as poor CYP2D6 metabolizers and non-poor metabolizers (ultra-extensive, extensive, intermediate metabolizers). The post hoc Bayesian individual parameter estimates for apparent clearance, dose-normalized AUC_{0-24}, C_{max}, and C_{min} at steady state were used in a Wilcoxon signed-rank test to evaluate the effect of CYP2D6 metabolizer status on the PK of CAR, DCAR and DDCAR. The final population PK models were evaluated using visual predictive check and bootstrapping methods. All population modeling was performed in NONMEM, Version 7.1.2, on an Intel cluster with the Linux operating system. The first-order conditional estimation (FOCE) method with interaction was used.

Results: A total of 14,613 CAR measurable plasma concentrations from 2,392 patients, 14,380 measurable DCAR plasma concentrations from 2,387 patients and 13,531 measurable DDCAR plasma concentrations from 2,344 patients were used in the development of the population PK models. The population PK analyses were performed using doses ranging from 1.5 to 18 mg/day. The most parsimonious structural model describing CAR was a two-compartment disposition model with first-order elimination and sigmoid absorption, characterized by a zero-order input of the dose in a depot compartment followed by a first-order transfer into the central compartment. Typical apparent clearance (CL/F) and central volume of distribution (Vc/F) of CAR were estimated to be 22.8 L/h and 454 L, respectively. The most parsimonious structural model describing DCAR or DDCAR was a one-compartment model with first-order elimination. Typical CL/F and Vc/F of DCAR were estimated to be 70.9 L/h and 176 L, respectively, and for DDCAR were 6.74 L/h and 2220 L, respectively. The CL/F and Vc/F of each moiety were statistically dependent upon a function of body weight. Race, gender, and age were also statistically significant predictors of the CL/F or Vc/F of some moieties. However, none of the covariates were found to be clinically relevant (their effect ranged between 2 and 32 %). Other variables describing hepatic (albumin and NCI liver dysfunction classification) and renal (creatinine clearance and classes of renal impairment) functions were found to be no statistical significance. The concomitant administration of CYP2D6 inhibitors ($N = 106$, 5.2 % of patients), mild or moderate CYP3A4 inhibitors ($N = 21$, 1 % of patients), and CYP inducers ($N = 52$, 2.5 % of patients) did not show a statistically significant effect on the apparent clearance of any of the moieties. A total of 895 patients were genotyped for CYP2D6 status. Of these, 39 patients were poor metabolizers. There were no statistical differences ($p > 0.05$) in CAR and DCAR exposures and no clinically relevant differences in DDCAR exposures for poor metabolizers as compared to others (16 % statistically higher in poor metabolizers, $p \leq 0.05$). Final CAR, DCAR, and DDCAR population PK models predicted the median time to achieve 90 % of absolute steady-state to be 4, 4, and 31 days, for CAR, DCAR, and DDCAR, respectively and the functional half-life was 1, 1, 9 days, respectively. The PK of CAR, DCAR and DDCAR were found to be linear within the 1.5-18 mg/day dose range.

Conclusions: The linear population PK models adequately described the PK profiles of CAR and its two major active metabolites in patients with schizophrenia or bipolar manic or mixed episodes associated with Bipolar I disorder after exposure to doses ranging from 1.5 to 18 mg/day. No statistically significant effect on the PK of any of the moieties were noted for hepatic function, renal function, concomitant administration of CYP2D6 inhibitors, CYP3A4 inhibitors, or CYP inducers. Patients classified as CYP2D6 poor metabolizers had no clinically relevant difference in exposure compared to non-poor metabolizers. The typical functional half lives of CAR, DCAR and DDCAR (1 day, 1 day, and 9 days, respectively) support once daily dosing for cariprazine in the patient population described above (Fig. 1).

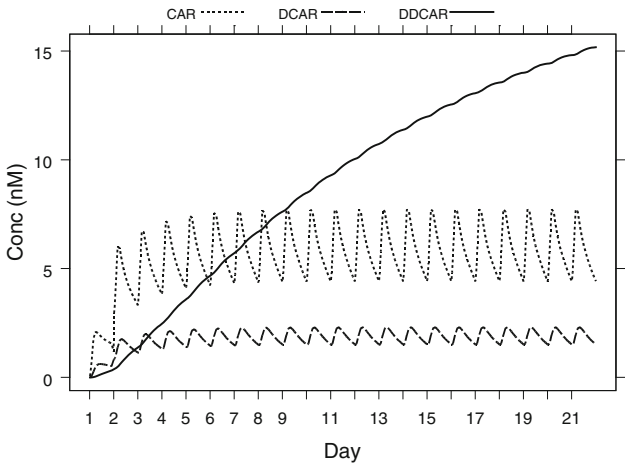

Fig. 1 Average CAR, DCAR, and DDCAR exposures for a typical patient following 21 days of dosing titrated to 12 mg/day dose by Day 10

W-040 Pharmacokinetic-Pharmacodynamic Modeling of Amyloid-Related Imaging Abnormalities of Edema Following Intravenous Administration of Bapineuzumab to Subjects with Mild to Moderate Alzheimer's Disease

Matt Hutmacher[1*], Chuanpu Hu[2], Volkmar Guenzler-Pukall[3], Michael Arrighi[3], Kaori Ito[4], Mahesh Samtani[5], Steven Xu[5], Sangeeta Raje[6], Brian Corrigan B[4], Ming Lu[2]

[1]Ann Arbor Pharmacometrics Group, Ann Arbor, MI, USA; [2]Janssen Research & Development, LLC, Spring House, PA, USA; [3]Janssen Alzheimer Immunotherapy Research & Development, LLC, South San Francisco, CA, USA; [4]Pfizer, Inc., Groton, CT; [5]Janssen Research & Development, LLC, Titusville, NJ, USA; [6]Pfizer, Inc., Collegeville, PA, USA

Objectives: Bapineuzumab is a humanized anti-amyloid-beta monoclonal antibody given intravenously and was evaluated in four phase 3 clinical trials for the treatment of Alzheimer's disease (AD). Amyloid-related imaging abnormalities—edema/effusion (ARIA-E) are radiological findings detected by magnetic resonance imaging (MRI) as an area of high signal intensity on T2-weighted or fluid-attenuated inversion recovery (FLAIR) sequences. ARIA-E occurrence appears to be related to bapineuzumab treatment (i.e., a treatment emergent event) in a dose dependent manner based on early phase clinical studies. The primary objectives of this pharmacokinetic/pharmacodynamic (PK/PD) modeling effort were (1) to develop a PK/PD model relating time to event (TTE) of ARIA-E to bapineuzumab exposure and (2) to develop a PK/PD model relating the total radiological score (RS), a measurement of severity of ARIA-E, to bapineuzumab exposure. The secondary objectives were to evaluate covariates of clinical interest that may affect the risk of an ARIA-E event, or given an event, modify the RS.

Methods: Data are from two phase 3 clinical studies of bapineuzumab in patients with mild to moderate Alzheimer's disease who are APOE ε4 carriers (Study 301) and non-carriers (Study 302). Total number of subjects enrolled, $n = 2{,}452$. Patients received either bapineuzumab (0.5 or 1.0 mg/kg) every 13 weeks for 6 doses and were followed until study endpoint at 78 weeks. MRIs were performed per protocol 6 weeks after bapineuzumab treatment at 13 weeks intervals. Two pharmacokinetic/pharmacodynamic (PK/PD) models have been developed: one relating TTE of an ARIA-E event to bapineuzumab exposure, and one relating RS as determined by MRI to bapineuzumab exposure in subjects with mild to moderate AD—from two phase 3 trials. The onset of an ARIA-E event was the interval starting at the time immediately after the prior MRI with no findings, up to and including the time of the following MRI at which the abnormalities were discovered, therefore, interval censoring methods were implemented for the TTE analysis. A log-additive hazard model was used to describe the TTE of ARIA-E. Overall goodness of fit was assessed using simulation-based diagnostics such as the Visual Predictive Check (VPC). Complete use of the observed trial design for simulation was not possible for ARIA-E; per protocol, once a patient was indentified with ARIA-E, the bapineuzumab treatment was stopped until the event resolution and subsequent treatment was initiated at a lower dose and additional MRIs were performed at intervals less than 13 weeks for clinical monitoring and evaluation. However, not all patients with ARIA-E underwent a temporary suspension of dose followed by a dose reduction. During the course of the clinical trial, a protocol amendment was implemented resulting in the downward titration of the 2 mg/kg cohort to 1 mg/kg. Therefore, models were constructed to account for the randomness in the scheduled MRI times and doses as well as the timing of the titration for the 2 mg/kg group. A traditional VPC for survival, concordance of observed and simulated survival curves, was computed using Turnbull's nonparametric estimator of survival for interval censoring. Comparisons of survival curves can lack resolution for determining the adequacy of a parametric hazard, because survival curves are based on the exponentiation of the area under the hazard curve (cumulative hazard function). Therefore, to aid in evaluating specific components of the hazard, a binned hazard VPC was also performed. The concept is to compute a data-based hazard profile to compare data and model on the scale on which the data are modeled.

RS is a bounded outcome score (BOS) ranging from 0 to 180, inclusive. Because a few placebo and approximately 20 percent of the treated patients had ARIA-E events, RS was modeled conditionally—considering RS data from patients who had an ARIA-E event. The BOS methodology as described by Hutmacher et al. was modified accordingly. A VPC was also performed to evaluate the RS model. Base models were developed for both endpoints. Study-specific effects were evaluated to check the adequacy of pooling the carrier versus non-carrier studies. Next, covariates which were pre-specified to a large extent were added in the attempt to formulate full models for the endpoints. The Wald approximation method was then implemented to determine a set of candidate models, one of which was selected as the final (most likely) covariate model. APOE ε4 copy number (the effect of 2 alleles) was then evaluated for its affect on risk of an event and severity in an ad hoc fashion.

Results: A total of 2423 subjects were included in the ARIA-E analysis, of whom 243 were identified with ARIA-E. The parameter estimates of the ARIA-E final model suggested that the hazard for an ARIA-E event is 988-fold greater in subjects with maximum drug effect (E_{max}; effect when bapineuzumab concentration are several fold higher than the EC_{50}) relative to placebo. The predicted incidence rate of an ARIA-E event was found to attenuate as time progresses. The baseline ARIA-E hazard (i.e., hazard without consideration of treatment) was 69 % lower for APOE ε4 non-carriers (Study 301) relative to carriers (Study 302). Microhemorrhage at baseline (presence versus absence) and an effect of APOE ε4 copy number of 2 alleles were added as covariates in the final model. Presence of microhemorrhage increased the baseline ARIA-E hazard 1.85-fold. Additionally an APOE ε4 copy number of 2 increased the maximum drug effect risk by 4.33 fold. The incidence of ARIA-E events was primarily driven by bapineuzumab concentration, as evidenced by the low number of placebo subjects that had events. In addition, the results demonstrated that the bapineuzumab exposure is

slightly higher in heavier subjects than in lighter subjects using the weight based dose and such an increase could amplify the risk of ARIA-E despite the slight difference. As a result, heavier subjects receiving higher doses of bapineuzumab, with microhemorrhage present at baseline, and with an APOE ε4 copy number of 2 had the greatest risk for an ARIA-E event.
A total of 243 subjects contributed to the RS analysis. The maximum effect of bapineuzumab concentration on RS response attenuated over time for both Study 302 (carriers) and Study 301 (non-carriers). A larger E_{max} value was observed in APOE ε4 carriers than non-carriers. No other covariates were found to be predictors of RS.
Conclusions: Overall, the results of the modeling indicate that the incidence of ARIA-E events and their severity (RS) are dose (concentration) dependent and attenuate with time since treatment initiation. The parameter estimates of the final model and the visual predictive check results indicate that the baseline risk is low, and the risk of an event is highest after the first dose of bapineuzumab. The incidence of ARIA-E events was driven by bapineuzumab concentration, confirming that the risk of an ARIA-E event is mechanism related. The primary risk factors for an event are serum bapineuzumab concentration, APOE ε4 copy number, and the presence of baseline microhemorrhage. The maximal effect of bapineuzumab concentration on severity (RS) attenuated over time, which might be due to the recovery of vascular integrity after removal of amyloid deposition.

W-041 Reduction in Interindividual Variability and Clinical Significance Ratio in Covariate Assessment

Susan Willavize*, Jill Fiedler-Kelly

Cognigen Corporation, Buffalo, NY, USA

Objectives: Covariate analysis has become a customary and expected part of population PK and PK/PD modeling [1]. The covariate submodel describes, explains, and predicts the impact of patient characteristics on drug exposure and effects. Various criteria have been discussed for assessing the utility of a covariate. These criteria include reduction in interindividual variability (IIV) [2] and measures of the clinical importance [3].
Using creatinine clearance (CrCL) as an example covariate, this study aims to investigate the relationships between the clinical significance ratio (CSR) and

- Reduction in inter-individual variability between base and covariate models
- Design factors such as the number of subjects, number of PK samples per subject (n) and the diversity of the covariate observations (in terms of the corrected sum of squares (CSS) of the observed covariates).

Methods: Basic statistical properties of the covariate submodel alone indicate that the probability of detecting a covariate relationship is dependent on the true value of the slope and CSS. A simulation study was undertaken to explore, in the population PK context, the effects of these factors as well as the sparseness of sampling within subjects on the CSR and the change in unexplained IIV. SAS9.2 was used to create the simulation data and to summarize the results. NONMEM 7.2 was used for nonlinear mixed-effect modeling.
Simulation data:

- 1-cmt, bolus dose PK model with first order elimination, single dose, CL = 3 L/h, Vc = 50 L, dose = 100 mg
- TVCL = $\theta_0 + \theta_C$ * CrCL; θ_0 = 50 mL/min, θ_C = 0, 0.0850, 0.4225, 0.83 (corresponding to true CSR values of 1, 0.9, 0.7, and 0.6, respectively)
- CrCL ranges from 30 to 140 mL/min; 4 differently distributed samples from this range of CrCL values which provide differing patterns of diversity, and hence different values of CSS
- R = 1,000 simulation replications/scenario
- N = 50, 100 subjects/simulated clinical trial
- n = 12 or 5 samples per subject (at times t = 0, 1, 2, 3, 4, 6, 8, 10, 12, 16, 20, 24 h or t = 0, 1, 4, 12, 24 h)
- ω_{CL} = 25 % CV, ω_{Vc} = 25 % CV ($CL_i = \theta_1 \cdot \exp(\eta_{1i})$, $Vc_i = \theta_2 \cdot \exp(\eta_{2i})$), σ = 30 % CV (proportional residual variability, variance = 0.09)

Estimation methods:

- NONMEM 7, with FOCEI
- Base model with covariate effect at null value
- Linear covariate model: TVCL = THETA(1) + THETA(2) * (CrCL − 80);
- Power function covariate model: TVCL = THETA(1) * (CrCL/80) **(THETA(2))
- Statistical significance based on P value computed by χ^2 (delta_MVOF, 1); where delta_MVOF is computed by difference in MVOF for base model (THETA(2) fixed at 0) versus covariate model
- Reduction in interindividual variability as the percent reduction in the estimated iiv (expressed as SD) for base model versus covariate model

Results: Example results for sparse sampling and the most extreme CSS values are provided below. Results for full profile sampling were essentially the same as those for sparse data and results for True CSR = 0.6 were essentially the same as those for True CSR = 0.7. While the proportional reduction in IIV decreased with increasing CSS, the estimated CSR was essentially constant.
When the True CSR was equal to 1 (indicating no clinically important effect), the estimated CSR was unbiased. P values for the null case averaged about 0.5, while the proportional reduction in IIV was low and sometimes negative (indicating an increase in IIV).

In non-null cases the CSR was underestimated, but seemed to plateau for values of True CSR <0.9. P-values for these cases usually indicated statistical significance (mean <0.01 and maximum was less than 0.1). Proportional reduction in IIV varied inversely with estimated CSR.

Scenario 1 (CSS = 83,000)

Mean (SD)		True CSR		
		1.0	0.9	0.7
Sparse	Proportional reduction in IIV	0.007 (0.011)	0.30 (0.035)	0.42 (0.047)
	Estimated CSR	1.00 (0.077)	0.54 (0.035)	0.43 (0.027)

Scenario 3 (CSS = 28,000)

Mean (SD)		True CSR		
		1.0	0.9	0.7
Sparse	Proportional reduction in IIV	0.007 (0.015)	0.13 (0.047)	0.21 (0.054)
	Estimated CSR	1.01 (0.15)	0.55 (0.071)	0.44 (0.058)

Conclusions:

1. Under the null-case, the p-value alone provided unreliable indication of the absence of effect. But the lack of reduction in IIV in this case provided an indication that there was no strong covariate effect.
2. In the null-case, the estimated CSR was unbiased and in the non-null cases, it was generally underestimated, but decreased with the True CSR, indicating the presence of a covariate effect.
3. For the scenarios studied, the findings were insensitive to the sparseness of the sampling strategy.
4. In the absence of a clearly defined clinical significance function, the proportional reduction in IIV together with statistical significance may provide an indication of the presence of a covariate effect, with the extent of reduction in IIV indicative of the size of the CSR.

References

[1] Dartois C, et al. (2007) Overview of Model-building Strategies in Population PK/PD Analyses: 2002-2004 Literature Survey. Br J Clin Pharmacol 64:503–612

[2] Lagishetty CV, Vajjah P, Duffull SB (2012) A reduction in between subject variability is not mandatory for selecting a new covariate. JPP 39:383–392

[3] Gastonguay MR (2004) A full model estimation approach for covariate effects: inference based on clinical importance and estimation precision. The AAPS J 6(S1), Abstract W4354

W-042 Utility of Model-based Meta-analyses for Evaluation of Phase 2 Results and Phase 3 Study Design for Trials in Patients with Advanced Pancreatic Cancer

Dana J Nickens*, Michael A Amantea

Pfizer, Inc., San Diego CA, USA

Objectives: New therapies are needed for pancreatic cancer as it is a difficult disease to treat and has a 5 year overall survival rate of less than 4 % [1]. A completed meta-analysis of the current literature on pancreatic cancer drug therapies [2] was used to (1) evaluate treatment effects of overall survival from a completed phase 2 study; (2) combine the phase 2 data with the meta-analysis results for an updated model for overall survival; (3) provide performance metrics for a proposed phase 3 design relative to the current knowledge about a new drug therapy; (4) compare the completed Phase 3 trial results with the model-based meta-analysis predictions.

Methods: A completed phase 2 study in pancreatic patients with gemcitabine as the control arm and gemcitabine + new drug therapy was available for comparison with a pancreatic cancer meta-analysis. A completed meta-analysis of drug therapies used a linear model for therapies based on drug class with between study random effects for median overall survival [2]. The model was used to generate a predictive distribution for the gemcitabine arm and for a 2 drug combination arm with gemcitabine with which to compare the phase 2 results.

Bayesian methods with non-informative priors were used to combine aggregate data from the phase 2 trial with the pancreatic meta-analysis to provide an updated model. Based on an assumed parametric survival distribution, the updated model was used to estimate the hazard ratio of gemcitabine versus the combination arm. The updated meta-analysis results were also compared to the actual phase 3 trial results.

The updated pancreatic meta-analysis with an assumed parametric survival distribution was used to generate results for 10,000 simulated future phase 3 trials based on a chosen study design. Comparisons were made between the simulated data-analytic results and the predictive distribution (10,000 simulations for 596 patients in each future clinical trial) for the hazard ratio of the treatment effect of using the updated meta-analysis model. Performance metrics (e.g., probability of technical success, probability of making a correct decision, probability of a go decision) were calculated and the phase 3 trial design evaluated based on these metrics

Results: The phase 2 overall survival result for gemcitabine (5.6 months; $n = 34$) was compared to the meta-analysis model based predictive distribution for that size study, and had probability of 18 % of being smaller indicating that the phase 2 gemcitabine result was toward the lower end of the predictive distribution. The overall survival result for gemcitabine + new drug (6.9 months; $n = 69$) was compared to the meta-analysis model based predictive distribution for a combination with gemcitabine arm of that size study and had probability of 82 % of being larger indicating that the phase 2 combination arm result was toward the lower end of the predictive distribution.

The updated Bayesian meta-analysis showed that the gemcitabine + new drug combination provided only a 0.3 month improvement over gemcitabine versus a 1.3 month improvement based on the phase 2 result alone. The observed phase 2 hazard ratio for gemcitabine vs. combination therapy was 0.79 while the updated model based hazard ratio was 0.97. The hazard ratio for the treatment comparison in the actual phase 3 trial was 1.04.

Based on the simulations using the updated meta-analysis model, the probability of success in a phase 3 trial is 13 %. The probability of a correct decision for the phase 3 trial was 54 %. A go decision had a probability of 59 %. These metrics relating the compound and study design performance indicated that overall success in phase 3 would be poor.

Conclusions: The availability of a meta-analysis of recent pancreatic trials was useful: (1) to evaluate the results of phase 2 trial; (2) to assess the performance of proposed phase 3 designs; (3) to augment phase 2 results in evaluating the future success of a compound under a selected phase 3 design.; (4) for providing a more systematic and quantitative framework to inform the transition strategy between phases of drug development.

References

[1] Greenlee RT, Murray T, Bolden S, et al (2000) Cancer statistics. CA Cancer J Clin 50 (1):7–33

[2] Nickens D, Khosravan R, Amantea M, French J (2011) A systematic review and meta-analysis of recent drug therapies for chemo-naïve patients with advanced pancreatic cancer. Poster at American Conference on Pharmacometrics, San Diego

W-043 Detection of Immunogenicity and Unbiased Estimation of Model Parameters for Monoclonal Antibodies

Leonid Gibiansky*, Ekaterina Gibiansky

QuantPharm LLC, North Potomac, MD, USS

Objectives: To propose and evaluate methods for detection of immunogenic increase of elimination using concentration–time data and for unbiased estimation of model parameters in the presence of immunogenicity.

Methods: A large dataset (1,000 subjects) was simulated with sampling scheme that included the rich data following the first and the last doses, and also trough and peak values for all other doses. Intravenous doses were administered on days 1, 8, 15, 28, and then every 4 weeks during the 24-weeks treatment period. A two-compartment model with parallel linear and Michaelis–Menten elimination, and pharmacokinetic parameters typical for the monoclonal antibodies with membrane-bound targets were used. Random effects with moderate (CV = 20 %) inter-subject variability were included for all parameters. The exponential residual error (CV = 20 %) was implemented as an additive error in the log-transformed variables. Immunogenicity was simulated in non-specific clearance in approximately 30 % of subjects as (a) 5-fold increase following the doses at days 56, 84, 112, or 140 (with equal probability of each of these onset times), or (b) according to a steep Hill function of time with inter-individual variability in E_{max} and T_{50} parameters.
First, the model that did not account for immunogenicity was fitted to evaluate bias of the parameter estimates. Then, two methods of accounting for immunogenicity were tested.

The first method (called ETA-on-epsilon method) introduced the random effect on the magnitude of the residual error, hypothesizing that subjects with immunogenicity would have higher magnitude of this parameter. The same model was then fitted to the sequence of datasets where the increasing fractions of subjects with the highest residual error were commented out. Association of subjects with immunogenicity and subjects with high residual error was investigated. The obtained parameter estimates of each model were compared with the true parameters of non-immunogenic subjects.

The second method used the Nonmem mixture model routine. For the data set (a) it was assumed that the study population consisted of 5 subpopulations. Subpopulation 1 did not have immunogenicity while subpopulations 2, 3, 4, and 5 were allowed to have an increase in clearance following the doses at days 56, 84, 112 or 140 (to match the simulated pattern of immunogenic increase in clearance). For the data set (b) 2 subpopulations represented non-immunogenic and immunogenic subjects with increase in non-specific clearance modeled by the Hill function of time. The parameter estimates were compared with the true parameters, and the ability of the models to correctly identify presence and onset time of immunogenic response was investigated.
Results: The parameter estimates of the model that did not account for immunogenic increase of clearance were significantly biased and the estimate of the inter-individual variability in clearance was greatly inflated. Introduction of ETA-on-epsilon reduced, but not eliminated bias. High individual ETA-on-epsilon values identified immunogenic subjects. When subjects with high magnitude of the residual error were removed from the datasets, bias due to the unaccounted immunogenic increase of clearance was eliminated. At the same time, the variance of the ETA-on-epsilon random effect decreased to zero indicating that the ETA-on-epsilon random effect indeed accounted for immunogenicity.
The mixture models provided the unbiased estimates of the model parameters in both cases (a) and (b). The simulated immunogenic subjects were correctly assigned to the appropriate subpopulations. Thus, the estimates of the mixture model can be used to identify the onset of immunogenic increase of clearance.

The proposed methods allowed identification of subjects with immunogenic increase of clearance; they also reduced or completely eliminated bias of the parameter estimates in the simulated datasets.
Conclusions: For the simulated datasets with rich sampling, the proposed ETA-on-epsilon and mixture model methods identified subjects with immunogenic increase of clearance, provided unbiased individual estimates of the onset time and magnitude of immunogenicity, and unbiased estimates of population parameters. The proposed methods offer the approach to evaluate and describe influence of immunogenicity on the population PK parameters of monoclonal antibodies.

This work should be viewed as proof-of-concept investigation as it was applied in nearly perfect simulated conditions, with rich sampling before and after the onset of immunogenic reaction. Application to the real data will likely face more difficulties. However, the proposed methods provide useful tools for detection and evaluation of changes in the PK parameters related to immunogenicity.

W-044 A Novel Method of Covariate Selection for Analyzing a Large Number of Covariates: Application to Pharmacogenetics Variables

Chaitali Passey[1,*], Kyle T. Baron[2], Pamala A. Jacobson[1], Richard C. Brundage[1], Angela K. Birnbaum[1]

[1]Department of Experimental and Clinical Pharmacology, University of Minnesota, Minneapolis, MN, USA; [2]Metrum Research Group LLC, Tariffville, CT, USA

Objectives: When the number of covariates is large, covariate analysis with the conventional forward selection-backward elimination approach in NONMEM® can be a very time consuming or impractical approach. Software limitations may also arise when such a large number of covariates need to be tested alone and in combination. We were presented with 119 single nucleotide polymorphisms (SNPs) (identified through standard regression analyses as potentially important) that could have an association with tacrolimus apparent clearance (CL/F). The objective of this analysis was to devise a novel "winnowing method" that could screen the 119 SNPs to (1) select important SNPs, (2) include SNPs that are only important in the presence of another covariate, and (3) remove noncontributory SNPs. We illustrated this method with the help of a simulated dataset.
Methods: We first obtained the base model (structural PK model with no covariates) and empirical Bayes estimates (EBEs) from NONMEM®. Next, a series of generalized additive modeling (GAM) runs were devised using the GAM function in the R statistical package. In the first GAM run, the EBEs of CL/F from the base model were regressed on a subset of 25 SNPs out of the 119 SNPs. In our method, we refer to this as the *group size* of the random selection process. The subset of 25 SNPs was randomly selected from the available 119 SNPs. The most important combination of SNPs in a set of 25 randomly chosen SNPs was identified based on the Akaike Information Criterion (AIC). The process of randomly selecting 25 SNPs and subjecting them to a GAM analysis was repeated 500 times and referred to as the *number of GAM repetitions*. A SNP index (0.0–1.0), which defines the relative importance of SNPs, was created. It was defined as the proportion of the number of times a SNP was selected to the number of times it was randomly sampled (Eq. 1).

$$\text{SNP Index} = \frac{\text{Number of times SNP is selected}}{\text{Number of times SNP is sampled}} \quad (1)$$

The most important SNPs (index = 1.0) were included in an updated NONMEM® model, while unimportant SNPs (index = 0.0) were removed from further consideration. The remaining ambiguous SNPs (index = 0.1–0.9) were subjected to this winnowing process again using the EBEs from the updated NONMEM model and the same *group size* and *number of GAM repetitions* as used previously. This process was repeated until all SNPs were categorized as 0.0 or 1.0. The important SNPs were obtained by this process. Backward elimination was then performed to obtain the final SNPs affecting tacrolimus CL/F.
Illustration of the method: We further explored this approach using a simulated dataset. PK data were simulated from a one-compartment intravenous (i.v.) bolus model. The dataset consisted of 500

individuals with 7 samples per individual drawn at 0.25, 0.5, 1, 2, 4, 6 and 8 h after administration of a 500 mg dose. The typical value of CL was set to 5 L/hr and the typical volume of distribution (V_d) was set to be 14.5 L. An exponential error model was assumed for inter-individual variability (IIV) on CL and V_d and was set to 30 % for both PK parameters. A proportional error model was assumed for random unexplained variability (RUV) and set to 10 %. Using the R statistical package, 100 SNPs with specific allele frequencies were simulated. The effects of 10 important SNPs on CL were incorporated into the model and the corresponding observed concentrations were simulated using NONMEM®. The objective was to determine if the 10 important SNPs were selected from the 100 SNPs in the simulated dataset by this approach. Type I (false positive) and type II (false negative) error rates were also calculated.

Results: The winnowing scheme selected 26 SNPs from the 119 SNPs as the full model from the clinical dataset. It involved a total of 5 updated NONMEM® covariate models and 5 runs in GAM to attain the full model. A total of 19 SNPs affecting tacrolimus CL/F were obtained after backward elimination.

For the simulated data set, a total of 18 SNPs were picked up by the winnowing method for the full model. All true positive SNPs ($n = 10$) and 8 false positive SNPs were selected by the winnowing approach. The type I and type II error rates were 9 and 0 %, respectively.

Conclusions: We developed a novel method for selection of significant covariates when a large number of potential covariates are available. We used tacrolimus pharmacogenetics as a motivating example to develop this method. Using this method, followed by backward selection, we were able to select 19 SNPs from the 119 SNPs. The SNPs selected included the widely established CYP3A5*1, which is well known to increase tacrolimus CL/F. We illustrated this method using a simulated dataset. The method was able to select all of the 10 important SNPs from the 100 SNPs in the simulated dataset yielding a 0 % false negative rate. In addition to the true positive SNPs, 8 false SNPs were also selected putting the false positive rate of the method in the simulated dataset to be about 10 %. It is to be noted that the clinical and simulated datasets are not comparable and the simulation was an illustration of the approach. More comprehensive simulation studies will help establish the performance of this method for covariate selection.

W-045 Fasting Glucose Model-Based Meta-analysis: A Tool for Designing and Interpreting Early Diabetes Studies

William S. Denney*, Gianluca Nucci

Pfizer, Clinical Pharmacology, Cambridge, MA, USA

Objectives: Fasting Glucose (FG) is a key parameter of the overall diabetes diagnosis, progression, and treatment, ideally complementing postprandial glucose (PPG) and comprehensive measurements (HbA1c) [1–2]. FG is also a critical parameter for assessment of glucose control in short term trials and as such it is important to be able to quantify the time course and FG effect of available oral anti-diabetic agents to offer a quantitative framework for decision making of novel agents undergoing early signal of efficacy studies. To this end, we have undertaken a model-based meta-analysis (MBMA) [3] of FG in published clinical studies with sulfonylureas (SU) thiazolidinediones (TZD), metformin (MET), dipeptidyl peptidase-4 inhibitors (DPP4), and sodium/glucose cotransporter 2 inhibitors (SGLT2).

Methods: A database of 169 published, double-blind, clinical trials of oral anti-diabetic treatments with a combined 66772 subjects was constructed by Pfizer and Quantitative Solutions. The meta-analysis was limited to summary level data from 0 to 26 weeks. Models were fit using R 2.15.1 using nonlinear mixed effect modeling (nlme library). Baseline fasting glucose (BFG) was reported in most studies; when not reported, it was estimated as a function of baseline HbA1c, prior treatment, and disease duration. The inverse standard error squared of FG was used as the per-measurement weighting. During stepwise-selection, models were chosen based on the Akaike information criterion (AIC) and physiological plausibility. Model forms tested included a combination of E_{max} time to effect (collapsed to step-changes in time when T50 was too small to be estimated) with E_{max} dose response (collapsed to step-changes in dose when ED50 was not estimated). Treatment effect was baseline-adjusted with a power function.

Results: Goodness of fit plots indicated that the model adequately described the trial data. All model parameters were estimated with low relative standard errors. The rate of FG change was fastest with SGLT2, SU, and DPP4 while MET and TZD were the longest consistent with the insulin sensitizing mechanism of action.

Conclusions: A FG model-based meta-analysis was developed informing the design of clinical studies of novel anti-diabetic agents by comparison to existing oral agents. The estimated times to half-maximal FG effect suggests the duration of FG studies to allow for this uncertainty range from <1 week to ~ 6 weeks and allowed to benchmark comparative effectiveness of novel agents in development against current oral anti-diabetic treatments.

References

[1] Stumvoll M, Goldstein BJ, van Haeften TW (2005) Type 2 diabetes: principles of pathogenesis and therapy. Lancet 365:1333–1346

[2] Monnier L, Lapinski H, Colette C (2003) Contributions of fasting and postprandial plasma glucose increments to the overall diurnal hyperglycemia of type 2 diabetic patients. Variations with increasing levels of HbA1c. Diabetes Care 26(3):881–885

[3] Mandema JW, Gibbs M, Boyd RA, Wada DR, Pfister M (2011) Model-based meta-analysis for comparative efficacy and safety: application in drug development and beyond. Clin Pharmacol Ther 90(6):766–769

W-046 Model-based Characterization of the Clinical Pharmacokinetics of Nivolumab, a Fully Human Anti-PD-1 Monoclonal Antibody

Yan Feng*, Shruti Agrawal, Georgia Kollia, Sally Saeger, Martin Ullmann, Vindira Sankar, Dan McDonald, Ashok Gupta, Eric Masson, Amit Roy

Bristol-Myers Squibb, Princeton, NJ, USA

Background: The immune checkpoint receptor programmed death-1 (PD-1) negatively regulates T cell activation. Nivolumab, a PD-1 receptor blocking antibody, demonstrated durable clinical benefit in a phase 1 study in pts with various tumors [1]. The aim of this study is to characterize the PK profile of nivolumab and to assess the effects of intrinsic and extrinsic factors on nivolumab exposure in support of the development of nivolumab for the treatment of melanoma, non-small cell lung cancer (NSCLC), and renal cell carcinoma (RCC).

Methods: Nivolumab time-concentration profiles were described by a population pharmacokinetic (PPK) model with 2,760 post-nivolumab treatment serum PK samples from 325 subjects enrolled in 2 clinical studies: a single ascending dose (SAD) and a multiple ascending dose

(MAD) study in with advanced solid malignancies. Nivolumab doses of 0.3–10 mg/kg single IV dose were tested in SAD study and doses of 0.1–10 mg/kg dose every 2 weeks were tested in the MAD study. The relationships between PK parameters (clearance (CL) and volume of central compartment (VC)) and various baseline covariates were examined, including: body weight (BW), age, sex, estimated glomerular filtration rate (eGFR), baseline lactate dehydrogenase, albumin, absolute lymphocyte count, C-reactive protein and total bilirubin. Visual predictive check was applied for PPK model validation.

Results: The PPK of nivolumab was well characterized by a linear two compartment model with zero-order IV infusion and first-order elimination. Typical CL and VC estimates are: 0.0104 L/h and 4.56 L, with 52.8 and 29.6 % interindividual variability. Baseline BW, sex, C-reactive protein, albumin, appear to have >20 % effect on clearance (CL); BW and sex also appear to have a >20 % effect on VC. BW normalized dosing produces relatively constant nivolumab steady-state exposures across a wide BW range (40–150 kg).

Conclusions: The PPK analysis indicate that nivolumab PK is linear and a BW-normalized dosing regimen is appropriate for nivolumab therapy. These results will be confirmed with additional data from the phase 2 and 3 studies of nivolumab in melanoma, NSCLC, and RCC.

Reference

[1] Topalian et al (2012) Safety, activity, and immune correlates of anti-PD-1 antibody in cancer. N Engl J Med 366:2443–2454

W-047 Power Calculations for Pharmacodynamic Crossover Studies Conducted to establish Bioequivalence of Inhaled Corticosteroids Through Monte Carlo Simulations

Bhargava Kandala[1,*], Benjamin Weber[1], Lawrence Winner[2], Guenther Hochhaus[1]

[1]Department of Pharmaceutics, University of Florida, Gainesville, FL, USA; [2]Department of Statistics, University of Florida, Gainesville, FL, USA

Background: To establish bioequivalence (BE) of generic inhaled corticosteroids (ICS) at the site of action, the FDA recommends pharmacodynamic/clinical studies[1] monitoring effects of ICS on fractional exhaled nitric oxide (FeNO). There is limited literature available on effects of ICS on surrogate markers of inflammation and there are no BE studies reported to date.

Objectives: To perform power calculations for pharmacodynamic (PD) crossover studies through a clinical trial simulation model by (a) predicting the dose response to ICS using FeNO, (b) incorporating different patient populations (high responders [2] vs. intermediate responders [3]), and (c) applying a bootstrap based non-parametric approach to construct distributions of relative bioavailability [4] # (F_{DS}).

Methods: Crossover studies (Fig. 1) were simulated with sample sizes of 48, 64 and 128 patients and a wide range of identical reference (R) and test (T) products. The mean responses for R and T doses were obtained from an E_{max} model (Eq. 1) with relevant E_{max} and ED_{50} values. Two patient populations, high responders and intermediate responders were simulated with E_{max} values of 75 and 50 % of E_0 respectively. Within- and between-subject variability estimates were obtained from literature.

FeNO values from each simulated dataset were analyzed using a linear mixed effects model with restricted maximum likelihood estimation. Dosing sequence, treatment (3 doses of R and one dose of T) and period were fixed effects, while patient nested within sequence was a random effect. Baseline FeNO values were added to the model as covariate. The study power, defined as the % of the 200 simulated datasets showing bioequivalence i.e. if 90 %CI of F_{DS} (Eq. 2) is within 0.8-1.2 was calculated via bootstrap procedure (R 2.14.1).

E_{max} **Model:**

$$\text{Response} = E_0 - \frac{E_{max} * \text{Dose}}{ED_{50} + \text{Dose}} \quad (1)$$

Relative Bioavailability:

$$F_{DS} = \frac{\phi_R^{-1}(E_T)}{D_T} \quad (2)$$

F_{DS} is the relative bioavailability of T and R at site of action; Φ_R is the E_{max} model describing the dose response of R, E_T, D_T are the response and claimed does of the T respectively.

Results: Highest power was achieved in general when the test dose is close to ED_{50} (Fig. 2). 90 % power was obtained in high responders using sample size of 128 subjects, whereas in intermediate responders it was 50 % with the same number of subjects (Figs. 2, 3). When the BE criteria is relaxed to 0.7–1.3, 90 % power was obtained using 64 and 128 subjects in high and intermediate responders respectively. A 33 % change in E_{max}, expressed as a percent of E_0 (75–50 %)

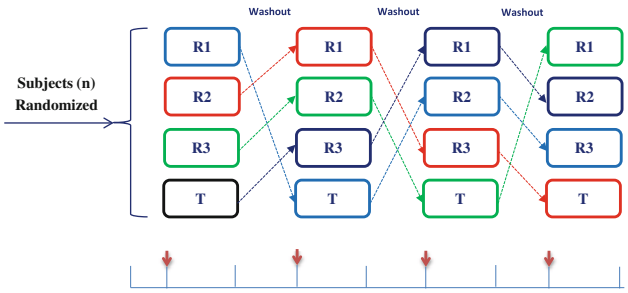

Fig. 1 Simulated crossover study design

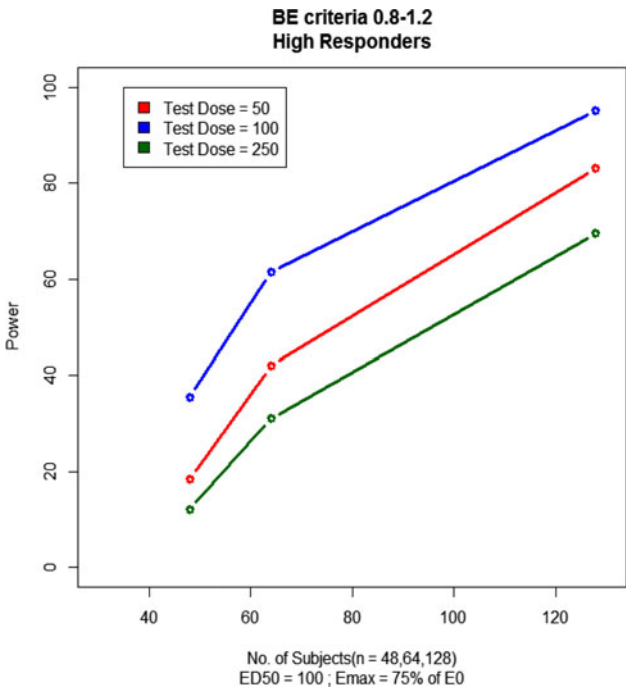

Fig. 2 Power versus test dose ($ED_{50} = 100$)

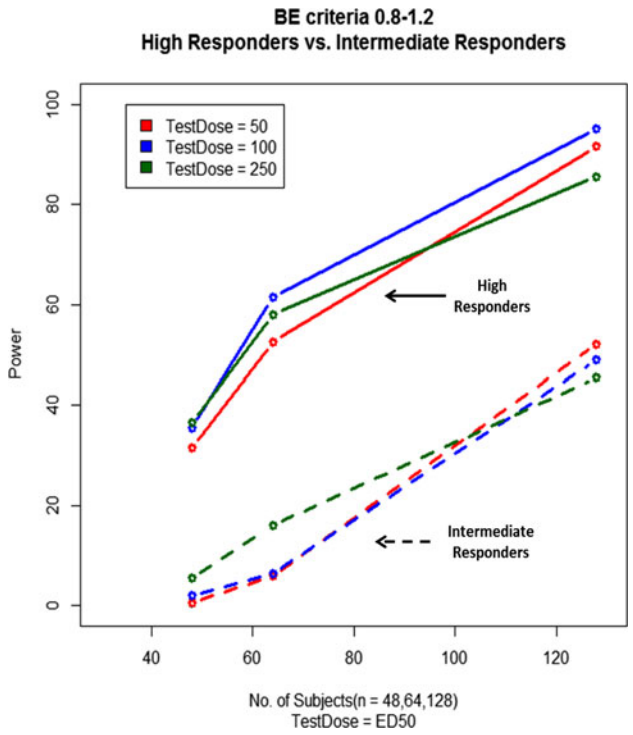

Fig. 3 Power in different patient populations

between high and intermediate responders decreased the study power by 44 % (Fig. 2).

Conclusions: Power calculations were performed by applying a bootstrap approach to crossover studies and constructing 90 % CI on F_{DS} without any distributional assumptions. The pharmacodynamic approach for establishing BE of ICS seems feasible only when the study population consists of high responders to establish a significant dose response relationship and the test dose chosen is close to the estimated ED_{50} value of the drug and biomarker combination. The clinical trial simulation model developed can be used to optimize other BE studies design.

References

[1] Lee Sl, Adams WP, Li BV, Conner DP, Chowdhury BA, Yu L (2009) In vitro considerations to support bioequivalence of locally acting drugs in dry powder inhalers for lung diseases. AAPS J 11(3):414–423

[2] Anderson WJ, Short PM, Williamson PA, Lipworth BJ (2012) Inhaled corticosteroid dose response using domiciliary exhaled nitric oxide in persistent asthma: the fenotype trial. Chest 142(6):1553–1561

[3] O'Connor BJ et al (2011) Rapid effects of extrafine beclomethasone dipropionate/formoterol fixed combination inhaler on airway inflammation and bronchoconstriction in asthma: a randomised controlled trial. BMC Pulmonary Med 11:60

[4] Food and drug administration center for drug evaluation and research. Draft guidance on orlistat. http://www.fda.gov/downloads/Drugs/GuidanceComplianceRegulatoryInformation/Guidances/UCM201268.pdf. Revised Aug 2010

W-048 A Technique for Identifying an Optimal Threshold Value of a Continuous Predictor of Clinical Outcomes

Cecilia Fosser[1,*], Sriram Krishnaswami[1], Matthew Hutmacher[2]

[1]Pharmacometrics, Pfizer Inc., Groton, CT, USA; [2]Clinical Pharmacology, SCBU, Pfizer Inc., Groton, CT, USA; [3]Ann Arbor Pharmacometrics Group (A2PG), Ann Arbor, MI, USA

Objectives: In situations where a clinical outcome (e.g. infection) is causally linked to a continuous measure (e.g. neutrophil counts), it is of interest to drug developers and clinical practitioners to determine a threshold value for the continuous measure that could be used to optimize outcomes (e.g. changing the dose, discontinuing treatment, seek alternative therapy), and/or characterize the therapeutic index during development. Various techniques have been employed to identify such thresholds including empirical methods based on years of clinical experience, contingency tables, and Receiver Operating Characteristics (ROC) analysis, all of which have their benefits and limitations. These approaches are limited by the fact that they are static with respect to time and do not take into account changes in the continuous measure over time, a common phenomenon in clinical trials. We propose a general profiling method using a Cox proportional hazards model that combines both the development of the relationship between the continuous measure and the clinical outcome, while providing a quantitative framework to identify the threshold value. The method captures nonlinear aspects of the relationship, yet can also be used to take advantage of software intended for linear models.

Methods: The 'extended' Cox proportional hazards model used includes a second covariate derived from the time-varying continuous measure of interest that estimates the contribution of this continuous predictor when it is beyond a specified, fixed threshold value. The profiling technique generates diagnostic statistics from the model fits as the threshold values are varied. These statistics are analyzed and the threshold value achieving the minimum such statistic is considered the optimal threshold. The process is similar to obtaining confidence intervals by likelihood profiling. We compare and discuss the merits of using the minimum of the sum of the relative standard errors as the indicator of the optimum threshold versus using the minimum objective function value.

Results: Example: Top plot: Incidence rates are graphed at the median values of the 5th percentiles of the continuous predictor. A threshold effect appears to exist in the data at low values of the continuous predictor. Bottom plots: various measures of model fits using the Cox PH model using different threshold values of the continuous predictor: Left: sum of the relative standard errors; Right: objective function values

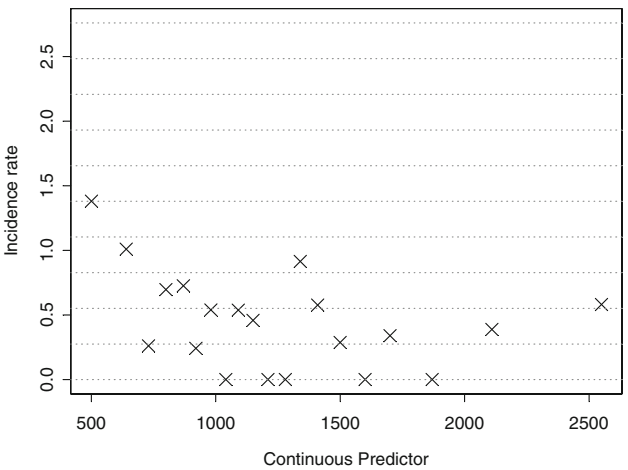

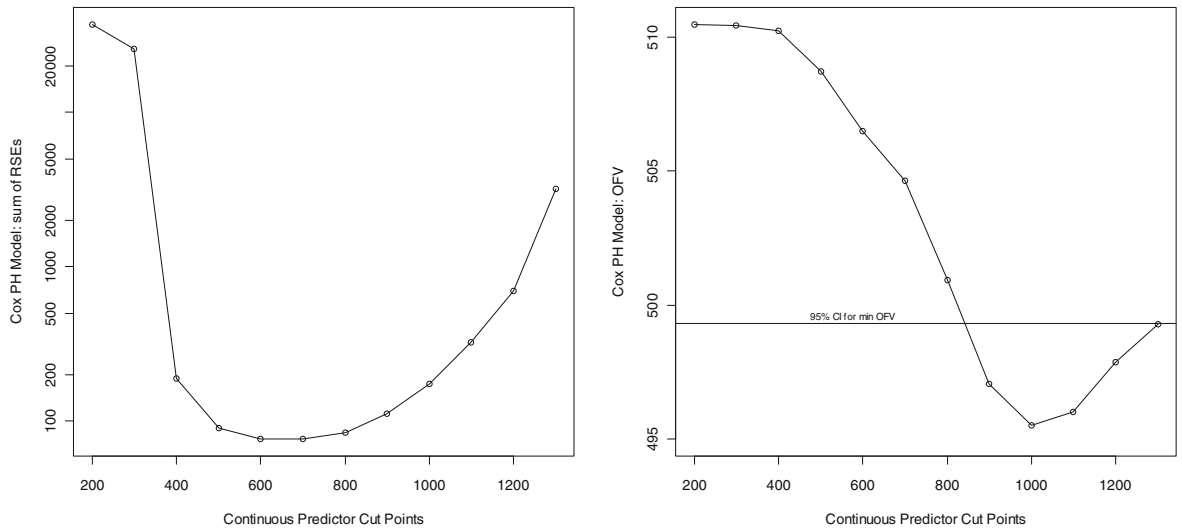

Conclusions: In situations when time-varying continuous measures may have a threshold value, for which values of the continuous measure above or below this threshold become predictive of a clinical outcome or of clinical concern, the threshold profiling technique proposed using diagnostic statistics from a Cox PH model, specifically the sum of the relative standard errors of the effects, can quantitatively identify the threshold value that provides a predictive range of the continuous measure. Identifying such thresholds for the continuous predictor may be valuable for advising on a change in dose, guiding a treatment decision, or helping to delineate a therapeutic index.

W-049 An R Function to Efficiently Screen for Relationships Between Drug and/or Disease Parameters and Rare Adverse Events

Anasuya Hazra[1,*], Cecilia Fosser[2], Steve Riley[1], Sujatha Menon[1], Vivek Purohit[1], Arnab Mukherjee[1], Jonathan French[3], Matt Hutmacher[4], Mark C Peterson[5], Manisha Lamba[1], Sriram Krishnaswami[1]

[1]Clinical Pharmacology, SCBU; [2]Pharmacometrics, Pfizer Inc., Groton, CT, USA; [3]Metrum Research Group, Tariffville, CT, USA; [4]Ann Arbor Pharmacometrics Group, Ann Arbor, MI, USA; [5]Pharmacometrics, Pfizer Inc., Cambridge, MA, USA

Objectives: One of the most difficult aspects of drug development is reliably detecting increased incidence of rare adverse events or events with significant latency and developing a sufficient understanding to assess the benefit-risk ratio, guide dosing, and/or inform clinical management decisions. Frequently, an ad hoc process based on clinical judgment is employed in order to associate the occurrence of an event with drug dose or a laboratory safety marker. While clinical judgment is a critical component to such decision making, pharmacometricians can play a role in informing those decisions by applying model-based approaches and doing so in an efficient and consistent manner across the plethora of safety data typically collected during the drug development process. The primary objective of this work was to develop a simple and informative screening method to explore such relationships in a consistent and timely manner to answer development/regulatory questions.
Methods: Data requirements to use this function are as follows, one record per subject with the following data, (a) subject identifier, (b) predictor variables, e.g., clinically relevant drug exposure metrics, such as time weighted average C_{max} or Cavg for the duration of the treatment, or complete blood counts (CBC) at baseline i.e. before a subject started therapy with the given drug, c) types of AE (dichotomous), i.e. occurrence of an event defined as 1 (yes) 0 (no); d) total duration of therapy for the patient up to the time of event or discontinuation or duration of follow-up. *Method of Analysis*: The exposure or biomarker values are sub-divided into a user-specified number of bins based on clinical relevance (e.g., quartiles or deciles). The observed mean incidence rates [IR] (e.g. events per 100 patient years) and 90 % confidence intervals (CI) are calculated using the "cipoisson" function (Terry Therneau, (http://mayoresearch.mayo.edu/mayo/research/biostat/splusfunctions.cfm). The model predicted IR is obtained by regressing the observed IR in each bin vs. the median of the predictor variable within each bin through a generalized linear model with log link and Poisson errors. This is implemented using the "glm" function in S-Plus 8.0 (Insightful Corporation, Seattle, Washington, USA) or R12.2.2 (http://www.R-project.org) (http://mayoresearch.mayo.edu/mayo/research/biostat/upload/81.pdf).
Results: The following flowchart illustrates the steps that are performed in the user defined (squares) and the function (circles) steps to obtain desired outcomes. Steps 1-8 do not need user input.

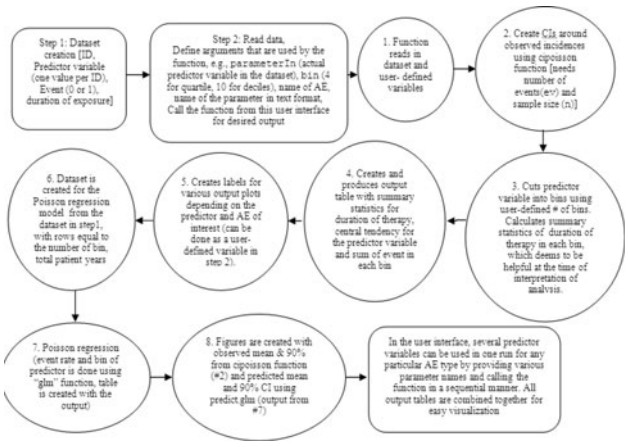

A typical plot from the function where quartiles of the predictor variable are used to model the incidence rate of an AE is given below.

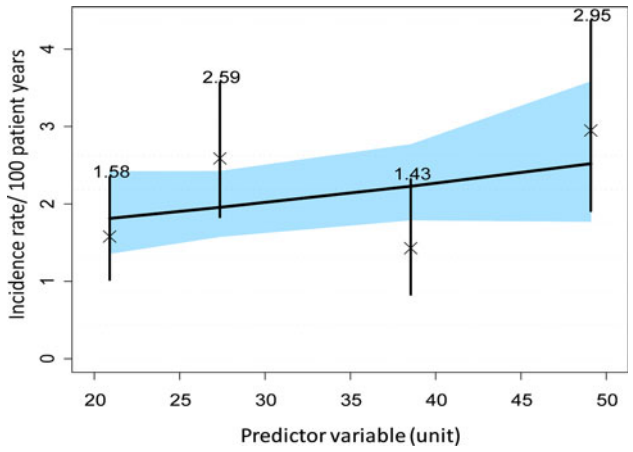

Symbol 'x' represents observed incidence rate (per 100 patient years for example); bars represent 90 % confidence intervals (CI) of the incidence rate; solid line represents mean model prediction and blue band represents 90 % CI of the model prediction;

Conclusions: A simple and computationally rapid methodology that allows for efficient screening of multiple endpoints and/or adverse event outcome relationships is proposed. The tool allows communication of results in a consistent and easy-to-visualize manner. Future efforts for moving from screening to inferential analysis using pharmacologically-based models (e.g. to better address latency) are warranted.

W-050 In Vitro Study to Characterize Antiplatelet Effect of Ticagrelor and its Active Metabolite (AR-C124910XX)

Namyi Gu, Kyun-Seop Bae, Hee Youn Choi, Mi Jo Kim, Yo Han Kim, Yook-Hwan Noh*, Jin A Jung, Eunhwa Kim, Hyeong-Seok Lim

Department of Clinical Pharmacology and Therapeutics, Asan Medical Center, Seoul, Republic of Korea

Objectives: Ticagrelor is a reversible P2Y12 receptor antagonist which has been developed as a treatment of acute coronary syndrome. Although both ticagrelor per se and its metabolite, AR-C124910XX, are known to be pharmacologically active for P2Y12 receptor, their pharmacodynamic interaction has not been studied. This is an in vitro study to evaluate the pharmacodynamic interaction between ticagrelor and AR-C124910XX.

Methods: Twenty pairs of the randomized concentrations of ticagrelor and AR-C124910XX were studied within 2 h using the plasma from an individual. The ranges of the randomized concentrations of ticagrelor and AR-C124910XX were 0–10,000 and 0–5,000 ng/mL, respectively. The primary variable was the platelet aggregation (%) of each mixture which was measured with a light transmission aggregometry using ADP as an agonist. NONMEM version 7 was used to analyze their pharmacodynamic interaction by building a response surface model.

Results: A total of healthy volunteers donated their blood to conduct the in vitro study. Platelet aggregation was measured in 576 samples including 96 blank ones. In the response surface model, the synergistic interaction was identified in the mixtures of ticagrelor and AR-C124910XX. Although both ticagrelor and AR-C124910XX inhibited platelet aggregation, ticagrelor was more potent than AR-C124910XX with the IC50 of approximately 17 % compared to AR-C124910XX in this study. The median predicted platelet aggregation response surface was visualized and compared to the observed values in Fig. 1. Figure 1 shows the median response surface with the reference lines of average steady state plasma concentrations of ticagrelor and AR-C124910XX on ticagrelor 90 mg q 12 h, at which dosing regimen, ticagrelor is predicted to exert its near-maximum anti-platelet effect.

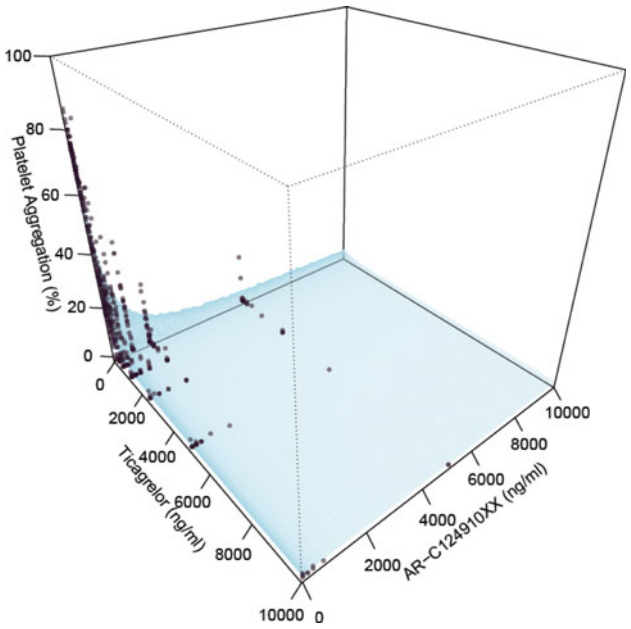

Fig. 1 Comparison of the predicted versus observed platelet aggregation (%) by the plasma concentrations of ticagrelor and AR-C124910XX

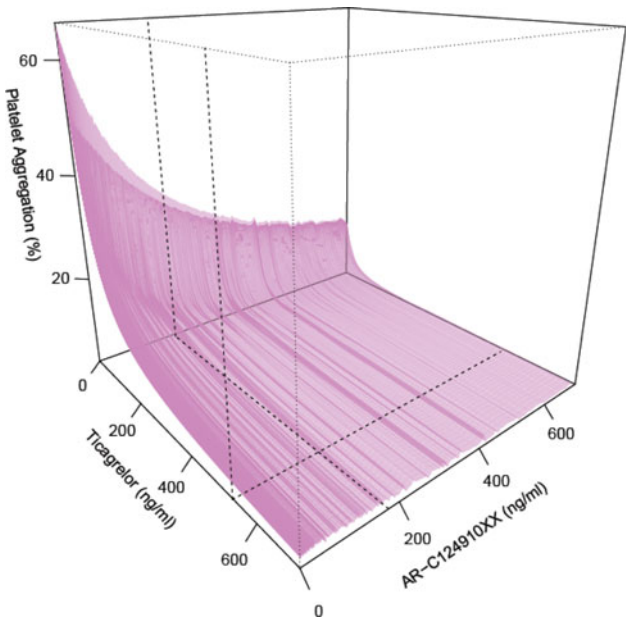

Fig. 2 Visualization of the median predicted platelet aggregation (%) in the concentration ranges around Css of ticagrelor and AR0C124910XX when orally administered with ticagrelor 90 mg twice a day

Conclusions: This study suggested that ticagrelor is more potent than AR-C124910XX and that there is the synergistic pharmacodynamic interaction on the inhibition of platelet aggregation between ticagrelor and AR-C124910XX.

References

[1] Minto CF, Schnider TW, Short TG, Gregg KM, Gentilini A, Shafer SL (2000) Response surface for anesthetic drug interactions. Anesthesiology 92:1603–1616

[2] Fidler M, Kern SE (2006) Flexible interaction model for complex interactions of multiple anesthetics. Anesthesiology 105:286–296

[3] Husted S, van Giezen JJ (2009) Ticagrelor: the first reversibly binding oral P2Y12 receptor antagonist. Cardiovasc Ther 27(4):259–274

W-051 In-Vitro In-Vivo Correlation (IVIVC) Using a Generic PBPK Model and Markov Chain Monte Carlo Analysis

Robin McDougall[1,2,*], Marc-Andre Verner[3,4], Conrad Housand[1]

[1]The AEgis Technologies Group, Orlando, FL, USA; [2]University of Ontario Institute of Technology, Oshawa, ON, Canada; [3]Channing Division of Network Medicine, Brigham and Women's Hospital, Harvard Medical School, Boston, USA; [4]Institute of Environmental Medicine, Karolinska Institutet, Stockholm, Sweden

Objectives: In-vitro in vivo correlation (IVIVC) methods can play an important role in improving the efficiency of drug development by providing predications for the physiological responses in multiple tissues to modest drug formulation changes without requiring the completion of costly clinical studies.

There are a number of different approaches to IVIVC described in the literature, but one that shows particular promise with respect to its flexibility is the direct, differential equation IVIVC (DDE-IVIVC) method presented in [1]. By removing the requirement for solving for convolutions to link the in vitro and in vivo components of IVIVC, DDE-IVIVC makes employing more sophisticated kinetic models relatively straightforward.

With this in mind, the goal of this work was to present a revised DDE-IVIVC approach with two proposed modifications. First, by using a physiologically based pharmacokinetic (PBPK) model in place of a classical one- or two-compartment pharmacokinetic model it becomes possible to monitor the effects of formulation changes not only on plasma concentration time-courses, but also tissue-specific time courses as well. And secondly, by employing Markov chain Monte Carlo techniques to solve for the IVIVC parameters we are able to not only incorporate prior knowledge about both the in vitro and in vivo models, but also to gain significantly more information about the relationships and correlations between the IVIVC parameters themselves.

Methods: We developed a generic, extensible "In-vitro Dissolution"/"In-vivo PBPK" model on which to apply DDE-IVIVC. The in vitro model components were modeled directly from [1], the in vivo dynamics modeled as a typical multi-compartment PBPK model with a scalable number of compartments set up to use drμg/formulation-specific parameters (intrinsic clearance and octanol:water coefficients) to describe the pharmacokinetics.

Next an MCMC statistical model was developed which can incorporate any prior information for the parameter values that solved for the probabilistic distributions of the in vitro and in vivo values via a likelihood function that considers the rate of dissolution and observations from clinical trials for available formulations.

After running the MCMC analysis to convergence, we use the resulting chains to make inferences about the distributions for the in vitro and in vivo parameters, and then forward Monte Carlo studies to generate tissue specific time-course predictions for different formulation candidates.

Results: The modified DDE-IVIVC approach employed here was able to predict levels of diltiazem that were relatively close to the values presented in [1], in that the median values from our study were within 10–20 % of the mean values reported by [1].

Conclusions: The approach employed was able to match the observations of the withheld data set as well as provide predictions for other tissues of interest for different formulations. By using a PBPK model in place of a classical pharmacokinetic model, predicted time-course concentrations for multiple tissues are available instead of just plasma (allowing us to ensure therapeutic dose levels in the desired tissues while monitoring toxicity in others). The use of MCMC analysis to quantify the relationship between the IVIVC parameters instead of deterministic optimization analysis we gain significant insight into the correlations of the IVIVC parameters as well as the physiological parameters that would otherwise be missed.

Reference

[1] Buchwald P (2003) Direct, differential-equation-based in vitro-in vivo correlation (IVIVC) method. J Pharm Pharmacol 55(4): 495–504

W-052 Population PK Model of Rectal 1 % Tenofovir (TFV) Gel in the Rectum and Plasma

Kuo-Hsiung Yang[1,*], Julie Elliot[2], Craig Hendrix[3], Peter Anton[2], Ross Cranston[4], Ian McGowan[4], Angela DM Kashuba[1]

[1]UNC Eshelman School of Pharmacy, Chapel Hill, NC, USA; [2]UCLA, Los Angeles, CA, USA; [3]Johns Hopkins University, Baltimore, MD, USA; [4]University of Pittsburgh, Pittsburgh, PA, USA

Objectives: There is evidence that TFV 1 % vaginal gel can be used for pre-exposure prophylaxis in women [1] and oral Truvada (tenofovir disoproxyl fumarate/emtricitabine) in men. [2] Rectal microbicides are currently being evaluated to reduce HIV transmission via unprotected receptive anal intercourse. This population PK model describes TFV gel's disposition in the rectum and plasma.

Methods: Subjects in the RMP-02/MTN-006 study were given a single oral dose TDF (300 mg), followed 4 weeks later by a single rectal dose of 1 % TDF gel (44 mg) [3]. Blood plasma and rectal sponge samples were collected at various times up to day 12 post dose. The dataset used for this model contains 12 subjects. TFV concentration was determined by validated LC–MS/MS methods [4, 5]. Mixed effects population modeling was done using NONMEM 7.2.0 (ICON, plc) with FOCE-interaction algorithm. Inter-individual variability is described with an exponential error model, and residual variability is described using an additive and proportional error model. The additive error is fixed to 1 ng/mL, and proportional error fixed to 32 % CV. Linear kinetics in the model is assumed. Model discrimination is with AIC. After model parameter estimates and inter-individual variability are obtained, 1000 simulations are performed for the visual predictive check. Data pre/post-processing and plotting is done with R [6]; additional R libraries used includes lattice, reshape2 and plyr [7–9] Initial parameter estimates and model exploration is done with Berkeley Madonna (UC Berkeley).

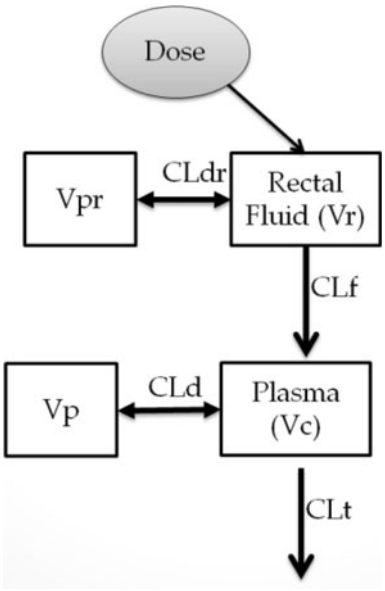

Fig. 1 Structural Model

Table 1 Parameter estimates

	Fixed effects	Random effects (CV %)
Vr	0.0247 L	33.3
Vpr	0.753 L	
Vc	5.66 L	30.9
Vp	16500 L	
CLt	77.4 L/h	70.5
CLd	169 L/h	27.3
CLf	0.027 L/h	127
CLdr	0.235 L/h	310

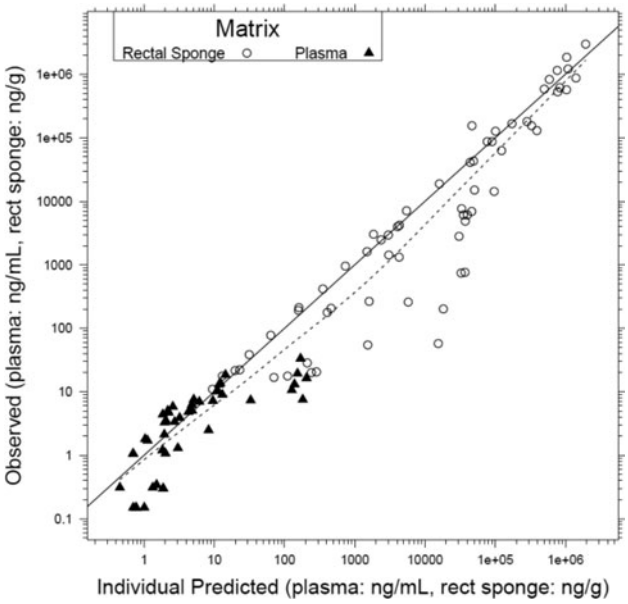

Fig. 2 Observed versus individual predicted (—LOESS line)

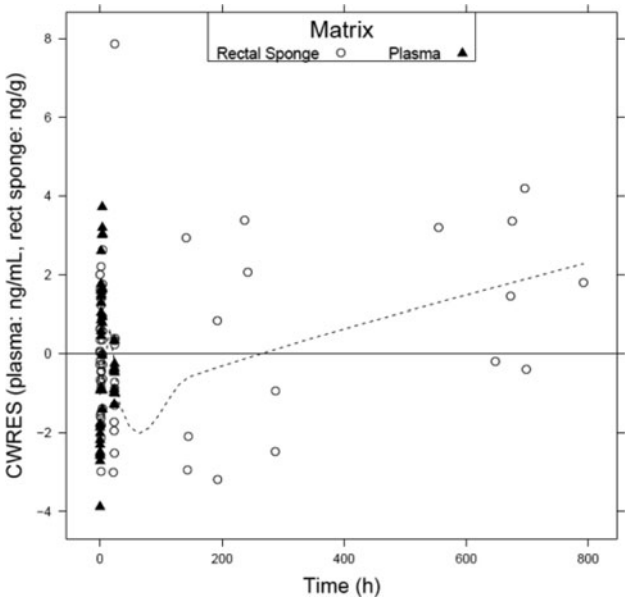

Fig. 3 Conditional weighted residuals versus time (—LOESS line)

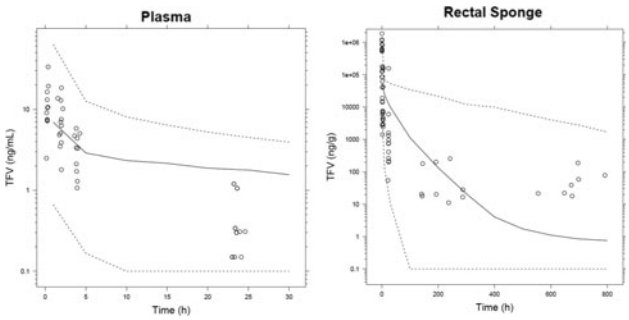

Fig. 4 Visual predictive checks (−50th percentile, —5th, 95th percentile, 1000 simulations)

Results: A four compartment, bolus input, linear kinetic model with a rectal compartment (Vr) leading to a plasma compartment (Vc) and a distributional compartment for each matrix (Vrp, Vp) best describes the data (Fig. 1) The parameter estimates are in Table 1. The goodness of fit plots shows that the model predicts TFV concentrations well in both matrices. There is good correlation between the individual predicted and observed (Fig. 2). There is no systematic under or over prediction in either compartment (Fig. 3). The visual predictive check shows good model performance and that the model adequately describes the data in both matrices, though there is some over-prediction in the plasma and under-prediction in rectal sponge at the later time points (Fig. 4).

Conclusions: This model is useful for predicting rectal and plasma TFV concentrations. The ability to predict and characterize rectal TFV exposure from the gel formulation is important once targets for preventing HIV transmission are defined. This model also allows for simultaneous prediction of plasma TFV concentration, which is important for estimating systemic toxicity. Finally, this model allows for prediction of plasma concentration based on rectal sponge concentration alone, eliminating blood draws. Once the required concentration is known for preventing transmission, this model can be used to optimize the dose and regimen by maximizing efficacy and

minimizing toxicity through simulations. A possible future direction would be to incorporate tissue and other intracellular compartments into the model with active TFV diphosphate concentrations.

References

[1] Abdool Karim Q, Abdool Karim SS, Frohlich JA, Grobler AC, Baxter C, Mansoor LE, Kharsany AB, Sibeko S, Mlisana KP, Omar Z, Gengiah TN, Maarschalk S, Arulappan N, Mlotshwa M, Morris L, Taylor D; CAPRISA 004 Trial Group (2010) Effectiveness and safety of tenofovir gel, an antiretroviral microbicide, for the prevention of HIV infection in women. Science. 329(5996):1168–1174

[2] Grant RM, Lama JR, Anderson PL, Glidden DV et al (2010) Preexposure chemoprophylaxis for HIV prevention in men who have sex with men. N Engl J Med. 363(27):2587–2599

[3] Anton PA, Cranston RD, Kashuba A, McGowan I, et al (2012) RMP-02/MTN-006: A phase 1 rectal safety, acceptability, pharmacokinetic, and pharmacodynamic study of tenofovir 1 % gel compared with oral tenofovir disoproxil fumarate. AIDS Res Hum Retroviruses 28(11):1412–1421. doi: 10.1089/AID.2012.0262

[4] King T, Bushman L, Kiser J, Anderson PL, Ray M, Delahunty T, Fletcher CV (2006) Liquid chromatography-tandem mass spectrometric determination of tenofovir-diphosphate in human peripheral blood mononuclear cells. J Chromatogr B Analyt Technol Biomed Life Sci. 843(2):147–156

[5] Keller MJ, Madan RP, Torres NM, Herold BC, et al (2011) A randomized trial to assess anti-HIV activity in female genital tract secretions and soluble mucosal immunity following application of 1 % tenofovir gel. PLoS One. 6(1):e16475

[6] R Core Team (2012) R: A language and environment for statistical computing. R Foundation for Statistical Computing, Vienna. ISBN 3-900051-07-0, URL:http://www.R-project.org/.

[7] Sarkar D (2008) Lattice: multivariate data visualization with R. Springer, New York. ISBN 978-0-387-75968-5

[8] Hadley W (2011) The split-apply-combine strategy for data analysis. J Stat Softw 40(1):1–29. URL:http://www.jstatsoft.org/v40/i01/

[9] Hadley W (2007) Reshaping data with the reshape package. J Stat Softw 21(12):1–20. URL:http://www.jstatsoft.org/v21/i12/

W-053 Quantitative Application of Learn: Apply to Support Go-No Go Decision to Phase III for a Back-up Compound

Rong Liu[1,*], Ellen Snyder[1], Carole Sable[2], Kevin Ashliman[3], Julie Stone[4], Pravin R Jadhav[4]

[1]Biostatistics and Research Decision Sciences, Merck Research Laboratories, Upper Gwynedd, PA, USA; [2]Project Leadership and Management, Merck Research Laboratories, Upper Gwynedd, PA, USA; [3]Global Marketing, Merck Research Laboratories, Upper Gwynedd, PA, USA; [4]Modeling and Simulation, Merck Research Laboratories, Upper Gwynedd, PA, USA

Objectives: With rising cost of phase III development and high failure rate, a decision to continue investment in a back-up compound is really critical. Quantitative approaches promise early No Go for compounds with low probability of success and faster path of phase III for those with high probability of success. We will present a case study incorporating probabilistic decision making where the lead compound showed favorable benefit-risk profile and back-up molecule demonstrated further improvement over the lead compound. The development of the back-up compound is then not only a public health decision but also an important business decision. The presentation will demonstrate rigorous approach to LEARN from the lead compound and APPLY to back-up compound to support Go-No Go to Phase III. We will also present a thought process and methodology to support the decision making.

Methods: For a lead compound, successful phase III studies demonstrating favorable risk benefit was available. However, with growing interest in the area, additional unmet medical needs were realized. For a back-up compound, a successful Phase II study was available. The key question to the product development team was: Does the compound represent best in class (BIC) efficacy and safety with clinically meaningful improvement? Realistically, a me-too compound from the same company is neither desired nor useful.

The lead and back up compound shared similar mechanism and target population with subtle differences in preclinical species and pharmacokinetic properties. The molecules also shared several important similarities in Phase II study designs (4 arm, placebo controlled, 4 week studies with 300 patients).

A multi-disciplinary team approached the decision in the following way:

1. *Learn*: Assessment of predictive value of Phase II study for the lead compound

Key question: Does Phase II study of the lead compound reasonably predict observed Phase III results? To answer the question, categorical data analysis to assess responder rate on a key endpoint was conducted using a proportional odds model using Phase II data. Model checking for was done by traditional diagnostics. The model was used to predict Phase III using covariate distribution similar to that of observed Phase III data. Similarity between observed and predicted Phase III results was assessed by comparing responder rates.

2. *Apply*: Prediction of Phase III results for the back-up compound and probabilistic assessment of improvement over the lead compound

Given reasonable predictive value of model based analysis for the lead compound, the team developed model for back-up compound using Phase II data and predicted Phase III results using clinical trial simulations. From the simulation, 1000 Phase III studies were simulated and probability of observing better outcome than the lead compound in the Phase III was assessed.

The following Figure demonstrates a quantitative application of Learn—Apply to support Go-No Go decision to Phase III for a back-up compound.

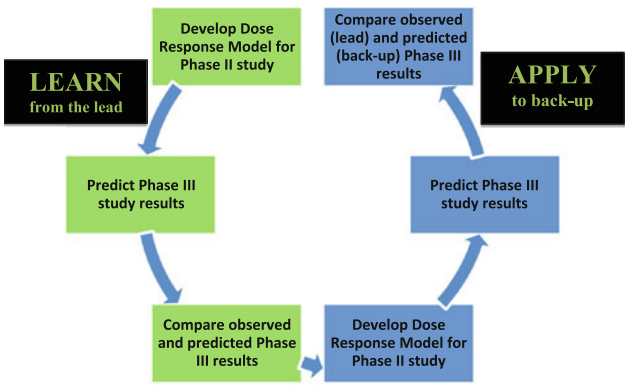

For the presentation, drug identity and therapeutics will be concealed for confidentiality purposes and it not central to the methodology.

Results: Using quantitative approach, a predictive value of Phase II study towards Phase III studies was successfully demonstrated. Using trial simulations, phase III studies were simulated for the back-up compound to demonstrate potential for improvement in efficacy and safety over the lead compound. Further, model approach allowed probabilistic approach to decision making. Most importantly, quantitative approach allowed assessment of areas of improvements for the back-up compound that is leading to design of a market research to understand commercial viability.

Conclusions: A decision to continue development of a back-up compound while comparing to the lead compound is an important business decision. Quantitative approach allows further insights into comparative benefit risk of compounds in development. With a rational thought process and appropriate statistical tools, such comparisons can be rigorously conducted. These insights are an important aspect of development with multi-disciplinary decision making.